

Jorge Alamán Aguilar

Digital fabrication of optical elements through inkjet printing of direct photocurable hybrid inks

Director/es

Sánchez Somolinos, Carlos

<http://zaguan.unizar.es/collection/Tesis>

© Universidad de Zaragoza
Servicio de Publicaciones

ISSN 2254-7606



Universidad
Zaragoza

Tesis Doctoral

DIGITAL FABRICATION OF OPTICAL ELEMENTS
THROUGH INKJET PRINTING OF DIRECT
PHOTOCURABLE HYBRID INKS

Autor

Jorge Alamán Aguilar

Director/es

Sánchez Somolinos, Carlos

UNIVERSIDAD DE ZARAGOZA
Escuela de Doctorado

2020

B/S/H/



Digital fabrication of optical elements through inkjet printing of direct photocurable hybrid inks

Author: Jorge Alamán Aguilar

Director: Carlos Sánchez Somolinos

Departamento de Física de la Materia Condensada

Facultad de Ciencias – Universidad de Zaragoza

CSIC – Consejo Superior de Investigaciones Científicas

ICMA – Instituto de Ciencia de Materiales de Aragón

BSH Electrodomésticos España, S.A.

Zaragoza, May 2020

Table of content

Compendium of publications	9
Resumen.....	11
Conclusiones	13
INTRODUCTION	17
1. Introduction to inkjet printing.....	19
2. Inkjet printing technology	25
3. Drop formation.....	27
4. Drop deposition.....	31
5. Drop fixation.....	33
6. Inkjet printing in micro- and integrated optics	37
7. Summary and outlook	40
MEMORY	43
1. Goals.....	45
2. Scope	47
3. Methodology	53
4. Conclusions	59
REFERENCES	61
PAPERS	71
1. Publication 1.	
Journal: Materials	
Title: Inkjet Printing of Functional Materials for Optical and Photonic Applications	73
2. Publication 2.	
Journal: Journal of Materials Chemistry C	
Title: Photoacid catalyzed organic-inorganic hybrid inks for the manufacturing of inkjet-printed photonic devices.....	123
3. Publication 3.	
Journal: Polymers	
Title: Digital Luminescence Patterning via Inkjet Printing of a Photoacid Catalysed Organic-Inorganic Hybrid Formulation	153
4. Publication 4.	
Journal: Sensors	
Title: Optical Planar Waveguide Sensor with Integrated Digitally-Printed Light Coupling-in and Readout Elements	177
5. Publication 5.	

Journal: Applied Surface Science

Title: Facile Fabrication of Microlenses with Controlled Geometrical Characteristics by Inkjet Printing on Nanostructured surfaces prepared by combustion chemical vapour deposition..... 197

Compendium of publications

The following thesis is presented as a compendium of publications.

This work comprises the following four published original research papers:

- Jorge Alamán, María López-Valdeolivas, Raquel Alicante, Francisco J. Medel, Jorge Silva-Treviño, José Ignacio Peña and Carlos Sánchez-Somolinos. “Photoacid catalyzed organic–inorganic hybrid inks for the manufacturing of inkjet-printed photonic devices”. *Journal of Materials Chemistry C* **2018**, *6*, 3882.
- Jorge Alamán, María López-Valdeolivas, Raquel Alicante, Jose Ignacio Peña and Carlos Sánchez-Somolinos. “Digital Luminescence Patterning via Inkjet Printing of a Photoacid Catalysed Organic-Inorganic Hybrid Formulation”. *Polymers* **2019**, *11*, 430.
- Jorge Alamán, María López-Valdeolivas, Raquel Alicante and Carlos Sánchez-Somolinos. “Optical Planar Waveguide Sensor with Integrated Digitally-Printed Light Coupling-in and Readout Elements”. *Sensors* **2019**, *19*, 2856.
- Jorge Alamán, Ana María López-Villuendas, María López-Valdeolivas, María Pilar Arroyo, Nieves Andrés and Carlos Sánchez-Somolinos. “Facile fabrication of microlenses with controlled geometrical characteristics by inkjet printing on nanostructured surfaces prepared by combustion chemical vapour deposition.” *Applied Surface Science* **2020**, *510*, 145422.

And one review paper:

- Jorge Alamán, Raquel Alicante, José Ignacio Peña and Carlos Sánchez-Somolinos. “Inkjet Printing of Functional Materials for Optical and Photonic Applications”. *Materials* **2016**, *9*, 910.

Resumen

La tecnología de impresión inkjet permite eyección controlada de gotas de tinta de volumen definido y su posicionamiento preciso en un sustrato. Esta tecnología, entre otras virtudes, ofrece una gran flexibilidad para la preparación de estructuras en superficies gracias a su carácter digital, siendo además un proceso fácilmente escalable a nivel industrial, distinguiéndose en estos aspectos de otras técnicas comúnmente utilizadas como, por ejemplo, la fotolitografía. Ya es posible, de hecho, encontrar la tecnología inkjet en aplicaciones de fabricación masiva como la impresión de cartelería o de elementos decorativos. Más allá de la impresión de texto y trabajos gráficos, la capacidad de depositar una gran variedad de materiales de manera digital en forma de recubrimientos homogéneos y patrones en superficies ha despertado gran interés para la preparación de superficies y dispositivos funcionales. Pese a ello, la penetración del inkjet en entornos industriales para la implementación de este tipo de aplicaciones es todavía muy limitada. Entre otras cosas, esto se debe a que los materiales a depositar requieren unas propiedades muy exigentes para poder ser eyectados en condiciones óptimas por los cabezales de impresión, lo que limita la disponibilidad de fluidos compatibles con esta tecnología. Por ello, se hace preciso una adaptación de la viscosidad de los fluidos para poder ser impresos sin que ello reduzca su estabilidad a lo largo de su vida útil ni se vea penalizada la funcionalidad de los depósitos finales, que han de cumplir unos requerimientos específicos, generalmente muy exigentes, para cada aplicación. Por ejemplo, en aplicaciones de micro-óptica u óptica integrada suele ser necesario que los materiales finales tengan buena transparencia y propiedades ópticas adecuadas como alto índice de refracción o luminiscencia según el caso de uso y que estas propiedades no se vean mermadas por el uso o el paso del tiempo.

En este ámbito concreto de las aplicaciones de micro-óptica u óptica integrada, se encuentran en la literatura diversas aproximaciones para el desarrollo de tintas inkjet con las que implementar guías de luz o microlentes. Una de las más prometedoras consiste en la preparación de tintas basadas en materiales híbridos orgánico-inorgánicos que ofrecen una gran flexibilidad para funcionalizar el material gracias a su componente orgánica, a la vez que presentan gran resistencia mecánica y química debido a la red inorgánica. Típicamente, se lleva a cabo la hidrólisis y condensación de un organosilano y se añade un disolvente para ajustar la viscosidad de modo que la formulación sea eyectable. Una vez depositada se elimina el disolvente y se cura la parte orgánica. La necesidad de eliminar el disolvente añade complejidad al proceso. Por otro lado, los procesos de hidrólisis y condensación previos a la impresión del fluido suelen penalizar la estabilidad de las tintas. Asimismo, también es frecuente la combinación del inkjet con el uso de tecnologías adicionales como la fotolitografía para el acondicionamiento de la superficie, previo a la impresión, o procesos térmicos para la posterior fijación de la tinta en el sustrato. Si bien se ha demostrado en la literatura el desarrollo de depósitos y dispositivos de buena calidad óptica con estos materiales híbridos, la falta de estabilidad de las tintas y la complejidad de los procesos envueltos para implementar estos dispositivos ópticos limitan la integración de la tecnología inkjet a nivel industrial en estos ámbitos de aplicación.

Buscando superar estas limitaciones, este trabajo se ha centrado en el desarrollo de tintas funcionales y la implementación con ellas, mediante impresión por tecnología inkjet, de elementos de micro-óptica y óptica integrada. Para ello, más allá de la formulación de tintas funcionales, se ha trabajado en la definición y optimización de todo el proceso, abordando desde

la preparación de la superficie hasta el proceso de impresión y fijación de la tinta al sustrato. Con esto, se ha perseguido conseguir depósitos funcionales mediante un proceso económico y viable en un entorno industrial.

Para ello, las tintas desarrolladas se han basado en precursores híbridos orgánico-inorgánicos comerciales y ampliamente empleados en la literatura. De manera distintiva, con el fin de mejorar la estabilidad de las tintas y controlar los procesos de impresión y fijación, se ha perseguido que las tintas desarrolladas no empleen disolventes y sea posible el curado simultáneo de ambas redes (orgánica e inorgánica) únicamente mediante la exposición a luz UV tras el proceso de impresión. Para ello se han incorporado en las formulaciones fotogeneradores de ácido. Además, se han incluido en las tintas los aditivos necesarios para implementar las funcionalidades deseadas y controlar su viscosidad y tensión superficial, lo que permite una adecuada eyección y mojado de las superficies, así como unas prestaciones satisfactorias para las aplicaciones perseguidas.

Siguiendo esta directriz, a lo largo de esta tesis se han desarrollado diferentes tintas inkjet, libres de disolventes y de curado directo. La primera de ellas, una tinta modelo eyectable sobre la cual se han incorporado posteriormente las funcionalidades deseadas. Así, se ha preparado otra tinta que resulta en depósitos de un elevado índice de refracción que ha permitido, por un lado, la fabricación de guías de luz planares cuando se imprime como un depósito homogéneo y, por otro lado, la preparación de microlentes cuando la tinta se imprime como gotas aisladas con geometrías controladas. Finalmente, también se han formulado dos tintas luminiscentes que permiten la preparación de elementos emisores de luz.

Además del diseño y formulación de las tintas, se han diseñado y optimizado los procesos que intervienen en la preparación de los depósitos con el fin de desarrollar un sistema integral viable a nivel industrial. Por un lado, se han desarrollado diferentes protocolos de preparación de superficies con el fin de controlar la mojabilidad de estas y conseguir, desde gotas aisladas con geometrías controladas y patrones de gotas, hasta líneas continuas o depósitos homogéneos. Por otro lado, el propio proceso de impresión también ha sido optimizado, ajustando la configuración correspondiente para eyectar cada una de las tintas en las condiciones deseadas. Por último, como se ha remarcado anteriormente, el proceso de fijación de la tinta sobre el sustrato también ha sido llevado a cabo exclusivamente por activación mediante luz actínica.

Para poner en valor la funcionalidad de las tintas y los procesos desarrollados, se han diseñado y preparado diferentes sistemas demostradores de casos de uso en micro-óptica y óptica integrada. Por ejemplo, como se ha mencionado con anterioridad, se ha llevado a cabo la impresión de guías de luz planares sobre diferentes sustratos, incluso flexibles, patrones de microlentes con geometrías controladas y un sensor óptico de temperatura planar con indicadores luminiscentes.

Conclusiones

En el marco de esta tesis, se ha desarrollado una plataforma eficiente para la funcionalización de superficies, mediante tecnología de impresión inkjet, para aplicaciones en los campos de la micro-óptica y la óptica integrada. Esta plataforma incluye tintas funcionales basadas en materiales híbridos orgánico-inorgánicos, los procesos necesarios para la preparación de las superficies de un modo eficiente, la optimización del proceso de impresión del material y la subsiguiente fijación de este en el sustrato.

En primer lugar, se han preparado formulaciones libres de disolventes, basadas en monómeros con grupos epoxi y silano, que contienen un fotogenerador de ácido y los aditivos adecuados para ser depositadas por tecnología de impresión inkjet. Gracias al fotogenerador de ácido incluido en la formulación de la tinta, la polimerización de ambas redes, orgánica e inorgánica, es activada de modo simultáneo mediante su exposición a la luz ultravioleta (UV). Esto permite retrasar el proceso de hidrólisis-condensación hasta que la tinta depositada es excitada con luz UV. Gracias a esto y a la ausencia de disolventes en la formulación, no son necesarias etapas adicionales de curado o evaporación, simplificando enormemente el proceso de fabricación. Además, la eliminación de la etapa de hidrólisis y condensación previa a la impresión confiere mayor estabilidad a las tintas a lo largo del tiempo, haciéndolas adecuadas para el uso en aplicaciones industriales.

Mediante el uso de la formulación adecuada, este proceso de impresión y curado ha permitido la preparación de películas sólidas con buena adhesión y transparencia, consiguiendo guías de luz planares con alto índice de refracción y bajas pérdidas.

Haciendo uso de la misma tinta formulada, se ha desarrollado un protocolo flexible y robusto para la preparación de superficies que permite crear microlentes con propiedades ópticas a la carta. Para controlar las propiedades geométricas de las microlentes y, por tanto, sus propiedades ópticas, este tratamiento consta de dos etapas. En la primera, mediante CCVD (de sus siglas en inglés Combustion Chemical Vapour Deposition), se deposita una capa de SiO₂ nanoestructurado. Posteriormente, mediante un proceso CVD (de sus siglas en inglés Chemical Vapour Deposition), esta superficie es funcionalizada con una capa de fluorosilano. En esta superficie así modificada, mediante el control del volumen de las gotas depositadas, se han preparado microlentes con geometrías a la carta, más allá incluso de la hemiesfera.

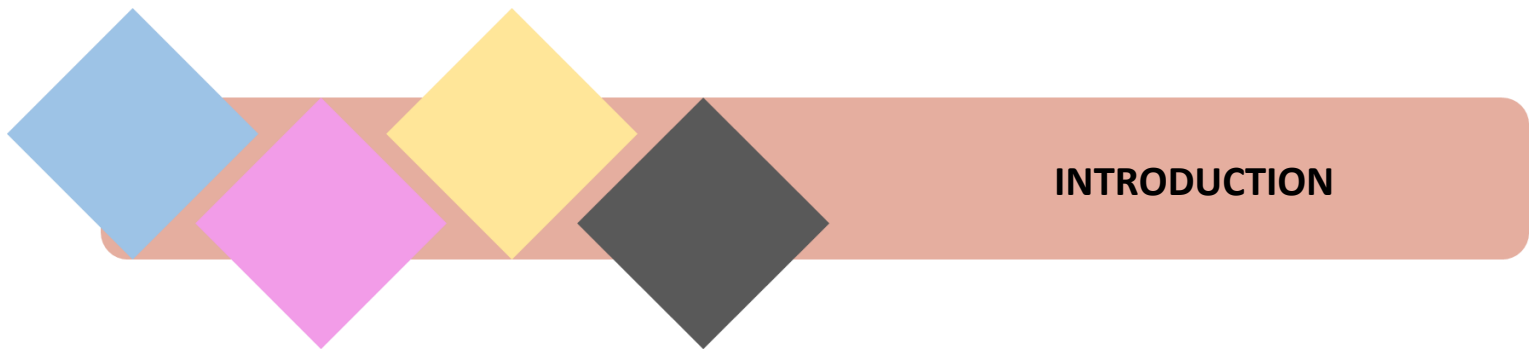
Posteriormente se han incluido también moléculas luminiscentes en las formulaciones desarrolladas sin que se viese penalizada su mojabilidad ni su capacidad de ser impresas por tecnología inkjet. Esto ha permitido la preparación de depósitos luminiscentes a través del mismo proceso de impresión por inkjet y el subsiguiente curado en un solo paso mediante excitación por luz UV. Estos depósitos han derivado en superficies con patrones luminiscentes para su uso en dispositivos ópticos, con buenas propiedades mecánicas, así como buena adhesión.

Para validar estas tintas luminiscentes en aplicaciones reales que demuestren su rendimiento, se ha preparado un sensor óptico de temperatura. Para ello se han combinado depósitos de tintas luminiscentes con otro recubrimiento de polímero cristal líquido, que responde modificando sus propiedades ópticas al cambiar la temperatura, sobre una guía de onda planar.

En resumen, se han desarrollado formulaciones funcionales adecuadas para su impresión por tecnología inkjet, así como los procesos de preparación de las superficies para la

implementación efectiva en ellas de diferentes elementos ópticos, todo ello con capacidad de ser escalado a producción industrial. Además de esto, se han preparado diferentes demostradores para validar el uso de las tintas formuladas en aplicaciones reales. Las tintas desarrolladas se han impreso sobre diversos sustratos como superficies planas de calidad óptica o sustratos convencionales usados normalmente en la industria, tanto flexibles como rígidos, demostrando la versatilidad de estas tintas para poder ser adaptadas a diferentes superficies.

Más allá de las tintas y elementos concretos implementados, la presente tesis ofrece nuevas vías para el desarrollo de tintas funcionales y procesos de preparación de superficies que puedan permitir la impresión digital de elementos funcionales con buenas prestaciones a través de una metodología sencilla e industrialmente viable.



INTRODUCTION

1. Introduction to inkjet printing

There currently are many different technologies used for the deposition of materials onto surfaces in order to generate films or patterns. For example, lithographic techniques such as photolithography are conventionally used for this purpose. These technologies make use of masks or molds to lead to well-defined patterns with submicron resolution, high-throughput and compatibility with wide range of materials. Nonetheless, these techniques rely on expensive and time-consuming processes and imply laborious steps. In contrast with them, a deposition process like inkjet printing has lately gained relevance thanks to its simplicity, its precision and the high material consumption efficiency that it offers. Despite it is difficult to achieve deposits with precision below micrometric order and materials require a specific adaptation of the fluid for being properly jetted, inkjet has become a valuable technology. Especially when it comes to patterning, it is particularly useful thanks to its capability to digitally control the deposition in comparison, for example, with mask photolithography, being possible to change the pattern from one sample to the next one simply by changing a digital file without the need of masks or molds [1].

As a general description, inkjet is a non-contact deposition technique that directly jets the fluid from a printhead to the substrate, which is placed under it. Different parts can be distinguished in an inkjet printing system, as seen in Figure 1a: typically, it counts with a printhead having multiple nozzles at the bottom, a small reservoir to store the ink to be printed, fluid connections to ensure that the printhead is fed with ink from an external larger reservoir and an electronic controller to command the jetting process. The system is digitally controlled by a computer, which sends an electrical signal to dictate the printhead when the ink should be jetted through each individual nozzle. When this occurs, a pressure change is induced inside the cavity and provoke the ejection of a small quantity of fluid in the order of picolitres trough the nozzle (in a subsequent section, the different activation methods will be detailed). In ideal conditions, this jetted fluid ends up in a spherically shaped droplet before it reaches the substrate, which is typically located at 1 mm distance below the printhead. Once these micrometric droplets reach the surface, they spread and relax to its final spherical cap shape. To provide an insight of the magnitudes and dimensions of these systems, Figure 1b shows a conventional industrial inkjet printhead with an active width of few centimeters that counts with more than 1000 nozzles.

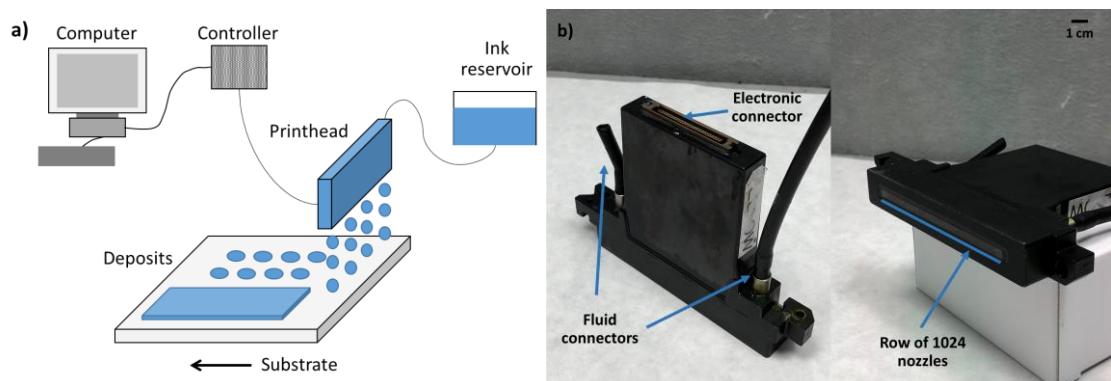


Figure 1. a) Schematic general representation of inkjet printing, b) conventional inkjet industrial printhead.

To understand the increasingly presence of inkjet technology for the preparation of deposits and patterns, these are some of the most significant benefits compared to other deposition technologies:

- **Digital patterns.** With no need of masks or complex multi-steps processes, inkjet allows the deposition of homogeneous films and complex patterns only with the use of adequate digital printing files. Each pixel of the digital file is correlated with a drop; hence, the designed pattern is directly printed on the surface.
- **Flexibility.** The control of each single nozzle of the printhead, together with the digitalization of the patterns to print, enable the preparation of completely different designs using the same process. Each printed pattern may be different from the preceding one and equally controlled. Moreover, one single electronic system is capable to control different printheads simultaneously, permitting the deposition of different materials in the same process, thus, making multimaterial patterning possible.
- **Precision.** The reduced size and the constant volume of the ejected drops and their precise positioning enable the printing of patterns and coatings with resolution in the order of tens of microns.
- **Control.** Multiple variables such as temperature of the ink during the deposition and the pressure changes in the cavity close to each nozzle can be regulated. Thanks to this, the jetting process can be controlled and optimized for multiple fluids and led to spherical droplets, avoiding the appearance of artifacts that may affect the final deposit.
- **Material consumption.** Ink is only deposited where the pattern or area requires and, on the other hand, the volume of the droplets is very low. This makes that very few volume of ink is deposited even when printing big areas and nearly zero waste of material is produced.

Concerning the use of the technology, inkjet is already present in our daily life. The most common well-known application is domestic printers as many of the printers used at home for document printing with ink use this technology. Beyond this, there already exist many examples of the use of inkjet printing in industrial and research applications. In the industry, the biggest sector where inkjet is already well settled down is graphics. Labeling, advertising or photography are some examples and efforts are now being dedicated to improve the quality of the images and provide high-throughput process for wide format sizes (Figure 2a). Another industry sector where inkjet is already well exploited too is packaging. Thanks to the possibility of printing different images and codes from one unit to another, being a non-contact technique and the low quality requirements of these patterns, inkjet technology is highly convenient for this application. Bar codes, Quick Response (QR) matrixes, expiration dates and other traceability indicators are usually printed with inkjet and can be seen in packaging of consumer products like soda cans, tetra bricks or food packaging.

There are other industrial sectors like home appliances (Figure 2b) and architecture where inkjet is already present and gaining relevance too despite its use is not yet as extended as these previous cases due to the high-performance requirements. Increasingly, consumers request for new, cheaper and personalized aesthetics that conventional technologies are not capable to meet. Even more, cost production can be reduced thanks to inkjet. On one side, the process makes an efficient use of materials, which reduces the consumable costs. On the other hand, expensive materials used in architecture and interiors design can be replaced by cheaper materials with highly realistic patterns printed on them, imitating the natural appearances, such as marble, wood or ceramic aesthetics. Additional advantages are given by the reduction of complexity in the production and, hence, logistics. Digitalization of decoration process allows

the manufacture of unitary lot size, which implies a more effective management of the production and stocks. For example, for the production of products that share a common construction but different aesthetics, like some home appliances, they can be decorated on demand instead of producing big batches at once and store them until they are ordered; drastically reducing the inventory in warehouses.

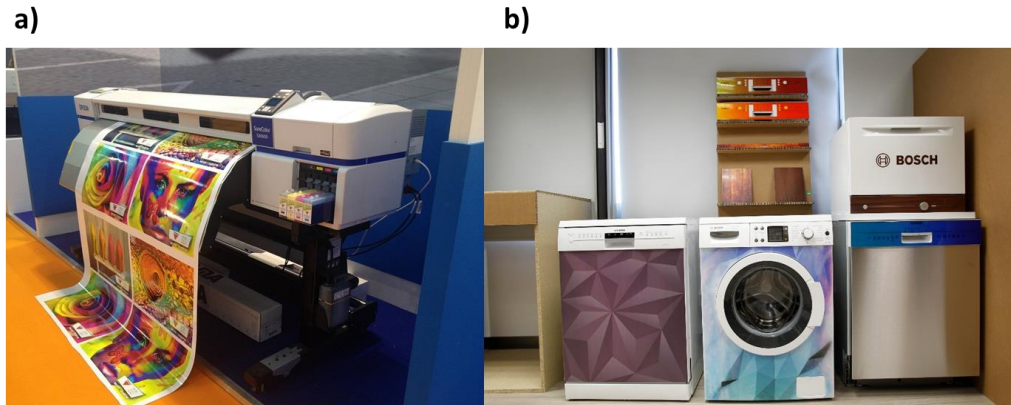


Figure 2. Example of commercial inkjet industrial use cases: a) wide format advertisement (Reproduced under the terms of Creative Commons CC0 license) and b) decoration of home appliances.

All these introduced industrial applications are oriented to decoration and, indeed, this sector actually covers a relevant portion of the overall industrial inkjet business [2, 3]. For this reason, the large majority of commercially available inks are decorative color inks of different natures that can be used for a wide range of substrates and printers.

Despite other functionalities besides decoration can be found in the industry, they find significant limitations to burst into industrial production in the same way as decoration does. On one side, inkjet technology requires high demanding fluid properties to allow the ink to be jetted; therefore, an adequate adaptation of the formulations is needed beforehand. In addition, the deposited inks should show a robust performance of the functionality over time, withstanding specific requirements for each use case. For instance, high conductivity is demanded for conductive inks used in micro-electro-mechanical systems (MEMS) and solar cells applications, good transparency and controlled optical properties are sought in microlenses and high emission efficiency is necessary in luminescent inks used in displays. Nevertheless, the versatility of inkjet to deposit multiple materials with high accuracy and precision over different substrates (even flexible ones), printing fine patterns over large areas and its compatibility with methodologies such as roll to roll, makes the efforts dedicated to the development of these applications worth [4-9]. Here it is briefly described some of the applications where inkjet is bringing additional value compared with existing deposition and production methods and where more presence in the industry can be foreseen:

- Organic Light Emitting Devices (OLEDs). These devices consist of multilayer structures that convert electricity in light. In Figure 3, a conventional layout of these systems is shown. For an adequate performance, they require highly efficient emission, brightness and uniformity in the different colors as well as quick response and clear contrast between on and off states. The fabrication of these devices foresees a miniaturization and flexibility of the technology to give response to trends and needs of consumer electronics, where small platforms and flexible screens are being demanded. Thanks to its accuracy, patterning capability, efficient

material management and the possibility to deposit inks with emissive or conductive material (such as PEDOT), inkjet printing can give response to these needs. Hence, the direct deposition of functional materials for this multilayer structure (Figure 3) is being developed for the preparation of OLEDs like displays in a more flexible and industrially scalable fashion [10-16].

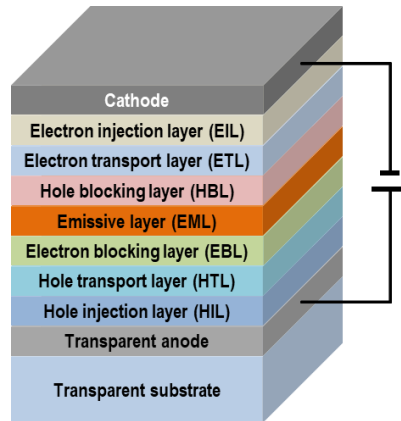


Figure 3. Schematic representation of the multilayer structure of a conventional OLED.

- Printed electronics. Due to the growth of electronics market and its goal to miniaturize and make flexible devices, inkjet has become a promising technology for the future production of electronics. The current technologies used for the production of electronic circuits provides low cost processes with good performance and high definition patterns and, hence, inkjet technology is not competitive enough to replace current processes. Nonetheless, it offers additional features that make it potentially interesting for certain applications. Its digital nature makes it compatible with other production techniques that are usually required too for the incorporation of microelectronic devices in the circuits such as LEDs, transistors, RFID antennas or memories. In order to make inkjet printing a successful fabrication technology in this field, printed circuits should show good performance, for example, stable and controlled conductivity is required. This objective is actually highly sought and, for instance, silver nanowires, carbon nanotubes or graphene have already been used to provide efficient conductive functionality to inkjet printed elements (Figure 4) [17-20].

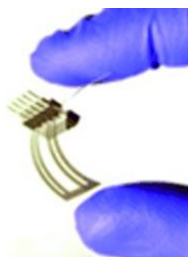


Figure 4. Flexible plastic substrate with printed conductive tracks based on graphene oxide and reduced graphene oxide inkjet inks. Adapted with permission from reference [20]. Copyright (2010) WILEY-VCH Verlag GmbH & Co. KGaA, Weinheim.

- Organic Photovoltaics. Photovoltaic energy is established worldwide as green energy source but still behind hydro and wind energy, among other reasons, because of its low efficiency. In this way, highly efficient crystalline silicon solar cells are normally used in current photovoltaic technologies but the cost of the material and the complicated production

process is still a limitation. In addition, as in the case of OLEDs, solar cells comprise a complex multilayer structure (Figure 5) where the control of the morphology and the interface between the layers is crucial for a proper performance. In this direction, inkjet may provide an accurate deposition of multiple materials in the same device and even print the conductive material to interconnect the layers, leading to a large-scale and low-cost production process compatible with roll to roll methodologies [21-24]. Nonetheless, the achieved efficiencies need to be still improved.

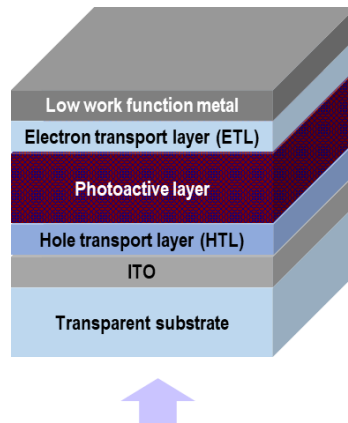


Figure 5. Schematic representation of the multilayer structure of conventional photovoltaic (PV) panels.

- Sensors. Sensors can be identified as devices that respond to an external stimulus, giving back feedback (as an electrical signal or an optical indicator for instance) to warn about it or using it as triggering systems (Figure 6). For example, in the field of optical sensors, chiral photonic structures based on liquid crystals have been explored as materials for sensing devices [25-27]. A change in the molecular order, produced by an external stimulus, may modify the pitch of the chiral periodic structures and, therefore the reflection wavelength, becoming a sensor for this stimulus. Inkjet printing has already been used to generate this type of liquid crystalline cholesteric photonic structures and, with an appropriate design, they respond against external stimuli like pressure, temperature, vapour or humidity [28-30].

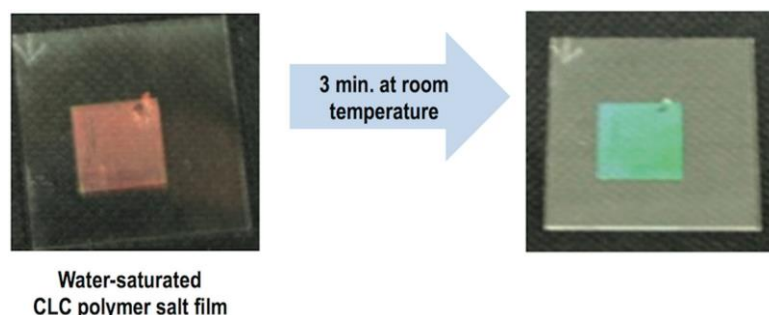


Figure 6. Example of humidity optical sensor made of water saturated cholesteric liquid crystal polymer salt film on polyimide coated glass in water (left red film) and after 3 min at room temperature (right green film). Adapted with permission from reference [31]. Copyright (2012) American Chemical Society.

- Micro-optics. With the purpose of miniaturizing optical devices such as mirrors or lenses, micro-optics has grown as a discipline of optics with highly demanding requirements from both the materials and process points of view. On one side, optical properties of the materials

should provide the desired functionality independently of the size of the systems. On the other hand, its performance becomes a challenge as long as the same requirements should be fulfilled but in smaller size. In addition, accuracy and precision in the deposition of materials is more difficult but inkjet is presented as a successful technology to overcome these issues as it is shown in many studies where this technology is used for the deposition of microlenses [32, 33] (Figure 7). Furthermore, the integration of micro-optical systems with other systems as lasers, sensors or LEDs, lead to a wide range of opportunities for the development of optical microsystem applications.

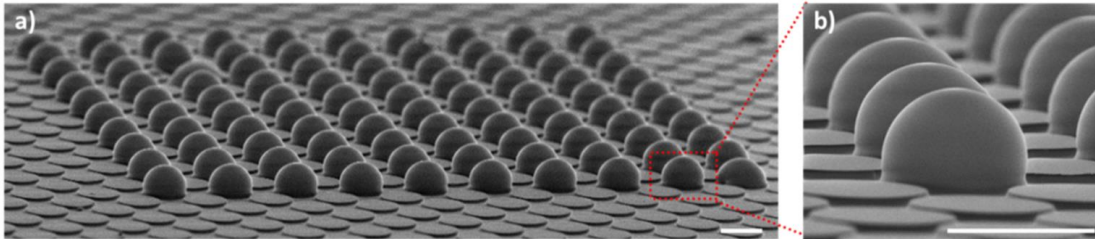


Figure 7. SEM image of inkjet printed microlenses based on hybrid organic-inorganic polymer inks deposited on platforms that help to fix position: a) full printed pattern and b) detail of few microlenses showing spherical profiles (scale bars: 100 μm). Adapted with permission from reference [34]. Copyright (2015) Optical Society of America.

- Integrated optics. Waveguides, able to guide light between different points, are key elements in optical-integrated circuits. For example, waveguides in planar integrated sensors enable the light to travel from the source to the detectors and sensor materials. In all these cases, planar waveguides need to present good optical properties for a suitable transmission of the light, high refractive index materials to ensure guiding and a reliable high-throughput fabrication process. Existing examples can be found in literature where combination of processing technologies, together with inkjet printing, are already used to prepare waveguiding structures [35-39] (Figure 8).

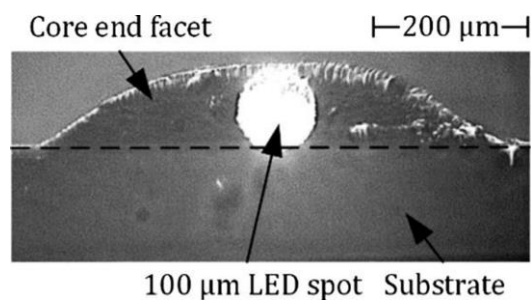


Figure 8. Cross section of an inkjet printed planar waveguide under optical measurement setup focused with LED spot. Adapted with permission from reference [36]. Copyright (2016) Elsevier.

Given the scope of this thesis, a more in-depth review of the use of inkjet in micro-optics and integrated optics fields will be done later in a subsequent section.

2. Inkjet printing technology

Inkjet technology can be classified attending to multiple criteria like the nature of materials that are deposited (e.g. inorganic or polymeric) or the kind of applications that are being implemented (e.g. functional or decorative). Another widely used and representative classification is the one that takes into account the physics of the printheads to generate the ink droplets and direct them to the substrate. Attending to this criterion, the following main technologies to eject the fluid through the nozzles can be defined:

- Continuous inkjet (CIJ): in this kind of printheads, the ink, stored in a reservoir inside the printhead, is pumped through the nozzles generating a stream of fluid. Consecutively, this stream of fluid derives into a continuous column of droplets, a phenomenon driven by the Rayleigh instability. Right after the nozzle, a small electrostatic charge is acquired by each drop while they are formed. Deflector plates at the exit of the nozzles determine afterwards which drops finally fall into the substrate and which ones are collected in a deposit and return back to the printhead to be reused (Figure 9). Thanks to the continuous firing of drops, the frequencies that are reached are considerable high, up to 175 kHz [40] and normally in the 20 – 60 kHz range [41]. These values make this technology especially useful for applications such as coding and marking for packaging, where high speed is needed, dielectric fluids are recommended and high definition is not demanded (conventionally, drop sizes are in the order of 100 μm of diameter [41]).

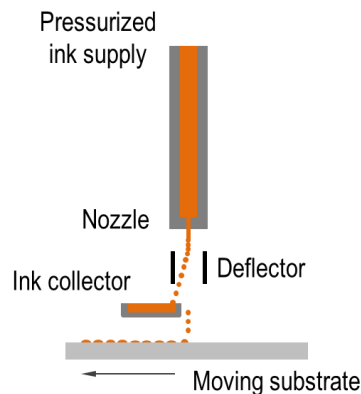


Figure 9. Schematic view of Continuous Inkjet (CIJ) printhead.

- Drop On Demand (DOD): in this method, the ink, which is also stored in a reservoir inside the printhead, is only jetted through the nozzles when necessary. The nozzles generate single drops only when required by the designed pattern, thus it is, material wise, a more efficient way of jetting the ink. The drops are formed by pressure pulses independently sent to each nozzle but the way these pulses are generated can substantially vary, as it is described below. This technology is conventionally used for printing patterns with a decorative or functional purpose as it offers better quality due to smaller drop sizes, similar to the inner diameter of the nozzle (around 20 – 50 μm) and higher precision than CIJ. On the other hand, it needs to operate at lower frequencies (1 – 20 kHz [41]) and, as it could be seen later, the activation signal should be highly controlled as acoustics and resonances in the ink chamber can affect the drop jetting process. The two main methods to generate pressure pulses are the following:

- Thermal. Inside the printhead chamber that contains the ink to be jetted, close to the nozzle, a resistive element can be found. This element is suddenly heated above the boiling temperature of the ink, causing the evaporation of part of the ink and thus, a bubble is generated. Once this small vapour volume collapses, it creates the pressure pulse needed to push the ink away and jet it through the nozzle (Figure 10). Due to this phenomenon, a very precise control of fluid properties is required, limiting the number of inks that can be used. Nonetheless, the small size of the nozzles, the compact format of the printheads and the reduced cost of this technology, have made this kind of printheads highly suitable for domestic printers [41].

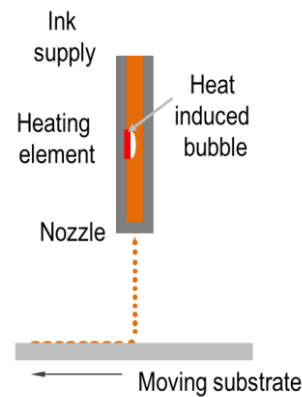


Figure 10. Schematic view of Thermal Drop On Demand Inkjet printhead.

- Piezoelectric. The walls close to the nozzle are in contact with a piezoelectric actuator that suddenly deforms the cavity when an electric pulse is applied to the piezoelectric element. The pressure caused by this quick deformation results into the jetting of the ink through the nozzle (Figure 11). The size of the ejected drops is normally in the order of tens of micrometers (the order of magnitude of the diameter of the nozzle) and the velocity of the drops reaches up to few meters per second. Despite the higher cost of production (in comparison with thermal DOD printheads), its robustness and the capability of being used with a wider range of fluids, make this technology more frequently used than thermal DOD.

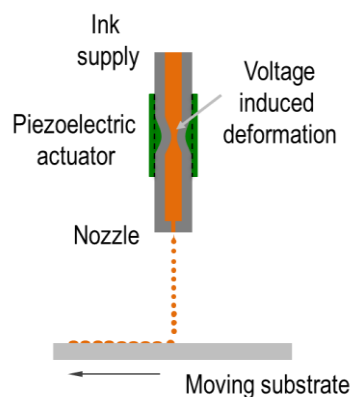


Figure 11. Schematic view of Piezoelectric Drop on Demand Inkjet Printhead.

As it can be seen, each technology is suitable for a certain kind of fluids and applications according to their properties. Because of this, the requirements of the application together with the material properties will define the most suitable type of printhead for each specific case. As

introduced before, CIJ is suitable for coding and use cases where speed and cost are prioritized against quality and precision while thermal DOD is widely used in desktop printers, as they are miniaturized enough and cost effective. Finally, due to the capability of control the pulse generation and its versatility to be used with a high variety of inks, piezoelectric DOD is the preferred one in many of the industrial and research printers.

3. Drop formation

There exists multiple piezoelectric DOD printhead sizes, from a single nozzle printhead up to more than a thousand as seen in Figure 1b. For industrial scenarios, printheads with large number of nozzles are convenient but the working principle behind the technology of the printhead is the same independently of the number of nozzles. In order to facilitate the understanding of the working principle, a single nozzle printhead (as represented in Figure 12a) is used to introduce the physics of the formation of a drop. This system can be schematically described as a feeding tube connected to a cavity with cylindrical geometry filled of ink and a tubular excitable piezoelectric element with its corresponding electrodes surrounding the wall of this cavity. As an example of activation signal reaching the mentioned piezoelectric element, a simple trapezoidal voltage excitation, as represented in Figure 12b is chosen. This trapezoidal signal consists of three differentiated phases: increasing, maintenance and decreasing of the voltage signal; each one with their corresponding duration (t_{rise} , t_{dwell} and t_{fall} respectively).

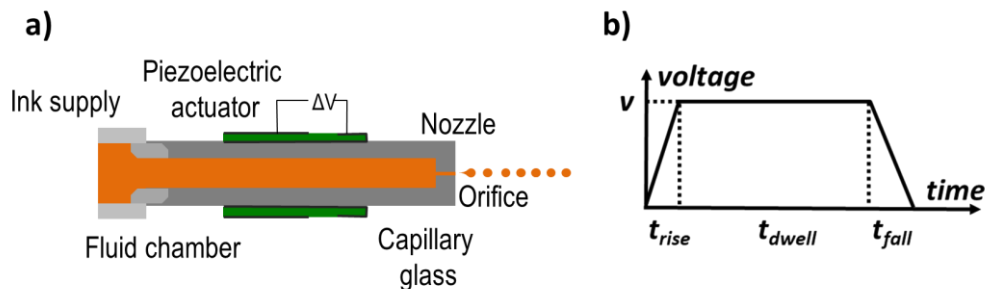


Figure 12. a) Schematic representation of piezoelectric printhead and b) example of a trapezoidal signal sent to the piezoelectric walls of the printhead.

Once this trapezoidal signal is sent to the piezoelectric actuator, it is deformed accordingly to generate the pressure pulses needed for the drop formation. In Figure 13, a schematic representation of the pressure pulse propagation is represented to conduct the explanation of the involved events. The rise stage of the signal generates a quick expansion of the cavity, producing a pressure decrease in the fluid. In ideal conditions, this pressure change can be ideally divided in two waves, each one with half amplitude of the original signal and propagating in opposite directions to both ends of the cavity. As detailed before, one of the two ends of the cavity is connected to an ink supply tube of larger diameter so it can be modelled as an open-end. Because of this, the negative signal arriving to this boundary is reflected with a π phase shift changing to a positive pressure pulse with same amplitude but travelling in opposite direction to the end of the nozzle. This other end of the cavity, with a very small nozzle aperture in comparison with the cavity diameter, can be modelled as a close-end. Therefore, the initial negative signal arriving to this side will be reflected with no change in the phase, being negative and with the same amplitude [42, 43]. During t_{dwell} there is no additional disturbance in the

system and the above-mentioned propagation of the signal takes place. When voltage starts the decreasing phase, the signal introduces in the cavity the opposite reaction of the initial rising one. This voltage drop causes a fast decrease of the diameter of the cylinder, generating a positive pressure disruption. In an analogous way than before, half positive pressure will move upwards and, if properly synchronized, it could compensate the existing half negative pressure that was going in that direction, while the other half positive pressure going downwards to the exit of the nozzle could add the previous half positive pressure moving in that direction too. Hence, every time that this positive pressure arrives to the open cavity of the nozzle, if kinetic energy is enough to overcome the surface tension that holds the fluid inside the cavity, the ink will be jetted and, eventually, a drop could be formed.

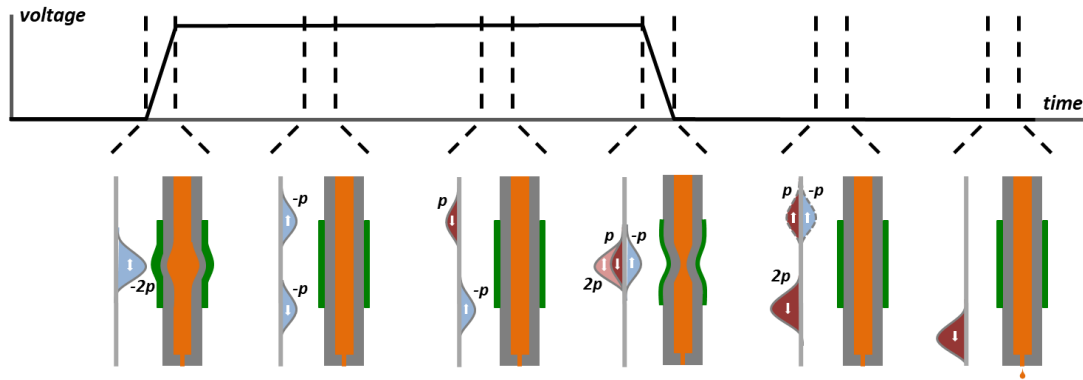


Figure 13. Generation, propagation and reflection of the cavity pressure perturbation by a trapezoidal voltage excitation.

As it can be seen, pulse characteristics have a strong impact on the jettability of the fluid and, hence, on the proper formation of drops [42, 44, 45]. For example, in order to reach the necessary pulse frequencies, t_{rise} and t_{fall} should just last a few microseconds. On the other hand, t_{dwell} influences this process too. As described before, during this phase, the generated pulses at t_{rise} are propagating along the cavity so its optimal value will depend on the length of the cavity in order to coordinate the cancellation and overlapping of the negative and positive pressures. In particular, the starting of the fluid compression at t_{fall} phase should take place at the same time that the reflected waves (originated by the initial fluid expansion) pass by the mid-point of the cavity, where the piezoelectric element is located. Thus, only a double positive amplitude pressure travels towards the nozzle to reach the exit.

In real conditions, there are additional factors that may affect the generation and propagation of the pulses and the fluid behavior such as damping of viscosity, non-ideal reflection or energy losses for example. In addition, this signal is not usually a single pulse but a series of consecutive pulses where residual pressure waves can generate disturbances in the subsequent ones. Therefore, the periodicity of these pulses can affect the performance too and the frequency of the signal is a relevant factor in the jetting process that should be controlled [42, 43, 46-48]. Due to this confluence of phenomena in the generation and propagation of the pulses, the voltage signal should be carefully designed according to the printhead characteristics and the fluids to be jetted and becomes a crucial contribution from the know-how of the printhead manufacturers.

As important as the acoustics of the printhead and the control of the piezoelectric system, fluid properties directly influence the good performance of the printing process too. Fluid

characteristics like surface energy, viscosity and density will define the drop generation process. These parameters merge into various non-dimensional numbers that allow to create a theoretical framework to understand the drop formation process. The principal ones are the Reynolds number (Re), which correlates inertial forces with viscosity and the Weber number (We), which do likewise with kinetic energy and surface energy when the fluid is being jetted. Equation 1 and Equation 2 provide the definition of Re and We respectively.

$$Re = \frac{v\rho a}{\eta} \quad (1)$$

$$We = \frac{v^2\rho a}{\gamma} \quad (2)$$

Where v is the velocity of the jetted drop, η is the viscosity, γ is the surface tension, ρ is the density of the fluid and a is the diameter of the nozzle.

For a proper drop formation, once the jet is formed, it thins before breaking up and form a drop. This thinning phase will directly depend on the surface tension and will be influenced by the viscosity of the fluid and the inertial forces. For Newtonian fluids with high viscosity, for instance, surface tension forces squeezing the fluid need to overcome viscosity to thin the jet. On the other hand, for fluids with low viscosity, inertial forces of the accelerating fluid will be the ones opposing the jet thinning [49, 50].

Apart from We and Re , Wolfgang von Ohnesorge defined an additional non-dimensional number (Equation 3) to set the fluid regimes that could be identified once the fluid is jetted. This equation does not involve the velocity of the drop and so only depends on intrinsic physical properties of the ink and the inner diameter of the nozzle [49, 51].

$$Oh = \frac{\sqrt{We}}{Re} = \frac{\eta}{\sqrt{\gamma\rho a}} \quad (3)$$

According to existing literature, Oh numbers in the range of 0.1 and 1 typically lead to stable drop formation [52] and even a narrower range between 0.07 and 0.25 is given by other groups [53]. In these cases, in the drop formation process, the jetted fluid is supposed to thin and break, generating a ligament that retracts and return back inside the cavity while the expelled fluid achieves a spherical drop shape before reaching the substrate (Figure 14a). Beyond these limits, high values of Oh , which means that viscous forces govern the thinning of the jet, can impede the ink to leave through the nozzle. On the other hand, too low Oh numbers indicate that the inertial forces are the ones that regulate the jetting. In this case, with very low viscosity, it can even result in a stream of fluid leaving the nozzle, leading to a drop surrounded of multiple smaller drops called satellites (Figure 14b) [49]. If these satellites are still present when the drop reaches the substrate, it can cause non-homogeneous circular drops after deposition, affecting the quality and accuracy of the printed deposits.

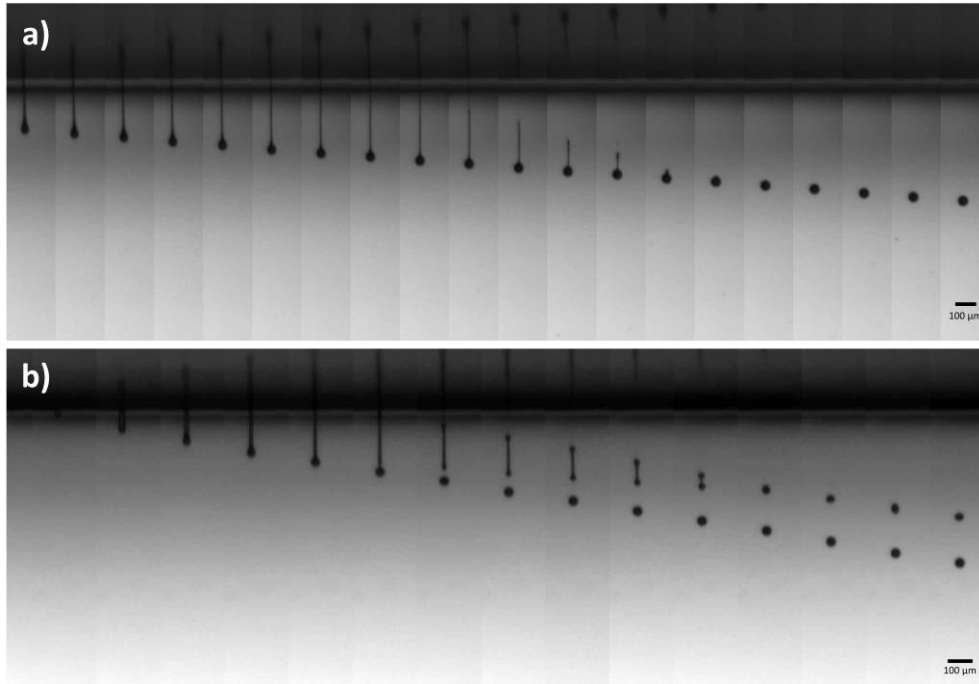


Figure 14. Sequence of photographs taken by a home-built dropwatcher, showing the sequence of the formation of drops of inks developed along this thesis a) in optimal situation, achieving spherical drop shape and b) with the formation of satellites (Advanced Manufacturing Laboratory – ICMA).

Despite speed is not considered in Oh number, kinetic energy, as previously indicated, should be considered for a proper jetting process. Researches carried out in this respect have defined limits for We and Re numbers to predict its effect on jettability. For instance, We numbers above 4 are supposed to have enough kinetic energy to exceed the surface tension and allow the jettability of the fluid [41, 54]. On the other side, Equation 4 defines a regime in which the energy that pushes the fluid is low enough to avoid the fluid splash and spread all over the surface when the drop reaches it [41, 55, 56].

$$(We)^{1/2}(Re)^{1/4} < 50 \quad (4)$$

Combining these thresholds into a common graphic, the printability of a fluid can be determined by the combination of certain values of Re , We and Oh , as represented in Figure 15.

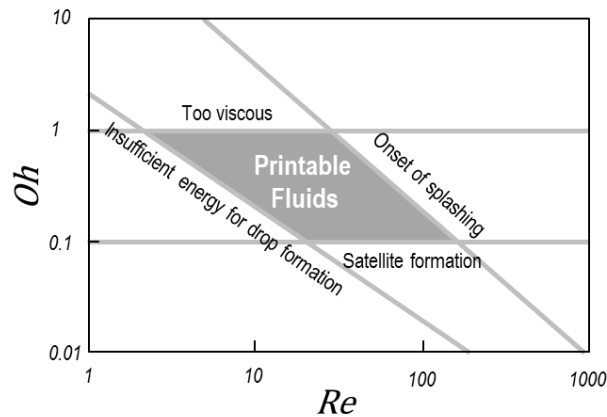


Figure 15. Printability limits of inkjet fluids.

The previous description is standardly defined for Newtonian fluids but, normally, the addition of high molecular weight polymers in the formulations to control the rheological properties of the ink and other additives to functionalize them can cause that these fluids do not always behave as purely Newtonian. Nonetheless, small concentration of polymers can positively contribute to reduce the risk of creating satellites by helping in the retraction of the tail after jet breaking thanks to the induced viscoelasticity [41]. This kind of phenomenon can lead to situations where, despite the Oh number is out from a defined range, the fluid leads to well-defined droplets.

As it can be foreseen, complex formulations are needed to fulfil the demanding requirements that certain application requires for a proper performance. This makes the modelling of the physics of the jetting of the ink highly difficult and, hence, additional models have been proposed trying to give response to the need of predict when a fluid is printable or not [49, 57]. Anyhow, experimental printability and direct observation of fluid jetting is the ultimate test to validate and ensure the proper jettability of a determined fluid with independency from theoretical models.

To facilitate proper drop formation, printheads typically count with thermoresistive control systems that enables the heating of the fluid. This feature is highly beneficial as it contributes to a better adaptation of the viscosity of the fluid, which is, indeed, particularly important due to the narrow range of fluid properties allowed by the printhead.

Within the printability limits, the fluid itself together with the generated pulses in the printhead will determine, therefore, the volume of jetted ink drop. For example, low Oh numbers or large pulse voltages will typically derive into bigger drop sizes [43, 58]. Apart from that, the inner diameter of the nozzle will affect drop dimensions too. In addition, a widely used alternative to control the dropsizes is the firing of several drops of the same size that merge together while flying before reaching the substrate, the so-called grey scale printing.

4. Drop deposition

Once the droplet has been formed in the air, it continues its descendant trajectory until it finally reaches the substrate. This step affects to the result of the deposition process too and the subsequent performance of the ink since it influences on the final geometry of the drop. It is mainly driven by the following forces: inertial, capillary and gravitational. Nonetheless, gravitational forces can be ignored for the conventional volume of inkjet droplets because its magnitude in comparison with the rest of the forces is negligible [40, 41].

In the deposition process, three principal phases can be normally identified (Figure 16) [40, 41]. The first one corresponds to the impact of the drop into the surface, where it begins to be deformed by the inertial forces generated by the impact with the substrate. In a second phase, the kinetic energy lead to surface energy and causes the droplet to spread in a radial direction, giving a ring-like film with a larger diameter (d_m) than the droplet in the air (d_o). Finally, in the last phase, there is a retraction of the extended drop due to the surface tension and, after several oscillations where the energy is dissipated by viscous forces, the drop acquires its definitive geometry with an equilibrium diameter d_{eq} and a contact angle θ_{eq} , being dictated by the interaction of the ink and substrate [59, 60].

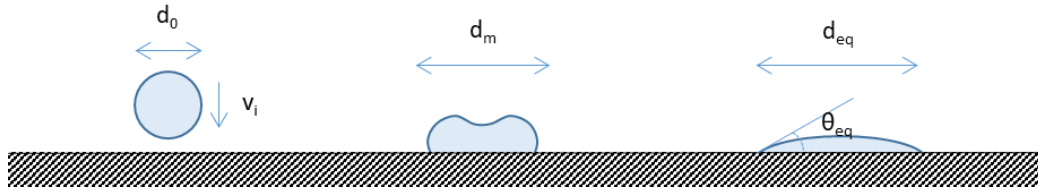


Figure 16. Three main phases of the drop when reaching the substrate.

In consequence, the volume of the ejected droplet directly affects to the size of the drop after being deposited as well as to the final resolution of the film or pattern. As explained before, gravitational effects can be ignored and so the shape of the drop once relaxed on the surface can be modelled by a spherical cap defined by the interaction between the fluid and the surface according to Equation 5 [60]:

$$d_{eq} = d_0 \left(\frac{8}{\tan\frac{\theta_{eq}}{2} \left(3 + \left(\tan\frac{\theta_{eq}}{2} \right)^2 \right)} \right)^{1/3} \quad (5)$$

If a sequence of single drops is consecutively deposited along one defined direction, it can lead to continuous lines where their definition will be dictated by the interaction of the fluid and the substrate. Moreover, printing process characteristics as pulse frequency and substrate speed with respect of the printhead permits the control of the spacing of the jetted drops and, hence, the quality of these lines. If the separation between subsequent droplets is large enough, they will not overlap and so a row of single isolated droplets can be deposited (Figure 17a). If the distance between droplets is diminished, they may coalesce and form a continuous line of fluid. Nonetheless, it exists an optimal spacing that will derive into an ideal straight line (Figure 17c). Out from this optimal range, two additional phenomena can be appreciated in the formed lines. When drops are still printed separately but they start merging when spreading due to wettability of the fluid and the surface, a continuous line with rounded contour can be appreciated (Figure 17b). On the other hand, if drops are deposited too close, the continuous line can present bulging along the width caused by the accumulation of ink in those areas (Figure 17d).

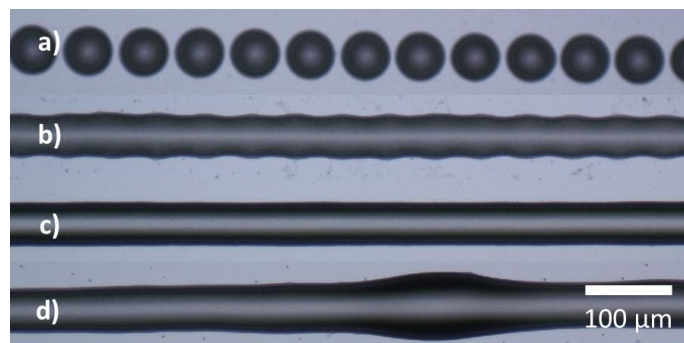


Figure 17. Sequence of droplets deposited in a row with decreasing distance between adjacent drops: a) spaced independent drops, b) line with rounded contour, c) straight line and d) line bulging (Advanced Manufacturing Laboratory – ICMA).

In the same manner, consecutive parallel lines could merge and derive in areas. In this case, wetting agents are normally used in the formulation of the inks to control the spreading after the deposition and avoid dewetting areas that lead to heterogeneous deposits.

5. Drop fixation

Once the ink is deposited, the fluid needs to be solidified to deploy the functionality into the surface as, for example, provide color for decorative applications or establish conductivity of the deposit for electronic devices. This solidification of the fluid depends on its composition and requires a large degree of control as in the previous stages of the ink droplet formation and deposition.

With regards of the nature of functional inkjet inks, fluids composed by a solvent and a solid load can be usually found (being this solid load, for instance, pigments, dyes or nanoparticles that provides the functionality to the ink). Besides this kind of inks, photopolymerizable inks are also commonly used. Even if solvent is used as a carrier too, these inks comprise different kind of monomers and oligomers that finally lead to a solid structure given by the polymeric chains or networks generated when irradiated with actinic light.

Concerning solvent inks, the principal component is typically the solvent itself, which should be evaporated by a drying step after deposition, while the solid phase elements present in the formulation remain afterwards on the surface, providing the desired functionality. In addition to the solvent and the solid load, other additives can be added too, such as viscosity or surface tension modifiers, in order to control the ink properties and make it jettable.

If a drop of pure solvent ink is deposited over a smooth surface, the contact angle will be continuously reduced due to its evaporation until the receding contact angle is reached and, hence, the diameter of the drop will also be reduced. On the contrary, if the surface is rough, the contact line will be pinned and, therefore, as long as solvent evaporation evolves, the contact angle is reduced too but the droplet is not retracted. If this solvent ink contains solid phase materials (as described before for certain inks), the evaporation of the solvent will lead to a ring of the material with the initial diameter of the drop. This pinned solid phase can avoid the recession of the liquid, anchoring the droplet to its initial size and controlling the dimensions of the final deposit. Nonetheless, as long as evaporation continues and reach the edges, the loss of solvent in the edge can be compensated by flow of liquid from the inner side of the drop, carrying additional solid phase material to the outer and being deposited. This is known as “*coffee ring effect*” and is one important effect caused by the solvent content of these kind of inks (Figure 18) [61-63]. To prevent this and achieve homogeneous deposits, mechanisms to control the flow of solids during the evaporation can be used. For example, controlled atmospheres while evaporating could reduce the solvent elimination rate in the pinning line, minimizing or precluding the formation of the ring. Besides, the use of more than one solvent with different boiling point and surface tension may cause Marangoni effect (flow driven by surface tension gradients) and, hence, compensate the *coffee ring effect* too. Therefore, despite the presence of solvent may contribute to make the jettable of the inks easier, it also leads to additional difficulties to control the process and the final deposit.

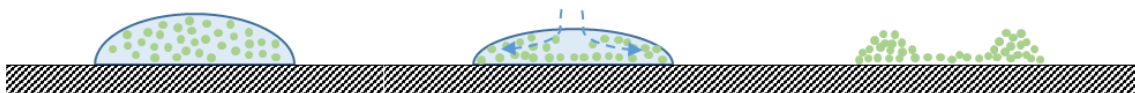


Figure 18. Schematic representation of *coffee ring effect*.

Additional difficulties that can cause damage in the printheads may arise when using solvent inks. As seen in previous sections, if printhead is not activated, the ink to be deposited remains stored in the reservoir of the printhead and lie down on the base of the nozzles, being its surface

tension what prevents it to be jetted. If the printhead is not in use for a certain period of time and the solvent is evaporated, it can cause the nozzles to clog because of the solid particles remaining in the apertures.

In contrast, photopolymerizable inks may prevent these problems. As described before, photopolymerizable inks experience a solidification when curing but, if no solvent is present in the formulation, there is no relevant loss of material after the deposition process and therefore, drop shape is retained with better fidelity on fixation. Nonetheless, this process also leads to inefficiencies as polymerization rates are usually below 100%. As long as the polymer is generated and the reaction progresses, viscosity increases and this makes more difficult for the monomers to move. Depending on the nature of the monomers, they will evolve to a different molecular structure, like linear chain when they are monoreactive or 3D network if they are multireactive. As a result, some molecules can find limited mobility around them and take more time to find accessible monomers to polymerize with or finally remain unreacted.

Attending to the chemistry of photopolymerizable inks, addition polymerization reaction (so-called chain growth polymerization reaction) is the most commonly employed for inkjet inks. This reaction usually involves monomers and a photoinitiator that is activated by light, triggering the addition of monomers to a polymeric chain. Depending on how this process is initiated, it is possible to identify different polymerization types, from which radical and cationic are normally used for inkjet inks.

In radical photopolymerization (Figure 19) the decomposition of the photoinitiator (I) upon light activation lead to the generation of radical species (A*) which can react with double carbon bonds. This reaction of a radical with an accessible monomer opens this bond and results into larger radical species that keeps reacting with new monomers in close proximity. This addition reaction continues until polymerization finishes, for example by a combination of polymer chains [1, 64].

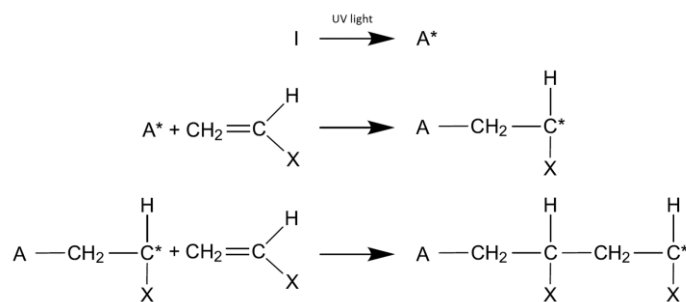


Figure 19. Initiation and chain growth of free radical polymerization.

As double carbon bonds are required in the reaction, acrylates are very commonly used monomers in this kind of ink formulations. In addition, due to the possibility to include monomers with several reactive groups, crosslinked networks are normally formed, providing structures with good mechanical and chemical resistance [1].

On the contrary, there exist some limitations too that should be controlled during the free radical photopolymerization reaction for a proper solidification of the ink like, for example, inhibition by oxygen, shrinkage caused by polymerization or, as introduced before, insufficient conversion rates.

In contrast with free radical photopolymerization, in cationic photopolymerization, cationic species are generated when the photoinitiator is excited. These cationic species react with the monomers of the formulation and causes the beginning of the polymerization chain reaction.

This atomic reaction avoids some of the above-mentioned problems that can be found in radical photopolymerization. For instance, cationic photopolymerization is not hindered by reasonable oxygen atmosphere conditions, shrinkage is not that relevant, polymerization continues once the process is activated even if there is no light and, in addition, it is compatible with a wider range of monomers [1, 65]. Nonetheless, because of the high viscosity ranges of cationic photopolymerizable inks, they have a limited compatibility with inkjet technology, reducing the number of existing cationic photopolymerizable inkjet inks [40].

As an example of cationic photopolymerization, epoxy ring polymerization can be commonly found in inkjet inks. An epoxy group is a cyclic ether consisting of a triangular ring with an oxygen atom and two adjacent carbons. When the cation reaches the ring, this is opened and the polymerization reaction starts, creating polyether molecules (Figure 20) [66].

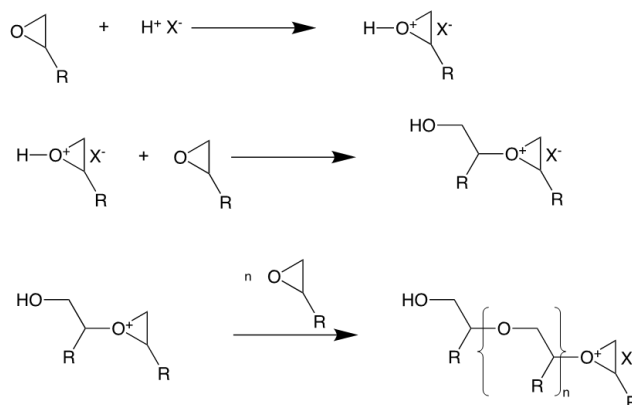


Figure 20. Cationic photopolymerization of epoxy ring.

With regards of the photoinitiator, onium salts (On^+X^-) such as triarylsulfonium are some of the most widely used in cationic photopolymerization, among other reasons, because they present good thermal stability and absorption at UV wavelengths [67-72].

The described chain photopolymerization reactions are typically used in purely organic monomers but it can be also found in the polymerization of the organic part of hybrid organic-inorganic materials. In these cases, to confer the inorganic nature, alkoxides groups are typically used as precursors. One example of these kind of materials frequently used is 3-glycidoxypropyltrimethoxysilane (GPTMS) that bears an epoxy group as the organic part and a trialkoxysilane as the inorganic one [73-78].

As stated above, the organic part of this molecule polymerizes through a chain polymerization reaction while the inorganic part requires a hydrolysis and condensation process to polymerize. To start this last reaction, the system requires the presence of water and besides, typically an acid that act as a catalyst. Once hydroxyl groups are generated after the hydrolysis step, the polycondensation phase starts leading to the Si-O-Si bonds and, hence, providing the inorganic structure to the network. In this step, together with siloxane molecules, water and alcohol are also released as byproducts (Figure 21).

Hydrolysis:



Alcohol condensation:



Water condensation:



Figure 21. Representation of hydrolysis and condensation reaction.

Once both organic and inorganic structures are formed, the resulting 3D network structure confers to the material a series of properties that make hybrid materials suitable for highly demanding applications. On one side, the organic part provides flexibility to the structure, facilitating the bonding between different kinds of molecules and, hence, permitting the introduction of additional functional molecules into the formulation that may lead to a better performance of the deposits. On the other hand, the inorganic nature confers a strong structure, presenting excellent chemical and mechanical stability as well as good adhesion to inorganic surfaces [79-83].

Despite these interesting properties, the use of hybrid materials for inkjet inks is still limited. The coexistence of two polymerization reactions and their different curing mechanisms, make the fluid properties of the ink, and the subsequent fixation process, difficult to be controlled. Typically, inks are prepared by carrying out the pre-hydrolysis and condensation of the organosilane. A solvent is normally added to adjust the rheology to the jetting requirements. Disadvantageously, once printing is performed, evaporation of solvent prior to curing needs to be carried out further complicating the process. Apart from this, pre-hydrolysis and condensation steps may imply additional stability problems as reactions do not go to completion and may continue during the life of the ink, therefore increasing its viscosity. This can eventually lead to clogging of the nozzles and reduction of the self-life of the inks. Besides, the need of additional pre-hydrolysis and condensation steps makes the overall process more complicated [84, 85].

In order to simplify and improve the efficiency in the curing process of these hybrid systems, Croutxè et al. have proposed the use of a photoacid generator (PAG) together with GPTMS to concomitantly activate both organic and inorganic networks, leading to a direct photopolymerization of hybrid materials [73-77]. In this way, when activated by UV light, the generated photoacid reacts with the epoxy ring and organic polymerization reaction starts, giving place to the organic chains as previously represented in Figure 20. At the same time, the acid molecules released by the decomposed PAG catalyze, in the presence of water, the hydrolysis and subsequent condensation process to create the inorganic network (Figure 22). Despite the potential of this approach to control in space and time the polymerization step, its use in inkjet inks formulations has not been explored yet.

influenced by the interaction of the surface and the liquid droplets, mainly given by the contact angle. Inkjet permits high accuracy in the control of the volume of each drop and therefore, this will have also a direct impact on its shape as well as the solidification process of the ink.

Some works firstly reported inkjet printed microlenses made of molten polymer being cooled down after deposition and getting diameters between 70 and 150 μm with focal lengths between 50 and 150 μm [33]. More recently, cap shaped microlenses made of prepolymers cured with UV light were also achieved [87-88]. Solvent inks have been commonly used too but, as explained in previous section, the curing process, implying solvent evaporation, brings more complexity to achieve spherical caps due to the need of evaporation rate control and to the volume changes taking place while the solidification phase [89, 90].

The control of the topography of the surfaces that will interact with these deposited droplets has been explored too. For this purpose, different approaches of pre-patterning with micro-platforms are used, combining wetting and non-wetting areas that will help to fix the fluid in the desired spots, confining the drop and controlling its geometry by the deposited volume (Figure 24). Photolithography, as shown before, has been commonly used for the creation of these patterned pillars [91] on top of which inkjet technology is employed to generate the microlenses [91, 92]. By precisely defining the geometry of these columns (their surface area and rim angle φ) and controlling the drop volume, it is possible to adjust the angle between the drop edge and the surface (θ_{eq}), allowing a wide range of geometries. For instance, using this methodology, differences up to 85° for platforms with 100 μm of diameter have been achieved [93, 94]. Despite inkjet has been introduced as an advantageously technology to make such microlenses with large angles at the contact point, the platforms needed to hold the droplets are still prepared by using sophisticated photolithographic steps, making the overall fabrication process less suitable for industrial production [95].

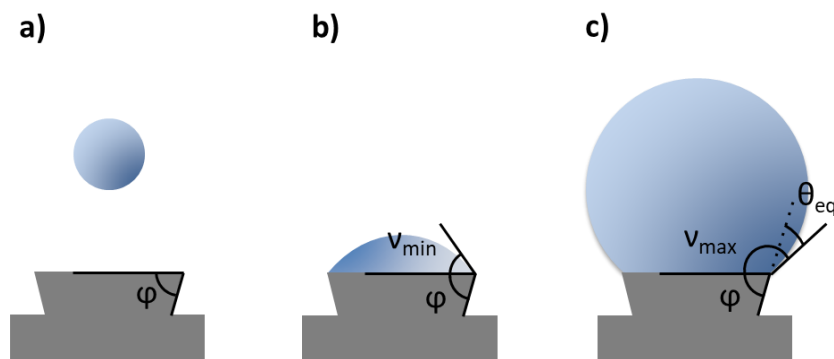


Figure 24. Schematic representation of droplet shape control by the use of pillars being a) the droplet before reaching the substrate, b) the minimum contact angle (ν_{min}) for a drop covering the area of the pillar and c) the maximum edge value (ν_{max}) that depends on the contact angle (θ_{eq}) and the angle of the platform rim (φ).

From the materials point of view, optically clear systems are sought. For this purpose, materials such as acrylates or epoxy resins (already described above) are good candidates for these micro-optic applications as they present high transparency, together with good mechanical properties as well as temperature and chemical resistance.

Besides, as remarked before, hybrid materials can provide a wide variety of advantages for the preparation of functional inkjet inks and, therefore, this family of materials have been studied before in literature for micro-optics too. For example, UV curable sol-gel hybrid-based inks have led to directly printed microlenses with good optical properties. With this approach, Aegerter et

al. achieved transparent spherical microlenses with diameters from 50 to 300 μm and focal lengths of 70 to 3000 μm [96]. With the same goal, the same authors, used epoxy-based hybrid inks to get diameters of 50 to 1000 μm and focal lengths from 100 to 2200 μm [84, 85].

Other groups like Brugger and coworkers have explored different strategies to develop microlenses arrays with inkjet. For that, their work is based on hybrid photocurable resist inks and a proper surface preparation to control its wettability. Thanks to this, they achieved initial microlenses with focal distances of 45-50 μm and radius of curvature up to 29 μm with 1.553 of refractive index at 635 nm. Going a step further, modifying the number of drops per microlens, hence, modifying their volume, the focal length was controlled from 64.1 to 175.1 μm . Furthermore, by combining microstructuration of the surface with a fluorinated treatment, parabolic-shaped microlenses were produced too [34, 97-99].

Anyway, in these cases where hybrid-based inks are used for the deposition of microlenses, different strategies are currently being used to release the polymerization and adapt the fluid properties for a proper jetability. For instance, a pre-hydrolysis and condensation steps are normally required, increasing the complexity of the process and penalizing the stability of the ink. Besides this, solvents are used too to adapt the viscosity of the ink, requiring an evaporation process after the deposition. In addition, short focal lengths and large curvature lenses typically need the preparation of the surfaces with sophisticated protocols to control the wettability. These additional steps in the preparation of the microlenses causes more limitations in their applicability and scalability.

Regarding the applications of these microlenses deposited by inkjet, we can find different fields of interest as already pointed before. Within photonics, for instance, they have been deployed to improve the coupling angle of light on fibers or waveguides and to improve the efficiency of light collimation in diode lasers. An additional example is the use of microdots on top of photodetectors to improve the amount of light collected [100-103]. On the other hand, microlenses can be also used for display backlighting applications by depositing light decoupling microlenses patterns over a light guiding plate [104, 105].

As described in previous sections, due to deposition control of inkjet, not only independent drops can be deposited but also thin lines and well-defined areas. Besides microlenses, other optical elements such as planar waveguides, key elements in integrated optical circuits, can be efficiently printed by using inkjet technology. This possibility brings relevant advantages with regards of cost, flexibility and easiness for patterning waveguides in comparison with other technologies such as lithography, direct writing or extrusion printing [32, 37, 106]. On the other hand, this application requires deposits with high transparency and homogeneity, having high refractive index and low optical losses. These properties are difficult to meet and constitute a challenge for inkjet due to the fluid restriction and the difficulty to control the application of deposits with high definition.

The first research carried out focused on the preparation of waveguides printed with inkjet is dated more than twenty years ago by Hayes et al., introducing a combination of printing processes of solders and polymers for electronic devices [32]. The inks they formulated were epoxy-based fluids, with which they deposited waveguides with a refractive index of 1.74 [107]. With a similar orientation, Chappel and coworkers provided a study of the stability of printed waveguides. In particular, they worked with a commercially available UV curable acrylate monomer with some concentration of solvent to control the viscosity of the fluid for a proper jetting. Nevertheless, this study was focused on the influence of temperature of the substrate

on the geometry of the printed material, leaving the characterization of the optical properties of the printed waveguides aside [108].

As an additional example, Vacirca and Kurzweg introduced SU-8 into the inkjet ink formulation: a photoresist polymer solution that was previously reported being used with other technologies such as photolithography and providing good optical properties for waveguides [109, 110]. In this case they combined UV and thermal curing processes, achieving good and uniform waveguides but with losses of 16.1 dB in 7.5 cm [111]. To put in perspective the difficulty of getting waveguides with low losses with inkjet and the room for improvement in this field is worthy to contrast these results with those achieved by alternative technologies. For instance, waveguides generated by a direct UV patterning of dip-coated films of hybrid organic-inorganic ORMOCER® materials led to higher quality channels, having rms surface roughness down to 2-5 nm and just 0.07 dB/cm of propagation losses, measured at 850 nm [112].

Despite the gap between the performance of digitally printed waveguides and those prepared by conventional technologies such as photolithography, inkjet printed ones have shown improvements in terms of transparency and promising low losses. Advantageously, when compared with other preparation techniques, inkjet printing provides flexibility and simplicity in terms of pattern preparation and deposition on different types of substrates [38, 39, 112].

In summary, inkjet printing offers a wide range of possibilities to generate micro and integrated optical elements showing good performance through a simple and flexible preparation process. Along this section the intense activity and interest around this field has been surveyed but additional research is needed to fit with the strict fluid properties required by the technology, provide high-throughput processes and assure a robust implementation of the functionalities afterwards. Different materials have already demonstrated to be highly efficient for these purposes. Among others, especially hybrid organic-inorganic materials provide excellent properties and, hence, they are presented as a promising solution but their use with inkjet technology still presents limitations in comparison with conventionally settled techniques. Formulation of jettable inks with suitable optical properties together with the implementation of industrial viable surface preparation and curing processes becomes the backbone to foster the use of inkjet printing in the manufacturing of optical elements in real-life applications.

7. Summary and outlook

Considering the current state of the art described along previous sections, we are in the position to assure that inkjet is a mature technology. Existing industrial massive production systems show a promising future for the upcoming applications that are being developed in different research and technology fields. Nonetheless, the demanding requirements of the materials in terms of printability and the required final performance seems to be the main limitation to find this technology present in more applications.

The technology itself shows high capability of adaptation. We can find from cheap and miniaturized printheads for conventional applications like desktop printers up to high-performance technology for printing conductive circuits on flexible substrates. Specially, the use of piezoelectric printheads has been highly extended because of their robustness and capability to accept a wide range of fluids. Even more, their working principles as well as the jetting process are widely studied and modelled, permitting a deep understanding of the physics behind.

Multiple studies can be found to model the behavior of the fluid to be jetted. Non-dimensional numbers like Re , We or Oh permit us to understand the interaction between the different forces taking part during the jetting and drop formation processes and predict the printability of the fluid. In any case, due to the existence of very different ink natures, as important as this modelling is the experimental observation of the jetted drop.

Once the drop is jetted, it is of paramount importance its interaction with the substrate to achieve the desired deposits. An adequate balance between inertial forces, surface tension, and viscosity, together with printing parameters like frequency or the speed of the substrate with respect of the printhead will enable the well-defined deposition of isolated droplets or continuous lines or areas.

The nature of the materials used in the ink formulation will determine the fixation process of the fluid onto the surface. Due to fluid properties restrictions, solvent inks are widely used but these inks present drawbacks that make their use and control challenging: for instance, they require a drying process after deposition and therefore, the volume of the deposit changes; in addition, the *coffee ring effect* can lead to imperfections in the final deposit.

As an alternative to solvent inks, photopolymerizable inks are also commonly used utilizing UV light as activation source to trigger the curing process. This provides several benefits as they may not use solvents and, therefore, relevant volume changes are avoided during curing. Disadvantageously, the change of viscosity caused by photopolymerization due to chain growth and crosslinking may lead to curing inefficiencies and curing conditions should be carefully controlled too for a proper fixation.

Chain polymerization reactions are typically used in inkjet inks, like acrylate or epoxy chemistries which are two representative examples of free radical and cationic polymerization respectively. Besides, these reactions can be found too in the polymerization of the organic part of hybrid organic-inorganic materials. Together with the organic polymerization, in order to complete the solidification of hybrid materials, it is also required the activation of the polymerization of the inorganic part, where alkoxides are conventionally used as precursors. For this, typically water and acid are needed to trigger the hydrolysis and condensation process that will create the Si-O-Si bonds of the inorganic network.

Hybrid organic-inorganic materials provide relevant advantages for those cases where demanding performance is required as they combine the flexibility of organic structures to implement functionalities into the material together with the chemical and mechanical robustness of the inorganic structure to withstand exigent conditions. On the other hand, due to the coexistence of both organic and inorganic natures, the control of the fluid properties of hybrid-based inkjet inks becomes more difficult.

Focusing on the viscosity of the inks, solvents are typically incorporated for its control. Rheology is also affected by the activation of the hydrolysis and condensation steps done prior to printing. Despite the proper jet of the fluid, in both cases, the ink stability is compromised.

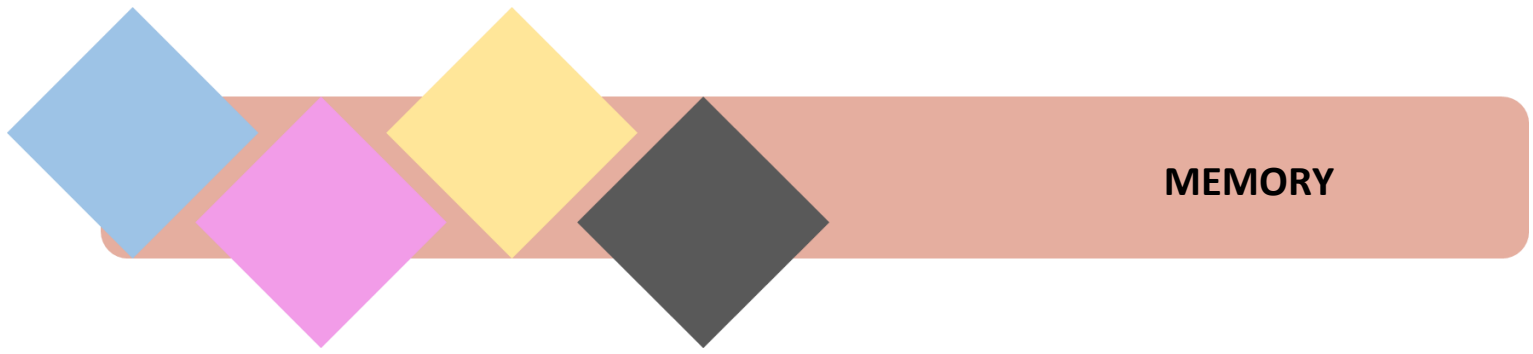
As a promising alternative, the use of photoacid generator (PAG) has been recently explored to trigger both, organic and inorganic reactions concomitantly. This photoinitiator activates the organic polymerization when irradiated with UV light and, at the same time the acid generated catalyzes the hydrolysis-condensation processes of the inorganic part. Nonetheless, literature does not show studies of this approach being used in combination with inkjet printing technology.

With regard to the applications, this thesis is focused on the use of inkjet applied to the micro- and integrated optics field. In this direction, inkjet printed microlenses and waveguides have been targeted, where good transparency is required in the final material. Apart from the optical properties of the final material, the interaction of the ink with the surface will have a direct influence on the performance of the optical element too.

In the case of microlenses, spherical geometries with large contact angles have been reported but, normally, laborious processes involving additional technologies like photolithography to structure the surface are needed. On the other hand, despite inkjet has shown promising results for the preparation of waveguides, their optical losses are still far away from those achieved by conventional technologies such as dip coating.

In summary, inkjet is already a well-known technology that provides considerable advantages to deposition processes, especially when patterning is necessary, but the fluid restrictions and the demanding performance of the use cases are the main reasons why some applications are still away from industrialization. To further exploit this technology, complex formulations are being developed. One of the most promising ones are hybrid organic-inorganic based fluids but still count with some limitations like the pre-hydrolysis and condensation steps carried out prior to print and the use of solvents to control the rheology of the inks. In addition, especially in micro-optics field, additional steps are required for the preparation of the surfaces prior to the deposition or for curing the ink.

In this framework, this thesis is focused on the development of photopolymerizable solvent-free hybrid organic-inorganic based formulations for inkjet printing with long term stability, leading after curing to deposits with good mechanical and optical properties. The implementation through inkjet printing of optical elements based on these photocurable inks has been explored to demonstrate their added value in real use cases.



1. Goals

The general goal of this thesis is the development of jettable inks and their use for the generation of surfaces and elements with optical functionalities and good mechanical performance by using inkjet printing technology and high-throughput industrially viable processes.

Firstly, from the materials point of view, hybrid organic-inorganic materials have demonstrated to be a highly suitable candidate for micro- and integrated optics applications. Nonetheless, there exist difficulties for their industrial use in combination with inkjet printing, hence, a proper adaptation of the fluid properties and stability improvement is nowadays pursued. In addition, not only ink printability and stability are required but good performance after deposition should be addressed too: good mechanical properties and proper optical functionality of the final deposits. Furthermore, versatile inks showing suitability for multiple substrates could provide and added value to expand their use to additional applications.

Secondly, from the process point of view, inkjet technology already provides a flexible and precise deposition process with high-throughput. Additional steps required for functional surfaces and elements preparation include the conditioning of the substrate or the fixation of the ink. For example, like masking or complex photolithographic, for the precise positioning of droplets or solvent evaporation, prior to ink fixation, may add complex and time-consuming steps. Therefore, developing robust and flexible printing and curing processes as well as minimizing complexity of the surface conditioning could facilitate the introduction of this technology in real industrial applications.

In this framework, to accomplish the above-mentioned general goal, the following specific goals have been defined:

1. Formulation of jettable solvent-free inks based on hybrid organic-inorganic photopolymerizable materials with direct UV curing leading to deposits with good mechanical properties and adhesion to the substrate as well as good optical transparency and suitable optical properties and functionality (e.g.: high refractive index or luminescence).
2. Control of the interaction between ink and substrate, assuring an adequate wettability that could permit a good performance of the deposited material.
3. Implementation of optical elements: waveguides, microlenses and luminescent deposits.
4. Validation of inkjet printed devices, demonstrating the applicability of the developed inks and preparation processes into specific relevant applications.

2. Scope

As described in previous sections inkjet printing is a powerful technique for the implementation of optical applications, in particular, functional elements such as microlenses or waveguides. In this direction, a literature research of inkjet technology and its use in different fields was done in first instance, giving place to the review paper “Inkjet Printing of Functional Materials for Optical and Photonic Applications” published in the journal *Materials* (**Publication 1**). In this review, an in-depth revision of the jetting and deposition phenomena was conducted as well as an overview of the use of inkjet for the manufacturing of different optical elements and photonic devices, with special emphasis in the materials used and the added value that inkjet provides in the manufacturing processes as well as the current challenges in each application field.

The present thesis is focused on the development of materials and their use with inkjet printing technology for the manufacturing of optical elements such as microlenses or waveguides. For this purpose, suitable fluids to be jetted in proper conditions and with good performance after deposition are needed. In particular, characteristics such as good transparency, high refractive index, good adhesion and flexibility are typically targeted in the different studied applications.

Within the different available materials, as remarked in previous sections, hybrid organic-inorganic ones are suitable candidates to fulfill these requirements. These materials provide good mechanical properties given by the inorganic structure as well as flexibility to be functionalized thanks to their organic nature.

Conventionally, inkjet inks described in literature based on hybrid organic-inorganic materials require multiple steps for curing and trigger polymerization of both organic and inorganic networks or they make use of solvents to adapt their rheology to the requirements of the printhead. As described in the introduction, these features penalize the efficiency and throughput of the process. To overcome these issues, in the article “Photoacid catalyzed organic–inorganic hybrid inks for the manufacturing of inkjet-printed photonic devices”, published in *Journal of Materials Chemistry C* (**Publication 2**), we present solvent-free photoacid catalyzed jettable hybrid organic-inorganic inks with good optical properties. These inks can be cured right after the deposition by UV light activation that triggers the concomitant polymerization of the organic and inorganic networks in an efficient manner, simplifying enormously the curing process.

These formulations are based on 3-glycidoxypropyltrimethoxysilane (GPTMS) as the principal component (Figure 25). This precursor counts with an epoxy ring and a triethoxysilyl group, providing the organic and inorganic nature respectively. Looking for a concomitant polymerization of both organic and inorganic reactive groups, a photoacid generator (PAG) is added in order to trigger the curing process. The selected PAG was a triarylsulfonium hexafluorophosphate salt (Figure 25) that reacts when excited with UV light. In addition, in order to adapt the fluid properties of the material and make it jettable, a surface tension modifier is used. In this case, a polyether-modified polydimethylsiloxane (BYK-333) was added to the formulation, giving place to the first printable fluid (so-called Model ink).

Looking for an adequate performance of this ink into optical applications, further additives are selectively introduced to tune the optical properties of this ink. On one side Epikote 157 (Figure 25) was added, an epoxy resin composed by 8 benzene rings each one bearing an epoxide ring, which is expected to react with the organic part of the network. On the other side,

dimethoxydiphenylsilane (dPDMS) (Figure 25), comprising two aromatic rings, having each one a silane group that can react to the inorganic network, was added too. Thanks to these additional multi-reactive components, the network is reinforced, favouring an improvement of mechanical properties of the final deposit while the aromatic rings help to increase its refractive index, what provides a better performance to this material for waveguiding applications. In this way, a new ink with high refractive index (so-called HRI ink) was formulated.

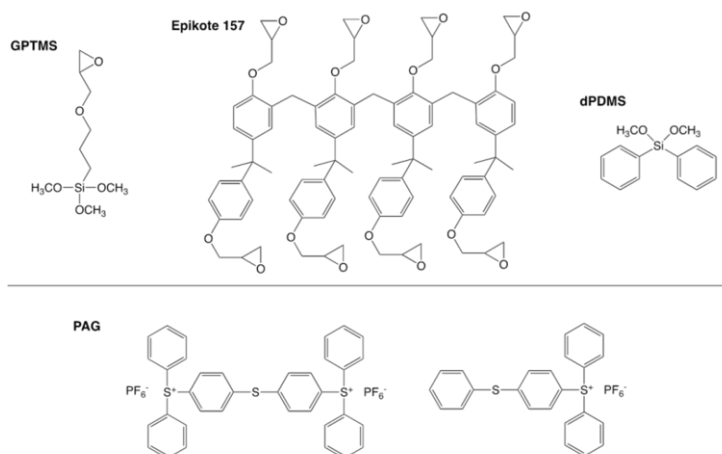


Figure 25. Molecular structure of GPTMS, Epikote 157, dPDMS and PAG.

Deposits of these inks with excellent adhesion to different substrates, refractive index of 1.56 and good transparency were obtained by properly adjusting the printing and curing conditions. Planar and channel optical waveguides were also successfully prepared on various substrates with propagation losses as low as 0.5 dB/cm (Figure 26).

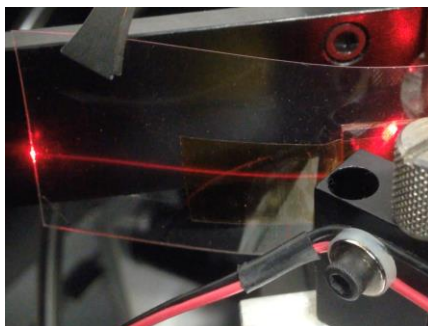


Figure 26. Photograph of flexible substrate with inkjet printed waveguide.

Apart from the deposition of waveguides, the precise deposition of luminescent materials with inkjet can be highly beneficial for different applications such as energy harvesting, optoelectronics or anti-counterfeiting. In this direction, a luminescent ink was presented in the article “Digital Luminescence Patterning via Inkjet Printing of a Photoacid Catalyzed Organic-Inorganic Hybrid Formulation”, published in the journal *Polymers* (**Publication 3**).

Taking advantage of the optical properties of the previously formulated HRI ink, luminescence functionality was included by adding a luminescent dye (Rhodamine B) into the formulation and resulting in a stable solution (so-called HRI-RhodB-02 ink). No penalty in the jetting, UV curing process nor its mechanical properties were noticeable due to the incorporation of this dye. Even more, the deposition on different types of substrates other than glass and even on flexible films was also demonstrated. Overall this study further demonstrates the potential and robustness of

these inks to keep its properties despite the modifications suffered in the formulation to introduce new functionalities (Figure 27).

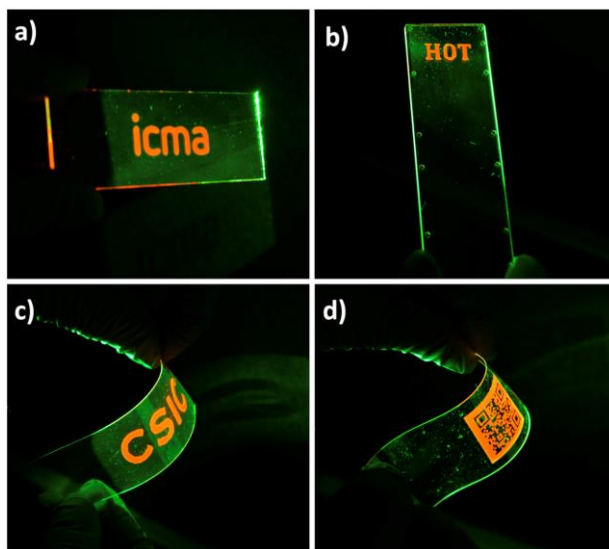


Figure 27. Examples of luminescent ink deposited on multiple substrates under green light excitation. Luminescent marks on (a) glass, (b) rigid cyclic olefin polymer (COP), (c) flexible indium tin oxide (ITO) coated poly(ethylene terephthalate) (PET) and (d) luminescent quick response (QR) code printed on flexible COP.

To put in value the capabilities of this luminescent ink and its applicability, an optical planar waveguide sensor was presented in the following article: “Optical Planar Waveguide Sensor with Integrated Digitally-Printed Light Coupling-in and Readout Elements”, published in the journal *Sensors* (**Publication 4**). An optical temperature sensor was developed by integrating two luminescent inkjet ink deposits as light coupling-in and readout elements respectively with matched emission and excitation together with a temperature responsive material.

Taking HRI-ink as base ink, a small percentage of the dye Fluorescein F27 was introduced in the formulation. Following an analogous process as the performed for HRI-RhodB-02, fluid properties did not show relevant changes when this dye was added to the ink formulation. Therefore, the so-called HRI-F27-02 ink was formulated and used to create a coupling-in film deposited by inkjet. When blue light excites this element, it emits light in the green wavelength in all directions. Light emitted by this deposit is partially coupled in the planar light guide where it is printed. Thanks to this, light coupling can be performed remotely by exciting this luminescent deposit without special alignment of the light source. In addition, a thermoresponsive Liquid Crystal Polymer (LCP) was formulated to be used as light controller and, hence, regulate the amount of light transmitted through the planar waveguide. This LCP has an isotropization temperature at 134 °C that causes the material to be translucent below this temperature and, hence, the light is dispersed and coupled out from the waveguide. On the contrary, if temperature is above this temperature, the order of the liquid crystal is lost and becomes transparent, allowing the light go straight through it, remaining coupled in the waveguide (Figure 28). On the other side of the planar waveguide, the previously described HRI-RhodB-02 inkjet ink was deposited, behaving as readout element. This second luminescent element absorbs part of the green light emitted by HRI-F27-02 ink and emits at longer wavelengths, therefore, it behaves as readout element through luminescence intensity measurements.

Thanks to this demonstrator (Figure 28), the capability of inkjet technology to efficiently print luminescent elements to facilitate the coupling-in and readout of light in waveguides as well as the miniaturization of sensing devices and the integration of their elements was evidenced.

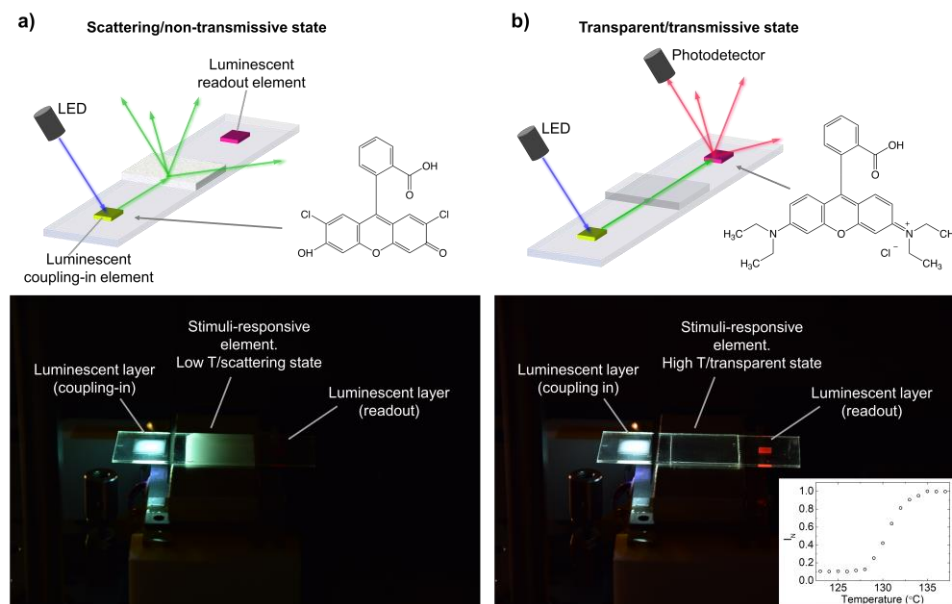


Figure 28. a) and b): schematic representation (top) and photograph (bottom) of an optical planar waveguide sensor comprising a luminescent coupling-in element and a luminescent temperature readout element (a) in the scattering/non-transmissive state, at low temperature, and (b) in the transmissive state, at high temperature. The inset in (b) shows a plot of the emitted red light (633 nm) measured as a function of temperature at the sensing region.

Finally, relying on the good optical properties of the HRI ink formulated in the framework of this thesis and the capability of precise deposition of single drops with inkjet, microlenses with tailored geometrical properties and, hence, optical properties, were prepared and characterized. Precise positioning of these microlenses can be of great interest to improve the efficiency in coupling of light in optical fiber communication systems, light extraction from LEDs or improve light collection in sensing devices. Nonetheless, currently used processes, such as photolithography, require complex steps to condition the surface in order to get the desired geometries in the lenses.

In the article “Facile fabrication of microlenses with controlled geometrical characteristics by inkjet printing on nanostructured surfaces prepared by combustion chemical vapour deposition”, published in the journal *Applied Surface Science* (**Publication 5**), we introduce a high-throughput process to prepare the surface and, therefore, control the geometry of the inkjet printed microlenses. This surface treatment protocol is based on a Combustion Chemical Vapour Deposition (CCVD) process, which generates a porous layer with nano-roughness on the substrate. This surface is subsequently processed through a silanization step with fluorosilane at mild vacuum conditions. After this treatment, HRI-ink is deposited by inkjet as independent droplets on the treated surface. Thanks to the absence of solvent in the formulation of the ink and the curing process in one single step by UV light activation, the geometry of these droplets is not significantly modified while curing, favouring the control of the final optical properties of the microlenses.

In order to tailor the geometry of these microlenses, the nano-roughness given by the CCVD process is controlled, allowing the preparation of microlenses with a large range of contact angles, achieving single droplet microlenses beyond the hemisphere (contact angles up to 115°) and reproducible well-defined digital patterns of microlenses (Figure 29).

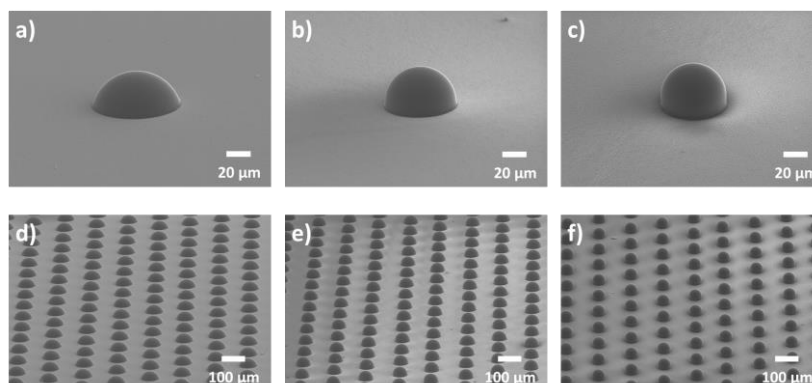


Figure 29. Oblique view FESEM images of a single-drop inkjet printed microlens using HRI-ink on a CCVD-fluorosilane treated glass substrate with (a) 2, (b) 4 and (c) 8 passes through the CCVD system. Oblique view FESEM images of arrays of single-drop inkjet printed microlenses on a CCVD-fluorosilane treated glass substrate with (d) 2, (e) 4 and (c) 8 passes through the flame.

In conclusion, through this thesis, we present how photoacid catalyzed formulations, containing hybrid organic-inorganic monomers with epoxy and silane functionalities can be innovatively applied for the preparation of jettable inks suitable for the generation of photonic devices such as planar waveguides, luminescent coatings or microlenses through inkjet printing. The capability of delaying the hydrolysis and condensation of the reactive inorganic precursor by protecting the ink from UV light confers high stability to the ink too. In addition, we have leveraged the advantages of concomitantly polymerize the organic and inorganic networks, providing a highly throughput process suitable for industrial production.

Apart from that, the interaction between the inks and the substrate has been thoroughly studied, leading to the definition of different surface treatments and protocols to control the wettability of the surface and, hence, the geometrical characteristics of the deposits and their adhesion to the underlying substrate.

Thanks to this, we have been capable to get solid films with good adhesion and mechanical properties together with tailored optical characteristics, achieving inks with high refractive index and low propagation losses or luminescent properties. Apart from films, controlled spherical caps with adjustable geometry have been also successfully targeted.

In addition, besides the development of the inks themselves, this research has focused its effort in demonstrating the applicability of the printed elements in specific applications in the areas of micro- and integrated optics that could be industrially scaled up.

The presented thesis also opens the door to further achievements by showing the versatility of these formulations to be used in other use cases where other functional materials are needed and even flexible substrates are used.

3. Methodology

Depending on the formulations and the substrate to be used, the preparation of the fluid and the surface, the analysis and characterization of materials differ from one case to another. Here, the different methods and procedures employed in the different studies carried out are detailed:

Ink preparation: for the formulation of the inks, the following materials were used in the concentrations detailed in the corresponding papers:

- GPTMS (3-glycidoxypropyltrimethoxysilane): hybrid organic-inorganic monomer bearing an epoxy and a trialkoxysilane group, purchased from Alfa Aesar.
- Epikote 157: an epoxy resin consisting of an average of eight aromatic benzene rings and eight epoxide reactive groups, acquired from Momentive.
- dPDMS (dimethoxydiphenylsilane): a disilane monomer having two aromatic rings, each having a methoxysilane group, supplied by Aldrich.
- Photoacid Generator (PAG): triarylsulfonium hexafluorophosphate salt (50% in propylene carbonate), acquired from Aldrich that, after excitation with UV light, it triggers the polymerization reaction of the organic epoxides and, concomitantly, catalyzes the hydrolysis and condensation of the alkoxide groups.
- BYK-333: a polyether-modified polydimethylsiloxane, from BYK Chemie, was used to adjust the surface tension of the inks and to promote the surface wetting.
- Rhodamine B: a luminescent dye that strongly absorbs in the green region of the spectrum and emits orange-red light, centered at 585 nm, was purchased from Lambda Physic.
- Fluorescein 27 (F27): a luminescent dye absorbing in blue region, having an emission centered at 520 nm (green light), was purchased from Lambda Physic.

Substrate preparation: a well-defined procedure was followed for the cleaning of the substrates in order to have reproducibility in the behavior of the printed inks. Nonetheless, depending on the application, additional surface modifications apart from cleaning were done to activate and functionalize the surface:

- Substrate cleaning: The glass slides used as substrate were cleaned using soapy water and gently hand rubbing the surface using nitrile gloves. After that, once rinsed, the substrates are introduced in an ultrasonic bath with soapy water too during 10 minutes. After this, mili-Q water was used to reflux them again and repeat ultrasonic bath for 10 minutes in mili-Q water. A third cleaning and 10 minutes of ultrasonic bath step, both with isopropyl alcohol, was done. The drying of the substrates was done using compressed air.
- Ozone treatment: Samples treated with UV Ozone were introduced into a UVO 342 reactor (Jeligh company Inc.) in order to remove the contamination on the surface of the glass. In this way, silanol groups of glass are left exposed after this activation, increasing the wettability behavior of the substrate [113].
- Combustion Chemical Vapour Deposition (CCVD): This surface treatment (Pyrosil[®], SURA) consists in a combustion chemical vapour deposition where a propane-air flame is put in close contact with the substrate. The air stream feeding the flame contains an organosilicon precursor, causing the deposition of a SiO₂ like thin coating (between 50-100 nm) [114].
- Chemical Vapour Deposition (CVD): Substrates are introduced into a desiccator together with a glass slide with ~50 µl of the reactive used for the coating, 1H,1H,2H,2H-Perfluorooctyltrichlorosilane (FOTS) in our case. Vacuum is then applied to diminish the

pressure to 100 mbar and samples are taken out after 30 minutes. The coated samples are rinsed with isopropyl alcohol, dried with compressed air and finally heated during 10 minutes in air at 110 °C [115].

Inkjet Printing: For the deposition of the different inks, the same equipment was used, although specific configuration of the printing system was needed for a proper jetting in each case. This configuration was set according to the analysis done with a dropwatcher that allowed analyzing the drops on the fly and achieving spherical isolated droplets prior to their deposition on the substrate.

- Printer: Specific equipment was used based on a custom-made printer system. For this, the chosen technology is piezoelectric DOD from Xaar. This printhead (Xaar-126/80) counts with 126 nozzles of 50 μm of diameter and 137 μm of pitch. The substrate to be printed moves in perpendicular direction to the line of nozzles with a distance gap of around 1 mm between both of them and a native resolution of 185 dpi. This printhead is driven by electronics provided by the same manufacturer who have also designed the signal command of the piezoelectric walls, allowing its adjustment (as well as the printing parameters) through its software. The printhead temperature is stabilized by making use of a heater and thermocouple assembled into the metallic block where the printhead is mounted. An additional printhead holder was mounted in series to the original one to allow the printing of two different inks in the same setup just by connecting the desired printhead to the electronic control board. For the movement of the substrate, an eTrack linear stage from Newmark Systems Inc. was used, being commanded by IMS-Terminal software and achieving a constant speed of around 20 mm/s. A picture of the equipment can be seen in Figure 30.

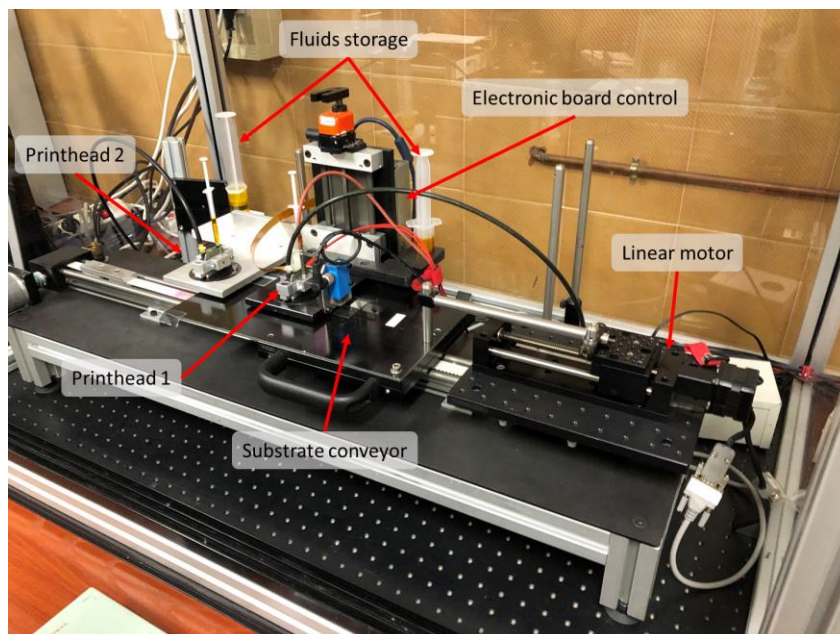


Figure 30. Image of the printer set-up used for the development of this thesis.

- Dropwatcher
This equipment is used for the observation of drops being jetted on the fly, allowing the analysis of the characteristics of these drops. It consists on a stroboscopic light and a

camera, both connected and synchronized with the printhead by using a pulse generator, following the scheme shown below (Figure 31a). For the work developed during this research, a home-built dropwatcher system was used. A pulse generator sends a voltage signal to the printhead to trigger the drop ejection process. The same generator sends another voltage pulse to trigger the camera image acquisition and a third pulse is sent to trigger a short pulse (50 to 200 ns duration) of light from a strobe LED. According to the following representation in Figure 31b, the three signals should be synchronized so the camera acquires a picture when the drop is flying through the camera field of view and the LED light is on. Using this setup (Figure 31c), images of ink jets and flying droplets like those of Figure 14 can be taken and, hence, analyze the jet formation process and the characteristics of the drops, adjust the system configuration and validate if the ink is jetted in proper conditions.

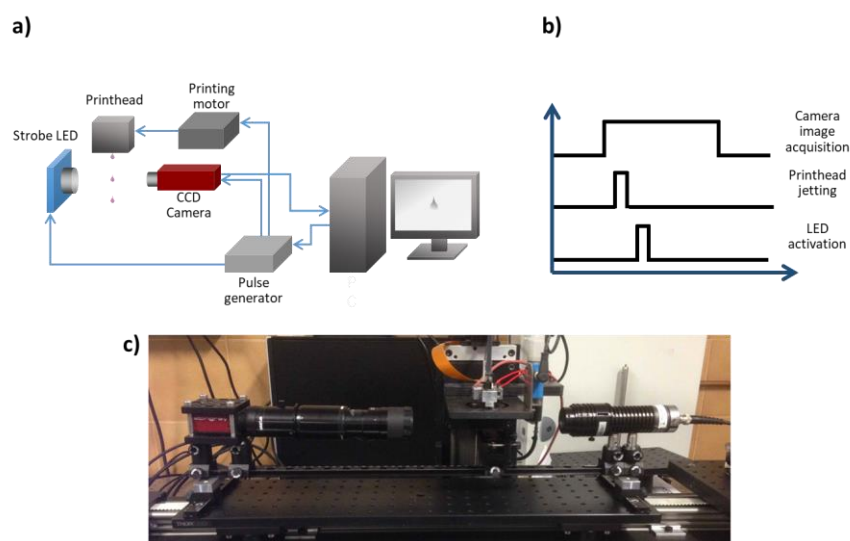


Figure 31. a) Schematic representation of dropwatcher system, b) representation of pulse coordination for visualization of drops and c) photograph of the home-built developed dropwatcher system.

Photocuring: After the deposition, the materials needs to be solidified. In this case, all the formulated inks are photopolymerizable fluids, which means that actinic light is used for the initiation of the polymerization process and, hence, the fixation of the fluid on the substrate.

- UV curing: For the curing of the samples, an UV lamp Exfo OmniCure S2000 UV was used with a bandpass filter to set the wavelength range to 320 – 390 nm. The power used was 10 mW/cm² and the coatings were exposed during 5 minutes at RT. Depending on the required conditions, the samples were cured at ambient atmosphere with relative humidity between 30 % and 40 % or under mild vacuum. When mild vacuum was required, the samples were introduced in a chamber with optical access through a quartz glass that allows the UV light to reach the substrate while a pressure of 100 mbar was set by using a vacuum pump. After this pressure was achieved, UV light was immediately applied to the sample.

Finally, once the patterns and films were prepared, each case has required specific characterization. Below, a brief description of the used techniques for the corresponding analysis is given.

Ink properties characterization:

- Viscosity: Viscosity of the inks was measured using a Haake Rheostress 1 rotational rheometer from Thermo Scientific.
- Surface tension: Surface tension were measured by using an Attension Goniometer Theta Lite.
- Density: Density measurements were carried out using a 10 ml pycnometer.

Ink-substrate interaction:

- Contact angle: Contact angle was measured by using an Attension Goniometer Theta Lite.

Morphology characterization:

- Microscopy: The shape of the drop after deposition and after curing as well as the quality of the printed material were analyzed by using an optical microscope OLYMPUS Eclipse i80. In those cases where liquid crystal is employed and so temperature dependence is required to be analyzed, this equipment counts with a Linkam LTSE420 heating stage to provide this feature.
- Atomic Force Microscopy (AFM): Characterization of the surface quality and topography was performed with the support of CEQMA Service by using a Ntegra Aura Scanning Probe Microscopy from NT-MDT.
- Field Emission Scanning Electron Microscopy (FE-SEM): Morphology of the surface was also studied by using a Merlin Carl Zeiss equipment that belongs to SAI – University of Zaragoza Service, who provided the necessary support for this characterization.

Thermal characterization:

- Thermogravimetry Analysis (TGA): TGA analysis was performed by using a Netzsch TG 209 Libre F1 equipment.

Spectroscopy characterization:

- UV-Vis Spectrophotometry: Absorption of the samples where measured by using a VARIAN Cary-500 spectrophotometer.
- Fourier Transform Infrared Spectroscopy (FTIR): A Perkin Elmer Spectrum 100 with Attenuated Total Reflectance (ATR) accessory was used to perform the FTIR spectroscopy. The measurements were done between 4000 cm^{-1} and 450 cm^{-1} .
- Spectrofluorometry: Luminescence properties were characterized with a Perkin Elmer LS 50B spectrofluorometer.

Mechanical characterization:

- Adhesion cross cut: Adhesion test were done following the ASTM D3359 standards. In this case, a round cutter provided by Neurtek was used to scratch the coating. After this, a normalized Tesa 4024 adhesive tape was applied over the coating and quickly removed at an angle of approximately 180° .

- Nanoindentation: Mechanical properties of the deposited cured films such as hardness and elastic module were characterized by using nanoindentation technique with support from CEQMA Service. A Nanoindenter G200 from Agilent Technologies equipment was used with a Vickers indenter tip.

Optical characterization:

- Digital transmission microscopy: For the analysis of geometrical characteristics of microlenses, a home-made digital transmission microscope at the Applied Physics Department (University of Zaragoza) was employed where a collimated laser beam ($\lambda = 514.5 \text{ nm}$) was used to illuminate the sample. Planachromat extra-long working distance microscope objectives were used to image the microlenses into a digital camera (2560x2160, $6.5 \mu\text{m}$ pixels). In addition, a home-made holder permitted the rotation of substrate, allowing the observation of the microlenses from any direction.

Waveguiding characterization:

- Prism coupler: Propagating modes were analyzed using a prism coupler Metricon 2010 equipped with a HeNe laser at 632.8 nm for the transverse electric (TE) and transverse magnetic (TM) polarization. For this technique, a laser beam is directed to a prism with a high refractive index and the light is then reflected to a photodetector. The film to be analyzed is placed against the base of the prism and, by using a pneumatic knee, it is pressured to minimize the air gap between the prism and the sample. The setup is, afterwards, rotated with respect to the laser beam. If the angle matches that of the waveguided modes, light may be coupled into the waveguide, causing a decrease in the intensity of the light reaching the detector. Thanks to this, the refractive index and thickness of the film can be measured. By using the same equipment, propagation losses can be also characterized. To do that, several cm of the surface to be analyzed are scanned with an optical fiber while the light is being propagated, detecting the scattered light that is considered to be proportional to the intensity of light being propagated at each position. The remaining intensity in the waveguide after propagating a distance x is given by Equation 6.

$$I(x) = I_0 10^{\left(-\frac{\alpha x}{10}\right)} \quad (6)$$

Where I_0 is the initial intensity, $I(x)$ is the transmitted intensity through the waveguide at position x (cm), and α is the attenuation coefficient measured in decibels per centimeter (dB cm^{-1}).

4. Conclusions

From a general perspective, we have developed a complete platform to implement micro- and integrated optic functionalities directly on glass surfaces. The platform comprises the formulation of hybrid organic-inorganic solvent-free based photoacid catalyzed inks, high-throughput processes for the preparation of the surfaces, the deposition of the material by inkjet printing and its subsequent fixation.

Firstly, solvent-free photoacid catalyzed formulations, based on epoxy and silane monomers have been prepared and properly adapted to be deposited by inkjet printing. These inks contain a photoacid generator that allows the polymerization of the organic and inorganic networks to occur concomitantly. This permits the delay of the hydrolysis-condensation after the printing step (by protecting the ink against UV light) and, hence, directly curing the ink by UV excitation. As a result, with no solvents involved, no additional post-printing steps are needed, advantageously simplifying the fabrication process and providing long-term stability to the inks, making them suitable for industrial applications.

By using an appropriate formulation, this deposition and curing process has led to the preparation of solid films with good adhesion, transparency and high refractive index leading to planar waveguides with low optical losses.

By making use of the same formulation, a flexible and robust methodology for the preparation of microlenses with tailored optical properties has been developed. In order to control the geometrical characteristics of the microlenses, a two-steps surface treatment has been defined to adjust the interaction between the ink and the substrate. Firstly, a CCVD step results into a SiO₂ nanostructured surface. Secondly, this surface is functionalized with a fluorosilane layer deposited by a CVD process. Later, by controlling the volume of the deposited drop and the described surface treatment, microlenses beyond the hemisphere have been prepared with this methodology.

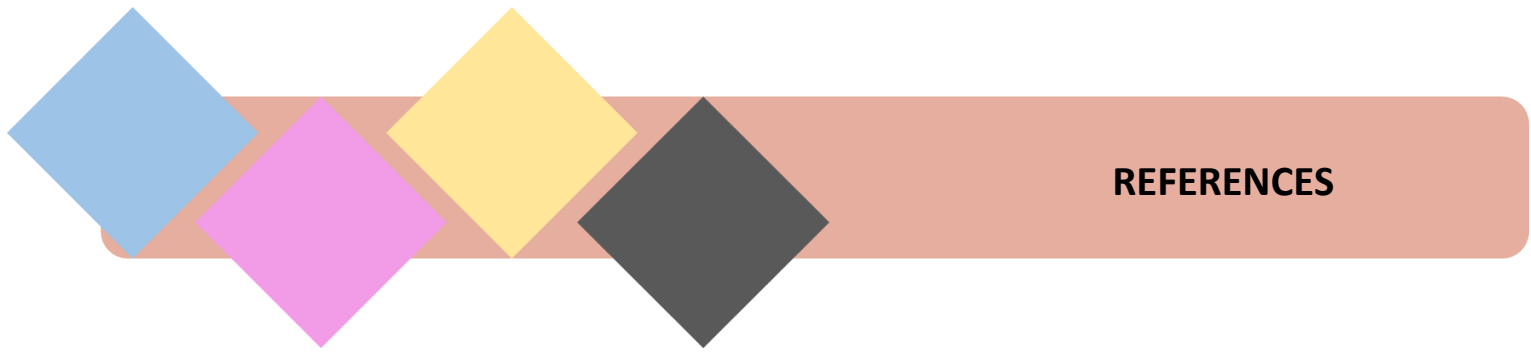
The inclusion of luminescent molecules in these formulations has not significantly affected the jettability of the inks and their wettability, allowing the preparation of luminescent deposits with the same simple inkjet printing process and the subsequent curing in one single step by UV light excitation. These deposits have led to patterned light emissive surfaces with good adhesion and mechanical properties for the fabrication of optical devices.

As a proof of concept, these luminescent inks have been used for the preparation of an optical temperature sensor by combining these deposits with a smart thermoresponsive liquid crystalline polymer on a planar waveguide architecture.

In summary, we have developed suitable functional formulations for inkjet and substrate conditioning processes to prepare optical elements with capability to be scaled into industrial production. In addition, different demonstrators have been prepared to highlight the use of the developed inks into real applications. Besides this, the formulated inks have been also deposited on additional rigid and flexible surfaces used in industry, showing the versatility of the developed inks to be adapted to different surfaces.

Beyond the formulated inks and their implementation in specific applications, the present thesis also provides new avenues for the development of jettable inks and processes for the

preparation of surfaces that could enable the digital printing of functional elements with good performance through a simple and industrially viable methodology.



REFERENCES

1. Del Barrio, J.M.; Sánchez-Somolinos, C. Light to Shape the Future: From Photolithography to 4D Printing. *Adv. Optical Mater.* **2019**, 1900598.
2. Smithers Pira. Fast-growing inkjet market to pass \$100 billion in 2023. Available online: [https://www.smitherspira.com/news/2018/july/fast-growing-inkjet-market-to-pass-\\$100-bn-in-2023](https://www.smitherspira.com/news/2018/july/fast-growing-inkjet-market-to-pass-$100-bn-in-2023) (accessed on 29 July 2019).
3. Future Market Insights. An Incisive, In-depth Analysis on the Inkjet Printers Market. Available online: <https://www.futuremarketinsights.com/reports/inkjet-printers-market> (accessed on 29 July 2019).
4. Lee, W.-H.; Park, Y.D. Inkjet Etching of Polymers and Its Applications in Organic Electronic Devices. *Polymers* **2017**, *9*, 441.
5. Homola, T.; Shekargoftar, M.; Dzik, P.; Krumpolec, R.; Durasova, Z.; Vesely, M.; Cernak, M. Low-temperature (70 C) ambient air plasma-fabrication of inkjet-printed mesoporous TiO₂ flexible photoanodes. *Flex. Print. Electron.* **2017**, *2*, 035010.
6. Ma, S.; Ribeiro, F.; Powell, K.; Lutian, J.; Møller, C.; Large, T.; Holbery, J. Fabrication of Novel Transparent Touch Sensing Device via Drop-on-Demand Inkjet Printing Technique. *ACS Appl. Mater. Interfaces* **2015**, *7*, 21628–21633.
7. Sun, J.Z.; Guo, Y.Z.; Cui, B.; Chu, F.Q.; Li, H.Z.; Li, Y.; He, M.; Ding, D.; Liu, R.P.; Li, L.H.; Song, Y. Inkjet printing bendable circuits based on an oil-water interface reaction. *Appl. Surf. Sci.* **2018**, *445*, 391–397.
8. Sun, J.Z.; Yun, C.; Cui, B.; Li, P.; Liu, G.; Wang, X.; Chu, F. A Facile Approach for Fabricating Microstructured Surface Based on Etched Template by Inkjet Printing Technology. *Polymers* **2018**, *10*, 1209.
9. Sun, J.Z.; Cui, B.; Chu, F.Q.; Yun, C.H.; He, M.; Li, L.H.; Song, Y.L. Printable nanomaterials for the fabrication of high-performance supercapacitors. *Nanomaterials* **2018**, *8*, 528.
10. Halls, J. Ink-Jet printing of PLED displays. *Inf. Disp.* **2005**, *2*, 11.
11. Bharathan, J.; Yang, Y. Polymer electroluminescent devices processed by inkjet printing: I. Polymer light-emitting logo. *Appl. Phys. Lett.* **1998**, *72*, 2660–2662.
12. Shimoda, T.; Kimura, M.; Seki, S.; Kobayashi, H.; Kanbe, S.; Miyashita, S.; Friend, R.H.; Burroughes, J.H.; Towns, C.R.; Millard, I.S. Technology for active matrix light emitting polymer displays. In Proceedings of the International Electron Devices Meeting Technical Digest, Washington, DC, USA, 5–8 December 1999; pp. 107–110.
13. Kobayashi, H.; Kanbe, S.; Seki, S.; Kiguchi, H.; Kimura, M.; Yudasaka, I.; Miyashita, S.; Shimoda, T.; Towns, C.R.; Burroughes, J.H. A novel RGB multicolor light-emitting polymer display. *Synth. Met.* **2000**, *111*, 125–128.
14. Haverinen, H.M.; Myllylä, R.A.; Jabbour, G.E. Inkjet printing of light emitting quantum dots. *Appl. Phys. Lett.* **2009**, *94*, 073108.
15. Wood, V.; Panzer, M.J.; Chen, J.; Bradley, M.S.; Halpert, J.E.; Bawendi, M.G.; Bulovic, V. Inkjet-Printed Quantum Dot-Polymer Composites for Full-Color AC-Driven Displays. *Adv. Mater.* **2009**, *21*, 2151–2155.
16. Haverinen, H.M.; Myllylä, R.A.; Jabbour, G.E. Inkjet printed RGB quantum dot-hybrid LED. *J. Disp. Technol.* **2010**, *6*, 87–89.
17. Lu, H.; Lin, J.; Wu, N.; Nie, S.; Luo, Q.; Ma, C.-Q.; Cui, Z. Inkjet printed silver nanowire network as top electrode for semi-transparent organic photovoltaic devices. *Appl. Phys. Lett.* **2015**, *106*, 093302.
18. Maisch, P.; Tam, K.C.; Lucera, L.; Egelhaaf, H.-J.; Scheiber, H.; Maier, E.; Brabec, C.J. Inkjet printed silver nanowire percolation networks as electrodes for highly efficient semitransparent organic solar cells. *Org. Electron.* **2016**, *38*, 139–143.

19. Kordás, K.; Mustonen, T.; Tóth, G.; Jantunen, H.; Lajunen, M.; Soldano, C.; Talapatra, S.; Kar, S.; Vajtai, R.; Ajayan, P.M. Inkjet Printing of Electrically Conductive Patterns of Carbon Nanotubes. *Small* **2006**, *2*, 1021–1025.
20. Dua, V.; Surwade, S.P.; Ammu, S.; Agnihotra, S.R.; Jain, S.; Roberts, K.E.; Park, S.; Ruoff, R.S.; Manohar, S.K. All-Organic Vapor Sensor Using Inkjet-Printed Reduced Graphene Oxide. *Angew. Chem. Int. Ed.* **2010**, *49*, 2154–2157.
21. Aernouts, T.; Aleksandrov, T.; Girotto, C.; Genoe, J.; Poortmans, J. Polymer based organic solar cells using ink-jet printed active layers. *Appl. Phys. Lett.* **2008**, *92*, 033306.
22. Hoth, C.N.; Choulis, S.A.; Schilinsky, P.; Brabec, C.J. High Photovoltaic Performance of Inkjet Printed Polymer: Fullerene Blends. *Adv. Mater.* **2007**, *19*, 3973–3978.
23. Hoth, C.N.; Schilinsky, P.; Choulis, S.A.; Brabec, C.J. Printing Highly Efficient Organic Solar Cells. *Nano Lett.* **2008**, *8*, 2806–2813.
24. Eom, S.H.; Park, H.; Mujawar, S.H.; Yoon, S.C.; Kim, S.-S.; Na, S.-I.; Kang, S.-J.; Khim, D.; Kim, D.-Y.; Lee, S.-H. High efficiency polymer solar cells via sequential inkjet-printing of PEDOT:PSS and P3HT:PCBM inks with additives. *Org. Electron.* **2010**, *11*, 1–7.
25. White, T.J.; McConney, M.E.; Bunning, T.J. Dynamic color in stimuli-responsive cholesteric liquid crystals. *J. Mater. Chem.* **2010**, *20*, 9832–9847.
26. Stumpel, J.E.; Broer, D.J.; Schenning, A.P.H.J. Stimuli-responsive photonic polymer coatings. *Chem. Commun.* **2014**, *50*, 15839–15848.
27. Moirangthem, M.; Arts, R.; Merckx, M.; Schenning, A.P.H.J. An Optical Sensor Based on a Photonic Polymer Film to Detect Calcium in Serum. *Adv. Funct. Mater.* **2016**, *26*, 1154–1160.
28. Wang, L.; Wang, J.; Huang, Y.; Liu, M.; Kuang, M.; Li, Y.; Jiang, L.; Song, Y. Inkjet printed colloidal photonic crystal microdot with fast response induced by hydrophobic transition of poly(N-isopropyl acrylamide). *J. Mater. Chem.* **2012**, *22*, 21405–21411.
29. Bai, L.; Xie, Z.; Wang, W.; Yuan, C.; Zhao, Y.; Mu, Z.; Zhong, Q.; Gu, Z. Bio-Inspired Vapor-Responsive Colloidal Photonic Crystal Patterns by Inkjet Printing. *ACS Nano* **2014**, *8*, 11094–11100.
30. Shen, W.; Li, M.; Ye, C.; Jiang, L.; Song, Y. Direct-writing colloidal photonic crystal microfluidic chips by inkjet printing for label-free protein detection. *Lab Chip* **2012**, *12*, 3089–3095.
31. Herzer, N.; Guneyusu, H.; Davies, D.J.D.; Yildirim, D.; Vaccaro, A.R.; Broer, D.J.; Bastiaansen, C.W.M.; Schenning, A.P.H.J. Printable Optical Sensors Based on H-Bonded Supramolecular Cholesteric Liquid Crystal Networks. *J. Am. Chem. Soc.* **2012**, *134*, 7608–7611.
32. Hayes, D.J.; Wallace, D.B.; Royall Cox, W. MicroJet printing of solder and polymers for multi-chip modules and chip-scale packages. *Proc. SPIE Int. Soc. Opt. Eng.* **1999**, *3830*, 242–247.
33. MacFarlane, D.L.; Narayan, V.; Tatum, J.A.; Cox, W.R.; Chen, T.; Hayes, D.J. Microjet fabrication of microlens arrays. *IEEE Photonics Technol. Lett.* **1994**, *6*, 1112–1114.
34. Jacot-Descombes, L.; Cadarso, V.J.; Schleunitz, A.; Grützner, S.; Klein, J.J.; Brugger, J.; Schiff, H.; Grützner, G. Organic-inorganic-hybrid-polymer microlens arrays with tailored optical characteristics and multi-focal properties. *Opt. Express* **2015**, *23*, 25365–25376.
35. Wolfer, T.; Bollgruen, P.; Mager, D.; Overmeyer, L.; Korvink, J.G. Flexographic and inkjet printing of polymer optical waveguides for fully integrated sensor systems. *Procedia Technol.* **2014**, *15*, 521–529.

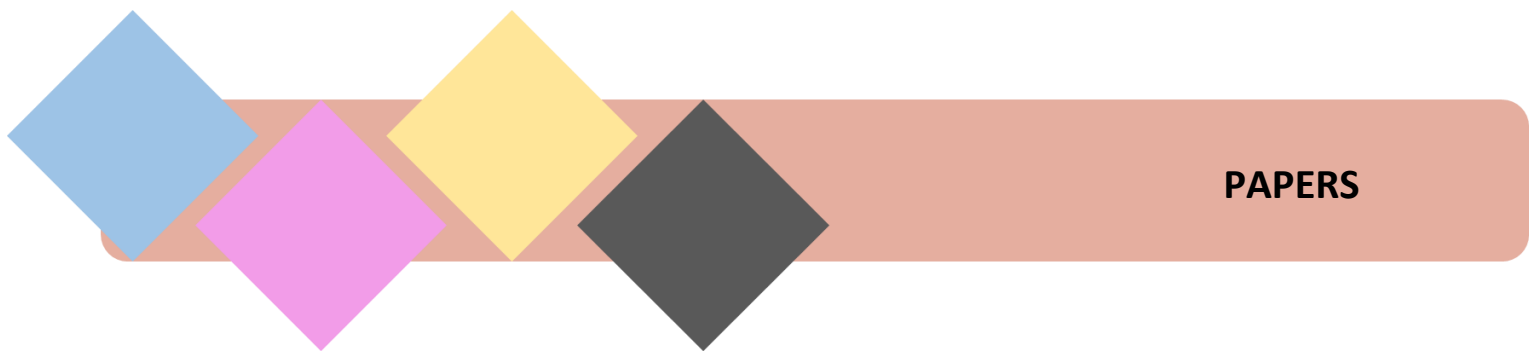
36. Wolfer, T.; Bollgruen, P.; Mager, D.; Overmeyer, L.; Korvink, J.G. Printing and preparation of integrated optical waveguides for optronic sensor networks. *Mechatronics* **2016**, *34*, 119–127.
37. Parker, S.T.; Domachuk, P.; Amsden, J.; Bressner, J.; Lewis, J.A.; Kaplan, D.L.; Omenetto, F.G. Biocompatible silk printed optical waveguides. *Adv. Mater.* **2009**, *21*, 2411–2415.
38. Samusjew, A.; Kratzer, M.; Moser, A.; Teichert, C.; Krawczyk, K.K.; Griesser, T. Inkjet Printing of Soft, Stretchable Optical Waveguides through the Photopolymerization of High-Profile Linear Patterns. *ACS Appl. Mater. Interfaces* **2017**, *9*, 4941–4947.
39. Bollgruen, P.; Wolfer, T.; Gleissner, U.; Mager, D.; Megnin, C.; Overmeyer, L.; Hanemann, T.; Korvink, J.G. Ink-jet printed optical waveguides. *Flex. Print. Electron.* **2017**, *2*, 045003.
40. Magdassi, S. *The Chemistry of Inkjet Inks*. World Scientific Publishing Co. Pte. Ltd. Singapore, 2010.
41. Derby, B. Inkjet Printing of Functional and Structural Materials: Fluid Property Requirements, Feature Stability, and Resolution. *Annu. Rev. Mater. Res.* **2010**, *40*, 395–414.
42. Bogy, D.B.; Talke, F.E. Experimental and theoretical study of wave propagation phenomena in drop-on-demand ink jet devices. *IBM J. Res. Dev.* **1984**, *28*, 314–321.
43. Reis, N.; Ainsley, C.; Derby, B. Ink-jet delivery of particle suspensions by piezoelectric droplet ejectors. *J. Appl. Phys.* **2005**, *97*, 094903.
44. Wu, H.-C.; Shan, T.-R.; Hwang, W.-S.; Lin, H.-J. Study of micro-droplet behavior for a piezoelectric inkjet printing device using a single pulse voltage pattern. *Mater. Trans.* **2004**, *45*, 1794–1801.
45. Kwon, K.-S. Experimental analysis of waveform effects on satellite and ligament behavior via in situ measurement of the drop-on-demand drop formation curve and the instantaneous jetting speed curve. *J. Micromech. Microeng.* **2010**, *20*, 115005.
46. Reis, N.; Derby, B. Ink jet deposition of ceramic suspensions: Modeling and experiments of droplet formation. *MRS Proc.* **2000**, *625*, 117.
47. Seerden, K.A.; Reis, N.; Evans, J.R.; Grant, P.S.; Halloran, J.W.; Derby, B. Ink-jet printing of wax-based alumina suspensions. *J. Eur. Ceram. Soc.* **2001**, *84*, 2514–2520.
48. Ainsley, C.; Reis, N.; Derby, B. Freeform fabrication by controlled droplet deposition of powder filled melts. *J. Mater. Sci.* **2002**, *37*, 3155–3161.
49. Clasen, C.; Phillips, P.M.; Palangetic, L.; Vermant, A.J. Dispensing of rheologically complex fluids: The map of misery. *AIChE J.* **2011**, *58*, 3242–3255.
50. Day, R.F.; Hinch, E.J.; Lister, J.R. Self-similar capillary pinchoff of an inviscid fluid. *Phys. Rev. Lett.* **1998**, *80*, 704–707.
51. McKinley, G.H.; Renardy, M. Wolfgang von Ohnesorge. *Phys. Fluids* **2011**, *23*, 127101.
52. Derby, B.; Reis, N.; Seerden, K.; Grant, P.S.; Evans, J. Freeform fabrication of ceramics by hot-melt ink-jet printing. *MRS Proc.* **2000**, *625*, 195.
53. Jang, D.; Kim, D.; Moon, J. Influence of Fluid Physical Properties on Ink-Jet Printability. *Langmuir* **2009**, *25*, 2629–2635.
54. Duineveld, P.C.; de Kok, M.M.; Buechel, M.; Sempel, A.; Mutsaers, K.A.; van de Weijer, P.; Camps, I.G.; van de Biggelaar, T.; Rubingh, J.-E.J.; Haskal, E.I. Ink-jet printing of polymer light-emitting devices. *Proc. SPIE* **2002**, *4464*, 59–67.
55. Stow, C.D.; Hadfield, M.G. An experimental investigation of fluid flow resulting from the impact of a water drop with an unyielding dry surface. *Proc. R. Soc. Lond. A Math. Phys. Eng. Sci.* **1981**, *373*, 419–441.
56. Bholra, R.; Chandra, S. Parameters controlling solidification of molten wax droplets falling on a solid surface. *J. Mater. Sci.* **1999**, *34*, 4883–4894.

57. Herran, C.L.; Coutris, N. Drop-on-demand for aqueous solutions of sodium alginate. *Exp. Fluids* **2013**, *54*, 1–25.
58. Fromm, J.E. Numerical calculation of the fluid dynamics of drop-on-demand jets. *IBM J. Res. Dev.* **1984**, *28*, 322–333.
59. Yarin, A.L. Drop impact dynamics: Splashing, spreading, receding, bouncing... . *Annu. Rev. Fluid Mech.* **2006**, *38*, 159–192.
60. Van Dam, D.B.; Le Clerc, C. Experimental study of the impact of an ink-jet printed droplet on a solid substrate. *Phys. Fluids* **2004**, *16*, 3403–3414.
61. Deegan, R.D.; Bakajin, O.; Dupont, T.F.; Huber, G.; Nagel, S.R.; Witten, T.A. Capillary flow as the cause of ring stains from dried liquid drops. *Nature* **1997**, *389*, 827–829.
62. Deegan, R.D.; Bakajin, O.; Dupont, T.F.; Huber, G.; Nagel, S.R.; Witten, T.A. Contact line deposits in an evaporating drop. *Phys. Rev. E* **2000**, *62*, 756.
63. Sun, J.; Bao, B.; He, M.; Zhou, H.; Song, Y. Recent advances in controlling the depositing morphologies of inkjet droplets. *ACS Appl. Mater. Interfaces* **2015**, *7*, 28086–28099.
64. Andrzejewska, E. Chapter 2 – Free Radical Photopolymerization of Multifunctional Monomers. *Micro and Nano Technologies* **2016**, 62-81.
65. Chatani, S.; Kloxin, C.J.; Bowman, C.N. The power of light in polymer science: photochemical processes to manipulate polymer formation, structure and properties. *Polym. Chem.* **2014**, *5*, 2187-2201.
66. Alamán, J.; López-Valdeolivas, M.; Alicante, R.; Medel, F.J.; Silva-Treviño, J.; Peña, J.I.; Sánchez-Somolinos, C. Photoacid catalyzed organic–inorganic hybrid inks for the manufacturing of inkjet-printed photonic devices. *J. Mater. Chem. C* **2018**, *6*, 3882–3894.
67. Shi, S.; Croutxé-Barghorn, C.; Allonas, X. Photoinitiating systems for cationic photopolymerization: Ongoing push toward long wavelengths and low light intensities. *Prog. Polym. Sci.* **2017**, *65*, 1-41.
68. Crivello J.V. Cationic polymerization—iodonium and sulfonium salt photoinitiators. *Adv. Polym. Sci.* **1984**, *62*, 1–48.
69. Crivello, J.V. The discovery and development of onium salt cationic photoinitiators. *J. Polym. Sci. A Polym. Chem.* **1999**, *37*, 4241–54.
70. Crivello, J.V.; Lam, J.Q.W. Diaryliodonium salts. A new class of photoinitiators for cationic polymerization. *Macromolecules* **1977**, *10*, 1307–15.
71. Crivello, J.V.; Lam, J.Q.W. A new preparation of triarylsulfonium and -selenonium salts via the copper(II)-catalyzed arylation of sulfides and selenides with diaryliodonium salts. *J. Org. Chem.* **1978**, *43*, 3055–8.
72. Crivello, J.V.; Lam, J.H.W. The Photoinitiated Cationic Polymerization of Epoxy Resins. *ACS Symp. Ser.* 1979, 114, 1-16.
73. Chemtob, A.; Versace, D.-L.; Belon, C.; Croutxé-Barghorn, C.; Rigolet, S. Concomitant organic-inorganic UV-curing catalyzed by photoacids. *Macromolecules* **2008**, *41*, 7390–7398.
74. Croutxé-Barghorn, C.; Belon, C.; Chemtob, A. Polymerization of hybrid sol-gel materials catalyzed by photoacids generation. *J. Photopolym. Sci. Technol.* **2010**, *23*, 129–134.
75. Chemtob, A.; Peter, M.; Belon, C.; Dietlin, C.; Croutxé-Barghorn, C.; Vidal, L.; Rigolet, S. Macroporous organosilica films via template-free photoinduced sol-gel process. *J. Mat. Chem.* **2010**, *20*, 9104-9112.
76. Chemtob, A.; Ni, L.; Dietlin, C.; Croutxé-Barghorn, C.; Kitzmann, P.; Brogly, M.; Vidal, L. Spontaneous photoinduced formation of hybrid polymer films with functionalized macroporous patterns. *Surf. Coat. Technol.* **2012**, *209*, 64–72.

77. Belon, C.; Chemtob, A.; Croutxé-Barghorn, C.; Rigolet, S.; Schmitt, M.; Bistac, S.; Le Houérou, V.; Gauthier, C. Nanocomposite coatings via simultaneous organic-inorganic photo-induced polymerization: synthesis, structural investigation and mechanical characterization. *Polym. Int.* **2010**, *59*, 1175-1186.
78. Brusatin, G.; Giustina, D.G.; Guglielmi, M.; Casalboni, M.; Proposito, P.; Schutzmann, S.; Roma, G. Direct pattern of photocurable glycidoxypropyltrimethosylsilane based sol-gel hybrid waveguides for photonic applications. *Mater. Sci. Eng. C* **2007**, *27*, 1022-1025.
79. Serra, A.; Ramis, X.; Fernández-Francos, X. Epoxy sol-gel hybrid thermosets. *Coatings* **2016**, *6*, 8.
80. Sanchez, C.; Lebeau, B.; Chaput, F.; Boilot, J.-P. Optical properties of functional hybrid organic-inorganic nanocomposites. *Adv. Mater.* **2003**, *15*, 1969–1994.
81. Houbertz, R.; Frohlich, L.; Popall, M.; Streppel, U.; Dannberg, P.; Bräuer, A.; Serbin, J.; Chichkov, B.N. Inorganic-Organic Hybrid Polymers for Information Technology: From Planar Technology to 3D Nanostructures. *Adv. Eng. Mater.* **2003**, *5*, 551–555.
82. Sanchez, C.; Belleville, P.; Popall, M.; Nicole, L. Applications of advanced hybrid organic–inorganic nanomaterials: From laboratory to market. *Chem. Soc. Rev.* **2011**, *40*, 696–753.
83. Parola, S.; Julian-Lopez, B.; Carlos, L.D.; Sanchez, C. Optical properties of hybrid organic-inorganic materials and their applications. *Adv. Funct. Mater.* **2016**, *26*, 6506–6544.
84. Danzebrink, R.; Aegerter, M.A. Deposition of micropatterned coating using an ink-jet technique. *Thin Solid Films* **1999**, *351*, 115–118.
85. Danzebrink, R.; Aegerter, M.A. Deposition of optical microlens arrays by ink-jet processes. *Thin Solid Films* **2001**, *392*, 223–225.
86. Popovic, Z.D.; Sprague, R.A.; Connell, G.N. Technique for monolithic fabrication of microlens arrays. *Appl. Opt.* **1988**, *27*, 1281–1284.
87. Voigt, A.; Ostrzinski, U.; Pfeiffer, K.; Kim, J.Y.; Fakhfour, V.; Brugger, J.; Gruetzner, G. New inks for the direct drop-on-demand fabrication of polymer lenses. *Microelectron. Eng.* **2011**, *88*, 2174–2179.
88. Xie, D.; Zhang, H.; Shu, X.; Xiao, J. Fabrication of polymer micro-lens array with pneumatically diaphragm-driven drop-on-demand inkjet technology. *Opt. Express* **2012**, *20*, 15186–15195.
89. Fakhfour, V.; Cantale, N.; Mermoud, G.; Kim, J.Y.; Boiko, D.; Charbon, E.; Brugger, J. Inkjet printing of SU-8 for polymer-based MEMS a case study for microlenses. In Proceeding of the 21st IEEE International Conference on Micro Electro Mechanical Systems, Tucson, AZ, USA, 13–17 January 2008; pp. 407–410.
90. Chen, C.T.; Chiu, C.L.; Tseng, Z.F.; Chuang, C.T. Dynamic evolution and formation of refractive microlenses self-assembled from evaporative polyurethane droplets. *Sens. Actuators A Phys.* **2008**, *147*, 369–377.
91. Chen, C.T.; Tseng, Z.F.; Chiu, C.L.; Hsu, C.Y.; Chuang, C.T. Self-aligned hemispherical formation of microlenses from colloidal droplets on heterogeneous surfaces. *J. Micromech. Microeng.* **2009**, *19*, 025002.
92. Chen, F.C.; Lu, J.P.; Huang, W.K. Using ink-jet printing and coffee ring effect to fabricate refractive microlens arrays. *IEEE Photonics Technol. Lett.* **2009**, *21*, 648–650.
93. Jacot-Descombes, L.; Gullo, M.R.; Cadarso, V.J.; Brugger, J. Fabrication of epoxy spherical microstructures by controlled drop-on-demand inkjet printing. *J. Micromech. Microeng.* **2012**, *22*, 074012.

94. Cadarso, V.J.; Perera-Núñez, J.; Jacot-Descombes, L.; Pfeiffer, K.; Ostrzinski, U.; Voigt, A.; Llobera, A.; Grützer, G.; Brugger, J. Microlenses with defined contour shapes. *Opt. Express* **2011**, *19*, 18665–18670.
95. Blattmann, M.; Ocker, M.; Zappe, H.; Seifert, A. Jet printing of convex and concave polymer micro-lenses. *Opt. Express* **2015**, *23*, 24525–24536.
96. Biehl, S.; Danzebrink, R.; Oliveira, P.; Aegerter, M.A. Refractive microlens fabrication by ink-jet process. *J. Sol-Gel Sci. Technol.* **1998**, *13*, 177–182.
97. Kim, J.Y.; Brauer, N.B.; Fakhfour, V.; Boiko, D.L.; Charbon, E.; Grutzner, G.; Brugger, J. Hybrid polymer microlens arrays with high numerical apertures fabricated using simple ink-jet printing technique. *Opt. Mater. Express* **2011**, *1*, 259–269.
98. Kim, J.Y.; Pfeiffer, K.; Voigt, A.; Gruetzner, G.; Brugger, J. Directly fabricated multi-scale microlens arrays on a hydrophobic flat surface by a simple ink-jet printing technique. *J. Mater. Chem.* **2012**, *22*, 3053–3058.
99. Kim, J.Y.; Martin-Olmos, C.; Baek, N.S.; Brugger, J. Simple and easily controllable parabolic-shaped microlenses printed on polymeric mesas. *J. Mater. Chem. C* **2013**, *1*, 2152–2157.
100. Cox, W.R.; Guan, C.; Hayes, D.J.; Wallace, D.B. Microjet printing of micro-optical interconnects. *Int. J. Microcircuits Electron. Packag.* **2000**, *23*, 346–352.
101. Cox, W.R.; Guan, C.; Hayes, D.J. Microjet printing of micro-optical interconnects and sensors. *Proc. SPIE Optoelectron. Interconnects VII: Photonics Packaging and Integration II* **2000**, 3952, 400–407.
102. Hayes, D.J.; Chen, T. Next-generation optoelectronic components enabled by direct-write microprinting technology. *Def. Secur.* **2004**, 5435, 83–90.
103. Cox, W.R.; Chen, T.; Ussery, D.; Hayes, D.J.; Tatum, J.A.; MacFarlane, D.L. Microjetted lenslet triplet fibers. *Opt. Commun.* **1996**, *123*, 492–496.
104. Tien, C.H.; Hung, C.H.; Yu, T.H. Microlens arrays by direct-writing inkjet print for LCD backlighting applications. *J. Disp. Technol.* 2009, *5*, 147–151.
105. Wang, M.W.; Pang, D.C.; Tseng, Y.E.; Tseng, C.C. The study of light guide plate fabricated by inkjet printing technique. *J. Taiwan Inst. Chem. E.* 2014, *45*, 1049–1055.
106. Cox, W.R.; Chen, T.; Hayes, D.J. Micro-Optics Fabrication by Ink-jet Printing. *Opt. Photonics News* **2001**, *12*, 32–35.
107. Wallace, D.; Hayes, D.; Chen, T.; Shah, V.; Radulescu, D.; Cooley, P.; Nallani, A. Think additive: Ink-jet deposition of materials for MEMS packaging. In Proceedings of the 6th Topical Workshop on Packaging of MEMS and Related Micro-Nano-Bio Integrated Systems, Long Beach, CA, USA, 18–20 November 2004.
108. Chappell, J.; Hutt, D.A.; Conway, P.P. Variation in the line stability of an inkjet printed optical waveguide-applicable material. In Proceedings of the 2nd Electronics System-Integration Technology Conference, Greenwich, UK, 1–4 September 2008; pp. 1267–1272.
109. Sum, T.; Bettiol, A.A.; van Kan, J.A.; Pun, E.Y.B.; Tung, K.K.; Watt, F. Proton beam wiring of low-loss optical waveguides. *Appl. Phys. Lett.* **2003**, *83*, 1707–1709.
110. Borreman, A.; Musa, S.; Kok, A.; Diemeer, M.; Driessen, A. Fabrication of polymeric multimode waveguides and devices in su-8 photoresist using selective polymerization. In Proceedings Symposium IEEE/LEOS Benelux Chapter, Amsterdam, 2002.
111. Vacirca, N.A.; Kurzweg, T.P. Inkjet printing techniques for the fabrication of polymer optical waveguides. *Proc. SPIE Int. Soc. Opt. Photonics* **2010**, 7591, 75910A.
112. Yoon, K.B. Low-loss multimode waveguides using organic-inorganic hybrid materials. *Macromol. Res.* **2004**, *12*, 290–292.

113. Stumpel, J.E.; Wouters, C.; Herzer, N.; Ziegler, J.; Broer, D.J.; Bastiaansen, C.W.M.; Schenning, A.P.H.J. An Optical Sensor for Volatile Amines Based on an Inkjet-Printed, Hydrogen-Bonded, Cholesteric Liquid Crystalline Film. *Adv. Opt. Mater.* **2014**, *2*, 459–464.
114. Schuhmacher, B.; Muschenborn, W.; Stratmann, M.; Schultrich, B.; Klages, C.-P.; Kretschmer, M.; Seyfert, U.; Forster, F.; Tiller, H.-J. Novel coating systems and surface technologies for continuous processing of steel sheet. *Adv. Eng. Mater.* **2001**, *3*, 681–689.
115. Davies, D.J.D.; Vaccaro, A.R.; Morris, S.M.; Herzer, N.; Schenning, A.P.H.J.; Bastiaansen, C.W.M. A Printable Optical Time-Temperature Integrator Based on Shape Memory in a Chiral Nematic Polymer Network. *Adv. Funct. Mater.* **2013**, *23*, 2723–2727.



PAPERS

1. Publication 1.

Journal: Materials

Title: Inkjet Printing of Functional Materials for Optical and Photonic Applications

Review

Inkjet Printing of Functional Materials for Optical and Photonic Applications

Jorge Alaman^{1,2}, Raquel Alicante¹, Jose Ignacio Peña³ and Carlos Sánchez-Somolinos^{1,*}

¹ Departamento de Física de la Materia Condensada, Instituto de Ciencia de Materiales de Aragón (ICMA), CSIC-Universidad de Zaragoza, C./Pedro Cerbuna 12, Zaragoza 50009, Spain; jorge.alaman@bshg.com (J.A.); raquela@unizar.es (R.A.)

² BSH, Polígono Industrial de PLA-ZA, Ronda del Canal Imperial de Aragón, 18-20, Zaragoza 50197, Spain

³ Departamento de Ciencia y Tecnología de Materiales y Fluidos, Instituto de Ciencia de Materiales de Aragón (ICMA), CSIC-Universidad de Zaragoza, C./María de Luna 3, Zaragoza 50018, Spain; jipena@unizar.es

* Correspondence: carlos.s@csic.es; Tel.: +34-876-553-770

Academic Editor: Dirk Poelman

Received: 21 September 2016; Accepted: 4 November 2016; Published: 10 November 2016

Abstract: Inkjet printing, traditionally used in graphics, has been widely investigated as a valuable tool in the preparation of functional surfaces and devices. This review focuses on the use of inkjet printing technology for the manufacturing of different optical elements and photonic devices. The presented overview mainly surveys work done in the fabrication of micro-optical components such as microlenses, waveguides and integrated lasers; the manufacturing of large area light emitting diodes displays, liquid crystal displays and solar cells; as well as the preparation of liquid crystal and colloidal crystal based photonic devices working as lasers or optical sensors. Special emphasis is placed on reviewing the materials employed as well as in the relevance of inkjet in the manufacturing of the different devices showing in each of the revised technologies, main achievements, applications and challenges.

Keywords: inkjet printing; functional materials; optical applications; photonic devices; microlenses; OLEDs; solar cells; liquid crystals; colloidal crystals; sensors

1. Introduction

Printing methods which allow inks to be precisely deposited have traditionally been used to reproduce written text and graphic works. Printing techniques have strongly fuelled information and knowledge conservation and spreading, ensuring the survival of ideas decisively contributing to progress of civilisation [1]. From cave painting to modern digital printing technologies, the development of ink deposition techniques has significantly evolved through centuries trying to adapt to existing needs and exploiting technological developments of each period. Among these technologies, inkjet printing has gained interest over the last decades due to its ability to digitally control the ejection of ink droplets of defined volume and precisely position them onto a substrate. Compared to analogical methodologies such as flexography, in which the use and preparation of complicated printing plates are needed, digital inkjet printing allows for the quick preparation of different designs with reduced cost becoming a very flexible tool for customisation.

Although the traditional and most wide use of inkjet printing has been centred in conventional applications such as graphics, text printing or marking, the ability to accurately position picoliter volumes of a large range of materials under digital control has been more recently exploited to pattern and manufacture novel functional surfaces and devices (Figure 1). Patterning at small length scales of materials with semiconducting, conducting, luminescent or magnetic functionalities has demonstrated

to be a key element to implement emerging technologies and applications such as electronic devices or displays, sensors, bio-arrays, radio frequency identifiers (RFIDs) or solar cells [2–4].

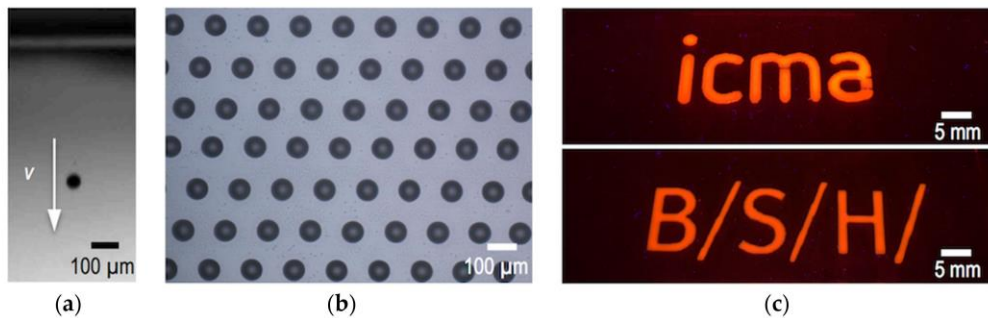


Figure 1. Inkjet printing process: (a) Picoliter volume ink droplets are generated and fly towards the substrate at speed v ; (b) Droplets are precisely deposited onto a surface; (c) Inclusion of functional materials (e.g., luminescent) leads to functional prints or structures.

Being an additive method, all the deposited material, except volatile carriers or by-products, is used in the final patterned surface or device, not needing any additional etching step and therefore using materials very efficiently. As a result, inkjet printing is an environmentally friendly technique. Besides, inkjet printing is a non-contact method so there is a large flexibility in the use of substrates of different materials, sizes, even non-flat or flexible ones. Despite inkjet printing is a serial process, it is a scalable technology able to deliver high throughput. For example, multiple printheads, each having a large number of nozzles ejecting at very high frequencies can be used, allowing multi-ink wide print-width with a single pass leading to a high productivity. Differently from other conventional printing processes, inkjet printing, as a digital technique, enables in-line correction of defects or distortions, by automatically adjusting the printing configuration of nozzles when a defect is detected, what is critical to obtain productions at high yield in certain defect-sensitive applications. In addition, inkjet printing is compatible with roll to roll (R2R) processing and can be effectively combined with other existing techniques such as gravure, screen-printing, offset lithography or flexography to optimize the production process.

After introducing some fundamental aspects of the inkjet printing process, this review will present an up-to-date overview of the use of inkjet printing in the implementation of different optical elements and photonic devices. In each of the reviewed technologies, main achievements attained, applications and remaining challenges to solve will be discussed.

In particular, a review of the use of inkjet printing in the preparation of microlenses, which are able to couple light in and out optical fibres or to beam shape the light from diode lasers, among other applications, will be presented. Efforts made in the use of inkjet printing in the implementation of waveguides and integrated splitters will also be surveyed.

Special attention will then be devoted to the role of inkjet printing in the field of large area photonic devices, such as organic light emitting diodes (OLED), liquid crystal displays (LCDs) or solar cells. According to the 2015th Roadmap of the Organic and Printed Electronics Association (OE-A), the market for organic and printed electronics was 23–24 billion US\$ in 2014 with a predicted increase of 20% in the next years [5]. Development of this application field relies on the effective integration of dielectric, semiconductors and conductive materials over large, flexible substrates leading to thin, light-weight, flexible, even rollable devices with reduced cost and waste of material. Within this large area electronics arena, inkjet printing appears to be a key enabler technology for the cost-effective and high quality manufacturing of the previously mentioned devices with good reliability and yield.

Finally, an overview on the combination of inkjet printing with self-organizing materials, such as colloidal inks containing monodisperse microspheres or liquid crystals, will be presented.

The preparation of different photonic devices, mainly comprising periodic structures, and its application as lasers or sensors will also be highlighted.

2. The Physics of Inkjet Printing: Drop Formation, Deposition and Fixation

The inkjet printing process essentially consists of the ejection of ink droplets of controlled properties and their precise deposition and fixation on a target substrate [3,6–10].

2.1. Drop Formation

Two major approaches are usually employed for the generation of ink droplets: Continuous Inkjet (CIJ) printing and Drop on Demand (DOD) inkjet printing (Figure 2). CIJ makes use of the Rayleigh instability to generate a continuous column of droplets that are selectively steered to position them on a target substrate (Figure 2a). Steering is done by the application of a voltage to the ejecting nozzle with respect to ground. When no printing is required the droplets are directed towards a reservoir where the ink is collected and potentially recycled. On the other hand, DOD inkjet printing generates a pressure impulse in the fluid within the printhead able to cause ejection of a droplet at the nozzle that is placed just above the target location of the substrate. Without pressure pulse, the liquid stays at the printhead retained at the nozzle by surface tension forces. The pressure impulse can be generated by the sudden formation and collapse of vapour bubbles at a current induced heating element placed close to the nozzle (Figure 2b). Despite this technology, named Thermal DOD, has become quite popular in many desktop printers, most of the industrial printers and most of the work carried out on functional material printing has been done using piezoelectric technology so this review will mainly focus on this last. This ejection method makes use of a piezoelectric element placed in contact with the fluid cavity (Figure 2c). The voltage applied to the piezoelectric generates a sudden deformation of the fluid cavity and induces a pressure impulse, origin of the ejected drop. With this method, droplets with sizes in the range of the nozzle orifice diameter, typically tens of micrometres, and linear speeds of few metres per second are typically generated at frequencies of 1 to 20 kHz.

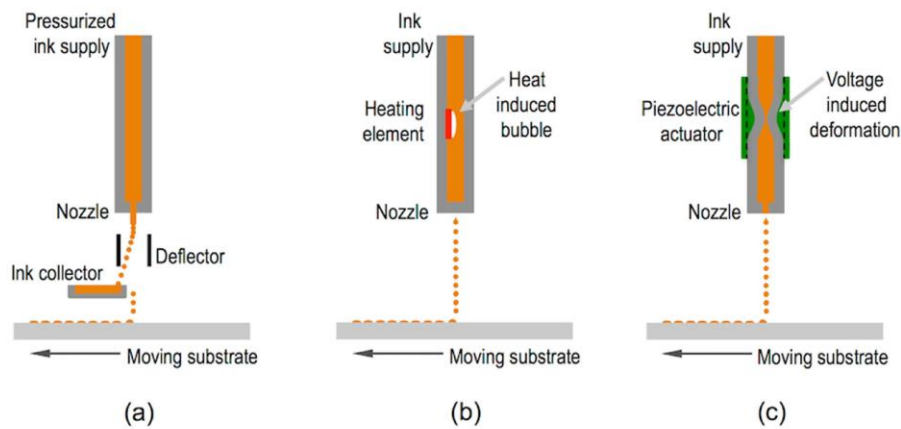


Figure 2. Schematic representation of (a) continuous inkjet (CIJ) and Drop on demand (DOD) inkjet printing systems using (b) thermal and (c) piezoelectric technology.

As mentioned, for industrial production purposes, printheads have a large number of nozzles, usually hundreds or thousands, that will eject ink droplets. For research purposes, printheads can be as simple as one single nozzle actuated by one single piezoelectric element. Although for practical large area applications single nozzle printheads are not useful and multi-head multi-nozzle inkjet systems are needed, the simplicity of the device helps to understand the underlying physics of the drop formation process so this configuration will be detailed in this section. Figure 3a shows a common

fluid tubular cavity geometry consisting of a glass tube with a nozzle and an orifice at one end, and a connection to a supply tube, generally of larger diameter, at the other extreme. The glass capillary has a tubular piezoelectric element bonded around with electrodes in the inner and outer surfaces of the piezo material. In the simplest case, a trapezoidal voltage piezo excitation as the one shown in Figure 3b is used. Initially voltage quickly increases from zero to a voltage V during a short period of time t_{rise} . After this, voltage is kept during t_{dwell} and finally it decreases to zero voltage, with t_{fall} being the time needed for this voltage to drop from V to zero.

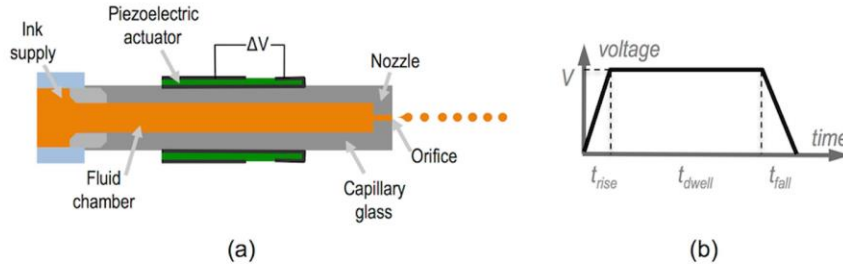


Figure 3. (a) Detailed schematic structure of a piezoelectric single nozzle printhead and (b) trapezoidal voltage piezoelectric excitation.

The initial voltage rise produces a fast enlargement of the cavity and a subsequent local pressure reduction of the fluid inside. If we assume no dispersion, this negative pressure perturbation can be modelled as splitting into two waves of half the initial amplitude that propagate with no deformation in opposite directions to both ends of the cavity at the speed of acoustic waves propagation in the fluid, as shown in Figure 4. Since the cavity enlarges its diameter at the supply end, we can assume an open-end boundary condition for this part of the cavity with the negative pressure being reflected with a π phase shift turning into a positive pressure pulse of the same amplitude and speed but propagating in opposite direction towards the nozzle end. This nozzle end, on the other hand, can be modelled as a closed-end since the orifice diameter is small compared with the inner diameter of the cavity, so there is no phase shift in the reflection, being the resultant reflected pressure perturbation a negative pressure wave of same amplitude propagating towards the supply end [11,12]. While the voltage is kept during t_{dwell} , no new pressure perturbation is introduced in the system. However, the final voltage drop introduces the opposite effect of the initial rise generating a quick decrease of the cylinder radius and therefore a positive pressure perturbation in the fluid that will propagate along the cavity and reflect at the cavity ends following the same described reflection rules at the cavity boundaries. Each time a positive pressure perturbation reaches the orifice end, if sufficient kinetic energy is provided to the fluid to overcome surface tension that retains the fluid within the tube, a column of ink leaves the cavity and a drop can eventually be formed.

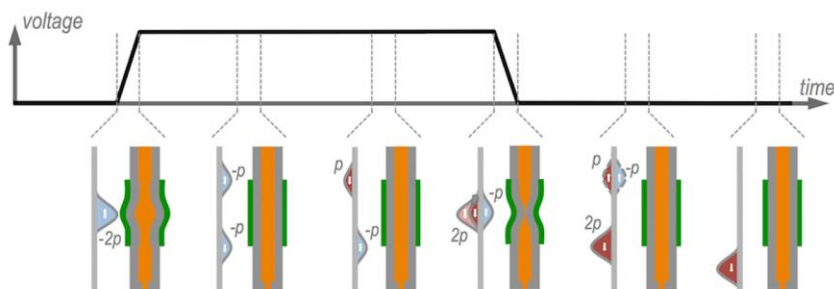


Figure 4. Pressure perturbation generation, propagation and reflection upon trapezoidal voltage application.

It has been experimentally observed that the drop formation process and ejected drop characteristics strongly depend on the pulse characteristics [11,13,14]. Short t_{rise} and t_{fall} times, in the order of few microseconds, are needed to have jet formation. Also voltage needs to be sufficient so the kinetic energy provided to the fluid at the orifice is enough to create new surface in the fluid and to finally generate a droplet. In addition, for a given cavity length, there is an optimum t_{dwell} for which the ejected drop velocity is maximum. This last optimal situation happens when the pulse is such that the final fluid compression (due to the final voltage drop) takes places when the reflected wave originated from the initial fluid expansion (due to initial voltage rise) passes through the piezo location in the middle point of the cavity. As schematically described in Figure 4, the positive pressure perturbation generated at this point cancels the negative pressure wave coming from the orifice end and reinforces the positive pulse coming from the supply end. As a result of this sequence of events only a double amplitude pressure perturbation travels towards the nozzle with no other residual perturbations within the cavity.

As mentioned, the picture described above assumes no energy dissipation of the fluid; however, in real systems, damping due to viscosity, non-ideal reflection and energy losses due to ejected droplets result in amplitude decrease of the pressure waves. The previous model also assumes an initial constant pressure within the cavity that is not the case when ejection of drops is periodically done. In this case, when subsequent pulses are applied, residual pressure waves, originated from previous piezo excitations, travel back and forth between the ends of the cavity. Optimum frequencies can be periodically found if the residual pressure from previous pulses is synchronized with newly created pressure waves being needed, as a result, smaller voltages for drop formation [11,12,15–17]. In industrial printers, cavity geometry and voltage actuating pulse are carefully designed to avoid pressure wave reflections reducing in this way this frequency dependence [12].

Besides the acoustics of the printhead and the voltage driven piezo actuation, which confers energy to the leaving column of ink, fluid properties such as surface energy, viscosity and density, strongly influence the process of drop formation after jet ejection. These magnitudes can be combined in a series of nondimensional numbers. While the Reynolds number (Re) relates inertial forces with viscosity (Equation (1)), the Weber number (We) compares kinetic energy with respect to surface energy of the moving fluid when the jet arises at the orifice (Equation (2)):

$$Re = \frac{v\rho a}{\eta} \quad (1)$$

$$We = \frac{v^2\rho a}{\gamma} \quad (2)$$

where v is the speed of the droplet, η is the viscosity, γ the surface tension, ρ is the density of the fluid and a the orifice diameter.

In order to eject well-controlled drops of material, the leaving jet needs to thin and break up after leaving the nozzle (Figure 5). This thinning, which is driven by surface tension forces, is balanced by viscous and inertial forces. For Newtonian liquids with a sufficiently high viscosity, the surface tension that induces jet squeezing is opposed by the viscous stresses within the filament. On the other hand, for liquids of low viscosity, the inertia of the accelerating fluid within the jet is the one opposing the thinning of the jet [18,19].

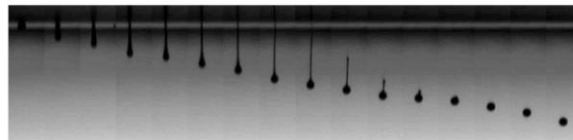


Figure 5. Sequence of photographs showing the drop formation process using a piezoelectric printhead of a hybrid organic-inorganic ink with a small amount of polymeric additive. The time interval between two adjacent frames is 5 μs .

Wolfgang von Ohnesorge introduced, well before the advent of inkjet printing, a new dimensionless grouping of numbers to understand and define the different regimes found for the jet breaking after it leaves the orifice. The Ohnesorge number Oh (Equation (3)) eliminates the speed of the drop and therefore depends only on the intrinsic physical properties of the fluid and the dimensions of the ejecting orifice (usually similar to the drop diameter):

$$Oh = \frac{\sqrt{We}}{Re} = \frac{\eta}{\sqrt{\gamma\rho a}} \tag{3}$$

The underlying physics behind this number can be better understood by seeing the expression above as the ratio of jet thinning characteristic times of a fluid of high viscosity ($t_\eta \sim \eta a/\gamma$), whose thinning is governed by viscous effects, and that of an inviscid liquid ($t_\rho \sim \sqrt{\rho a^3/\gamma}$), dominated by inertial effects (Equation (4)) [18,20].

$$Oh = \frac{t_\eta}{t_\rho} = \frac{\eta a/\gamma}{\sqrt{\rho a^3/\gamma}} \tag{4}$$

It is known from experimental studies that stable drop ejection typically takes place for certain range of Oh numbers, between 0.1 and 1 according to Reis and co-workers [21]. Slightly narrower range was given by Moon with Oh numbers, between 0.07 and 0.25 [22]. Regardless of the chosen limits, for too large Oh numbers, viscous forces dissipate the pressure perturbation precluding drop formation. On the other side, too low Oh numbers usually lead to columns of fluid leaving the nozzle that finally break into a main drop accompanied by drop satellites.

As said above, the Oh number does not depend on the velocity of the drop, however kinetic energy of the fluid is determinant for a successful drop formation and printing. On one side, a certain threshold of kinetic energy must be transferred to the jet to overcome the surface energy required to generate the droplet. As quantified by Duineveld and co-workers, We numbers should be higher than 4 in order to have ejection ($We > 4$) [7,23]. On the other side, and related to the landing of the droplet on the substrate, the energy should be low enough to avoid splashing of the fluid when reaching the substrate [24]. This condition has been quantified with the following inequality (Equation (5)) for smooth surfaces [7,24,25]:

$$(We)^{1/2} (Re)^{1/4} < 50 \tag{5}$$

This set of limits for Oh , We and Re dimensionless numbers allows us to delimitate the properties of fluids that can be printable by using inkjet as schematically presented in Figure 6.

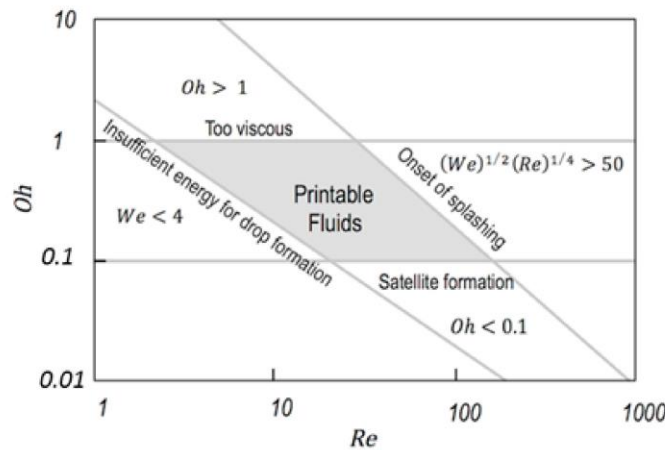


Figure 6. Parameter space of inkjet printable fluids [20].

The discussion above has been centred in fluids with Newtonian properties, however it is quite common the inclusion in inks of small amounts of high molecular weight polymers to improve the printability of fluids. In this way, satellites typically formed during jetting of low viscosity fluids can be sometimes suppressed by incorporating viscoelasticity to the ink (see Figure 5). Besides surface tension, viscosity and fluid inertia, the elasticity arising from extensional deformation of the polymer chains within the fluid needs then to be taken into consideration [26–28]. Additional dimensionless numbers need to be defined in order to account for all the relevant aspects of the fluid dynamics. For example, the Deborah number (De) establishes the ratio between elastic and inertial forces in a thinning filament, while the Elastocapillary number (Ec) relates the elastic and viscous ones [18,29]. Going back to the previously mentioned example of the addition of traces of polymers to inviscid inks, this makes the De number to increase above certain threshold and turns the material into printable despite the Oh number is not within the established values of printability for Newtonian fluids of Figure 6. As more demanding applications and accurate dispensing of more complex fluids, such as polymeric solutions or colloids with complex rheological properties, are required, the phenomenology and its description in terms of fluid properties becomes increasingly difficult and challenging making the applied field of inkjet printing a challenging playground for basic research of Physics of Fluids.

Concerning the size of the formed drop after filament breaking, it is dictated not only by the fluid ejection conditions but also by intrinsic properties of the fluid. It has been experimentally observed that drop volume increase with decreasing Oh numbers [12], being this fact consistent with the modelling predictions of Fromm [30]. Besides, drop volume can also be controlled by printhead pressure pulse excitation being larger for larger applied voltages [30]. Firing consecutive drops of the same size that fuse together in fly before they reach the substrate is also used to modulate drop volume, a technique that is named greyscale printing. Going back to the voltage excitation pulse, beyond the simple trapezoidal positive one, more complex waveforms, consisting of sequences of positive and negative voltage trapezoidal wave excitations have allowed us to gain control of drop quality, velocity and size. The pinch off of the fluid column from the nozzle can be induced by a properly designed driving waveform generating a negative pressure in the fluid cavity [31]. Fine adjustment of pulse wave parameters allows us to influence the leaving fluid at all the stages of the drop formation process, being also possible a significant reduction of drop diameter with respect to nozzle dimensions [32,33].

2.2. Drop Deposition on the Substrate and Ink Fixation

After leaving the nozzle, the droplet flies towards the target substrate. In order to turn flying droplets into a functional device or surface, they need to be precisely positioned on a substrate. During flight, drops lose kinetic energy due to drag of the atmosphere being the positioning of droplets sensitive to air currents that may change the target positioning [23]. For typical inkjet drop sizes and speeds, significant drop speed reduction takes places in distances of the order of few mm. As a consequence, the nozzles should be positioned at distances between 1 and 2 mm to the substrate in order to have precise positioning of the ink on it. This deceleration is more pronounced for smaller size drops and therefore closer distances between nozzle and substrate are required being this an intrinsic limitation of the resolution and printing quality of inkjet technology [34].

The drop finally reaches the target substrate and its behaviour and the underlying mechanism after impact can be again understood by performing nondimensional analysis using We , Re and Oh numbers [35]. For the usual inks and conditions of inkjet printing with droplets of diameter of tens of microns impacting with speeds of few metres per second, gravitational effects can be neglected and splashing is not expected to happen. The drop initially spreads just after impact being this behaviour controlled by inertial forces (impact driven regime). The kinetic energy of the drop is transformed into surface energy by spreading over the dry substrate. After the spreading there is a surface tension driven retraction of the extended drop followed by oscillations of the droplet in which energy is dissipated by viscous forces taking more and more importance capillary forces (capillary driven regime) until the deposited drop reaches the stationary shape that is dictated by surface energy forces [7,36]. As a

result, the size of the relaxed deposited drop, and therefore the resolution of inkjet printing technique depends on the size of the ejected drop and the equilibrium contact angle of the ink on the substrate. Since gravitational effects are negligible, the shape of the deposited drop is accurately modelled to that of a spherical cap with base equilibrium diameter d_{eq} given by [37]:

$$d_{eq} = d_0 \left(\frac{8}{\tan \frac{\theta_{eq}}{2} \left(3 + \left(\tan \frac{\theta_{eq}}{2} \right)^2 \right)} \right)^{1/3} \quad (6)$$

being θ_{eq} the equilibrium contact angle and d_0 the initial droplet diameter (Figure 7).

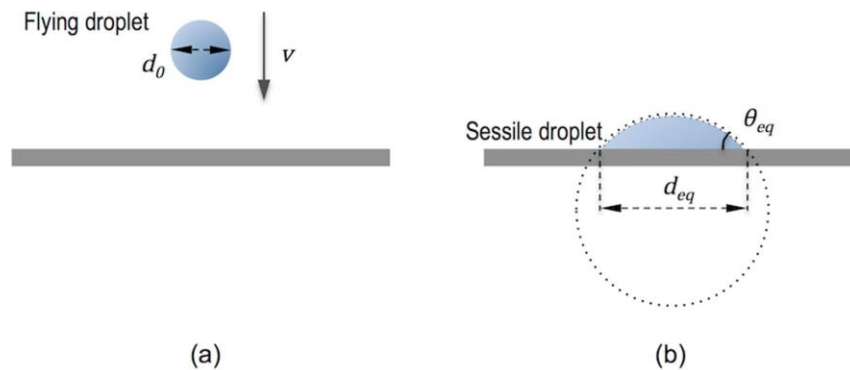


Figure 7. (a) Flying and (b) sessile droplet dimensions.

High resolution inkjet printheads can produce drops with a volume in the range of one picoliter that corresponds to a diameter of about 10 microns. With a typical equilibrium contact angle of 30° , this flying drop size typically leads to resolutions in the order of 30 microns. As mentioned above, the size can be diminished by adjusting the driving voltage and/or using printheads of smaller nozzle diameter [38]. However, going below 10 microns is problematic not only because clogging is each time much easier to happen but also because such small droplets are quickly decelerated so precise placement becomes more difficult, as mentioned above [23,34].

Beyond the printing of isolated dots, functional devices need also continuous printed tracks or areas so individual droplets have to be overlapped and the resultant features should be stable to maintain their shape and functionality. When drops of ink are deposited along a line, each overlapping with the previously deposited one, they coalesce into a single liquid bead. If the bead has a freely moving contact line it will be inherently unstable as a jet of water experiences a Rayleigh instability. Conversely, for the case of pinned contact line, the bead can be stable if the contact angle is below 90° [39,40]. Experimental studies carried out by Soltman and coworkers, printing adjacent dots of a water-soluble polyelectrolyte system consisting of poly(3,4-ethylenedioxythiophene) and poly(styrene-sulfonic acid) (PEDOT:PSS), fall within this case since this ink shows zero receding contact angle with the substrate [41]. A rich phenomenology was observed when varying the distance between sequentially ejected drops that is common for many other sets of inks and substrates (Figure 8). For large distances between drops, such that they do not interact on spreading, the individual printed droplets appear as a linear train of dots (Figure 8a). As the distance between printed dots becomes smaller, drop coalescence takes place, forming a line with a rounded contour, reminiscent of the individual contact lines of the original landed droplets (Figure 8b). If drop spacing is further decreased, the undulated contact lines disappear and a transition to parallel side edges is observed (Figure 8c). As mentioned above, for the length scales of inkjet printed drops, gravitational effects can be neglected so the profile of these parallel side edges liquid lines can be modelled in this case as a circular segment

determined by the contact angle as done by Stringer and Derby [42–44]. If spacing decreases even more, line widening can occur however eventually a bulging instability with regions that outflow the line and other where the line remains uniform might appear (Figure 8d). The appearance of this bulging instability revealed to be deposition rate dependent, as demonstrated by Duineveld [45]. Rapid rate deposition of the liquid in the line produces a local increase of the contact angle that exceeds the advancing contact angle, producing spreading out of the line and therefore a bulge.

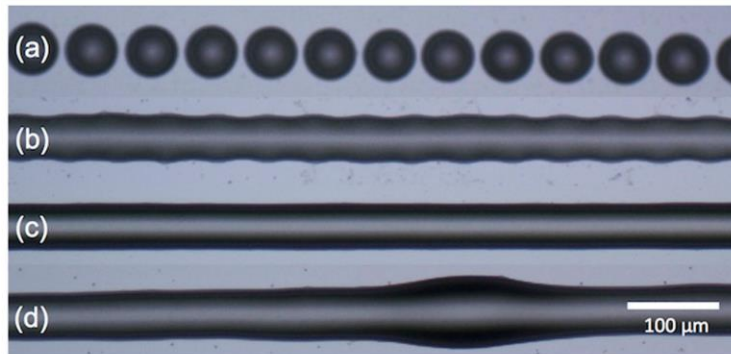


Figure 8. Droplets deposited along a line with decreasing distance between adjacent drops (from a to d) showing different behaviours: (a) isolated dots; (b) line with rounded contour; (c) line with straight contour and (d) line bulging.

Continuous surfaces are also essential features in the preparation of different functional devices such as OLEDs, solar cells or sensors. As in the case of lines, the printed features need to be well defined. Some inks show strong spreading when applied to substrates so the contours of features are not regular or the details are lost. In these cases, the material can be confined by barriers, applied for example photolithographically, limiting the spreading of the ink and therefore defining the contour of the printed features [23,46]. On the other hand, inkjet printing of squared shaped features, with inks showing partial wetting on a flat substrate, has also been studied by several authors. For example, Tekin and coworkers identified that sequential printing of spatially offset dot matrices covering the whole area can lead to continuous and homogeneous thickness polymeric films if solvents and printing speed are set properly [47]. Seeking also the formation of well-defined rectangular films, Kang, Soltman and coworkers studied different printing schemes. The search of conditions, for example line spacing or line printing sequence, that lead to a liquid bead having a contact angle smaller than the advancing and larger than the receding contact angle is pursued in order to avoid bulging and dewetting respectively, and therefore poor quality in the rectangular film definition [48,49]. These deleterious effects can be overcome by using printing algorithms in which areas are not printed by sequential application of equidistant dots forming lines that later coalesce into areas but sequences of prints heterogeneously distributed in the substrate, a methodology that contributes to have contact angle under control between the limits, therefore keeping well-defined feature shape [49].

Once the ink has been applied, the liquid needs eventually to turn into a solid to effectively implement functional elements and devices. Inks based on waxes, for example, lead to stable features upon a phase transition to the solid state. Inks comprising photopolymerizable monomers can be fixed by its exposure to actinic light. In other cases, inks are polymer solutions or particle dispersions in a solvent. The solvent is, in these last cases, just a carrier for the functional material, and it disappears after evaporation. In this type of inks, the drying process needs to be carefully analysed in order to have the desired quality of the prints.

When a drop of a pure solvent is deposited on a substrate with a smooth surface, evaporation will lead to a continuous reduction of the contact angle until the receding contact angle is reached and the diameter of the deposited drop start to decrease. If the surface is rough the contact line is pinned

so that, as evaporation proceeds, the contact angle decreases; however, the droplet does not retract. In case the solvent carries a solid phase, such as a polymer or a small amount of dispersed particles, evaporation of the applied drop, leads to a deposited ring of material with the dimensions of the initial drop. This solid phase at the contact line can prevent the liquid to recede, pinning the droplet to its initial size and controlling in this way the size of the final deposit. However, as evaporation further proceeds in the edge, the loss of liquid in this region can be compensated, as explained by Deegan and coworkers, by flow of liquid from the inner part of the droplet bringing more solid material to the edge where it deposits, what is known as the “coffee stain effect” [50–52]. Although this circular ring accumulation of material can be seen as an opportunity for patterning of materials [53,54], usually it has been found as a limitation since it results in poorer device performance [55]. The use of solvent mixtures has demonstrated to be a powerful tool to control the flow of solids and sometimes inhibit the formation of the solid phase ring [47,56]. For example, the use of a mixture of two solvents, one of them having higher boiling point and lower surface tension than the other can lead to a flow that compensates the evaporation induced flow towards the edge described above. The larger evaporation of the highly volatile solvent in the outer part of the deposited droplet generates a compositional gradient in the radial direction and therefore a surface tension gradient. This can generate a Marangoni flow that inhibits the formation of the ring leading in certain cases to a homogeneous deposit [55,57].

3. Inkjet Printing for Micro-Optics and Integrated Optics Fabrication

Despite the origins of micro-optics going back a long way (more than two centuries) with the first studies on diffractive gratings by Rittenhouse, later more systematically described by Fraunhofer, it has only been in the last three decades when micro-optics has gained entity and a name as a clear subdiscipline of Optics. Classical passive optical elements such as lenses or mirrors were miniaturized into micro-optical elements, such as microlenses or micromirrors, by the use of well-established photolithographic techniques due to the huge development of the semiconductor industry. Beyond gratings and microlenses, micro-optics has intimately merged with other disciplines of Optics over the last decades. Seeking miniaturisation of optical technologies, micro-optical systems have been integrated together with lasers, LEDs, sensors or fibre communication systems. Nowadays, many optical microsystems rely on combination of micro-optics (usually referring to free-space optical elements) and guided wave optics with the interface between both disciplines blurred. Being at the intersection of many different technologies, advances in micro-optics can broaden the scope of a wide variety of optical microsystems applications [58].

Focusing on micro-optics, the Physics to describe classical optical elements, such as cm sized lenses or mirrors, is exactly the same as that used in homologous micro-optical components, with features in the micron range. The effects of diffraction are more important in the latter, or even dominant, as in the case of gratings due to their small feature size in the same length scale of the wavelength of light. After the initial efforts in the field and focus on the preparation of diffractive Fresnel elements through photolithographic techniques, true microlenses were prepared by starting with circular posts obtained with a photoresist, that were subsequently thermally annealed to lead to a spherical cap of molten photoresist, that upon curing results in a lens [59]. Other approaches make use of greyscale photolithographies to obtain polymeric structures that work as refractive microlenses [60]. More recently, inkjet printing has been used in the production of these elements due to the possibility to apply different materials on virtually any type of substrate. Different from photolithographies, inkjet only adds material where it is needed so it allows for the precise application of functional materials at precise locations of prefabricated devices with no or minimal post processing. By using this technology, microlenses with large numerical aperture and short focal lengths can be prepared as an efficient, simple and cost-effective alternative to photolithography (Figure 9).

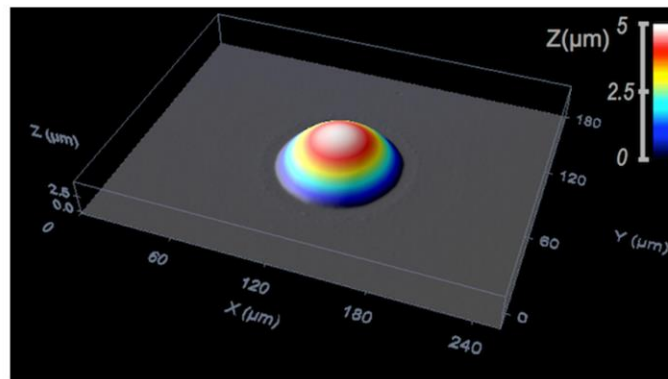


Figure 9. Confocal microscope image of an inkjet printed hybrid organic-inorganic UV-cured microlens deposited on a glass substrate.

Final properties of the microlenses can be finely tuned by appropriately selecting the refractive index of the resultant material and by controlling the final shape of the deposited microlens. As mentioned above, for typical sizes of inkjet printing ejected single drops, the sessile drop reaches, after relaxation, a spherical shape that, in the absence of any surface structuring, is mainly dictated by contact angle and the amount of deposited ink (see Equation (6)). This spherical cap shape can be frozen after relaxation for inks based on molten polymers when they are cooled down. MacFarlane and coworkers already reported in 1994 spherical cap convex microlenses made of molten polymer printed by inkjet with diameters ranging between 70 and 150 μm , and focal lengths between 50 and 150 μm [61]. The spherical shape is also kept for prepolymers that are fixed by exposure to UV light after inkjet deposition [62,63].

Other inks contain solvents that need to be eliminated after deposition. This is the case for many studies reported in the literature using SU-8 based inks containing solvents. As in the previously described ink types, wetting plays a very important role in the final properties. Studies carried out printing the same material on substrates with different wetting properties led to microlenses with different geometrical and therefore optical parameters. Besides the wetting, final shape can also be affected by evaporation of ink solvents and subsequent material transfer within the deposited drop [64].

Polymer based solutions have also been used for microlens preparation. Evaporation of solvents in deposited droplets usually leads to large changes in morphology. Pinning of the evaporating droplet fix the radius and induces the flow of the polymer solute within the droplet during evaporation, strongly influencing the final shape of the deposit, usually with a non-spherical profile. However, appropriate selection of the polymer solvent or solvents and target substrate has been demonstrated to lead to an evaporation mode in which the droplet is not pinned and spherical cap polymeric microlenses can be formed [65].

Fabrication of microlenses on substrates with patterned wettability has also been explored to gain control of microlens properties. The preparation of a non-wetting area surrounding the region where the optical material is deposited enables the control of the equilibrium position of the liquid on the surface and therefore the fabrication of several shapes of microlenses. Pre-patterning can be performed by means of photolithographic steps leading to wettability patterned substrates [66]. Pre-patterning can also be assisted by inkjet printing as done by Chen and co-workers [67]. In this last case, during the first patterning step, a solvent (anisole) is deposited by inkjet on a thin layer of PMMA previously casted on top of a flat glass. The solvent acts as an etchant creating, as a result of the coffee stain effect, reproducible well structures with a thinner layer in the centre and a thicker perimeter at the edges. After controlled etching of these patterned polymer layer with O_2 and CF_4 plasma, the thinner

part of the film is eliminated leaving the bare glass while the thicker rest of the polymer acquires a repellent character. Drops of photocurable optical glue are deposited using again inkjet printing on the generated holes. Self-positioning of the deposited materials is achieved due to the surface tension pattern established during the first step. Fine control of the focal length can be achieved by adjusting the diameter of the wells obtained in the first step and the amount of ink deposited in the second step that is confined by the wells [67].

Topographical features have also been used to control microlens characteristics. Fabrication of large arrays of micro-spherical caps with well-defined height, radius of curvature and edge angles was also performed by pre-patterning substrates with micro-platforms on top of which controlled amounts of an SU-8 based epoxy solution were deposited by inkjet (Figure 10). The deposition of a different number of resin drops in each platform having a well-defined rim angle φ , allows us to gain a precise control of the cap edge angle within a large range between a minimum ν_{min} defined by the equilibrium contact angle θ_{eq} and a maximum angle ν_{max} defined by $\theta_{eq} + \pi - \varphi$. Differences between ν_{max} and ν_{min} up to 85° for 100 micron diameter platforms have been achieved by this method [68]. Pre-patterning pillars on substrates has also been used to obtain different lens contour shapes such as circular, elliptical or toroidal [69]. The generation of concave microlenses has also been demonstrated by inkjetting droplets of UV curable prepolymers on photolithographically prepared SU-8 wells [70].

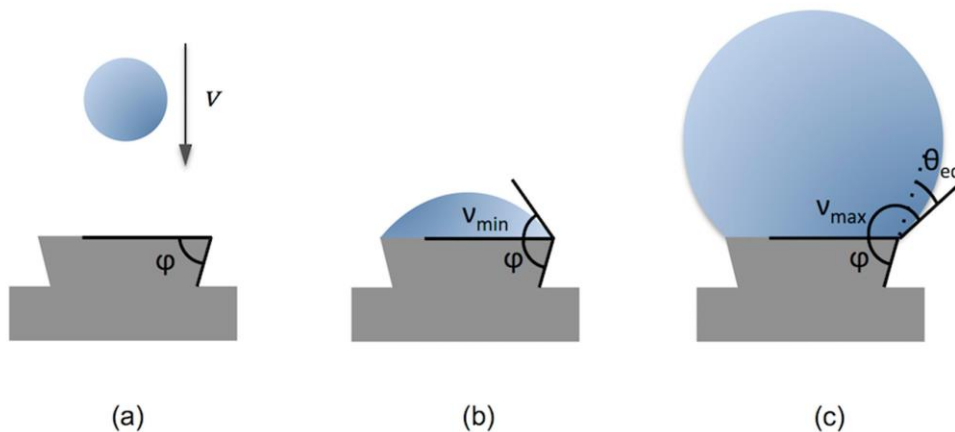


Figure 10. (a) Schematic view of a drop being deposited on top of a micro-platform with a rim angle φ ; (b) The deposited drops are confined by the elevated area fixing the contour shape of the drop. The minimum contact angle ν_{min} for a drop covering the elevated area is the contact angle θ_{eq} of the ink on a flat substrate; (c) Further addition of droplets leads to an increase of the edge angle until the maximum angle ν_{max} , defined by $\theta_{eq} + \pi - \varphi$, is reached. Above this angle the rounded drop overflows the platform [68].

With respect to the materials, besides the molten polymers and typical UV-curable inks, more sophisticated material strategies, seeking enhanced properties such as improved adhesion or higher transparency window, have been investigated. Aegerter and coworkers used sol-gel based inks containing UV curable 3-Methacryloxypropyltrimethoxysilane to make microlenses. They produced plano-convex spherical microlenses transparent from 375 to 2700 nm with diameters between 50 and 300 μm , focal lengths from 70 to 3000 μm and f-numbers (defined as the ratio of the focal length to the diameter of the entrance pupil) as low as 0.61 [71]. Later, the same group went further by printing epoxy-based inks, with similar optical transparency, in the form of plano-convex microlenses of 50 to 1000 μm diameter and focal lengths between 100 and 2200 μm . The smallest separation of the lenses in arrays was approximately 5% of the lens radius and the average surface roughness was as low as 40 nm [72,73].

Hybrid organic-inorganic materials were also used to prepare microlenses with high numerical aperture by Brugger and co-workers [62,74]. These lenses achieved a focal distance of 45–50 μm , and a small curvature radius of 29 μm . Periodic arrays of almost semi-spherical microlenses of 50 μm were obtained by treating the substrate with fluorinated silanes. High quality arrays of microlenses with good uniformity and reproducibility, transparency from 400 to 1600 nm and a refractive index of 1.553 at 635 nm were prepared with these materials. By increasing the number of drops per microlens, the focal length increased from 64.1 μm to 175.1 μm and the numerical aperture ranged from 0.41 to 0.30 [75]. By using microstructured SU-8 substrates treated with a fluorinated organosilane, parabolic-shaped microlenses with high numerical aperture, up to 0.86, has also been produced using these same hybrid materials (Figure 11) [76]. Combination of nanoimprinting lithography, to prepare microstructured arrays of pillars, and inkjet printing, to create microlenses on top of the pillars, using the same hybrid organic-inorganic material in both structuring techniques, has allowed for the preparation of arrays of microlenses with superior optical performance and high reproducibility. In addition, microlenses with different characteristics, different focal lengths and therefore focal planes have been prepared in the same substrate, separated by just few microns by using this combination of techniques [77].

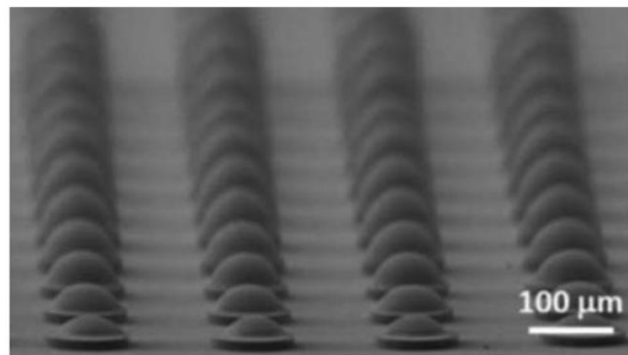


Figure 11. SEM images of microstructured polymeric pillars (diameter 100 μm , height 10 μm) treated with a fluorinated organosilane, with SU-8 microlenses on top formed by inkjet deposition of different numbers of drops (one to ten drops). Reprinted from reference [76] with permission of The Royal Society of Chemistry.

The typical wavelength application range of microlenses fabricated by inkjet printing has usually been in the visible and near-infrared, however novel materials, as chalcogenides have also been explored to manufacture microlenses for the mid-infrared potentially integrable with quantum cascade lasers in this wavelength range [78]. Fine tuning of lens geometrical parameters with diameters between 10 and 350 μm and estimated focal lengths from 10 to 700 μm were achieved by dispensing small amounts of an As_2S_3 solution on a hydrophobic substrate surface and carefully controlling the baking time.

Although, typically all or part of the ink material is intended to remain after the inkjet process, jetting of solvents that eventually completely evaporate has also demonstrated to be a powerful tool in the preparation of microstructured functional surfaces. Inkjet etching using drops of solvents on PS substrates has also been proposed to obtain polymer microstructures which can be used as microlenses [79–81]. Depending on the ratio of solvents in the jetted mixture the profile of the surface can be finely tuned going from concave to convex profiles in the same target substrate [80]. Later on, the inverse replica of these microlenses can be obtained by template casting using an elastomeric silicone (Sylgard 184, Dow Corning, Midland, MI, USA) [81].

Microlenses arrays, obtained by inkjet printing, are being explored in different photonic applications. Microlenses have been deposited by inkjet on fibre tips to increase the acceptance angle and more efficiently couple in light from diode lasers. On the other side, microlenses deposited

on the fibre tip can collimate the output beam. Inkjet printed microlenses have demonstrated to be a feasible approach to beam-shape the light from edge emitting diode lasers. On the other hand, microlenses precisely positioned on top of arrays of photodetectors can improve their efficiency collecting light [82–85]. As a result, inkjet is a very attractive technique for the in situ preparation of microlenses for Optical Input/Output (I/O) interconnections for massive high speed switching or parallel processing of information. Integration of different devices such as lasers, photodetectors of fibres has been demonstrated by using inkjet. Microlenses prepared in front of the aperture of a wire-bonded Vertical Cavity Surface Emitting Laser (VCSEL) can help to control the collimation of emitted light and improve the coupling efficiency into fibres being therefore inkjet printing a very effective technology for optical interconnection [86,87]. Recently, Chen and co-workers demonstrated inter-board optical connections between polymeric waveguides using inkjet printed microlenses deposited on top of total internal reflection mirrors. Microlenses of 70 μm in diameter deposited by inkjet printing improved the transmission by 2–4 dB per coupler [88]. Also seeking the coupling out of light from a waveguide, arrays of microlenses with controllable curvature and filling factor, were printed on top of light guide plates by Tseng and coworkers. The prepared systems were able to efficiently extract light with large uniformity (up to 84%) demonstrating the feasibility of this approach for the manufacturing of low-cost LCD backlights [89,90]. Inkjet printed microlenses have also recently been used in the implementation of optofluidic devices for analysis [91].

Waveguide manufacturing has also been accomplished by using inkjet printing technology. As mentioned in Section 2, printing of lines with parallel ridges can be achieved by sequential printing of closely spaced dots. These lines, that have a spherical cap cross-section, can be used as waveguides if the deposited material has a higher refractive index than the underlying substrate. Planar waveguides can also be obtained by printing larger flat areas (Figure 12). Besides the low cost and rapid fabrication process, an interesting advantage of inkjet printing versus traditional techniques such as photolithography, is the ability of inkjet to directly print high-aspect-ratio complex geometries such as multiple waveguides and splitters taking a simple image file as a design [92,93]. When compared to other printing techniques such as direct writing of cylindrical lightguides using extrusion printing [94], inkjet printing presents pros and cons. While the liquid character of the inkjet printing formulations allows for the preparation of smooth interconnections between optical elements, extrusion printing allows for the manufacturing of free standing optical fibres not achievable by inkjet printing.

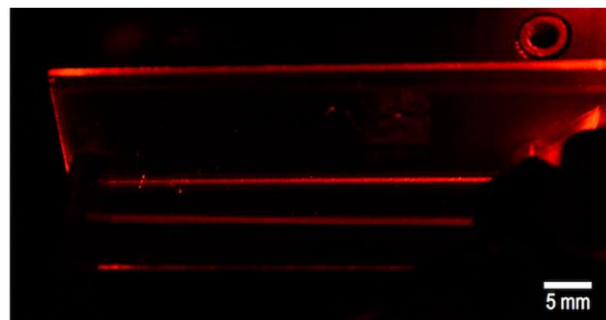


Figure 12. Inkjet printed hybrid organic-inorganic UV-cured planar waveguide deposited on a glass substrate. The 633 nm light propagates from right to left through the waveguide.

The first reference found in the scientific literature about the inkjet printing of waveguides, comes from Microfab Technologies Inc. scientists who reported in 1999 the printing of 100 μm epoxy based waveguides/splitter [92]. The description of these waveguides is detailed in a later publication in 2004, as a 1.74-index material printed on glass with a 1 to 16 splitter with 120 μm wide branches. Edge smoothness of the waveguide-substrate interface was on the order of the wavelength of the transmitted light demonstrating the viability of this technology [95].

In order to make inkjet printing a feasible technology for the preparation of optical waveguides, apart from a precise control of the geometrical parameters, materials with low losses need to be employed. Only few papers after the seminal work of MicroFab have been done in this direction. Chappell and co. employed a commercially available core material (Truemode[®], a UV-curable acrylate monomer manufactured by Exxelis Ltd., Edinburgh, UK) mixed with solvents to achieve a suitable viscosity to be jetted, and studied the influence of substrate wettability in the deposition process. Despite the authors demonstrate the preparation of lines of core material having a waveguide geometry there is no waveguide optical characterisation reported [96]. SU-8 has also been investigated as a candidate material for the manufacturing of waveguides by inkjet printing; however, loss measurements by Vacirca and co-workers showed high values [97].

Waveguides also constitute a key element in planar optoelectronic sensors for temperature, strain or chemical concentration detection. These are composed of integrated light sources, detectors and sensors, connected by optical waveguides on thin polymer films. A combination of flexographic and inkjet printing technique has also been proposed to prepare these waveguides by using the commercial hybrid organic-inorganic inks InkOrmo as the cladding and InkEpo as core material (Microresist Technology GmbH, Berlin, Germany) [98,99].

To conclude, a recent example has been reported in the preparation of photonic structures using inkjet printing. Patterns were obtained by printing a solvent etchant on a thin film of polystyrene. The solvent dissolves the polymer and this is accumulated at the outer region of the droplet due to the coffee stain effect previously described. After solvent evaporation, a microring of typical radius of 50 μm , width of 5 μm and a height of 500 nm is formed. Straight lines were also created following this procedure, acting as waveguides, while microrings including a luminescent dye (1,4-bis(a-cyano-4-diphenylaminostyryl)-2,5-diphenylbenzene) were characterized as lasers showing a quality factor higher than 4×10^5 , which is comparable to that of silicon-based resonators [54].

To summarize this section, inkjet printing has been employed in the preparation of microlenses and optical waveguides. A large degree of control of the final properties of microlenses has been achieved through appropriate selection of jetted materials, wetting and topographical features of the receiving substrate as well as post-processing of the deposited materials. On the other hand, the preparation of optical waveguides using inkjet has been much less explored. While photolithographies require complicated or difficult steps to be carried out, sometimes in combination with other technologies, inkjet printing, being a digital, contactless, additive material deposition technique, can be applied as a final step with minimal or no post-processing gaining positions as a relevant technology in the integration of optical micro-devices.

4. Inkjet Printing of Light Emitting Devices

Organic Light Emitting Diodes are solid-state lighting thin multilayered devices able to transform electricity into light. The structure of OLEDs comprises, in the most simplified version, a thin emissive layer (EL) of an organic emitting material sandwiched between a low work-function cathode (e.g., Ca or Ba) and a transparent anode (e.g., Indium Tin Oxide: ITO) [100]. Additional layers such as hole and electron injection, transport and blocking layers can be integrated in the structure to optimize the transport of charge carriers to the light emissive film (Figure 13) [101]. The inclusion of these layers improves device performance, mainly brightness, threshold voltage, lifetime and efficiency. When a voltage is applied between the electrodes, electrons are injected from the cathode and holes from the anode. Electrons and holes migrate to the emissive layer where they recombine into an exciton that can radiatively decay emitting light. Colour of the emitted light can be tuned through the introduction of changes in the molecular structure of the emitting material. This affects the energy gap of the $\pi-\pi^*$ transition that dictates the wavelength of the emitted light [102,103].

Currently, OLED emission can be produced with high efficiency, brightness, and uniformity at different colours. OLEDs present excellent contrast ratio (luminance ON/OFF) and fast response time as well as no angle-view dependence. Red, green and blue (RGB) colours can be generated with

OLEDs so other colours can be obtained just by combining these three without the need of any colour filters. In addition, the simple thin film structure can be manufactured at room temperature and in some cases from solution processes. All these characteristics, together with the improved lifetime reached over the last years, have made OLEDs systems to already penetrate the market of displays and further improvements in the area can turn this technology in the standard in the flat panel display arena nowadays dominated by LCDs. The ultrathin character of OLEDs allows for the production of flexible devices by preparing them on top of polymeric substrates paving the road for future disruptive display applications. More recently, beyond displays, lighting applications are also gaining a great deal of attention. Besides efficiency, other factors such as durability and intrinsic lightweight, the possibility to combine colours closely matching virtually any power distribution (for example sunlight) with no UV and the ability to adopt complex shapes or bend, make OLEDs a promising approach for future lighting applications [2,5,104–106].

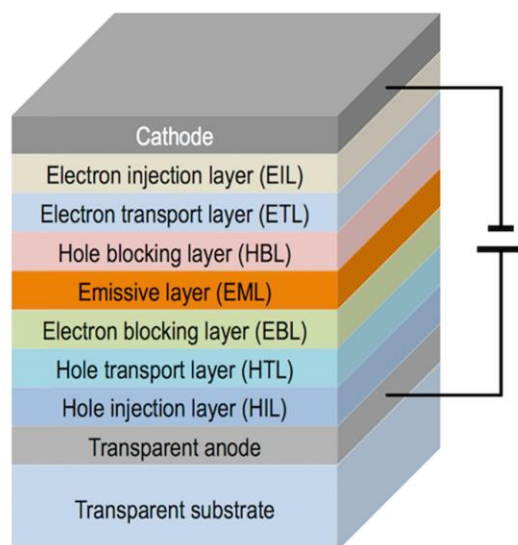


Figure 13. General schematic multilayer structure of an organic light emitting diode.

Patterning of different emissive materials is a key element in the manufacturing of OLED displays. Vacuum evaporation of small emissive molecules is the prevalent technology to deposit the electroluminescent layers. In combination with masks, this evaporation method is used to manufacture small and medium size displays; however, for large size displays the technical difficulties of this patterning methodology lead to low yields being not competitive with well-established LCD technology. As a result, alternative cost-effective manufacturing methodologies are needed to apply the emitting materials in displays. There is a trend to shift from evaporation techniques to solution based processes for which there is a need of emissive soluble materials. While the solubilisation and wet processing of small emissive molecules have traditionally presented many difficulties, polymeric light emitting materials have excellent solution processability properties being suitable materials for the manufacturing of OLED flat-panel displays [100]. Among the different patterning techniques, inkjet printing has been explored as a solid candidate to produce low cost RGB OLED displays due to its ability to precisely deposit different emissive inks at different positions with minimum waste of material. In addition, it is a scalable technique with reasonably high production speed and can be combined with other R2R processes. Even more inkjet allows us to correct defects in-line increasing with this the reliability and yield of the display production process.

Pixelation of RGB OLEDs by inkjet is done by precisely position droplets of the three colour emissive materials on the substrate [107]. To do this, the receiving substrate provided with the electrodes is patterned with polymer walls surrounding each pixel (Figure 14). The polymer walls are hydrophobic while the substrate is hydrophilic, so when a drop of hydrophilic ink reaches the well, it wets the substrate. If the printhead and the substrate are slightly misaligned or the droplets deviate during flying, these can touch the polymer wall and dewet eventually falling inside the well confining the emissive material. As a result, electroluminescent pixels with position and size accuracy within one micrometre, required for this technology, can be processed. High resolutions exceeding 200 pixels per inch, that are suitable for large size but also for medium and small size displays can be created using this approach [108].

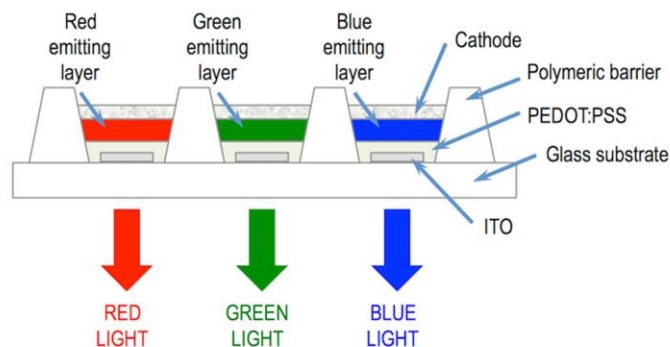


Figure 14. Schematic pixel structure of a red, green and blue (RGB) organic light emitting diodes (OLED) display.

The first attempts to incorporate inkjet printing technology in the production of OLEDs were disclosed at the end of last century. Hebner and co-workers prepared patterned emitting devices by inkjet printing three different chloroform solutions of polyvinylcarbazole as a hole transport polymer doped respectively with coumarin 6 (C6), coumarin 47 (C47), and Nile red as light emitting chromophores. Low threshold voltage and luminescence similar to that obtained by spin-coated devices was found for these processed with inkjet [109].

Almost simultaneously, the group of Yang at the University of California developed different configurations of OLED devices [110]. In a first example, they inkjet printed a solution of PEDOT on an ITO substrate. After this PEDOT patterning, a layer of Poly[2-methoxy-5-(2'-ethylhexyloxy)-1,4-phenylenevinylene] (MEH-PPV) was applied by spin-coating and finally a Ca cathode was deposited. The differences in conductivity between the PEDOT patterned areas and the non-printed regions led to differences in emission, allowing for the definition of logos and images [111]. The same group developed new different devices using inkjet technology. They built a dual colour polymer based emitting pixels by initially applying by spin-coating on an ITO substrate a blue emitting water soluble polymer, poly[2,5-bis[2-(*N,N,N*-triethylammonium)ethoxy]-1,4-phenylene-alt-1,4-phenylene]dibromide (PPP-Net+3). On top of it, a red-orange emitting, water soluble polymer, poly(5-methoxy-(2-propanoxysulfonide)-1,4-phenylene vinylene) (MPS-PPV), was patterned as pixels by inkjet printing. The inkjet patterned ink partially diffuses into the underlying layer. After the evaporation of the cathode the film presented blue emitting areas where no red ink was deposited whereas the printed areas showed the same red-orange electroluminescent spectrum of the MPS-PPV that was ascribed to the dopant diffusion and energy transfer effects [112]. A more sophisticated version of a multicolour RGB OLED was prepared by the same group. To implement it, a blue emitting polymer, poly-9-vinylcarbazole (PVK), was applied by spin-coating on top of an ITO glass substrate. Similar as in the previous case, two different methanol solutions of tris(4-methyl-8-quinolinolato)Al(III) (Almq3) and (4-(dicyano-methylene)-2-methyl-6-(4-dimethylaminostyryl)-4*H*-pyran) (DCM) were

inkjet-printed on the PVK layer. After the elimination of the solvents and the deposition of the cathodes, the application of voltage led to blue emission in the PVK area, orange-red emission in the PVK/DCM regions and green-blue emission in the PVK/Almq3 ones [113].

Beyond these initial attempts, Kobayashi and coworkers incorporated a thin film transistor (TFT) array in the substrate, as the one used in LCDs, to individually address the deposited RGB pixels. Despite only red and green pixels were deposited by inkjet printing, this work was a clear precursor for the preparation of active matrix OLED (AMOLED) displays by inkjet printing technology [114,115].

The effective incorporation of inkjet to OLED display manufacturing requires efforts and developments in different aspects of the inkjet process that comprehend the material to be deposited, the ink formulations, their deposition and drying process, the post-processing after inkjet as well as the equipment to pattern the large area devices.

As in the case of other solution processes, the deposited materials by inkjet need to have the appropriate optical and electrical properties to fulfil the stringent demands of display applications. Focusing in the electroluminescent materials, light emitting polymers such as poly(phenylene vinylene) (PPV) derivatives, MEH-PPV for example, which are soluble in common organic solvents, have been used in the preparation of OLEDs by inkjet printing [114,116]. The lifetime of the emitting materials and the device itself has been crucial in the effective incorporation of OLED technology in real applications, especially critical for blue OLEDs [101,117]. New macromolecular architectures, such as polyfluorenes and poly(spirofluorene)s, have led to solution processable materials with increased lifetime suitable for inkjet fabrication of OLEDs (Figure 15) [114,116,118]. Purification of these polymeric materials is a key element to make lifetime longer in OLED materials. When compared to polymers, higher levels of purity can be achieved in small emissive molecules, typically used in the preparation of OLEDs by evaporation, however these cannot easily be processed from solution as already mentioned. As a result an intense effort has been made towards the chemical modification of these molecules to make them soluble and inkjet-processable [119,120] and also towards the manufacturing of devices using them [121,122]. Exposure to moisture and oxygen results in degradation of the performance and lifetime reduction so the encapsulation of devices after printing is nowadays a standard step in the manufacturing of OLEDs [123,124].

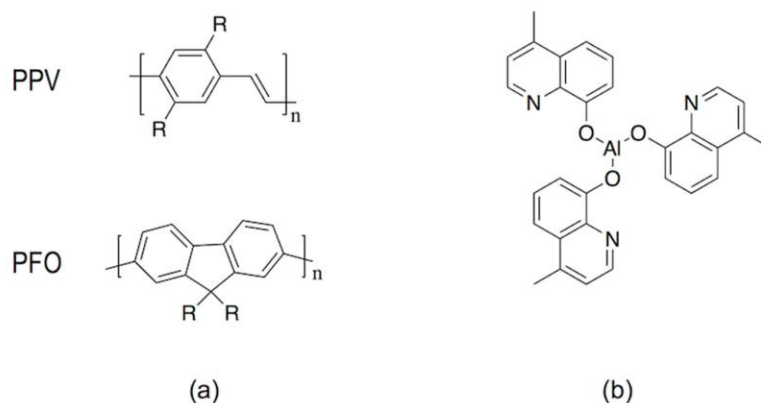


Figure 15. Chemical structure of materials used in OLEDs preparation: (a) light emitting polymers poly(phenylene vinylene) (PPV), polyfluorenes (PFO) and (b) light emitting small molecule Tris(4-methyl-8-hydroxyquinoline)aluminum.

PEDOT:PSS has been widely employed as an organic material to planarize the ITO electrode and to facilitate the transport of holes towards the electroluminescent layer (Figure 16) [125]. Inks of this polyelectrolyte system have been prepared and processed by using inkjet for the manufacturing of OLEDs [116,126–128]. Control of the PEDOT:PSS ratio, the solvents employed or the addition of

surfactants to inks, strongly influence the morphology and the electric properties of the final applied materials after solvent evaporation [129]. Due to the excellent optical and electrical properties of PEDOT:PSS, this is ubiquitous in OLED literature usually in combination with the ITO layer. However, motivated by the scarcity of Indium, it has been also tested in the manufacturing, also using inkjet, of devices with no ITO layer being PEDOT:PSS the anode material [128,130–132].

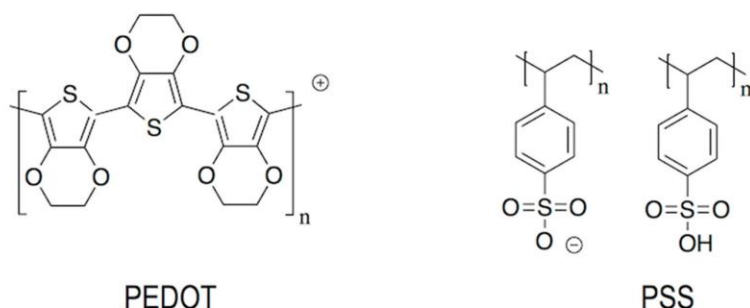


Figure 16. Chemical structure of poly(3,4-ethylenedioxythiophene) and poly(styrene-sulfonic acid) (PEDOT:PSS) polyelectrolyte commonly used in OLEDs preparation.

Besides suitable deposited materials properties, inkjet processing imposes additional demands with respect to conventional solution based processes. Functional inks must fulfil the requirements of rheology and surface tension to be successfully ejected [126]. They usually comprise a solvent and the functional materials, with a typical solid content between 0.2% and 2.5% w/v, leading to a solid film in the order of 100 nanometres after solvent evaporation [133]. These solvents need to be carefully selected to facilitate ejection without nozzle clogging. In addition, being OLEDs multilayer structures, the solvents used should not attack previously deposited layers. Crosslinking of the applied layers is a commonly used strategy to avoid damage caused by subsequently deposited materials [134]. Recently, Coenen, Gorter and co-workers at the Holst Centre in Eindhoven, demonstrated the fabrication of OLEDs with three adjacent organic functional layers [121,122]. In one of the examples disclosed by this group, a PEDOT:PSS layer, an additional thermally crosslinkable hole injection thin film and an emissive layer were successfully stacked by using inkjet printing [122].

Although the general trend is that the deposited material should not affect the properties of the underlying layer, inkjet can also be employed to locally induce chemical reactions in the substrate through the so called Reactive Inkjet Printing (RIP) technique. In the field of OLEDs, the group of Jabbour used this technique to locally modify the resistivity of PEDOT:PSS. The deposition using inkjet printing of a hydrogen-peroxide-based ink on top of the conductive layer produces oxidation and an increment of the sheet resistivity. This local modification of electrical properties allows for the preparation of logo and greyscale systems by using this simple approach [130,135].

The properties of the applied film after drying, especially morphology, thickness and its uniformity, must be also carefully controlled since they strongly influence electrical current density and emission properties of the deposited layer. As mentioned in Section 2, solvent evaporation can lead to pinning and coffee stain effect. This effect poses a challenge in OLED manufacturing since it results in inhomogeneous film thickness with detrimental consequences in OLED performance. The proper selection of solvents or mixtures of them have demonstrated to be key elements for the preparation of uniform thickness devices [56,57,136]. Ink concentration, substrate temperature and inkjet printing dot spacing also largely affects the evaporation process as already described in this review. Control of all these variables has allowed for the preparation of uniform thickness, good quality deposits for OLED applications [137].

Besides being a tool for device micromanufacturing, inkjet printing has demonstrated to be a valuable tool for material and process evaluation and optimisation since it can generate

batteries of samples processed with different conditions in a very reproducible fashion [56,138–142]. For instance, Tekin and co-workers prepared thin film libraries of six alkoxy-substituted poly(p-phenylene-ethynylene)-alt-poly(p-phenylene-vinylene)s (PPE-PPVs) with a systematic variation of thickness. The evaluation of the optical properties of the different inkjetted films allowed us to identify the influence of alkoxy side chain substituents and film thickness in the luminescence properties of the materials [139]. Studies on the printability of MEH-PPV solutions of different concentrations and solvents via inkjet were also carried out by the Schubert group. The morphology and surface quality of the obtained films was studied as a function of printing parameters [140]. The influence of other variables such as ink composition, dot spacing and the substrate temperature has also been explored in poly-(phenylene-ethynylene)-poly(phenylene-vinylene)s copolymer systems by evaluating thin film libraries prepared by inkjet printing. Fast parameter screening allows us to identify adequate conditions to obtain homogeneous films of fixed thickness being therefore a valuable tool for device manufacturing [141]. Relevant relationships between ink viscosity, polymer molecular weight, and film thickness and roughness have also been established by using this combinatorial approach [142].

Another shortcoming to be addressed in OLED technology has been the lack of pure colours due to the broad emission of organic materials, usually showing a full-width half-maximum (FWHM) of around 70 to 100 nm. To overcome this issue quantum dots (QDs) have attracted a great deal of attention since they present highly efficient narrow band emissions (FWHM of 20 to 30 nm) whose wavelength emission peak can be tuned simply by changing the size of the nanoparticle. QDs can be in situ prepared by Reactive Inkjet Printing as demonstrated by Song and co-workers. In this case, the deposition of a polymer and a cadmium precursor done by inkjet printing, followed by a treatment with hydrogen sulphide gas, led to CdS QD polymeric composites [143]. However more common approaches to synthesize QDs are carried out in solution. Once prepared, they are surface-modified to make them compatible with common solvents allowing for the processing from solution. This enables the preparation of QD light emitting diodes (QDLEDs) that present high colour purity leading to improved colour saturation and colour gamut with respect to conventional OLED displays prepared using organic molecules [144–146]. As a remarkable example, Samsung scientists have demonstrated the patterning of QDs and the preparation of QD displays by transfer printing using an elastomeric stamp. Although this step is a major breakthrough, handling of large area stamps, needed for large area display manufacturing, is not trivial and stamps can be damaged due to repeated use resulting in a loss of printing quality [147]. As for other solution processable materials, inkjet printing appears as a suitable candidate for the preparation of QD displays.

The inkjet printing of QD formulations consisting of a CdSe core and a CdS/ZnS double shell dissolved in chlorobenzene was demonstrated by Jabbour and co-workers. QD single pixel light emitting devices were prepared by inkjet printing a layer of QDs as the emissive layer embedded between a spin-coated hole transport polymer and a thermally evaporated organic molecule electron transport layer (Figure 17). Quarter video graphics array (QVGA) monochrome displays (320×240 pixels) were built using inkjet printing of these materials [148]. The group of Bulovic at MIT demonstrated the inkjet printing of QD–polymer composites leading to narrow band emissions in the red and in the green region [149]. RGB QD AC-driven displays were prepared by using a layer of a blue electroluminescent emitting layer of a commercial phosphor powder that constitutes the blue pixels and illuminates QDs that down-convert blue light into red a green depending on the pixel. Jabbour and co-workers also demonstrated patterning by inkjet printing technology of QVGA displays with QDs inks emitting in the red, green and blue [150]. Besides QDs, fluorescent inks based on semiconductor nanorods have also demonstrated to lead to highly concentrated printed layers with little emission shift and high quantum emission yield [151].

Large format (60 inch), Ultra High Definition (4K UHD) format are being attempted to be inkjet printed with QDs inks [152]. On the other hand, efficient (Quantum efficiencies larger than 10% for all three RGB colours), long lifetime (300,000 h) and well controlled RGB peak wavelengths potentially

leading to a colour gamut largely exceeding current colour standards for television, has been achieved using QDs solution processable materials by researchers from Nanophotonica Inc. and the University of Florida [153,154]. These studies demonstrate that inkjet printing of this type of material represents an extremely attractive approach for the manufacturing of ultra high definition-large format displays.

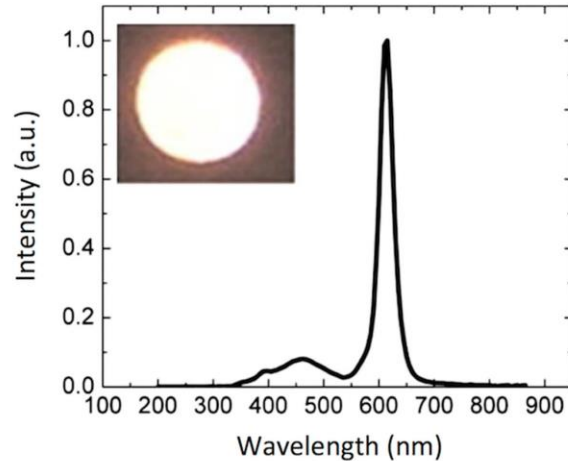


Figure 17. Electroluminescence of a QDLED showing emission from the quantum dots (sharp peak near 600 nm). A real operating device with an area of 0.14 cm^2 is shown in the top-left part of the plot. Adapted from [148], with the permission of AIP Publishing.

Beyond the materials, in which large chemical companies as Merck KGaA are heavily involved [120,155], a large effort is also being devoted to optimize the industrial manufacturing process. For example, DuPont Displays is trying to simplify the production process removing the polymer walls surrounding each pixel and therefore eliminating one photolithographic step reducing therefore cost production. To do this they have developed the nozzle printing technique in which a continuous liquid jet moves across the substrate aligned with previously defined wetting and non-wetting areas. As a result, continuous lines of emissive material instead of aligned pixels are obtained [156].

Focusing on the manufacturing equipment, the company Kateeva, that counts with the financial support from Samsung, has developed an inkjet printing platform for the production of flexible and large scale OLEDs. This equipment produces in a dust-free, nitrogen environment, avoiding oxygen and moisture leading to improved device lifetime. In addition, through process-control monitoring and printhead control algorithms, visual heterogeneities in the printing, referred to as mura, due to nozzle to nozzle non uniformities, are strongly reduced [157].

Summarizing this section, OLED technology has tremendously improved over the last two decades. Although small OLED displays can be routinely manufactured by evaporation processes, production of large area displays present still many challenges. Nowadays, solution-processable materials present excellent performance and equipment for OLED inkjet printing with reasonably high throughput, reliability and yield is being developed. With all this background it can be stated that inkjet printing is well positioned to become a key enabling technology to manufacture future large format, high-resolution displays.

5. Inkjet Printing of Other Flat Panel Displays Beyond OLEDs

Advantageous aspects of inkjet printing for OLED display manufacturing such as the digital character of the technique, its scalability, the low waste of material and the possibility to combine with R2R production techniques for flexible devices are also of great relevance in the production of other

types of displays such as LCDs or electrophoretic displays (EPD) [158]. As a result, inkjet has also been explored as a valuable tool in other flat panel display technologies.

LCDs, the dominant technology nowadays in flat panel displays, are, as OLEDs displays, multilayer structures able to deliver digital visual information to users. High-resolution full-colour images are nowadays a standard in LCD technology; however, the search of new approaches to reduce costs in a mature market is an always-present target for the LCD industry. A LCD typically consists of two thin transparent substrates. These substrates are separated few micrometres having electrodes and alignment layers in the inner part of the assembly. The gap between the glass plates is filled with a liquid crystal (LC) whose orientation in the absence on an electric field is controlled by the alignment layers. The application of an electric field changes the orientation of the LC and therefore the polarisation state of the light passing through the LC layer. This electrically controlled change of light polarisation in conjunction with properly oriented thin film polarisers allows for the control of the transmission at each individual pixel. Differently from OLEDs, pixels in LCDs are not self-emitting, and therefore a backlight is required for illumination. To generate colour images each pixel is subdivided into three independent adjacent subpixels having RGB colour filters. An absorbing structure, named Black Matrix, is placed in the area between the colour filters preventing light leakage between subpixels and acting as a light shield for TFT elements. Figure 18a shows a simplified version of a typical LCD. Electrophoretic displays, based on the spatial reorganisation of pigment particles under the action of an electric field, can also be manufactured having a similar RGB colour filter architecture as shown in Figure 18b.

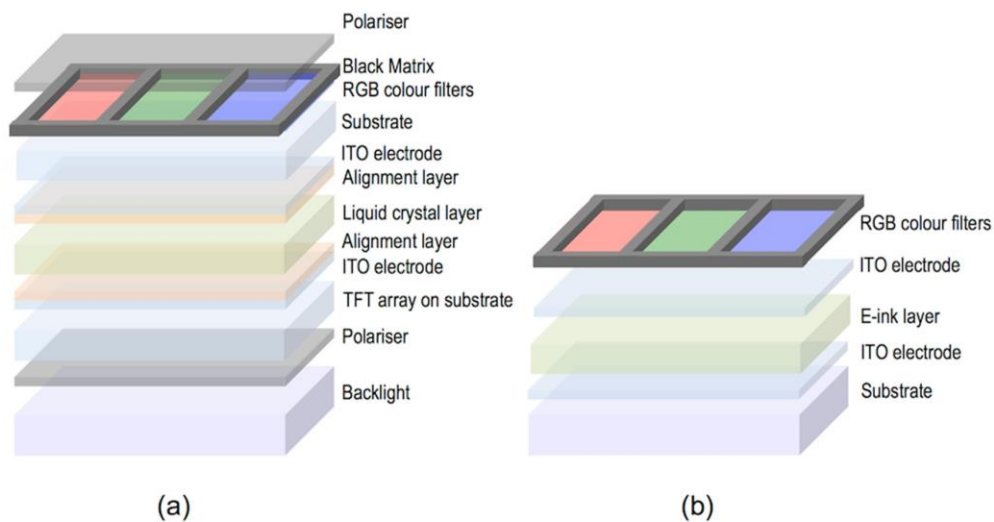


Figure 18. Schematic multilayer structure (a) an RGB liquid crystal display (LCD) and (b) a RGB e-ink display.

The fabrication of the colour filters, currently done in the LCD industry through numerous complex photolithographic steps, takes up to 25% of the overall material cost of the display [159]. A way to reduce costs in display manufacturing is to replace photolithography by other printing technologies, with inkjet printing being especially appealing. Besides the advantages mentioned at the beginning of this section, the number of steps for patterning is drastically reduced with respect of photolithography potentially reducing production costs. Efforts in developing inkjet printing technology and deposition strategies have been done to pattern colour filters in LCD panels [160–162]. Many of the challenges and difficulties to print colour filters are common to those found in the printing of light emitting materials in OLED display manufacturing so solutions will also be common or at least

parallel. As an example, the non-uniformity of the colourant film thickness leads to undesired visual effects, so accurate control of drop volume and positioning are crucial. Colour filters for LCDs can be applied into a pixel size wall structure pre-patterned on the top substrate of the LCDs similar to that typically used in OLED manufacturing. Actually, the black matrix can perform this function by acting as a barrier that precludes ink to mix with that of adjacent pixels. Although this black matrix structure is currently prepared by photolithographic techniques, its preparation using inkjet technology has also been reported [163].

Wettability and therefore treatments of the pre-patterned substrate are, as in OLED manufacturing, a determinant for the quality of the printed elements [164]. The group of Chang and co-workers showed that CF_4 plasma treatment of the substrate prior to printing leads to improved colour uniformity of inkjet printed colour filters when compared to O_2 plasma treatment [165,166].

Efforts have also been made in the study of formulations, usually based on inorganic pigments or dyes, towards the improvement of colour characteristics, ink stability and printability. Additives such as hyperbranched polymers have been added to tune the ink rheology and therefore its printability [167]. Diblock copolymers have been included too as dispersants in ink pigmented formulations leading to improvements of the mechanical properties and chemical resistance of printed colour filters [168]. Improvements in transmittance, colour purity as well as spectral and thermal stability have been sought by the inclusion of nanoparticles [169,170] or specifically designed dyes such as perylenes and phthalocyanines [171].

Although the research carried out in the inkjet printing of colour filters for displays has demonstrated that is a feasible technology, it still presents some challenges to be effectively introduced in the display manufacturing industry. As mentioned, some of them, such as the control over the manufacturing process, control of droplet volume of different nozzles or jetting failure, are common to those found in OLED displays manufacturing. Solutions for these issues, relying on the development of process-controlled production equipment in a clean and controlled environment could make inkjet printing technology to be an effective part in the industrial display mass production.

Finally, inkjet printing has also been explored by some groups as a tool for the preparation of electrochromic devices. A simplified version of this device, as the one shown in Figure 19, is quite similar to an electrochemical cell consisting of two conductive substrates (at least one of them being transparent to let the light go through). In one of them there is a layer of electrochromic material as a working electrode while in the other it is deposited a counter electrode. Between the two layers there is an electrolyte [172–174]. When a small voltage is applied, an electrochemically induced oxidation–reduction reaction takes place leading to changes in the absorption bands of the material.

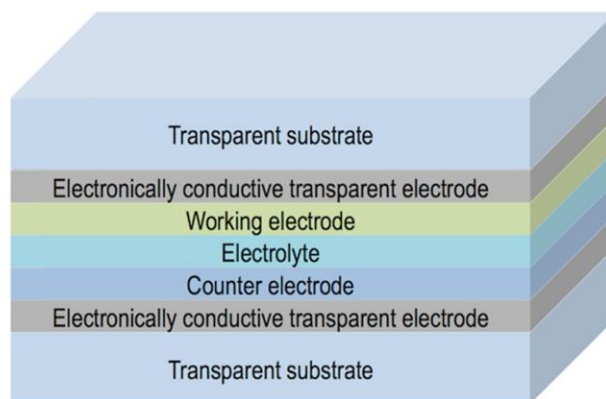


Figure 19. Schematic multilayer structure of an electrochromic device.

Wallace, in het Panhuis and coworkers disclosed water based jettable formulations containing polyaniline and a large fraction (up to 32%) of functionalized multi-wall carbon nanotubes. Printed films of these inks on platinized indium tin oxide coated glass and gold coated poly(vinylidene fluoride) substrates displayed polyelectrochromic behaviour switching between yellow, green and blue [175].

Tungsten oxide nanoparticles have also been used for the preparation of electrochromic inks [176–178]. As an example, Laia and co-workers prepared water based formulations containing these nanoparticles that were inkjet printed on flexible ITO-coated polyethylene terephthalate (PET) substrates to form both, the working electrode and the counter electrode having an electrolyte in between. The application of an external voltage led to the formation of different images demonstrating the possibility of displaying information in these inkjet printed devices [176]. Lee, Magdassi and co-workers recently developed, besides tungsten oxide inks, nickel oxide formulations to prepare electrochromic devices by inkjet printing. By using layers of these two materials as complementary electrodes, a large optical modulation of 75% at 633 nm was achieved, attributed by the authors to the synergistic and complementary electrochromic behaviour of the two printed layers [179].

Multicolour electrochromic devices have also been inkjet printed by using solutions of two metallo-supramolecular polymers, derived from iron and ruthenium, presenting two primary colours, blue and red respectively. Besides the formation of bicolour images, digital control of the deposition of the two inks in dot arrays with different red and blue dot ratio allows us to create areas with various colours without the need of premixing or new material synthesis (Figure 20) [180]. More recently, the group of Reynolds at the Georgia Institute of Technology has developed Cyan/Magenta/Yellow to colourless electrochromic inks based on alkoxy-functionalized poly(3,4-propylenedioxythiophene)-based polymers. By appropriate application of the inks, either layered or patterned over the conducting electrode, a broad range of colours can be achieved while keeping fast switching and high contrast. This makes inkjet printing a robust methodology for the preparation of patterned colourful electrochromic devices for the displaying of information [181].

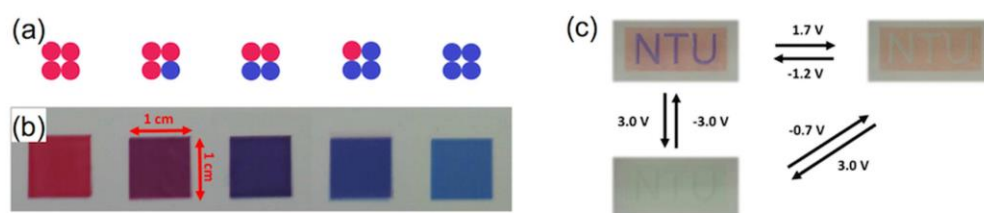


Figure 20. (a) Colour-mixing patterns resulting in (b) electrochromic material thin films with different mixing ratios of red and blue; (c) Multicolour patterns and colour states under different applied potentials. Adapted with permission from reference [180]. Copyright (2015) American Chemical Society.

6. Inkjet Printing of Organic Photovoltaics

The Sun provides Earth with 174 petawatts (PW) of solar radiation being by far the most abundant energetic resource on Earth [182]. Nevertheless, photovoltaic energy is still after hydro and wind energy in terms of global installed capacity with a total of at least 227 GW by the end of 2015 [183]. Among the existing photovoltaic technologies available, highly efficient crystalline silicon solar cells, which have reached a mature state, currently dominates the market, however the elevated costs of the materials employed and their processing, limits a widespread integration of photovoltaics in the Energy landscape. Although attempts to reduce costs in silicon solar cell manufacturing have been undertaken, for example, by substituting some of the photolithographic or spatially selective doping steps by inkjet printing based processes [184,185], there is a need of major breakthroughs to put photovoltaics in a prevalent position in the Renewable Energy field.

As an alternative to silicon photovoltaics, the use of solution processable conjugated polymers that strongly absorb light in the UV-Vis-NIR region has been largely recognized as a viable route towards cheaper and sustainable large-scale photovoltaic modules [186]. The most common organic photovoltaic device structure comprises an anode, a photoactive layer and a cathode with at least one of the electrodes being transparent to allow the light to reach the photoactive material. As in the case of OLEDs, additional layers are usually introduced between the electrodes and the photoactive layer, in this case of solar cells to facilitate charge extraction from the photoactive layer. An electron transport layer is usually placed at the cathode side while a hole transport layer is placed close to the anode. A differentiation is done depending on the location of the cathode with respect to the transparent substrate. If the cathode is away from the substrate, the solar cell architecture is termed as conventional (Figure 21a) while the solar cell is named inverted if the cathode is on the substrate (Figure 21b).

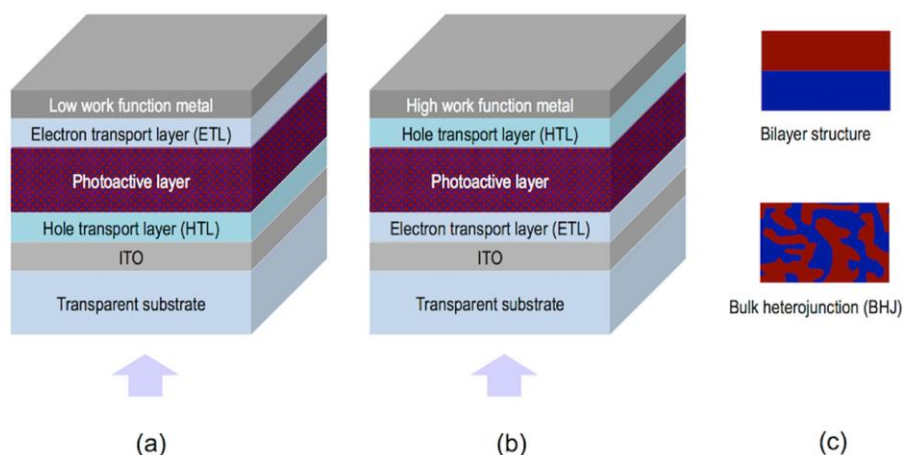


Figure 21. Schematic layer structure of a (a) conventional and an (b) inverted OPV device; (c) The photoactive layer, comprising electron donor and acceptor materials can have a bilayer or bulk heterojunction structure.

Concentrating on the photoactive layer, bulk heterojunction (BHJ) solar cells comprising an electron donor conjugated polymer and an electron acceptor fullerene based material, have received great attention as one of the most promising approaches to produce low-cost solar energy. Compared to bilayer architectures in which the photoactive layer comprises two separate films of the electron donor and acceptor materials with well-defined interface, bulk heterojunctions are based on a blend of the two systems (Figure 21c). The phases of the two components are interpenetrated forming a bicontinuous heterojunction. Absorption of light generates bound electron–hole pairs or excitons in the electron donor material that can diffuse, before recombination, to the interface of the two materials and dissociate to generate free charge carriers. The large interfacial area of the heterojunction with typical length scales below the exciton diffusion length, improves the efficiency of exciton dissociation since it diminishes the exciton travel distance. Therefore, control of the morphology of the heterojunction is crucial to optimize device performance. On one hand, exciton dissociation at the interface of the materials needs to be maximized and on the other hand charge carrier extraction to the electrodes must be as efficient as possible through the donor and acceptor continuous channels of the two materials [187]. Efficiencies larger than 10% have already been achieved with this type of BHJ solar cells [188]. Besides these single photoactive layer devices, multijunction solar cells, so called tandem solar cells, can be created by judiciously combining several junctions in one single solar cell. The complementary absorption of the different layers broadens the effective absorption window of the stack covering a larger part of the solar spectrum further increasing the power conversion efficiency [189,190].

Although important milestones have been reached and improvements are still in progress in terms of power conversion efficiency of organic photovoltaic (OPV) solar cells, their stability needs to be concurrently improved. Also, low-cost and high-throughput production processes need to be developed to make this technology successful and to penetrate the market.

As in the case of OLEDs, materials used in OPV can be processed at low temperature from solution and scaled up by using R2R technologies. In particular inkjet printing of OPV materials has drawn a lot of attention. Although inkjet has lower throughput when compared to other well established printing techniques such as screen printing, inkjet is a noncontact, digital technology able to print a wide variety of materials as layers, even several of them in the same device, and also apply conductive tracks needed to interconnect photovoltaic modules. All this makes inkjet a very attractive technology for the large-scale production of low-cost photovoltaic modules [191–197].

Research efforts have been done in the inkjet printing of the different layers of the device focusing especially in the photoactive materials (Figure 22). For example, Schubert's group has undertaken the preparation by inkjet printing of thin-film libraries of different polymer:fullerene materials for potential application in BHJ solar cells. They systematically prepared libraries of materials with a variety of blend ratios and solid concentrations, different solvent ratios, and film thicknesses and later on performed combinatorial screening of the optical and morphological properties of the films. Beyond fundamental knowledge acquired in these particular studies, these works present a fast and powerful experimental approach to establish processing-structure-properties relationships in OPV materials of crucial importance for the preparation of solar cells [198–200].

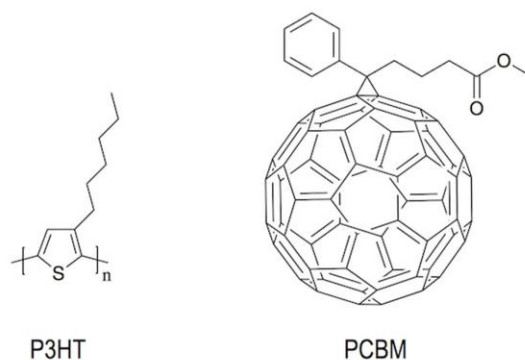


Figure 22. Materials such as poly(3-hexylthiophene) (P3HT) in its regioregular form and 1-(3-methoxycarbonyl)propyl-1-phenyl-(6,6)C₆₁ (PCBM) typically used in the preparation of BHJ.

Several studies can be found in the literature on the Fabrication of Organic OPV cells by inkjet printing of polymer:fullerene blends as photoactive layer [201–204]. Hoth, Brabec and co-workers reported inkjet formulations based on mixtures of high and lower boiling solvent (ortho-dichlorobenzene and 1,3,5-trimethylbenzene respectively) with reliable jetting behaviour, appropriate wetting, spreading and drying leading to smooth thin films with appropriate morphology and intermixing of polymer and fullerene phases. Photovoltaic devices prepared with these optimized formulations led to power conversion efficiencies in the range of 3% [202]. Studies carried out by the same group demonstrated that the control of the regioregularity of the polymer donor also plays a relevant role in the final morphology achieved and therefore in the performance of the device, allowing for further optimisation and reaching power conversion efficiencies of 3.5% [203]. Later on, Eom and co-workers further evaluated the influence of the addition of other high boiling point additives such as 1,8 octanedithiol, ortho-dichlorobenzene or chloronaphthalene to the photoactive layer ink based on chlorobenzene. As in the case of Hoth, morphology and solar cell performance were highly dependent on the presence of high boiling point additives reaching power conversion efficiencies of 3.71% [204]. Since morphology development of the photoactive layer is crucial for device performance, it is obvious

that not only the composition, but also other inkjet printing processing parameters such as substrate temperature during printing or drying can be relevant for the performance of the printed photovoltaic devices [200,205,206].

Inkjet printing has also been used for the deposition of PEDOT:PSS as in the abovementioned case of OLEDs. The role of additives in device efficiency was explored by Eom and co-workers finding that the addition of glycerol and ethylene glycol butyl ether resulted in improved surface morphologies and conductivities leading to power conversion efficiencies up to 3.16% for solar cells with inkjet printed PEDOT:PSS layers [207]. As for the photoactive layer, substrate temperature or subsequent film annealing have also a large impact in the final morphology and therefore in the device performance [208]. The efficiency values attained in these devices are in the range of those obtained with other techniques such as spin or spray coating making inkjet very attractive for the preparation of PEDOT:PSS layers ubiquitous in OPV, as inkjet introduces a high degree of flexibility in the manufacturing process [209].

Apart from the hole transport layer, it is highly desirable for the R2R manufacturing of OPV solar cells that the rest of the electrodes can also be printed. ITO has usually been employed as transparent electrode in the preparation of solar cells. Although some attempts to prepare conductive ITO layers and patterns have been performed by inkjet printing of ITO nanoparticle formulations, they require, after deposition, a high temperature annealing (usually at temperatures higher than 450 °C) to reach the desired conductivity for OPV applications, making these approaches not compatible with flexible substrates [210]. In addition, as already mentioned in the OLED section, indium is a scarce element that increases the price of the photovoltaic device. It is brittle, compromising the performance and stability of devices and it presents relatively high sheet resistance, which limits the width of the active area of an individual solar cell [211]. As a result, the elimination of ITO from solar cell R2R fabrication is highly desirable and it is being intensively pursued. This issue is also relevant in the display industry and in general in flexible electronics, so the development of transparent alternative electrodes has pushed the research on different materials and strategies for this purpose. Inkjet printing of silver nanowires [212,213], carbon nanotubes [214] or graphene [215] has already been demonstrated. Besides novel materials, an interesting and cost-effective alternative consists in the application on a substrate of a highly conductive metallic mesh (e.g., Ag, Al or Cu), preferably by printing techniques, that partially allows for the transmission of light in combination with another transparent conductive material (e.g., PEDOT:PSS) [216]. Galagan and co-workers, at the Holst Centre in Eindhoven, implemented ITO-free photovoltaic devices by inkjet-printing current-collecting grids with a silver nanoparticle ink and a layer of high-conductivity PEDOT:PSS forming a composite anode. BHJ solar cells with an active area of $2 \times 2 \text{ cm}^2$ led to power conversion efficiencies of 1.54% [217]. Larger active areas have also been achieved with high power conversion efficiencies (8 cm² active area cell with 2.34% efficiency) as shown by Huang and co-workers [218]. Aspects such as the sintering of the printed grids by thermal and laser based methodologies have also been evaluated and optimized [219]. The overall geometry and features of the grid and the width of the conductive tracks can be finely controlled through inkjet printing. Even embedding of the inkjet printed silver grids within the substrate has been demonstrated to lead to a smoother surface for the deposition of the PEDOT:PSS layer, resulting in an overall good photovoltaic performance [220]. All these aspects play an important role in the final device efficiency demonstrating the strength of inkjet digital manufacturing for the preparation of patterned electrodes. Also, the back electrodes have been successfully processed by using inkjet printing technology to implement OPV cells with conventional and inverted configurations reaching, in some of the cases, similar efficiencies similar to those obtained in solar cells with evaporated back electrodes [221–225].

When thinking about the massive production of solar cells in an industrial production environment, large amounts of ink are expected to be deposited per unit of time and therefore also large amounts of solvents need to be evaporated. A large effort is being made to eliminate halogenated solvents, typically used in research for OPV device preparation, from industrial inks trying to reduce environmental impact [226,227]. Chlorine-free solvent mixtures have been demonstrated to lead to

device efficiencies closer to those reached when using chlorinated solvents in the application of the photoactive layer as shown by Lange and coworkers [226].

As in the case of OLEDs, the fabrication of OPV multilayer devices by inkjet requires solvent compatibility with the underlying deposited layers in order not to deteriorate the device. Recently, Eggenhuisen and co-workers have shown the printing of four different layers using inkjet printing. Again, non-halogenated solvents have been used in the processing of the photoactive layer leading to devices with similar performance to those processed with chlorinated solvents. OPV modules with 92 cm² active area and efficiency of 0.98% have been achieved [228]. Seeking the industrialisation of OPV solar cells, efforts have been made in the production of all-inkjet printed devices produced in air atmosphere. Recently Jung and co-workers reported power conversion efficiency of 2% for an all-inkjet-printed solar cell with a small active area of 0.5 cm² [193]. Eggenhuisen and coworkers subsequently presented improved values with an all-inkjet-printed photovoltaic device with an active area larger than 1 cm² and power conversion efficiency of 4.1%, all this using environmentally friendly solvents in ambient atmosphere (Figure 23) [229].

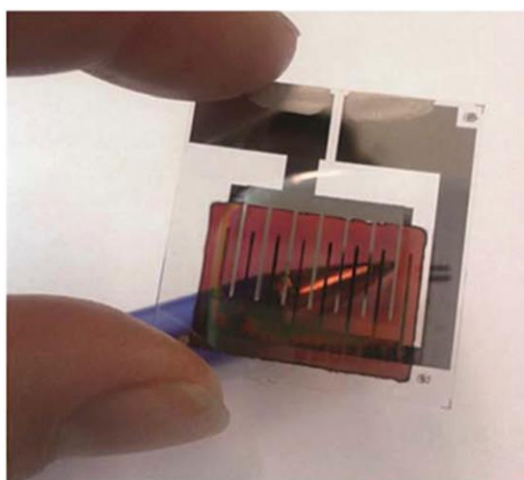


Figure 23. Semitransparent all-inkjet-printed solar cell with 1 cm² active area. Reprinted from reference [229] with permission of The Royal Society of Chemistry.

As described in this section, polymeric solar cells have been widely studied in combination with inkjet printing processing methodologies. Dye sensitized solar cells, that are also promising candidates for cheap production of PV modules, have been only recently explored in combination with R2R methodologies and in particular with inkjet printing [230–232]. Despite the impressive advances in the production of laboratory size polymeric photovoltaic devices showing good stability and efficiencies that demonstrate the potential of organic solar cell technology, the industrialisation and commercialisation of these devices is still to come. Inkjet printing has largely been demonstrated to be a solid candidate to replace or complement other techniques in R2R production of OPV and can contribute to the marketisation and future success of the OPV technology. Several companies (Merck, BASF, Plextronics, etc.) already commercialize organic semiconducting materials and research institutions, some of them mentioned in this review, and companies like BELECTRIC OPV GmbH are devoting large efforts to make large area inkjet printed organic solar cells closer to the market [233,234]. Reduction in cost of the materials and effective realisation of R2R production processes keeping a high efficiency and long lifetimes are required to make this technology penetrate the market.

7. Inkjet Printing of Self-Organizing Materials: Liquid Crystals and Colloidal Crystals

Top-down approaches make use of advanced tools, such as photolithographic, e-beam, ion-beam or inkjet printing setups, to generate patterns on top of or into a substrate. In contrast, bottom-up strategies rely on the ability of certain molecules or larger size entities to self-assemble, that is to autonomously organize, into defined structures or patterns through different kinds of interactions even if these are very weak [235]. The effective combination of both strategies, “bottom-up” and “top-down”, allows us to generate hierarchical structures crossing several length scales from the nanometre dimension of the molecule or self-assembling unit to the size of the device [236]. In this sense, the combination of self-organizing materials with inkjet printing represents an opportunity for the preparation of devices with different levels of organisation and complex functionality.

Liquid crystals are a well-known example of self-organizing soft molecular materials showing orientational order that extends to macroscopic distances. Orientational order in these materials has its origin in the shape anisotropy of the constituent molecules that align around a common orientation named director. In principle, the direction of the director is arbitrary in space; however, in practice, this direction is dictated by external forces, even when these are very small. Liquid crystals can be aligned along small grooves in the substrate surface, by the action of external electrical or magnetic fields or by surface tension forces [237]. When liquid crystal molecules are provided with reactive groups such as acrylates, orientation of the liquid crystal can be frozen by in situ photopolymerisation [238]. Reactive mesogens, as the ones of Figure 24a,b, can be oriented in their low molecular weight state. By including a small percentage of a radical photoinitiator, irradiation with UV light starts polymerisation. The incorporation in the reactive mixture of monomers with two reactive diacrylate groups (Figure 24b) results in crosslinked systems (liquid crystalline elastomers or mesogenic networks) that can freeze the initial orientation achieved in the monomeric state, as shown in Figure 24c.

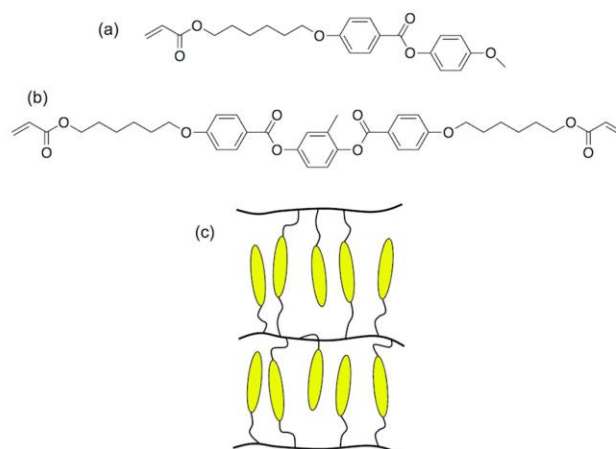


Figure 24. Reactive mesogens with (a) one or (b) two acrylate groups; (c) Diacrylate monomers establish crosslinks between polymeric chains.

Inkjet printing of liquid crystalline materials containing photoisomerizable azobenzene moieties has been successfully employed in the processing of soft light-driven micro actuators. Irradiation with light in the absorption bands of the photoisomerizable azobenzene unit induces isomerisation and therefore local molecular disorder generating internal stresses in the material that lead to light controlled deformations [239]. Inkjet printing has also been used in the production of polymeric liquid crystalline optical films showing genuine polarisation effects that can be applied, as disclosed by Moia and Johnson, to the protection of documents or goods [240]. These liquid crystalline prints are only

visible under special observation conditions using polarisers, acting as anti-counterfeiting features, as luminescent marks, that can also be obtained by inkjet printing, and are visible under certain light excitation conditions [241–245].

The inclusion of chiral molecules in a nematic liquid crystal induces the formation of a helical structure of the director having a pitch P that depends on the chiral dopant concentration and its helical twisting power (HTP) or ability to twist the nematic phase (Figure 25). Due to the optical anisotropy of the nematic phase, the introduced helical structure generates a periodic modulation of the refractive index leading to a photonic structure. These structures selectively reflect circularly polarised light of the same handedness of the helical structure and the reflected wavelength λ is given by the expression:

$$\lambda = \frac{n}{HTP \cdot c} \quad (7)$$

where n is the mean refractive index, that is the average of the ordinary and extraordinary refractive index, and c is the concentration of chiral dopant in weight percent [246].

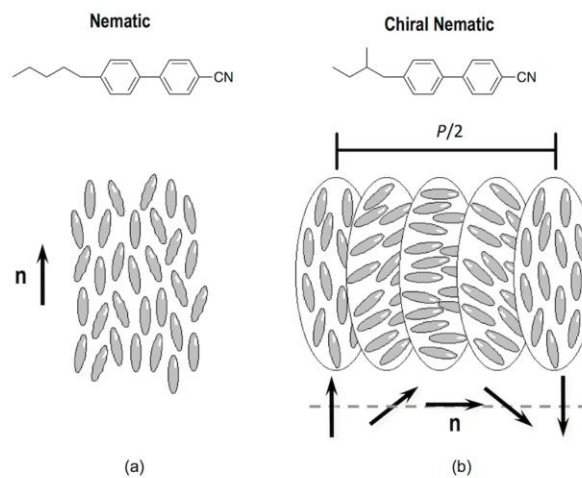


Figure 25. Chemical structure and mesophase arrangement of molecules in (a) a conventional nematic and in (b) a chiral nematic or cholesteric mesophase. The ability of inkjet printing to precisely deposit small amounts of material has been explored for the preparation of novel display concepts based on these cholesteric liquid crystals. Using a wall structure similar to that described in Sections 4 and 5 of this review, a chiral material can be deposited into each individual well and be filled afterwards with a cholesteric gel. The resulting pixels reflect different colours depending of the deposited materials and the reflection properties can be electrically addressed forming a multicolour cholesteric liquid crystal display [247].

The photonic structure spontaneously formed in chiral nematic liquid crystals has also been used for the preparation of lasers. The inclusion of a luminescent chromophore in the photonic structure can lead to laser emission if the photonic band gap overlaps with the fluorescence maximum of the dye [248]. Manufacturing of LC laser arrays has been performed by Coles and Hutchings groups at the University of Cambridge. By inkjet printing of a dye containing cholesteric liquid crystal mixture onto a wet film of polyvinyl alcohol, round, uniform sessile droplets with the helical axis orthogonal to the substrate can be obtained. The inkjet deposited drops in this way showed laser emission under optical excitation at the maximum of absorption the dye, with very narrow linewidths below 1 nm and well defined laser thresholds [249].

This type of chiral structures has also been explored in the preparation of optical sensing devices for different types of stimuli [246,250,251]. A change in the molecular order, produced for example

by temperature variation, can modify the cholesteric pitch and therefore the reflection wavelength becoming the system a temperature sensor. By including photoisomerizable molecules such as azobenzene chromophores, the cholesteric structure can act as a smart sensor that changes its colour with light. Light induced isomerisation of the azobenzene chromophores generates molecular disorder with a subsequent change in the helix pitch and reflected colour. Chemical sensors can also be prepared by the inclusion of selective receptor molecules into the chiral liquid crystalline material. Selective swelling of the helical structure can take place by selective molecular recognition, resulting in a change of the cholesteric reflection band.

Inkjet printing of humidity and temperature-sensitive films based on cholesteric liquid crystal layers has been demonstrated with potential application in sensing or anti-counterfeiting applications [252,253]. The work carried out by Schenning, Bastiaansen, Broer and co-workers has consistently demonstrated the preparation of battery-free sensors by inkjet printing of reactive mesogens and subsequent photopolymerisation. For example, films based on chiral nematic LC networks H-bonded through carboxylic acid groups, are converted to a hygroscopic polymer salt that shows a fast and reversibly change of their colour in response to humidity. Water saturated sensors based on this system can act as temperature/time integrators of interest for the control of the cold chain of food and pharmaceuticals (Figure 26) [253]. Inkjet printing has also been used in the preparation of other type of irreversible temperature/time integrators based this time in mechanical embossing of previously printed films, at temperatures above the glass transition temperature (T_g), followed by quenching below this temperature [254]. Trimethylamine sensors have also been prepared by inkjet printing using hydrogen-bonded cholesteric liquid crystals [255].

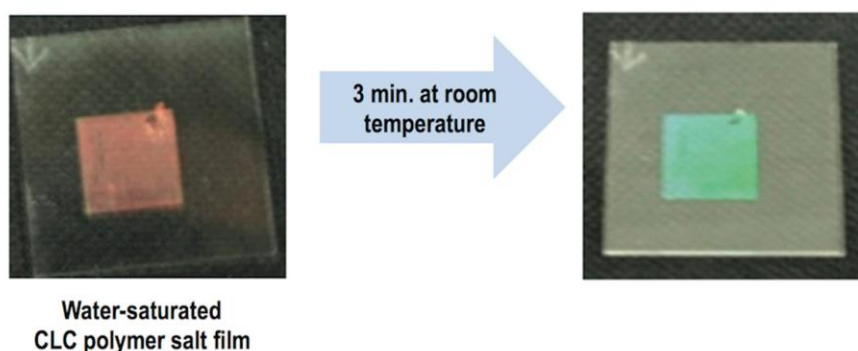


Figure 26. Inkjet printed water saturated cholesteric liquid crystal polymer salt film on polyimide coated glass in water (**left red film**) and after 3 min at room temperature (**right green film**). Adapted with permission from reference [253]. Copyright (2012) American Chemical Society.

All the research carried out in this topic demonstrates the feasibility of inkjet printing to produce this type of low-cost, battery-free cholesteric liquid crystal devices. The possibility to pattern the sensor materials and to generate different stimuli arrays in a single substrate/device makes inkjet printing an attractive tool for the massive production of sensors.

Besides liquid crystals, submicrometre-size, monodisperse colloidal particles can self-assemble into periodically well-organized structures that strongly interact with visible and IR light [256,257]. Compared to photolithographies, self-assembly offers a low-cost route for the manufacturing of these photonic structures over large areas, having the additional advantage of the easy inclusion of functionalities through their constituent colloidal particles. Patterning of these photonic structures has attracted extensive interest due to their potential application in the preparation of full colour displays, light waveguides, microfluidic devices or sensing arrays. Combination of bottom-up self-organisation of colloidal particles with top-down approaches has been explored to attain these patterned well-organised structures with hierarchical order. In particular, inkjet printing of colloidal

dispersions has demonstrated to be an interesting approach for the patterned growth of colloidal photonic crystals. Patterns deposited by inkjet become the template for colloidal self-assembly, which is a highly precise, high-throughput scalable approach for the preparation of patterned photonic structures (Figure 27).

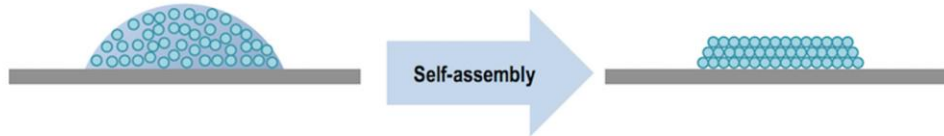


Figure 27. Monodisperse colloidal particles confined in a deposited drop self-assemble into well-ordered photonic structures during drying.

Fan and co-workers demonstrated the fabrication of hierarchically organized structures by an evaporation-induced self-assembly in combination with ink-jet printing [258]. They prepared an ink composed of oligomeric silica sols in ethanol/water with a surfactant concentration well below the critical micelle concentration (c.m.c.). After drop deposition by inkjet printing onto a surface, evaporation of ethanol makes the surfactant exceed the c.m.c., especially at the liquid-vapour interfaces, thus triggering the formation of micelles and their self-organization into long-range periodic structures. The possibility of generating microstructures with hierarchical organisation at the nanometre scale was demonstrated to be of interest in the fabrication of pH sensors for fluidic systems and with potential application in photonic devices and displays.

Besides the printing of silica sols, Moon and co-workers demonstrated the formation of photonic structures by evaporation-induced self-assembly of monodisperse microspheres of silica or polystyrene deposited as droplets by inkjet printing [259–262]. Morphology and size of the colloidal crystals can be controlled by adjusting the wettability of the substrate and the ink composition [259–265]. For example, evaporation of microsphere containing droplets showing a high contact angle, usually leads to dome like colloidal crystals of small radius, compared with the initial deposited drop size, since the contact line freely recedes without changing the angle. On the other hand, low contact angles usually lead to colloidal crystals with ring-like morphology. In this last case the liquid layer is very thin at the contact line and evaporation produces pinning of particles at the three-phase contact line. Further evaporation with this pinned contact line prevents the receding of the drop and drags the suspension toward the outer region, leading to concentration of the colloidal particles in the ring-like geometry, that is the coffee stain effect mentioned in Section 2 [259]. As in the case of polymer solutions, this effect can be suppressed or controlled by using a rationally designed mixture of solvents. Convective flow of particles towards the contact line can be compensated by the Marangoni flow induced by the surface tension gradient obtained when a small amount of higher boiling point/lower surface tension solvent is added to a lower boiling point/higher surface tension majority ink solvent. This can lead to homogenous round-shaped photonic crystals for isolated deposited droplets or line-shaped photonic structures when a continuous line of colloidal ink is deposited [261].

Another further development was carried out by Song's group when they printed large area patterned photonic crystals by ink-jet printing technology [266]. They used a polymer latex suspension of core-shell microspheres having a polystyrene core and a hydrophilic and soft poly(methyl methacrylate)/polyacrylic acid shell that favours self-assembly. By printing colloidal inks with microspheres of different diameter, namely 280, 220 and 180 nm, patterned photonic crystals showing respectively light reflections centred at 646, 541 and 465 nm, that is red, green and blue light were demonstrated. As in previous works from Moon, an adequate wettability of the substrate and the introduction of a co-solvent as ethylene glycol revealed to be crucial to obtain homogeneous photonic deposits of high quality. This facile fabrication method of patterned photonic crystals by ink-jet printing is promising for the preparation of photonic devices and optical circuits. Anti-counterfeiting

holograms for documents and goods protection have also been recently demonstrated by Nam and co-workers by using this technique [267].

As in the case of liquid crystalline cholesteric photonic structures, the colloidal photonic crystals can be made responsive to external stimuli by incorporation of appropriate functionalities in the structure. Colloidal photonic crystals prepared using inkjet printing have been employed in the implementation of humidity, vapour or protein sensors [268–270]. As an example, the group of Song has demonstrated the fabrication by inkjet printing of humidity sensors based on photonic crystals. The inclusion into the photonic crystal of poly(*N*-isopropyl acrylamide), presenting a reversible phase transition between a collapsed dehydrated state to a swollen hydrated form, is responsible of the fast and visible colour change in the order of seconds in response to the presence of water vapour [268]. Vapour responsive multicolour patterns were also reported by Bai and co-workers. They inkjet printed mesoporous silica microparticles with large active surface area and also large adsorption capability that can self-assemble forming colloidal photonic crystals. Vapour adsorption leads to changes in the average refractive index and therefore different reflection of the photonic structures as shown in Figure 28 [269].

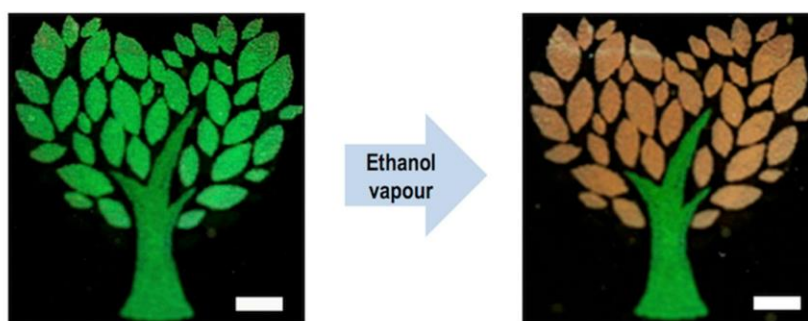


Figure 28. Inkjet printed colloidal photonic crystal pattern. The printed leaves are composed of self-assembled mesoporous silica microparticles with large adsorption capability while the tree trunk is made of solid silica microparticles. When exposed to N_2 (left) both photonic crystals present the same reflected colour. Exposure to ethanol vapour (right) reveals a change of colour in the mesoporous colloidal photonic crystal. Scale bar: 0.5 cm. Adapted with permission from Reference [269]. Copyright 2014 American Chemical Society.

Finally, inkjet printing can also be carried out on top of photonic crystals structures previously prepared by other methodologies locally varying the optical properties in these regions. This strategy has recently been used in the preparation of sensors for metal ions recognition [271]. Besides sensing, when droplets of other materials are infused into the photonic crystal, local swelling takes place in these regions, changing the reflected colours, an effect that has been used in the preparation of high resolution multicolour images [272].

Summarizing this section, the combination of self-assembly and inkjet printing has demonstrated to be an interesting approach for the preparation of functional surfaces and devices. Liquid crystal and colloidal microparticle based inks can be deposited by inkjet printing leading to hierarchical structures showing special optical behaviour. Control of the chemical functionality and the optical properties of the deposited materials as well as of the deposition process allows us to implement complex optical components as well as photonic devices such as lasers, sensors, anticounterfeiting elements or displays.

8. Summary and Conclusions

Beyond its use in graphics and marking, inkjet printing has become a very attractive tool for the digital manufacturing of functional surfaces and devices due to its ability to precisely position, with no-contact, a wide range of materials on a manifold of substrates. Besides this flexibility in

pattern formation, inkjet printing is an additive method that makes a very efficient use of materials, being therefore an environmentally friendly technique. Although inkjet printing is a serial patterning process, it can be scaled up by using multi-nozzle multi-heads with different inks allowing for the manufacturing of complex multi-material patterns with high throughput. The large interest in this technology has fed research in the fundamental physical processes that encompasses the generation of droplets, the interaction of the droplet with the substrate and the final transformation of the ink into a solid material. Understanding the relation between printhead architecture and dynamics, the acoustics and jet formation has allowed us to gain control on the drop generation process. The printability of different fluids has been largely explored identifying favourable regimes for stable drop formation at certain combinations of fluid properties (mainly viscosity, surface tension and density). However, as more demanding applications require the deposition of inks carrying polymers and/or microparticles with complex rheological behaviour, more research needs to be done to understand the drop formation mechanism in these fluids.

This review has presented an overview of the use of inkjet printing in the preparation of different optical elements and photonic devices. Inkjet printing has extensively been demonstrated to be a valuable tool for the manufacturing of microlenses with accurate control of the final optical parameters through appropriate selection of used materials and wetting characteristics of the substrate. Much less work has been carried out in the field of integrated optics despite interesting advances in the fabrication, using inkjet technology, of planar waveguides, inter-board optical connections between polymeric waveguides as well as integrated microring lasers have been done. Compared to other competitor technologies, such as photolithographies, inkjet printing has demonstrated to require less processing steps potentially being an interesting approach for the effective fabrication and integration of optical micro-devices.

In the field of large area photonic devices, a great effort has been done over the last two decades in the development of solution-processable materials for display and organic photovoltaic devices. The production using inkjet printing technology of OLED devices with excellent performance in terms of efficiency and durability, as well as colour gamut, as in the case of devices incorporating QDs, has been demonstrated in the laboratory. Efficient and stable BHJ solar cells have also been successfully produced at small scales by using this printing technology. Large efforts are being made to effectively integrate inkjet printing of these materials with R2R fabrication to reach high-efficiency and low-cost devices and make them closer to the market. Thinking in large-scale production, environmental issues are especially relevant, and attempts to eliminate chlorinated solvents of the production process are being done. Already, several small and large companies, covering the whole value chain, are already involved in finding a way towards the industrial production of large area photonic devices. Chemical companies commercialize organic semiconducting materials and industrial inkjet printing equipment with reasonably high throughput and yield is being developed specifically for these applications. Overall, inkjet printing technology appears to be a key enabling technology for the industrialisation and commercialisation of large area photonic devices in the near future.

Finally, the combined use of self-organizing materials and inkjet printing technology has been reviewed. In particular the use of liquid crystal and colloidal microparticle based inks has demonstrated to be an interesting approach for the preparation of hierarchical structures with striking optical behaviour. Introduction of specific functionalities in the inks has allowed us to implement photonic devices such as lasers or battery-free sensors for light, temperature or chemical vapour detection.

As an overall conclusion, inkjet printing has been demonstrated to be a valuable tool for the preparation of different optical components and photonic devices. As applications become closer to the market, requirements for inkjet printing are more demanding in terms of the used materials and also in the technology itself. Materials and processes resulting in cheaper and better performance devices are needed. More complex and extreme fluids, such as polymer solutions or colloidal dispersions, are nowadays being used requiring each time better performance printheads as well as a better understanding of fluid properties covering aspects that go from drop formation to its interaction with

the substrate and fixation. All this makes the field of inkjet printing research an extremely active and challenging area with fundamental research and industrial development advancing together towards applications.

Acknowledgments: This paper is dedicated to Rafael Alcalá on the occasion of his 70th anniversary. Carlos Sánchez-Somolinos thanks the Spanish MINECO project SAF2014-54763-C2-2-R, Gobierno de Aragón, and FEDER (EU).

Conflicts of Interest: The authors declare no conflict of interest.

References

1. Winckler, P.A. *Reader in the History of Books and Printing*; Greenwood Publishing Group; Information Handling Services: Englewood, CO, USA, 1983; Volume 26.
2. Singh, M.; Haverinen, H.M.; Dhagat, P.; Jabbour, G.E. Inkjet Printing-Process and Its Applications. *Adv. Mater.* **2010**, *22*, 673–685. [[CrossRef](#)] [[PubMed](#)]
3. Hutchings, I.M.; Martin, G.D. *Inkjet Technology for Digital Fabrication*; Wiley: Chichester, UK, 2013.
4. Tekin, E.; Smith, P.J.; Schubert, U.S. Inkjet printing as a deposition and patterning tool for polymers and inorganic particles. *Soft Matter* **2008**, *4*, 703–713. [[CrossRef](#)]
5. Clemens, W.; Lupo, D.; Hecker, K.; Breitung, S. *Roadmap for Organic and Printed Electronics*, 6th ed.; Hecker, K., Ed.; VDMA—The German Engineering Federation: Frankfurt am Main, Germany, 2015. Available online: www.oe-a.org/roadmap (accessed on 4 August 2016).
6. Basaran, O.A.; Gao, H.; Bhat, P.P. Nonstandard Inkjets. *Annu. Rev. Fluid Mech.* **2013**, *45*, 85–113. [[CrossRef](#)]
7. Derby, B. Inkjet Printing of Functional and Structural Materials: Fluid Property Requirements, Feature Stability, and Resolution. *Annu. Rev. Mater. Res.* **2010**, *40*, 395–414. [[CrossRef](#)]
8. Derby, B. Inkjet printing ceramics: From drops to solid. *J. Eur. Ceram. Soc.* **2011**, *31*, 2543–2550. [[CrossRef](#)]
9. Wijshoff, H. The dynamics of the piezo inkjet printhead operation. *Phys. Rep.* **2010**, *491*, 77–177. [[CrossRef](#)]
10. Hoath, S.D. (Ed.) *Fundamentals of Inkjet Printing: The Science of Inkjet and Droplets*; Wiley-VCH Verlag GmbH & Co.: Weinheim, Germany, 2016.
11. Bogy, D.B.; Talke, F.E. Experimental and theoretical study of wave propagation phenomena in drop-on-demand ink jet devices. *IBM J. Res. Dev.* **1984**, *28*, 314–321. [[CrossRef](#)]
12. Reis, N.; Ainsley, C.; Derby, B. Ink-jet delivery of particle suspensions by piezoelectric droplet ejectors. *J. Appl. Phys.* **2005**, *97*, 094903. [[CrossRef](#)]
13. Wu, H.-C.; Shan, T.-R.; Hwang, W.-S.; Lin, H.-J. Study of micro-droplet behavior for a piezoelectric inkjet printing device using a single pulse voltage pattern. *Mater. Trans.* **2004**, *45*, 1794–1801. [[CrossRef](#)]
14. Kwon, K.-S. Experimental analysis of waveform effects on satellite and ligament behavior via in situ measurement of the drop-on-demand drop formation curve and the instantaneous jetting speed curve. *J. Micromech. Microeng.* **2010**, *20*, 115005. [[CrossRef](#)]
15. Reis, N.; Derby, B. Ink jet deposition of ceramic suspensions: Modeling and experiments of droplet formation. *MRS Proc.* **2000**, *625*, 117. [[CrossRef](#)]
16. Seerden, K.A.; Reis, N.; Evans, J.R.; Grant, P.S.; Halloran, J.W.; Derby, B. Ink-jet printing of wax-based alumina suspensions. *J. Eur. Ceram. Soc.* **2001**, *84*, 2514–2520. [[CrossRef](#)]
17. Ainsley, C.; Reis, N.; Derby, B. Freeform fabrication by controlled droplet deposition of powder filled melts. *J. Mater. Sci.* **2002**, *37*, 3155–3161. [[CrossRef](#)]
18. Clasen, C.; Phillips, P.M.; Palangetic, L.; Vermant, A.J. Dispensing of rheologically complex fluids: The map of misery. *AIChE J.* **2011**, *58*, 3242–3255. [[CrossRef](#)]
19. Day, R.F.; Hinch, E.J.; Lister, J.R. Self-similar capillary pinchoff of an inviscid fluid. *Phys. Rev. Lett.* **1998**, *80*, 704–707. [[CrossRef](#)]
20. McKinley, G.H.; Renardy, M. Wolfgang von Ohnesorge. *Phys. Fluids* **2011**, *23*, 127101. [[CrossRef](#)]
21. Derby, B.; Reis, N.; Seerden, K.; Grant, P.S.; Evans, J. Freeform fabrication of ceramics by hot-melt ink-jet printing. *MRS Proc.* **2000**, *625*, 195. [[CrossRef](#)]
22. Jang, D.; Kim, D.; Moon, J. Influence of Fluid Physical Properties on Ink-Jet Printability. *Langmuir* **2009**, *25*, 2629–2635. [[CrossRef](#)] [[PubMed](#)]

23. Duineveld, P.C.; de Kok, M.M.; Buechel, M.; Sempel, A.; Mutsaers, K.A.; van de Weijer, P.; Camps, I.G.; van de Biggelaar, T.; Rubingh, J.-E.J.; Haskal, E.I. Ink-jet printing of polymer light-emitting devices. *Proc. SPIE* **2002**, *4464*, 59–67.
24. Stow, C.D.; Hadfield, M.G. An experimental investigation of fluid flow resulting from the impact of a water drop with an unyielding dry surface. *Proc. R. Soc. Lond. A Math. Phys. Eng. Sci.* **1981**, *373*, 419–441. [[CrossRef](#)]
25. Bhola, R.; Chandra, S. Parameters controlling solidification of molten wax droplets falling on a solid surface. *J. Mater. Sci.* **1999**, *34*, 4883–4894. [[CrossRef](#)]
26. Meyer, J.D.; Bazilevsky, A.V.; Rozhkov, A.N. Effects of polymeric additives on thermal ink jets. In Proceedings of the IS&T's NIP 13: International Conference on Digital Printing Technologies, Society for Imaging Science and Technology, Seattle, WA, USA, 2–7 November 1997; pp. 675–680.
27. Hoath, S.D.; Hutchings, I.M.; Martin, G.D.; Tuladhar, T.R.; Mackley, M.R.; Vadillo, D. Links Between Ink Rheology, Drop-on-Demand Jet Formation, and Printability. *J. Imaging Sci. Technol.* **2009**, *53*, 041208. [[CrossRef](#)]
28. Hoath, S.D.; Vadillo, D.C.; Harlen, O.G.; McIlroy, C.; Morrison, N.F.; Hsiao, W.-K.; Tuladhar, T.R.; Jung, S.; Martin, G.D.; Hutchings, I.M. Inkjet printing of weakly elastic polymer solutions. *J. Non-Newton. Fluid Mech.* **2014**, *205*, 1–10. [[CrossRef](#)]
29. Herran, C.L.; Coutris, N. Drop-on-demand for aqueous solutions of sodium alginate. *Exp. Fluids* **2013**, *54*, 1–25. [[CrossRef](#)]
30. Fromm, J.E. Numerical calculation of the fluid dynamics of drop-on-demand jets. *IBM J. Res. Dev.* **1984**, *28*, 322–333. [[CrossRef](#)]
31. Dong, H.; Carr, W.W.; Morris, J.F. An experimental study of drop-on-demand drop formation. *Phys. Fluids* **2006**, *18*, 072102. [[CrossRef](#)]
32. Chen, A.U.; Basaran, O.A. A new method for significantly reducing drop radius without reducing nozzle radius in drop-on-demand drop production. *Phys. Fluids* **2002**, *14*, L1–L4. [[CrossRef](#)]
33. Gan, H.Y.; Shan, X.; Eriksson, T.; Lok, B.K.; Lam, Y.C. Reduction of droplet volume by controlling actuating waveforms in inkjet printing for micro-pattern formation. *J. Micromech. Microeng.* **2009**, *19*, 055010. [[CrossRef](#)]
34. Derby, B. Additive Manufacture of Ceramics Components by Inkjet Printing. *Engineering* **2016**, *1*, 113–123. [[CrossRef](#)]
35. Schiaffino, S.; Sonin, A.A. Molten droplet deposition and solidification at low Weber numbers. *Phys. Fluids* **1997**, *9*, 3172–3187. [[CrossRef](#)]
36. Yarin, A.L. Drop impact dynamics: Splashing, spreading, receding, bouncing *Annu. Rev. Fluid Mech.* **2006**, *38*, 159–192. [[CrossRef](#)]
37. Van Dam, D.B.; Le Clerc, C. Experimental study of the impact of an ink-jet printed droplet on a solid substrate. *Phys. Fluids* **2004**, *16*, 3403–3414. [[CrossRef](#)]
38. Park, J.-U.; Hardy, M.; Kang, S.J.; Barton, K.; Adair, K.; Mukhopadhyay, D.K.; Lee, C.Y.; Strano, M.S.; Alleyne, A.G.; Georgiadis, J.G.; et al. High-resolution electrohydrodynamic jet printing. *Nat. Mater.* **2007**, *6*, 782–789. [[CrossRef](#)] [[PubMed](#)]
39. Davis, S.H. Moving contact lines and rivulet instabilities. Part 1. The static rivulet. *J. Fluid Mech.* **1980**, *98*, 225–242. [[CrossRef](#)]
40. Schiaffino, S.; Sonin, A.A. Formation and stability of liquid and molten beads on a solid surface. *J. Fluid Mech.* **1997**, *343*, 95–110. [[CrossRef](#)]
41. Soltman, D.; Subramanian, V. Inkjet-Printed Line Morphologies and Temperature Control of the Coffee Ring Effect. *Langmuir* **2008**, *24*, 2224–2231. [[CrossRef](#)] [[PubMed](#)]
42. Stringer, J.; Derby, B. Limits to feature size and resolution in ink jet printing. *J. Eur. Ceram. Soc.* **2009**, *29*, 913–918. [[CrossRef](#)]
43. Stringer, J.; Derby, B. Formation and Stability of Lines Produced by Inkjet Printing. *Langmuir* **2010**, *26*, 10365–10372. [[CrossRef](#)] [[PubMed](#)]
44. Smith, P.J.; Shin, D.Y.; Stringer, J.E.; Derby, B.; Reis, N. Direct ink-jet printing and low temperature conversion of conductive silver patterns. *J. Mater. Sci.* **2006**, *41*, 4153–4158. [[CrossRef](#)]
45. Duineveld, P.C. The stability of ink-jet printed lines of liquid with zero receding contact angle on a homogeneous substrate. *J. Fluid Mech.* **2003**, *477*, 1–26. [[CrossRef](#)]

46. Tekin, E.; Holder, E.; Marin, V.; de Gans, B.-J.; Schubert, U.S. Ink-Jet Printing of Luminescent Ruthenium- and Iridium-Containing Polymers for Applications in Light-Emitting Devices. *Macromol. Rapid Commun.* **2005**, *26*, 293–297. [[CrossRef](#)]
47. Tekin, E.; de Gans, B.-J.; Schubert, U.S. Ink-jet printing of polymers—From single dots to thin film libraries. *J. Mater. Chem.* **2004**, *14*, 2627–2632. [[CrossRef](#)]
48. Kang, H.; Soltman, D.; Subramanian, V. Hydrostatic Optimization of Inkjet-Printed Films. *Langmuir* **2010**, *26*, 11568–11573. [[CrossRef](#)] [[PubMed](#)]
49. Soltman, D.; Smith, B.; Kang, H.; Morris, S.J.S.; Subramanian, V. Methodology for Inkjet Printing of Partially Wetting Films. *Langmuir* **2010**, *26*, 15686–15693. [[CrossRef](#)] [[PubMed](#)]
50. Deegan, R.D.; Bakajin, O.; Dupont, T.F.; Huber, G.; Nagel, S.R.; Witten, T.A. Capillary flow as the cause of ring stains from dried liquid drops. *Nature* **1997**, *389*, 827–829. [[CrossRef](#)]
51. Deegan, R.D.; Bakajin, O.; Dupont, T.F.; Huber, G.; Nagel, S.R.; Witten, T.A. Contact line deposits in an evaporating drop. *Phys. Rev. E* **2000**, *62*, 756. [[CrossRef](#)]
52. Sun, J.; Bao, B.; He, M.; Zhou, H.; Song, Y. Recent advances in controlling the depositing morphologies of inkjet droplets. *ACS Appl. Mater. Interfaces* **2015**, *7*, 28086–28099. [[CrossRef](#)] [[PubMed](#)]
53. Magdassi, S.; Grouchko, M.; Toker, D.; Kamyshny, A.; Balberg, I.; Millo, O. Ring Stain Effect at Room Temperature in Silver Nanoparticles Yields High Electrical Conductivity. *Langmuir* **2005**, *21*, 10264–10267. [[CrossRef](#)] [[PubMed](#)]
54. Zhang, C.; Zou, C.L.; Zhao, Y.; Dong, C.H.; Wei, C.; Wang, H.; Liu, Y.; Guo, G.C.; Yao, J.; Zhao, Y.S. Organic printed photonics: From microring lasers to integrated circuits. *Sci. Adv.* **2015**, *1*, e1500257. [[CrossRef](#)] [[PubMed](#)]
55. Lim, J.A.; Lee, W.H.; Lee, H.S.; Lee, J.H.; Park, Y.D.; Cho, K. Self-Organization of Ink-jet-Printed Triisopropylsilylethynyl Pentacene via Evaporation-Induced Flows in a Drying Droplet. *Adv. Funct. Mater.* **2008**, *18*, 229–234. [[CrossRef](#)]
56. Tekin, E.; Smith, P.J.; Hoepfener, S.; van den Berg, A.M.J.; Susha, A.S.; Rogach, A.L.; Feldmann, J.; Schubert, U.S. Inkjet Printing of Luminescent CdTe Nanocrystal–Polymer Composites. *Adv. Funct. Mater.* **2007**, *17*, 23–28. [[CrossRef](#)]
57. De Gans, B.-J.; Schubert, U.S. Inkjet Printing of Well-Defined Polymer Dots and Arrays. *Langmuir* **2004**, *20*, 7789–7793. [[CrossRef](#)] [[PubMed](#)]
58. Zappe, H. *Fundamentals of Micro-Optics*, 1st ed.; Cambridge University Press: Cambridge, UK, 2010.
59. Popovic, Z.D.; Sprague, R.A.; Connell, G.N. Technique for monolithic fabrication of microlens arrays. *Appl. Opt.* **1988**, *27*, 1281–1284. [[CrossRef](#)] [[PubMed](#)]
60. Wu, M.H.; Park, C.; Whitesides, G.M. Fabrication of arrays of microlenses with controlled profiles using gray-scale microlens projection photolithography. *Langmuir* **2002**, *18*, 9312–9318. [[CrossRef](#)]
61. MacFarlane, D.L.; Narayan, V.; Tatum, J.A.; Cox, W.R.; Chen, T.; Hayes, D.J. Microjet fabrication of microlens arrays. *IEEE Photonics Technol. Lett.* **1994**, *6*, 1112–1114. [[CrossRef](#)]
62. Voigt, A.; Ostrzinski, U.; Pfeiffer, K.; Kim, J.Y.; Fakhfour, V.; Brugger, J.; Gruetzner, G. New inks for the direct drop-on-demand fabrication of polymer lenses. *Microelectron. Eng.* **2011**, *88*, 2174–2179. [[CrossRef](#)]
63. Xie, D.; Zhang, H.; Shu, X.; Xiao, J. Fabrication of polymer micro-lens array with pneumatically diaphragm-driven drop-on-demand inkjet technology. *Opt. Express* **2012**, *20*, 15186–15195. [[CrossRef](#)] [[PubMed](#)]
64. Fakhfour, V.; Cantale, N.; Mermoud, G.; Kim, J.Y.; Boiko, D.; Charbon, E.; Brugger, J. Inkjet printing of SU-8 for polymer-based MEMS a case study for microlenses. In *Proceeding of the 21st IEEE International Conference on Micro Electro Mechanical Systems*, Tucson, AZ, USA, 13–17 January 2008; pp. 407–410.
65. Chen, C.T.; Chiu, C.L.; Tseng, Z.F.; Chuang, C.T. Dynamic evolution and formation of refractive microlenses self-assembled from evaporative polyurethane droplets. *Sens. Actuators A Phys.* **2008**, *147*, 369–377. [[CrossRef](#)]
66. Chen, C.T.; Tseng, Z.F.; Chiu, C.L.; Hsu, C.Y.; Chuang, C.T. Self-aligned hemispherical formation of microlenses from colloidal droplets on heterogeneous surfaces. *J. Micromech. Microeng.* **2009**, *19*, 025002. [[CrossRef](#)]
67. Chen, F.C.; Lu, J.P.; Huang, W.K. Using ink-jet printing and coffee ring effect to fabricate refractive microlens arrays. *IEEE Photonics Technol. Lett.* **2009**, *21*, 648–650. [[CrossRef](#)]

68. Jacot-Descombes, L.; Gullo, M.R.; Cadarso, V.J.; Brugger, J. Fabrication of epoxy spherical microstructures by controlled drop-on-demand inkjet printing. *J. Micromech. Microeng.* **2012**, *22*, 074012. [[CrossRef](#)]
69. Cadarso, V.J.; Perera-Núñez, J.; Jacot-Descombes, L.; Pfeiffer, K.; Ostrzinski, U.; Voigt, A.; Llobera, A.; Grützer, G.; Brugger, J. Microlenses with defined contour shapes. *Opt. Express* **2011**, *19*, 18665–18670. [[CrossRef](#)] [[PubMed](#)]
70. Blattmann, M.; Ocker, M.; Zappe, H.; Seifert, A. Jet printing of convex and concave polymer micro-lenses. *Opt. Express* **2015**, *23*, 24525–24536. [[CrossRef](#)] [[PubMed](#)]
71. Biehl, S.; Danzebrink, R.; Oliveira, P.; Aegerter, M.A. Refractive microlens fabrication by ink-jet process. *J. Sol-Gel Sci. Technol.* **1998**, *13*, 177–182. [[CrossRef](#)]
72. Danzebrink, R.; Aegerter, M.A. Deposition of micropatterned coating using an ink-jet technique. *Thin Solid Films* **1999**, *351*, 115–118. [[CrossRef](#)]
73. Danzebrink, R.; Aegerter, M.A. Deposition of optical microlens arrays by ink-jet processes. *Thin Solid Films* **2001**, *392*, 223–225. [[CrossRef](#)]
74. Kim, J.Y.; Brauer, N.B.; Fakhfour, V.; Boiko, D.L.; Charbon, E.; Grützer, G.; Brugger, J. Hybrid polymer microlens arrays with high numerical apertures fabricated using simple ink-jet printing technique. *Opt. Mater. Express* **2011**, *1*, 259–269. [[CrossRef](#)]
75. Kim, J.Y.; Pfeiffer, K.; Voigt, A.; Gruetzner, G.; Brugger, J. Directly fabricated multi-scale microlens arrays on a hydrophobic flat surface by a simple ink-jet printing technique. *J. Mater. Chem.* **2012**, *22*, 3053–3058. [[CrossRef](#)]
76. Kim, J.Y.; Martin-Olmos, C.; Baek, N.S.; Brugger, J. Simple and easily controllable parabolic-shaped microlenses printed on polymeric mesas. *J. Mater. Chem. C* **2013**, *1*, 2152–2157. [[CrossRef](#)]
77. Descombes, L.J.; Cadarso, V.J.; Schleunitz, A.; Grützer, S.; Klein, J.J.; Brugger, J.; Schiff, H.; Grützer, G. Organic-inorganic-hybrid-polymer microlens arrays with tailored optical characteristics and multi-focal properties. *Opt. Express* **2015**, *23*, 25365–25376. [[CrossRef](#)] [[PubMed](#)]
78. Sanchez, E.A.; Waldmann, M.; Arnold, C.B. Chalcogenide glass microlenses by inkjet printing. *Appl. Opt.* **2011**, *50*, 1974–1978. [[CrossRef](#)] [[PubMed](#)]
79. Bonaccorso, E.; Butt, H.J.; Hankeln, B.; Niesenhaus, B.; Graf, K. Fabrication of microvessels and microlenses from polymers by solvent droplets. *Appl. Phys. Lett.* **2005**, *86*, 124101. [[CrossRef](#)]
80. Grimaldi, I.A.; De Girolamo Del Mauro, A.; Nenna, G.; Loffredo, F.; Minarini, C.; Villani, F. Microstructuring of polymer films by inkjet etching. *J. Appl. Polym. Sci.* **2011**, *122*, 3637–3643. [[CrossRef](#)]
81. Pericet-Camara, R.; Best, A.; Nett, S.K.; Gutmann, J.S.; Bonaccorso, E. Arrays of microlenses with variable focal lengths fabricated by restructuring polymer surfaces with an ink-jet device. *Opt. Express* **2007**, *15*, 9877–9882. [[CrossRef](#)] [[PubMed](#)]
82. Cox, W.R.; Guan, C.; Hayes, D.J.; Wallace, D.B. Microjet printing of micro-optical interconnects. *Proc. SPIE Int. Soc. Opt. Eng.* **2000**, *3952*, 220–225.
83. Cox, W.R.; Guan, C.; Hayes, D.J. Microjet printing of micro-optical interconnects and sensors. *Proc. SPIE Optoelectron. Interconnects VII* **2000**, *3952*, 400–407.
84. Hayes, D.J.; Chen, T. Next-generation optoelectronic components enabled by direct-write microprinting technology. *Def. Secur.* **2004**, *5435*, 83–90.
85. Cox, W.R.; Chen, T.; Ussery, D.; Hayes, D.J.; Tatum, J.A.; MacFarlane, D.L. Microjetted lenslet triplet fibers. *Opt. Commun.* **1996**, *123*, 492–496. [[CrossRef](#)]
86. Ishii, Y.; Koike, S.; Arai, Y.; Ando, Y. Ink-jet fabrication of polymer microlens for optical-I/O chip packaging. *Jpn. J. Appl. Phys.* **2000**, *39*, 1490. [[CrossRef](#)]
87. Lee, H.S.; Park, I.; Jeon, K.S.; Lee, E.H. Fabrication of micro-lenses for optical interconnection using micro ink-jetting technique. *Microelectron. Eng.* **2010**, *87*, 1447–1450. [[CrossRef](#)]
88. Lin, X.; Hosseini, A.; Dou, X.; Subbaraman, H.; Chen, R.T. Low-cost board-to-board optical interconnects using molded polymer waveguide with 45 degree mirrors and inkjet-printed micro-lenses as proximity vertical coupler. *Opt. Express* **2013**, *21*, 60–69. [[CrossRef](#)] [[PubMed](#)]
89. Tien, C.H.; Hung, C.H.; Yu, T.H. Microlens arrays by direct-writing inkjet print for LCD backlighting applications. *J. Disp. Technol.* **2009**, *5*, 147–151. [[CrossRef](#)]
90. Wang, M.W.; Pang, D.C.; Tseng, Y.E.; Tseng, C.C. The study of light guide plate fabricated by inkjet printing technique. *J. Taiwan Inst. Chem. E.* **2014**, *45*, 1049–1055. [[CrossRef](#)]

91. Chen, C.-T.; Tsai, T.-W. Multilayer polymer light guides integrated with refractive microlenses and liquid by micromolding and inkjet printing. *Sens. Actuators A* **2016**, *244*, 252–260. [[CrossRef](#)]
92. Hayes, D.J.; Wallace, D.B.; Royall Cox, W. MicroJet printing of solder and polymers for multi-chip modules and chip-scale packages. *Proc. SPIE Int. Soc. Opt. Eng.* **1999**, *3830*, 242–247.
93. Cox, W.R.; Chen, T.; Hayes, D.J. Micro-Optics Fabrication by Ink-jet Printing. *Opt. Photonics News* **2001**, *12*, 32–35. [[CrossRef](#)]
94. Parker, S.T.; Domachuk, P.; Amsden, J.; Bressner, J.; Lewis, J.A.; Kaplan, D.L.; Omenetto, F.G. Biocompatible silk printed optical waveguides. *Adv. Mater.* **2009**, *21*, 2411–2415. [[CrossRef](#)]
95. Wallace, D.; Hayes, D.; Chen, T.; Shah, V.; Radulescu, D.; Cooley, P.; Nallani, A. Think additive: Ink-jet deposition of materials for MEMS packaging. In Proceedings of the 6th Topical Workshop on Packaging of MEMS and Related Micro-Nano-Bio Integrated Systems, Long Beach, CA, USA, 18–20 November 2004.
96. Chappell, J.; Hutt, D.A.; Conway, P.P. Variation in the line stability of an inkjet printed optical waveguide-applicable material. In Proceedings of the 2nd Electronics System-Integration Technology Conference, Greenwich, UK, 1–4 September 2008; pp. 1267–1272.
97. Vacirca, N.A.; Kurzweg, T.P. Inkjet printing techniques for the fabrication of polymer optical waveguides. *Proc. SPIE Int. Soc. Opt. Photonics* **2010**, *7591*, 75910A.
98. Wolfer, T.; Bollgruen, P.; Mager, D.; Overmeyer, L.; Korvink, J.G. Flexographic and inkjet printing of polymer optical waveguides for fully integrated sensor systems. *Procedia Technol.* **2014**, *15*, 521–529. [[CrossRef](#)]
99. Wolfer, T.; Bollgruen, P.; Mager, D.; Overmeyer, L.; Korvink, J.G. Printing and preparation of integrated optical waveguides for optronic sensor networks. *Mechatronics* **2016**, *34*, 119–127. [[CrossRef](#)]
100. Burroughes, J.H.; Bradley, D.; Brown, A.R.; Marks, R.N.; Mackay, K.; Friend, R.H.; Burns, P.L.; Holmes, A.B. Light-emitting diodes based on conjugated polymers. *Nature* **1990**, *347*, 539–541. [[CrossRef](#)]
101. Li, Z.R. (Ed.) *Organic Light-Emitting Materials and Devices*, 2nd ed.; CRC Press: Boca Raton, FL, USA, 2015.
102. Akcelrud, L. Electroluminescent polymers. *Prog. Polym. Sci.* **2003**, *28*, 875–962. [[CrossRef](#)]
103. Grimsdale, A.C.; Leok Chan, K.; Martin, R.E.; Jokisz, P.G.; Holmes, A.B. Synthesis of Light-Emitting Conjugated Polymers for Applications in Electroluminescent Devices. *Chem. Rev.* **2009**, *109*, 897–1091. [[CrossRef](#)] [[PubMed](#)]
104. Cantatore, E. (Ed.) *Applications of Organic and Printed Electronics*; Springer: New York, NY, USA, 2013.
105. Kamtekar, K.T.; Monkman, A.P.; Bryce, M.R. Recent Advances in White Organic Light-Emitting Materials and Devices (WOLEDs). *Adv. Mater.* **2010**, *22*, 572–582. [[CrossRef](#)] [[PubMed](#)]
106. Sekine, C.; Tsubata, Y.; Yamada, T.; Kitano, M.; Doi, S. Recent progress of high performance polymer OLED and OPV materials for organic printed electronics. *Sci. Technol. Adv. Mater.* **2014**, *15*, 034203. [[CrossRef](#)]
107. Halls, J. Ink-Jet printing of PLED displays. *Inf. Disp.* **2005**, *2*, 11.
108. Chen, P.-Y.; Chen, C.-C.; Hsieh, C.-C.; Lin, J.-M.; Lin, Y.-S.; Lin, Y. High resolution organic light-emitting diode panel fabricated by ink jet printing process. *SID Symp. Dig. Tech. Pap.* **2015**, *46*, 1352–1354. [[CrossRef](#)]
109. Hebner, T.R.; Wu, C.C.; Marcy, D.; Lu, M.H.; Sturm, J.C. Ink-jet printing of doped polymers for organic light emitting devices. *Appl. Phys. Lett.* **1998**, *72*, 519–521. [[CrossRef](#)]
110. Yang, Y.; Chang, S.-C.; Bharathan, J.; Liu, J. Organic/polymeric electroluminescent devices processed by hybrid ink-jet printing. *J. Mater. Sci. Mater. Electron.* **2000**, *11*, 89–96. [[CrossRef](#)]
111. Bharathan, J.; Yang, Y. Polymer electroluminescent devices processed by inkjet printing: I. Polymer light-emitting logo. *Appl. Phys. Lett.* **1998**, *72*, 2660–2662. [[CrossRef](#)]
112. Chang, S.-C.; Bharathan, J.; Yang, Y.; Helgeson, R.; Wudl, F.; Ramey, M.B.; Reynolds, J.R. Dual-color polymer light-emitting pixels processed by hybrid inkjet printing. *Appl. Phys. Lett.* **1998**, *73*, 2561–2563. [[CrossRef](#)]
113. Chang, S.-C.; Liu, J.; Bharathan, J.; Yang, Y.; Onohara, J.; Kido, J. Multicolor organic light-emitting diodes processed by hybrid inkjet printing. *Adv. Mater.* **1999**, *11*, 734–737. [[CrossRef](#)]
114. Shimoda, T.; Kimura, M.; Seki, S.; Kobayashi, H.; Kanbe, S.; Miyashita, S.; Friend, R.H.; Burroughes, J.H.; Towns, C.R.; Millard, I.S. Technology for active matrix light emitting polymer displays. In Proceedings of the International Electron Devices Meeting Technical Digest, Washington, DC, USA, 5–8 December 1999; pp. 107–110.
115. Kobayashi, H.; Kanbe, S.; Seki, S.; Kiguchi, H.; Kimura, M.; Yudasaka, I.; Miyashita, S.; Shimoda, T.; Towns, C.R.; Burroughes, J.H. A novel RGB multicolor light-emitting polymer display. *Synth. Met.* **2000**, *111*, 125–128. [[CrossRef](#)]

116. Dijkman, J.F.; Duineveld, P.C.; Hack, M.J.J.; Pierik, A.; Rensen, J.; Rubingh, J.E.; Schram, I.; Vernhout, M.M. Precision ink jet printing of polymer light emitting displays. *J. Mater. Chem.* **2007**, *17*, 511–522. [[CrossRef](#)]
117. Lee, J.-H.; Ho, Y.-H.; Lin, T.-C.; Wu, C.-F. High-Efficiency Fluorescent Blue Organic Light-Emitting Device with Balanced Carrier Transport. *J. Electrochem. Soc.* **2007**, *154*, J226–J228. [[CrossRef](#)]
118. Haskal, E.I.; Büchel, M.; Duineveld, P.C.; Sempel, A.; van de Weijer, P. Passive-matrix polymer light-emitting displays. *MRS Bull.* **2002**, *27*, 864–869. [[CrossRef](#)]
119. Huang, J.; Liu, Q.; Zou, J.-H.; Zhu, X.-H.; Li, A.-Y.; Li, J.-W.; Wu, S.; Peng, J.; Cao, Y.; Xia, R.; et al. Electroluminescence and Laser Emission of Soluble Pure Red Fluorescent Molecular Glasses Based on Dithienylbenzothiadiazole. *Adv. Funct. Mater.* **2009**, *19*, 2978–2986. [[CrossRef](#)]
120. Hayer, A.; Anémian, R.; Eberle, T.; Heun, S.; Ludemann, A.; Schulte, N.; Buchholz, H. Concepts for solution-processable OLED materials at Merck. *J. Inf. Display* **2011**, *12*, 57–59. [[CrossRef](#)]
121. Gorter, H.; Coenen, M.J.J.; Slaats, M.W.L.; Ren, M.; Lu, W.; Kuijpers, C.J.; Groen, W.A. Toward inkjet printing of small molecule organic light emitting diodes. *Thin Solid Films* **2013**, *532*, 11–15. [[CrossRef](#)]
122. Coenen, M.J.J.; Slaats, T.M.W.L.; Eggenhuisen, T.M.; Groen, P. Inkjet printing the three organic functional layers of two-colored organic light emitting diodes. *Thin Solid Films* **2015**, *583*, 194–200. [[CrossRef](#)]
123. Burrows, P.E.; Bulovic, V.; Forrest, S.R.; Sapochak, L.S.; McCarty, D.M.; Thompson, M.E. Reliability and degradation of organic light emitting devices. *Appl. Phys. Lett.* **1994**, *65*, 2922–2924. [[CrossRef](#)]
124. Caironi, M.; Noh, Y.Y. (Eds.) *Large Area and Flexible Electronics*; John Wiley & Sons: Weinheim, Germany, 2015.
125. Groenendaal, L.; Jonas, F.; Freitag, D.; Pielartzik, H.; Reynolds, J.R. Poly (3, 4-ethylenedioxythiophene) and its derivatives: Past, present, and future. *Adv. Mater.* **2000**, *12*, 481–494. [[CrossRef](#)]
126. Aleeva, Y.; Pignataro, B. Recent advances in upscalable wet methods and ink formulations for printed electronics. *J. Mater. Chem. C Mater. Opt. Electron. Devices* **2014**, *2*, 6436–6453. [[CrossRef](#)]
127. Shimoda, T.; Morii, K.; Seki, S.; Kiguchi, H. Inkjet printing of light-emitting polymer displays. *MRS Bull.* **2003**, *28*, 821–827. [[CrossRef](#)]
128. Ren, M.; Gorter, H.; Michels, J.; Andriessen, R. Ink jet technology for large area organic light-emitting diode and organic photovoltaic applications. *J. Imaging Sci. Technol.* **2011**, *55*, 40301. [[CrossRef](#)]
129. Meixner, R.M.; Cibis, D.; Krueger, K.; Goebel, H. Characterization of polymer inks for drop-on-demand printing systems. *Microsyst. Technol.* **2008**, *14*, 1137–1142. [[CrossRef](#)]
130. Yoshioka, Y.; Calvert, P.D.; Jabbour, G.E. Simple Modification of Sheet Resistivity of Conducting Polymeric Anodes via Combinatorial Ink-Jet Printing Techniques. *Macromol. Rapid Commun.* **2005**, *26*, 238–246. [[CrossRef](#)]
131. Ummartyotin, S.; Juntaro, J.; Wu, C.; Sain, M.; Manuspiya, H. Deposition of PEDOT: PSS Nanoparticles as a Conductive Microlayer Anode in OLEDs Device by Desktop Inkjet Printer. *J. Nanomater.* **2011**, *2011*, 1–7. [[CrossRef](#)]
132. Hermerschmidt, F.; Burgués-Ceballos, I.; Savva, A.; Sepos, E.D.; Lange, A.; Boeffel, C.; Nau, S.; List-Kratochvil, E.J.W.; Choulis, S.A. High performance indium tin oxide-free solution-processed organic light emitting diodes based on inkjet-printed fine silver grid lines. *Flex. Print. Electron.* **2016**, *1*, 035004. [[CrossRef](#)]
133. De Gans, B.J.; Duineveld, P.C.; Schubert, U.S. Inkjet Printing of Polymers: State of the Art and Future Developments. *Adv. Mater.* **2004**, *16*, 203–213. [[CrossRef](#)]
134. Zuniga, C.A.; Barlow, S.; Marder, S.R. Approaches to Solution-Processed Multilayer Organic Light-Emitting Diodes Based on Cross-Linking. *Chem. Mater.* **2011**, *23*, 658–681. [[CrossRef](#)]
135. Yoshioka, Y.; Jabbour, G.E. Inkjet Printing of Oxidants for Patterning of Nanometer-Thick Conducting Polymer Electrodes. *Adv. Mater.* **2006**, *18*, 1307–1312. [[CrossRef](#)]
136. Eales, A.D.; Routh, A.F.; Dartnell, N.; Goddard, S. Evaporation of pinned droplets containing polymer—An examination of the important groups controlling final shape. *AIChE J.* **2015**, *61*, 1759–1767. [[CrossRef](#)]
137. Villani, F.; Vacca, P.; Nenna, G.; Valentino, O.; Burrasca, G.; Fasolino, T.; Minarini, C.; della Sala, D. Inkjet Printed Polymer Layer on Flexible Substrate for OLED Applications. *J. Phys. Chem. C* **2009**, *113*, 13398–13402. [[CrossRef](#)]
138. Sun, T.X.; Jabbour, G.E. Combinatorial screening and optimization of luminescent materials and organic light-emitting devices. *MRS Bull.* **2002**, *27*, 309–315. [[CrossRef](#)]
139. Tekin, E.; Wijlaars, H.; Holder, E.; Egbe, D.A.; Schubert, U.S. Film thickness dependency of the emission colors of PPE–PPVs in inkjet printed libraries. *J. Mater. Chem.* **2006**, *16*, 4294–4298. [[CrossRef](#)]

140. Tekin, E.; Holder, E.; Kozodaev, D.; Schubert, U.S. Controlled Pattern Formation of Poly[2-methoxy-5-(2'-ethylhexyloxy)-1,4-phenylenevinylene] (MEH-PPV) by Ink-Jet Printing. *Adv. Funct. Mater.* **2007**, *17*, 277–284. [[CrossRef](#)]
141. Teichler, A.; Eckardt, R.; Friebe, C.; Perelaer, J.; Schubert, U.S. Film formation properties of inkjet printed poly(phenylene-ethynylene)-poly(phenylene-vinylene)s. *Thin Solid Films* **2011**, *519*, 3695–3702. [[CrossRef](#)]
142. Teichler, A.; Shu, Z.; Wild, A.; Bader, C.; Nowotny, J.; Kirchner, G.; Harkema, S.; Perelaer, J.; Schubert, U.S. Inkjet printing of chemically tailored light-emitting polymers. *Eur. Polym. J.* **2013**, *49*, 2186–2195. [[CrossRef](#)]
143. Bao, B.; Li, M.; Li, Y.; Jiang, J.; Gu, Z.; Zhang, X.; Jiang, L.; Song, Y. Patterning Fluorescent Quantum Dot Nanocomposites by Reactive Inkjet Printing. *Small* **2015**, *11*, 1649–1654. [[CrossRef](#)] [[PubMed](#)]
144. Wood, V.; Panzer, M.; Sullivan, S.C.; Bulovic, V. Colloidal quantum dot light-emitting devices. In *Colloidal Quantum Dot Optoelectronics and Photovoltaics*; Konstantatos, G., Sargent, E.H., Eds.; Cambridge University Press: Cambridge, UK, 2013.
145. Mattoussi, H.; Radzilowski, L.H.; Dabbousi, B.O.; Thomas, E.L.; Bawendi, M.G.; Rubner, M.F. Electroluminescence from heterostructures of poly(phenylene vinylene) and inorganic CdSe nanocrystals. *J. Appl. Phys.* **1998**, *83*, 7965–7974. [[CrossRef](#)]
146. Shirasaki, Y.; Supran, G.J.; Bawendi, M.G.; Bulović, V. Emergence of colloidal quantum-dot light-emitting technologies. *Nat. Photonics* **2013**, *7*, 13–23. [[CrossRef](#)]
147. Kim, T.-H.; Cho, K.-S.; Lee, E.K.; Lee, S.J.; Chae, J.; Kim, J.W.; Kim, D.H.; Kwon, J.-Y.; Amaratunga, G.; Lee, Y.; et al. Full-colour quantum dot displays fabricated by transfer printing. *Nat. Photonics* **2011**, *5*, 176–182. [[CrossRef](#)]
148. Haverinen, H.M.; Myllylä, R.A.; Jabbour, G.E. Inkjet printing of light emitting quantum dots. *Appl. Phys. Lett.* **2009**, *94*, 073108. [[CrossRef](#)]
149. Wood, V.; Panzer, M.J.; Chen, J.; Bradley, M.S.; Halpert, J.E.; Bawendi, M.G.; Bulović, V. Inkjet-Printed Quantum Dot-Polymer Composites for Full-Color AC-Driven Displays. *Adv. Mater.* **2009**, *21*, 2151–2155. [[CrossRef](#)]
150. Haverinen, H.M.; Myllylä, R.A.; Jabbour, G.E. Inkjet printed RGB quantum dot-hybrid LED. *J. Disp. Technol.* **2010**, *6*, 87–89. [[CrossRef](#)]
151. Halivni, S.; Shemesh, S.; Waiskopf, N.; Vinetsky, Y.; Magdassi, S.; Banin, U. Inkjet printed fluorescent nanorod layers exhibit superior optical performance over quantum dots. *Nanoscale* **2015**, *7*, 19193–19200. [[CrossRef](#)] [[PubMed](#)]
152. Han, J.; Ko, D.; Park, M.; Roh, J.; Jung, H.; Lee, Y.; Lee, C. Toward High Resolution Inkjet-Printed Quantum Dot Light-Emitting Diodes for Next Generation Display. In Proceedings of the SID Symposium Digest of Technical Papers, San Francisco, CA, USA, 22–27 May 2016; Volume 47, pp. 1354–1357.
153. Manders, J.R.; Qian, L.; Titov, A.; Hyvonen, J.; Tokarz-Scott, J.; Acharya, K.P.; Holloway, P.H. High efficiency and ultra-wide color gamut quantum dot LEDs for next generation displays. *J. Soc. Inf. Disp.* **2015**, *23*, 523–528. [[CrossRef](#)]
154. Yang, Y.; Zheng, Y.; Cao, W.; Titov, A.; Hyvonen, J.; Manders, J.R.; Xue, J.; Holloway, P.H.; Qian, L. High-efficiency light-emitting devices based on quantum dots with tailored nanostructures. *Nat. Photonics* **2015**, *9*, 259–266. [[CrossRef](#)]
155. Levermore, P.; Schlenk, T.; Tseng, H.-R.; Wang, H.-J.; Heil, H.; Jatsch, A.; Buchholz, H.; Böhm, E. Ink-jet printed OLEDs for display applications. *SID Symp. Dig. Tech. Pap.* **2016**, *47*, 484–486. [[CrossRef](#)]
156. Chesterfield, R.; Johnson, A.; Lang, C.; Stainer, M.; Ziebarth, J. Solution-coating technology for AMOLED displays. *Inf. Disp.* **2011**, *1*, 11.
157. Madigan, C.F.; Hauf, C.R.; Barkley, L.D.; Harjee, N.; Vronsky, E.; Van Slyke, S.A. Invited Paper: Advancements in Inkjet Printing for OLED Mass Production. In Proceedings of the SID Symposium Digest of Technical Papers, San Diego, CA, USA, 3–6 June 2014; Volume 45, pp. 399–402.
158. Choi, M.C.; Kim, Y.; Ha, C.S. Polymers for flexible displays: From material selection to device applications. *Prog. Polym. Sci.* **2008**, *33*, 581–630. [[CrossRef](#)]
159. Shin, D.Y.; Brakke, K.A. Issues in Color Filter Fabrication with Inkjet Printing. In *Inkjet-Based Micromanufacturing*; Korvink, J.G., Smith, P.J., Shin, D.-Y., Eds.; Wiley-VCH Verlag GmbH & Co.: Weinheim, Germany, 2012; pp. 191–215.
160. Kashiwazaki, A. Color Filter, Process for Producing It, and Liquid Crystal Panel. U.S. Patent No. 6475683, 5 November 2002.

161. Shin, D.Y.; Smith, P.J. Theoretical investigation of the influence of nozzle diameter variation on the fabrication of thin film transistor liquid crystal display color filters. *J. Appl. Phys.* **2008**, *103*, 114905. [[CrossRef](#)]
162. Moon, K.S.; Choi, J.H.; Choi, D.-J.; Kim, S.H.; Ha, M.H.; Nam, H.-J.; Kim, M.S. A new method for analyzing the refill process and fabrication of a piezoelectric inkjet printing head for LCD color filter manufacturing. *J. Micromech. Microeng.* **2008**, *18*, 125011. [[CrossRef](#)]
163. Lu, G.S.; You, P.C.; Lin, K.L.; Hong, C.C.; Liou, T.M. Fabricating high-resolution offset color-filter black matrix by integrating heterostructured substrate with inkjet printing. *J. Micromech. Microeng.* **2014**, *24*, 055008. [[CrossRef](#)]
164. Chen, C.T.; Wu, K.H.; Lu, C.F.; Shieh, F. An inkjet printed stripe-type color filter of liquid crystal display. *J. Micromech. Microeng.* **2010**, *20*, 055004. [[CrossRef](#)]
165. Chang, C.J.; Chang, S.J.; Wu, F.M.; Hsu, M.W.; Chiu, W.W.; Chen, K. Effect of compositions and surface treatment on the jetting stability and color uniformity of ink-jet printed color filter. *Jpn. J. Appl. Phys.* **2004**, *43*, 8227. [[CrossRef](#)]
166. Chang, C.J.; Wu, F.M.; Chang, S.J.; Hsu, M.W. Influence of UV-curable compositions and rib properties on ink-jet-type color filter performance. *Jpn. J. Appl. Phys.* **2004**, *43*, 6280. [[CrossRef](#)]
167. Chang, C.J.; Lin, Y.H.; Tsai, H.Y. Synthesis and properties of UV-curable hyperbranched polymers for ink-jet printing of color micropatterns on glass. *Thin Solid Films* **2011**, *519*, 5243–5248. [[CrossRef](#)]
168. Chang, C.J.; Chang, S.J.; Shih, K.C.; Pan, F.L. Improving mechanical properties and chemical resistance of ink-jet printer color filter by using diblock polymeric dispersants. *J. Polym. Sci. B Polym. Phys.* **2005**, *43*, 3337–3353. [[CrossRef](#)]
169. Koo, H.S.; Chen, M.; Pan, P.C. LCD-based color filter films fabricated by a pigment-based colorant photo resist inks and printing technology. *Thin Solid Films* **2006**, *515*, 896–901. [[CrossRef](#)]
170. Koo, H.S.; Chen, M.; Pan, P.C.; Chou, L.T.; Wu, F.M.; Chang, S.J.; Kawai, T. Fabrication and chromatic characteristics of the greenish LCD colour-filter layer with nano-particle ink using inkjet printing technique. *Displays* **2006**, *27*, 124–129. [[CrossRef](#)]
171. Do Kim, Y.; Kim, J.P.; Kwon, O.S.; Cho, I.H. The synthesis and application of thermally stable dyes for ink-jet printed LCD color filters. *Dyes Pigments* **2009**, *81*, 45–52. [[CrossRef](#)]
172. Somani, P.R.; Radhakrishnan, S. Electrochromic materials and devices: Present and future. *Mater. Chem. Phys.* **2003**, *77*, 117–133. [[CrossRef](#)]
173. Mortimer, R.J.; Dyer, A.L.; Reynolds, J.R. Electrochromic organic and polymeric materials for display applications. *Displays* **2006**, *27*, 2–18. [[CrossRef](#)]
174. Cai, G.; Wang, J.; Lee, P.S. Next-generation multifunctional electrochromic devices. *Acc. Chem. Res.* **2016**, *49*, 1469–1476. [[CrossRef](#)] [[PubMed](#)]
175. Small, W.R.; Masdarolomoor, F.; Wallace, G.G.; in het Panhuis, M. Inkjet deposition and characterization of transparent conducting electroactive polyaniline composite films with a high carbon nanotube loading fraction. *J. Mater. Chem.* **2007**, *17*, 4359–4361. [[CrossRef](#)]
176. Costa, C.; Pinheiro, C.; Henriques, I.; Laia, C.A. Inkjet printing of sol-gel synthesized hydrated tungsten oxide nanoparticles for flexible electrochromic devices. *ACS Appl. Mater. Interfaces* **2012**, *4*, 1330–1340. [[CrossRef](#)] [[PubMed](#)]
177. Wojcik, P.J.; Santos, L.; Pereira, L.; Martins, R.; Fortunato, E. Tailoring nanoscale properties of tungsten oxide for inkjet printed electrochromic devices. *Nanoscale* **2015**, *7*, 1696–1708. [[CrossRef](#)] [[PubMed](#)]
178. Layani, M.; Darmawan, P.; Foo, W.L.; Liu, L.; Kamyshny, A.; Mandler, D.; Magdassi, S.; Lee, P.S. Nanostructured electrochromic films by inkjet printing on large area and flexible transparent silver electrodes. *Nanoscale* **2014**, *6*, 4572–4576. [[CrossRef](#)] [[PubMed](#)]
179. Cai, G.; Darmawan, P.; Cui, M.; Chen, J.; Wang, X.; Eh, A.L.-S.; Magdassi, S.; Lee, P.S. Inkjet-printed all solid-state electrochromic devices based on NiO/WO₃ nanoparticle complementary electrodes. *Nanoscale* **2016**, *8*, 348–357. [[CrossRef](#)] [[PubMed](#)]
180. Chen, B.-H.; Kao, S.-Y.; Hu, C.-W.; Higuchi, M.; Ho, K.-C.; Liao, Y.-C. Printed multicolor high-contrast electrochromic devices. *ACS Appl. Mater. Interfaces* **2015**, *7*, 25069–25076. [[CrossRef](#)] [[PubMed](#)]
181. Österholm, A.M.; Shen, D.E.; Gottfried, D.S.; Reynolds, J.R. Full color control and high-resolution patterning from inkjet printable cyan/magenta/yellow colored-to-colorless electrochromic polymer inks. *Adv. Mater. Technol.* **2016**. [[CrossRef](#)]

182. Luo, F.L.; Hong, Y. *Renewable Energy Systems: Advanced Conversion Technologies and Applications*; Wilamowski, B.M., Irwin, J.D, Eds.; CRC Press: Boca Raton, FL, USA, 2013.
183. Brunisholz, G. (Ed.) *Snapshot of Global Photovoltaic Markets*; Report IEA PVPS T1-29:2016; International Energy Agency (IEA): Paris, France, 2015.
184. Stüwe, D.; Mager, D.; Biro, D.; Korvink, J.G. Inkjet Technology for Crystalline Silicon Photovoltaics. *Adv. Mater.* **2014**, *27*, 599–626. [[CrossRef](#)] [[PubMed](#)]
185. Pi, X.; Zhang, L.; Yang, D. Enhancing the Efficiency of Multicrystalline Silicon Solar Cells by the Inkjet Printing of Silicon-Quantum-Dot Ink. *J. Phys. Chem. C* **2012**, *116*, 21240–21243. [[CrossRef](#)]
186. Darling, S.B.; You, F. The case for organic photovoltaics. *RSC Adv.* **2013**, *3*, 17633–17648. [[CrossRef](#)]
187. Dennler, G.; Scharber, M.C.; Brabec, C.J. Polymer-Fullerene Bulk-Heterojunction Solar Cells. *Adv. Mater.* **2009**, *21*, 1323–1338. [[CrossRef](#)]
188. Liu, Y.; Zhao, J.; Li, Z.; Mu, C.; Ma, W.; Hu, H.; Jiang, K.; Lin, H.; Ade, H.; Yan, H. Aggregation and morphology control enables multiple cases of high-efficiency polymer solar cells. *Nat. Commun.* **2014**, *5*, 1–8. [[CrossRef](#)] [[PubMed](#)]
189. Chen, C.-C.; Chang, W.-H.; Yoshimura, K.; Ohya, K.; You, J.; Gao, J.; Hong, Z.; Yang, Y. An Efficient Triple-Junction Polymer Solar Cell Having a Power Conversion Efficiency Exceeding 11%. *Adv. Mater.* **2014**, *26*, 5670–5677. [[CrossRef](#)] [[PubMed](#)]
190. Li, N.; Baran, D.; Spyropoulos, G.D.; Zhang, H.; Berny, S.; Turbiez, M.; Ameri, T.; Krebs, F.C.; Brabec, C.J. Environmentally Printing Efficient Organic Tandem Solar Cells with High Fill Factors: A Guideline Towards 20% Power Conversion Efficiency. *Adv. Energy Mater.* **2014**, *4*, 1400084. [[CrossRef](#)]
191. Helgesen, M.; Søndergaard, R.; Krebs, F.C. Advanced materials and processes for polymer solar cell devices. *J. Mater. Chem.* **2010**, *20*, 36–60. [[CrossRef](#)]
192. Carlé, J.E.; Krebs, F.C. Technological status of organic photovoltaics (OPV). *Sol. Energy Mater. Sol. Cells* **2013**, *119*, 309–310. [[CrossRef](#)]
193. Jung, S.; Sou, A.; Banger, K.; Ko, D.-H.; Chow, P.C.Y.; McNeill, C.R.; Sirringhaus, H. All-Inkjet-Printed, All-Air-Processed Solar Cells. *Adv. Energy Mater.* **2014**, *4*, 1400432. [[CrossRef](#)]
194. Sun, Y.; Zhang, Y.; Liang, Q.; Zhang, Y.; Chi, H.; Shi, Y.; Fang, D. Solvent inkjet printing process for the fabrication of polymer solar cells. *RSC Adv.* **2013**, *3*, 11925–11934. [[CrossRef](#)]
195. Krebs, F.C. Fabrication and processing of polymer solar cells: A review of printing and coating techniques. *Sol. Energy Mater. Sol. Cells* **2009**, *93*, 394–412. [[CrossRef](#)]
196. Søndergaard, R.; Hösel, M.; Angmo, D.; Larsen-Olsen, T.T.; Krebs, F.C. Roll-to-roll fabrication of polymer solar cells. *Mater. Today* **2012**, *15*, 36–49. [[CrossRef](#)]
197. Burgués-Ceballos, I.; Stella, M.; Lacharmoise, P.; Martínez-Ferrero, E. Towards industrialization of polymer solar cells: Material processing for upscaling. *J. Mater. Chem. A Mater. Energy Sustain.* **2014**, *2*, 17711–17722. [[CrossRef](#)]
198. Marin, V.; Holder, E.; Wienk, M.M.; Tekin, E.; Kozodaev, D.; Schubert, U.S. Ink-Jet Printing of Electron Donor/Acceptor Blends: Towards Bulk Heterojunction Solar Cells. *Macromol. Rapid Commun.* **2005**, *26*, 319–324. [[CrossRef](#)]
199. Teichler, A.; Eckardt, R.; Hoepfener, S.; Friebe, C.; Perelaer, J.; Senes, A.; Morana, M.; Brabec, C.J.; Schubert, U.S. Combinatorial Screening of Polymer:Fullerene Blends for Organic Solar Cells by Inkjet Printing. *Adv. Energy Mater.* **2011**, *1*, 105–114. [[CrossRef](#)]
200. Teichler, A.; Perelaer, J.; Schubert, U.S. Inkjet printing of organic electronics—Comparison of deposition techniques and state-of-the-art developments. *J. Mater. Chem. C* **2013**, *1*, 1910–1925. [[CrossRef](#)]
201. Aernouts, T.; Aleksandrov, T.; Giroto, C.; Genoe, J.; Poortmans, J. Polymer based organic solar cells using ink-jet printed active layers. *Appl. Phys. Lett.* **2008**, *92*, 033306. [[CrossRef](#)]
202. Hoth, C.N.; Choulis, S.A.; Schilinsky, P.; Brabec, C.J. High Photovoltaic Performance of Inkjet Printed Polymer:Fullerene Blends. *Adv. Mater.* **2007**, *19*, 3973–3978. [[CrossRef](#)]
203. Hoth, C.N.; Schilinsky, P.; Choulis, S.A.; Brabec, C.J. Printing Highly Efficient Organic Solar Cells. *Nano Lett.* **2008**, *8*, 2806–2813. [[CrossRef](#)] [[PubMed](#)]
204. Eom, S.H.; Park, H.; Mujawar, S.H.; Yoon, S.C.; Kim, S.-S.; Na, S.-I.; Kang, S.-J.; Khim, D.; Kim, D.-Y.; Lee, S.-H. High efficiency polymer solar cells via sequential inkjet-printing of PEDOT:PSS and P3HT:PCBM inks with additives. *Org. Electron.* **2010**, *11*, 1–7. [[CrossRef](#)]

205. Neophytou, M.; Cambarau, W.; Hermerschmidt, F.; Waldauf, C.; Christodoulou, C.; Pacios, R.; Choulis, S.A. Inkjet-printed polymer-fullerene blends for organic electronic applications. *Microelectron. Eng.* **2012**, *95*, 102–106. [[CrossRef](#)]
206. Lange, A.; Wegener, M.; Boeffel, C.; Fischer, B.; Wedel, A.; Neher, D. A new approach to the solvent system for inkjet-printed P3HT:PCBM solar cells and its use in devices with printed passive and active layer. *Sol. Energy Mater. Sol. Cells* **2010**, *94*, 1816–1821. [[CrossRef](#)]
207. Eom, S.H.; Senthilarasu, S.; Uthirakumar, P.; Yoon, S.C.; Lim, J.; Lee, C.; Lim, H.S.; Lee, J.; Lee, S.-H. Polymer solar cells based on inkjet-printed PEDOT:PSS layer. *Org. Electron.* **2009**, *10*, 536–542. [[CrossRef](#)]
208. Singh, A.; Katiyar, M.; Garg, A. Understanding the formation of PEDOT:PSS films by ink-jet printing for organic solar cells applications. *RSC Adv.* **2015**, *5*, 78677–78685. [[CrossRef](#)]
209. Steirer, K.X.; Berry, J.J.; Reese, M.O.; van Hest, M.F.A.M.; Miedaner, A.; Liberatore, M.W.; Collins, R.T.; Ginley, D.S. Ultrasonically sprayed and inkjet printed thin film electrodes for organic solar cells. *Thin Solid Films* **2009**, *517*, 2781–2786. [[CrossRef](#)]
210. Jeong, J.-A.; Lee, J.; Kim, H.; Kim, H.-K.; Na, S.-I. Ink-jet printed transparent electrode using nano-size indium tin oxide particles for organic photovoltaics. *Sol. Energy Mater. Sol. Cells* **2010**, *94*, 1840–1844. [[CrossRef](#)]
211. Cui, Z.; Ma, C.; Chen, Z.; Su, W.; Zhao, J.; Lin, J.; Qui, S. (Eds.) *Printed Electronics: Materials, Technologies and Applications*; John Wiley & Sons: Singapore, 2016.
212. Lu, H.; Lin, J.; Wu, N.; Nie, S.; Luo, Q.; Ma, C.-Q.; Cui, Z. Inkjet printed silver nanowire network as top electrode for semi-transparent organic photovoltaic devices. *Appl. Phys. Lett.* **2015**, *106*, 093302. [[CrossRef](#)]
213. Maisch, P.; Tam, K.C.; Lucera, L.; Egelhaaf, H.-J.; Scheiber, H.; Maier, E.; Brabec, C.J. Inkjet printed silver nanowire percolation networks as electrodes for highly efficient semitransparent organic solar cells. *Org. Electron.* **2016**, *38*, 139–143. [[CrossRef](#)]
214. Kordás, K.; Mustonen, T.; Tóth, G.; Jantunen, H.; Lajunen, M.; Soldano, C.; Talapatra, S.; Kar, S.; Vajtai, R.; Ajayan, P.M. Inkjet Printing of Electrically Conductive Patterns of Carbon Nanotubes. *Small* **2006**, *2*, 1021–1025. [[CrossRef](#)] [[PubMed](#)]
215. Dua, V.; Surwade, S.P.; Ammu, S.; Agnihotra, S.R.; Jain, S.; Roberts, K.E.; Park, S.; Ruoff, R.S.; Manohar, S.K. All-Organic Vapor Sensor Using Inkjet-Printed Reduced Graphene Oxide. *Angew. Chem. Int. Ed.* **2010**, *49*, 2154–2157. [[CrossRef](#)] [[PubMed](#)]
216. Galagan, Y.; Rubingh, J.-E.J.M.; Andriessen, R.; Fan, C.-C.; Blom, P.W.M.; Veenstra, S.C.; Kroon, J.M. ITO-free flexible organic solar cells with printed current collecting grids. *Sol. Energy Mater. Sol. Cells* **2011**, *95*, 1339–1343. [[CrossRef](#)]
217. Galagan, Y.; Coenen, E.W.C.; Sabik, S.; Gorter, H.H.; Barink, M.; Veenstra, S.C.; Kroon, J.M.; Andriessen, R.; Blom, P.W.M. Evaluation of ink-jet printed current collecting grids and busbars for ITO-free organic solar cells. *Sol. Energy Mater. Sol. Cells* **2012**, *104*, 32–38. [[CrossRef](#)]
218. Huang, Y.-C.; Hsu, F.-H.; Cha, H.-C.; Chuang, C.-M.; Tsao, C.-S.; Chen, C.-Y. High-performance ITO-free spray-processed polymer solar cells with incorporating ink-jet printed grid. *Org. Electron.* **2013**, *14*, 2809–2817. [[CrossRef](#)]
219. Galagan, Y.; Coenen, E.W.C.; Abbel, R.; van Lammeren, T.J.; Sabik, S.; Barink, M.; Meinders, E.R.; Andriessen, R.; Blom, P.W.M. Photonic sintering of inkjet printed current collecting grids for organic solar cell applications. *Org. Electron.* **2013**, *14*, 38–46. [[CrossRef](#)]
220. Burgués-Ceballos, I.; Kehagias, N.; Sotomayor-Torres, C.M.; Campoy-Quiles, M.; Lacharmoise, P.D. Embedded inkjet printed silver grids for ITO-free organic solar cells with high fill factor. *Sol. Energy Mater. Sol. Cells* **2014**, *127*, 50–57. [[CrossRef](#)]
221. Eom, S.H.; Senthilarasu, S.; Uthirakumar, P.; Hong, C.-H.; Lee, Y.-S.; Lim, J.; Yoon, S.C.; Lee, C.; Lee, S.-H. Preparation and characterization of nano-scale ZnO as a buffer layer for inkjet printing of silver cathode in polymer solar cells. *Sol. Energy Mater. Sol. Cells* **2008**, *92*, 564–570. [[CrossRef](#)]
222. Angmo, D.; Sweelssen, J.; Andriessen, R.; Galagan, Y.; Krebs, F.C. Inkjet Printing of Back Electrodes for Inverted Polymer Solar Cells. *Adv. Energy Mater.* **2013**, *3*, 1230–1237. [[CrossRef](#)]
223. Galagan, Y.; Shanmugam, S.; Teunissen, J.P.; Eggenhuisen, T.M.; Biezemans, A.F.K.V.; van Gijsegem, T.; Groen, W.A.; Andriessen, R. Solution processing of back electrodes for organic solar cells with inverted architecture. *Sol. Energy Mater. Sol. Cells* **2014**, *130*, 163–169. [[CrossRef](#)]

224. Yu, J.-S.; Kim, I.; Kim, J.-S.; Jo, J.; Larsen-Olsen, T.T.; Søndergaard, R.R.; Hösel, M.; Angmo, D.; Jørgensen, M.; Krebs, F.C. Silver front electrode grids for ITO-free all printed polymer solar cells with embedded and raised topographies, prepared by thermal imprint, flexographic and inkjet roll-to-roll processes. *Nanoscale* **2012**, *4*, 6032–6040. [CrossRef] [PubMed]
225. Patil, B.R.; Shanmugam, S.; Teunissen, J.-P.; Galagan, Y. All-solution processed organic solar cells with top illumination. *Org. Electron.* **2015**, *21*, 40–46. [CrossRef]
226. Lange, A.; Schindler, W.; Wegener, M.; Fostiropoulos, K.; Janietz, S. Inkjet printed solar cell active layers prepared from chlorine-free solvent systems. *Sol. Energy Mater. Sol. Cells* **2013**, *109*, 104–110. [CrossRef]
227. Lamont, C.A.; Eggenhuisen, T.M.; Coenen, M.J.J.; Slaats, T.W.L.; Andrieessen, R.; Groen, P. Tuning the viscosity of halogen free bulk heterojunction inks for inkjet printed organic solar cells. *Org. Electron.* **2015**, *17*, 107–114. [CrossRef]
228. Eggenhuisen, T.M.; Galagan, Y.; Coenen, E.W.C.; Voorthuijzen, W.P.; Slaats, M.W.L.; Kommeren, S.A.; Shanmugan, S.; Coenen, M.J.J.; Andrieessen, R.; Groen, W.A. Digital fabrication of organic solar cells by Inkjet printing using non-halogenated solvents. *Sol. Energy Mater. Sol. Cells* **2015**, *134*, 364–372. [CrossRef]
229. Eggenhuisen, T.M.; Galagan, Y.; Biezemans, A.F.K.V.; Slaats, T.M.W.L.; Voorthuijzen, W.P.; Kommeren, S.; Shanmugam, S.; Teunissen, J.P.; Hadipour, A.; Verhees, W.J.H.; et al. High efficiency, fully inkjet printed organic solar cells with freedom of design. *J. Mater. Chem. A Mater. Energy Sustain.* **2015**, *3*, 7255–7262. [CrossRef]
230. Hashmi, S.G.; Özkan, M.X.; Halme, J.; Zakeeruddin, S.M.; Paltakari, J.; Grätzel, M.; Lund, P.D. Dye-sensitized solar cells with inkjet-printed dyes. *Energy Environ. Sci.* **2016**, *9*, 2453–2462. [CrossRef]
231. Hashmi, S.G.; Ozkan, M.; Halme, J.; Mistic, K.D.; Zakeeruddin, S.M.; Paltakari, J.; Grätzel, M.; Lund, P.D. High performance dye-sensitized solar cells with inkjet printed ionic liquid electrolyte. *Nano Energy* **2015**, *17*, 206–215. [CrossRef]
232. Dodoo-Arhin, D.; Howe, R.C.T.; Hu, G.; Zhang, Y.; Hiralal, P.; Bello, A.; Amaratunga, G.; Hasan, T. Inkjet-printed graphene electrodes for dye-sensitized solar cells. *Carbon* **2016**, *105*, 33–41. [CrossRef]
233. Ultra-Thin Glass Membranes for Advanced, Adjustable and Affordable Quadruple Glazing Windows for Zero-Energy Buildings. Publishable Summary European Project MEM4WIN, Project Nr. European Union's Seventh Framework Programme Project. Grant Agreement No. 314578. Available online: http://cordis.europa.eu/docs/results/314/314578/periodic2-mem4win_publishable-summary_m36_v20151223.pdf (accessed on 18 August 2016).
234. Brabec, C.J.; Ameri, T. Special Section Guest Editorial: Solution-Processable Organic Solar Cells. *J. Photonics Energy* **2015**, *5*, 057201. [CrossRef]
235. Whitesides, G.M.; Grzybowski, B. Self-assembly at all scales. *Science* **2002**, *295*, 2418–2421. [CrossRef] [PubMed]
236. Cabrini, S.; Kawata, S. (Eds.) *Nanofabrication Handbook*; CRC Press: Boca Raton, FL, USA, 2012.
237. De Gennes, P.G.; Prost, J. *The Physics of Liquid Crystals*, 2nd ed.; Oxford University Press: Oxford, UK, 1995.
238. Broer, D.J.; Boven, J.; Mol, G.N.; Challa, G. In-situ photopolymerization of oriented liquid-crystalline acrylates, 3. Oriented polymer networks from a mesogenic diacrylate. *Die Makromol. Chem.* **1989**, *190*, 2255–2268. [CrossRef]
239. Van Oosten, C.L.; Bastiaansen, C.W.M.; Broer, D.J. Printed artificial cilia from liquid-crystal network actuators modularly driven by light. *Nat. Mater.* **2009**, *8*, 677–682. [CrossRef] [PubMed]
240. Moia, F.; Johnson, G.A. Optical Device and Method for Manufacturing Same. U.S. Patent No. 7201948, 10 April 2007.
241. You, M.; Zhong, J.; Hong, Y.; Duan, Z.; Lin, M.; Xu, F. Inkjet printing of upconversion nanoparticles for anti-counterfeit applications. *Nanoscale* **2015**, *7*, 4423–4431. [CrossRef] [PubMed]
242. Andres, J.; Hersch, R.D.; Moser, J.-E.; Chauvin, A.-S. A new anti-counterfeiting feature relying on invisible luminescent full color images printed with lanthanide-based inks. *Adv. Funct. Mater.* **2014**, *24*, 5029–2036. [CrossRef]
243. DaLuz, L.L.; Milani, R.; Felix, J.F.; Ribeiro, I.R.B.; Talhavini, M.; Neto, B.A.D.; Chojnacki, J.; Rodrigues, M.O.; Júnior, S.A. Inkjet printing of lanthanide-organic frameworks for anti-counterfeiting applications. *ACS Appl. Mater. Interfaces* **2015**, *7*, 27115–27123. [CrossRef] [PubMed]

244. You, M.; Lin, M.; Wang, S.; Wang, X.; Zhang, G.; Hong, Y.; Dong, Y.; Jin, G.; Xu, F. Three-dimensional quick response code based on inkjet printing of upconversion fluorescent nanoparticles for drug anti-counterfeiting. *Nanoscale* **2016**, *8*, 10096–10104. [[CrossRef](#)] [[PubMed](#)]
245. Baride, A.; Meruga, J.M.; Douma, C.; Langerman, D.; Crawford, G.; Kellar, J.J.; Cross, W.M.; May, P.S. A NIR-to-NIR upconversion luminescence system for security printing applications. *RSC Adv.* **2015**, *6*, 101338–101346. [[CrossRef](#)]
246. White, T.J.; McConney, M.E.; Bunning, T.J. Dynamic color in stimuli-responsive cholesteric liquid crystals. *J. Mater. Chem.* **2010**, *20*, 9832–9847. [[CrossRef](#)]
247. Ding, J.M.; Lin, Y.R.; Chen, C.H.; Chen, R.D.; Lin, C.Y.; Wang, H.L.; Lu, C.C.; Liao, C.C.; Hou, W.H. Inkjet printed multicolor cholesteric liquid crystal display. In Proceedings of the 13th International Display Workshops (IDW '06), Otsu, Japan, 6–8 December 2006.
248. Coles, H.; Morris, S. Liquid-crystal lasers. *Nat. Photonics* **2010**, *4*, 676–685. [[CrossRef](#)]
249. Gardiner, D.J.; Hsiao, W.K.; Morris, S.M.; Hands, P.J.W.; Wilkinson, T.D.; Hutchings, I.M.; Coles, H.J. Printed photonic arrays from self-organized chiral nematic liquid crystals. *Soft Matter* **2012**, *8*, 9977–9980. [[CrossRef](#)]
250. Stumpel, J.E.; Broer, D.J.; Schenning, A.P.H.J. Stimuli-responsive photonic polymer coatings. *Chem. Commun.* **2014**, *50*, 15839–15848. [[CrossRef](#)] [[PubMed](#)]
251. Moirangthem, M.; Arts, R.; Merkx, M.; Schenning, A.P.H.J. An Optical Sensor Based on a Photonic Polymer Film to Detect Calcium in Serum. *Adv. Funct. Mater.* **2016**, *26*, 1154–1160. [[CrossRef](#)]
252. Khan, M.K.; Bsoul, A.; Walus, K.; Hamad, W.Y.; MacLachlan, M.J. Photonic patterns printed in chiral nematic mesoporous resins. *Angew. Chem.* **2015**, *127*, 4378–4382. [[CrossRef](#)]
253. Herzer, N.; Guneyso, H.; Davies, D.J.D.; Yildirim, D.; Vaccaro, A.R.; Broer, D.J.; Bastiaansen, C.W.M.; Schenning, A.P.H.J. Printable Optical Sensors Based on H-Bonded Supramolecular Cholesteric Liquid Crystal Networks. *J. Am. Chem. Soc.* **2012**, *134*, 7608–7611. [[CrossRef](#)] [[PubMed](#)]
254. Davies, D.J.D.; Vaccaro, A.R.; Morris, S.M.; Herzer, N.; Schenning, A.P.H.J.; Bastiaansen, C.W.M. A Printable Optical Time-Temperature Integrator Based on Shape Memory in a Chiral Nematic Polymer Network. *Adv. Funct. Mater.* **2013**, *23*, 2723–2727. [[CrossRef](#)]
255. Stumpel, J.E.; Wouters, C.; Herzer, N.; Ziegler, J.; Broer, D.J.; Bastiaansen, C.W.M.; Schenning, A.P.H.J. An Optical Sensor for Volatile Amines Based on an Inkjet-Printed, Hydrogen-Bonded, Cholesteric Liquid Crystalline Film. *Adv. Opt. Mater.* **2014**, *2*, 459–464. [[CrossRef](#)]
256. Joannopoulos, J.D.; Johnson, S.G.; Winn, J.N.; Meade, R.D. (Eds.) *Photonic Crystals: Molding the Flow of Light*, 2nd ed.; Princeton University Press: Princeton, NJ, USA, 2011.
257. Arpin, K.A.; Mihi, A.; Johnson, H.T.; Alfred, J.B.; Rogers, J.A.; Lewis, J.A.; Braun, P.V. Multidimensional Architectures for Functional Optical Devices. *Adv. Mater.* **2010**, *22*, 1084–1101. [[CrossRef](#)] [[PubMed](#)]
258. Fan, H.; Lu, Y.; Stump, A.; Reed, S.T.; Baer, T.; Schunk, R.; Brinker, C.J. Rapid prototyping of patterned functional nanostructures. *Nature* **2000**, *405*, 56–60. [[CrossRef](#)] [[PubMed](#)]
259. Ko, H.-Y.; Park, J.; Shin, H.; Moon, J. Rapid Self-Assembly of Monodisperse Colloidal Spheres in an Ink-Jet Printed Droplet. *Chem. Mater.* **2004**, *16*, 4212–4215. [[CrossRef](#)]
260. Wang, D.; Park, M.; Park, J.; Moon, J. Optical properties of single droplet of photonic crystal assembled by ink-jet printing. *Appl. Phys. Lett.* **2005**, *86*, 241114. [[CrossRef](#)]
261. Park, J.; Moon, J. Control of colloidal particle deposit patterns within picoliter droplets ejected by ink-jet printing. *Langmuir* **2006**, *22*, 3506–3513. [[CrossRef](#)] [[PubMed](#)]
262. Park, J.; Moon, J.; Shin, H.; Wang, D.; Park, M. Direct-write fabrication of colloidal photonic crystal microarrays by ink-jet printing. *J. Colloid Interface Sci.* **2006**, *298*, 713–719. [[CrossRef](#)] [[PubMed](#)]
263. Wang, J.; Wang, L.; Song, Y.; Jiang, L. Patterned photonic crystals fabricated by inkjet printing. *J. Mater. Chem. C* **2013**, *1*, 6048–6058. [[CrossRef](#)]
264. Sowade, E.; Blaudeck, T.; Baumann, R.R. Inkjet printing of colloidal nanospheres: Engineering the evaporation-driven self-assembly process to form defined layer morphologies. *Nanoscale Res. Lett.* **2015**, *10*. [[CrossRef](#)] [[PubMed](#)]
265. Yoo, H.; Kim, C. Experimental studies on formation, spreading and drying of inkjet drop of colloidal suspensions. *Colloids Surfaces A Physicochem. Eng. Asp.* **2015**, *468*, 234–245. [[CrossRef](#)]
266. Cui, L.; Li, Y.; Wang, J.; Tian, E.; Zhang, X.; Zhang, Y.; Song, Y.; Jiang, L. Fabrication of large-area patterned photonic crystals by ink-jet printing. *J. Mater. Chem.* **2009**, *19*, 5499–5502. [[CrossRef](#)]

267. Nam, H.; Song, K.; Ha, D.; Kim, T. Inkjet printing based mono-layered photonic crystal patterning for anti-counterfeiting structural colors. *Sci. Rep.* **2016**, *6*, 30885. [[CrossRef](#)] [[PubMed](#)]
268. Wang, L.; Wang, J.; Huang, Y.; Liu, M.; Kuang, M.; Li, Y.; Jiang, L.; Song, Y. Inkjet printed colloidal photonic crystal microdot with fast response induced by hydrophobic transition of poly(N-isopropyl acrylamide). *J. Mater. Chem.* **2012**, *22*, 21405–21411. [[CrossRef](#)]
269. Bai, L.; Xie, Z.; Wang, W.; Yuan, C.; Zhao, Y.; Mu, Z.; Zhong, Q.; Gu, Z. Bio-Inspired Vapor-Responsive Colloidal Photonic Crystal Patterns by Inkjet Printing. *ACS Nano* **2014**, *8*, 11094–11100. [[CrossRef](#)] [[PubMed](#)]
270. Shen, W.; Li, M.; Ye, C.; Jiang, L.; Song, Y. Direct-writing colloidal photonic crystal microfluidic chips by inkjet printing for label-free protein detection. *Lab Chip* **2012**, *12*, 3089–3095. [[CrossRef](#)] [[PubMed](#)]
271. Chen, T.; Deng, Z.-Y.; Yin, S.-N.; Chen, S.; Xu, C. The fabrication of 2D and 3D photonic crystal arrays towards high performance recognition of metal ions and biomolecules. *J. Mater. Chem. C* **2016**, *4*, 1398–1404. [[CrossRef](#)]
272. Kang, P.; Ogunbo, S.O.; Erickson, D. High resolution reversible color images on photonic crystal substrates. *Langmuir* **2011**, *27*, 9676–9680. [[CrossRef](#)] [[PubMed](#)]



© 2016 by the authors; licensee MDPI, Basel, Switzerland. This article is an open access article distributed under the terms and conditions of the Creative Commons Attribution (CC-BY) license (<http://creativecommons.org/licenses/by/4.0/>).

2. Publication 2.


Journal: Journal of Materials Chemistry C

Title: Photoacid catalyzed organic-inorganic hybrid inks for the manufacturing of inkjet-printed photonic devices



Cite this: DOI: 10.1039/c7tc05178f

Photoacid catalyzed organic–inorganic hybrid inks for the manufacturing of inkjet-printed photonic devices†

Jorge Alamán,^{ab} María López-Valdeolivas,^a Raquel Alicante,^a Francisco J. Medel,^c Jorge Silva-Treviño,^a Jose Ignacio Peña^d and Carlos Sánchez-Somolinos *^{ae}

Photoacid catalyzed jettable inks containing monomers with epoxy and silane functionalities have been successfully formulated. In contrast to inks based on conventional sol–gel processes, the hydrolysis and condensation processes in these materials are triggered after printing using UV light favoring the long-term stability of the ink, a prerequisite for industrial applications. UV light can trigger the photocuring reaction of the epoxy groups and the hydrolysis and condensation of the silane groups leading to a crosslinked organic–inorganic hybrid polymeric network. Advantageously, the inks use no solvents and therefore the deposited material can be polymerized immediately after the deposition step by exposure to UV light. No additional baking steps are required allowing the use of thermally sensitive substrates and notably simplifying the process to one single step. Deposits with excellent adhesion and good transparency can be obtained by proper selection of the curing conditions through this process. Planar and channel optical waveguides have been prepared using these formulations by inkjet printing technology on a variety of substrates. The waveguides support optical modes with propagation losses as low as 0.5 dB cm⁻¹, demonstrating the potential of these photoacid catalyzed organic–inorganic hybrid formulations and inkjet printing for the preparation of photonic devices.

Received 13th November 2017,
Accepted 9th January 2018

DOI: 10.1039/c7tc05178f

rsc.li/materials-c

Introduction

The controlled propagation of light along planar dielectric layers is a basic pillar for the implementation of integrated optical circuits.¹ Planar waveguides can act as optical interconnects between light sources and detectors in these photonic circuits or can themselves be active elements such as amplifiers and lasers.^{2–4} Far from being limited to signal processing and telecommunication applications, planar waveguides have a tremendous role in the development of other technological fields. A large R&D effort is being demanded towards the development of sensors based on planar-guided optics for environmental and

biomedical monitoring, and solar concentrators for energy harvesting or lighting devices such as backlights for displays.^{5–8}

Hybrid organic–inorganic polymeric networks have been demonstrated to be suitable materials for the preparation of planar optical waveguides.^{2,3,9–17} Highly transparent films with precisely controlled thickness, a prerequisite for this application, can be prepared from these materials and their refractive indexes are adjusted by proper selection of the initial formulation and processing conditions.^{11,15} In addition, once prepared, they present excellent chemical and mechanical stability and good adhesion to inorganic substrates such as silicon and silicon oxide.^{2,18} As a prevalent example, in the ORMOCER[®] materials, alkoxy silanes bearing organic polymerizable groups are used as precursors for the preparation of, through a sol–gel route, nanoscale inorganic oligomers decorated with reactive organic functionalities.¹⁹ By incorporating suitable photoinitiators, structured waveguides can be prepared by applying the sol–gel processed material to a flat substrate and subsequently using photolithographic techniques (involving patterned UV-exposure, wet development and thermal curing steps) to crosslink and fix the organic part.^{3,10–12,15,20–22} Despite the variety of light based patterning techniques available for fabrication, mainly mask and holographic lithographies or direct laser writing (DLW) are used. These usually lack (except DLW)

^a Instituto de Ciencia de Materiales de Aragón (ICMA), CSIC-Universidad de Zaragoza, Departamento de Física de la Materia Condensada, Zaragoza, Spain. E-mail: carlos.s@csic.es

^b BSH Electrodomésticos España, S.A., Polígono Industrial de PLA-ZA, Ronda del Canal Imperial de Aragón, 18-20, 50197 Zaragoza, Spain

^c Instituto de Ciencia de Materiales de Aragón (ICMA), CSIC-Universidad de Zaragoza, Departamento de Ingeniería Mecánica, Zaragoza, Spain

^d Instituto de Ciencia de Materiales de Aragón (ICMA), CSIC-Universidad de Zaragoza, Departamento de Ciencia y Tecnología de Materiales y Fluidos, Zaragoza, Spain

^e CIBER in Bioengineering, Biomaterials and Nanomedicine (CIBER-BBN), Spain

† Electronic supplementary information (ESI) available. See DOI: 10.1039/c7tc05178f

flexibility for the rapid prototyping of structures and devices and they always require wet etching and thermal baking steps making the overall process complex and precluding their use with heat and chemically sensitive surfaces. As a result, using flexible fabrication techniques for the micromanufacturing of optical waveguides and their integration with other already processed optical elements and devices is important, all this being possible in different types of substrates.

Inkjet printing has been demonstrated over the last few years to be a powerful tool for the patterning of functional materials to implement elements and devices not only in optics and photonics but also in other application fields such as biomedicine, energy and electronics.^{23–26} In contrast to conventional coating techniques, such as spin-coating or dip-casting, inkjet printing allows fine structuring of the applied materials, beyond the preparation of continuous unstructured films. Compared to photolithography, which also enables patterning, inkjet printing allows digital deposition of different functional materials at precise locations on virtually any type of substrate even non-flat or flexible ones. With an additional advantage compared to light based lithographies, inkjet printing requires minimal post-processing, eliminating wet etching steps and therefore is an environmentally friendly technique. All these features make inkjet printing a very attractive technology for the implementation of functional optical devices. For example, a great deal of control has been achieved in the preparation of microlenses in which a numerical aperture and focal length can be controlled by using this technique as a simple and cost-effective alternative to existing methods.^{27–33} In this context, there is growing interest in the preparation of functional waveguides using additive manufacturing techniques; however the type and number of available materials for waveguide printing are quite limited.³⁴ Besides recently proposed stretchable materials obtained from polyurethane based inks,³⁵ other alternative systems are the commercial UV-curable solvent-containing hybrid organic–inorganic inks from Fraunhofer ISC and MicroResist technologies GmbH with excellent transparency and mechanical stability.³⁶ These solvent-containing acrylate based inks require soft baking steps to eliminate the solvent prior to UV curing in a nitrogen atmosphere and usually a post-baking step is also carried out.^{32,37,38} Acrylate solvent-free based inks have also been recently proposed by Hofmann and Bollgruen.^{39–42}

Here we present new jettable solvent-free inks based on photoacid catalyzed formulations containing monomers with epoxy and silane functionalities. Recently these types of photoacid catalyzed polymerization reactions have demonstrated to be efficient for the preparation of hybrid materials. Compared to other sol–gel methods it presents higher reactivity and it is a solvent-free process starting with the low molecular weight alkoxysilanes. Due to the presence of suitable photoinitiators in the formulation, UV irradiation induces the curing of the organic part. A subsequent thermal annealing step allows the formation of the inorganic network.^{43–45} For certain formulations, the polymerization of the organic and inorganic networks can concomitantly take place in a very efficient manner, enormously

simplifying the process and avoiding the use of postbaking steps.^{46–48} We try to leverage the advantages of this reaction to generate novel low viscosity formulations suitable for inkjet printing and having tailored final properties. Compared to conventional hybrid inks based on prehydrolyzed-condensed reactive inorganic precursors, in the presented approach, hydrolysis and condensation are advantageously delayed (by protecting the ink from UV light) after the printing step favouring the long-term stability of the inks, a prerequisite for industrial applications. Once applied through inkjet printing, actinic UV light reaching photoacid generators (PAGs) included in the formulation induces the release of acids that catalyze both the cationic ring opening polymerization of epoxy groups and, in the presence of atmospheric water, the hydrolysis and condensation of organosilanes. The light triggered reaction of the two functional groups leads, under controlled processing conditions, to solid films with good adhesion and transparency without the need for any further postprocessing step. By including appropriate monomers in the formulation, high refractive index planar and channel waveguides with low propagation losses can be generated through this material-processing platform on a variety of substrates.

Experimental section

Materials, ink preparation and characterization

The chemical structure of the main components of the ink is shown in Scheme S1 in the ESI.† 3-Glycidoxypropyltrimethoxysilane (GPTMS), a trialkoxysilane with an epoxy group, therefore having a hybrid organic and inorganic nature was acquired from Alfa Aesar. GPTMS is a low viscosity liquid at RT. The polymeric epoxy resin Epikote 157 (main component in SU-8 resists), with a monomer having an average of eight aromatic benzene rings and eight epoxide groups, was purchased from Momentive and it comes in a solid form as flakes at RT. Dimethoxydiphenylsilane (dPDMS) is a liquid disilane monomer with two aromatic rings. Triarylsulfonium hexafluorophosphate salts (50% in propylene carbonate) acquired from Aldrich act as a photoacid generator (PAG). Upon UV actinic illumination this compound leads to the formation of an acid (H^+X^- , with $X^- = PF_6^-$), which acts as an initiator for the polymerization of organic epoxide groups as well as a catalyst for the hydrolysis and condensation of the alkoxides. BYK-333 is a polyether-modified polydimethylsiloxane supplied by BYK Chemie which strongly reduces the surface tension of the ink also favoring surface wetting. All the materials were used as received.

Two photocurable inks, namely a model ink and a High Refractive Index (HRI) ink, were prepared by mixing different percentages of the above mentioned materials. To facilitate mixing, Epikote 157 was thoroughly grinded previous to its addition to the mixtures. These mixtures were stirred at room temperature (RT) using a magnetic stirrer at 600 rpm until a transparent solution was achieved.

Viscosity measurements of the inks were carried out using a Rheometer HaakeMars, rotors DC60/11 of Thermo Scientific, Germany. Surface tension of the inks was characterized using

an Attension Goniometer Theta Lite and using the pendant droplet method. The given values are the result of an average of three independent measurements. Density measurements were carried out using a 10 ml pycnometer.

Cleaning and surface treatment of substrates

Conventional microscope glass slides with refractive index $n_g = 1.514$ at 632.8 nm were employed for the HRI ink; however quartz substrates with refractive index $n_q = 1.457$ were used for the model ink deposits to prepare thin films of the materials.

Pre-cleaning of the substrates was performed by gently hand rubbing the surface using nitrile gloves and a solution of soapy water. After thoroughly rinsing the substrates with water, they were ultrasonicated with soapy water for 10 min, immediately after the substrates were refluxed with milli-Q water and ultrasonicated in milli-Q water for 10 min. After the water cleaning step, the substrates were refluxed with isopropyl alcohol and ultrasonicated in isopropyl alcohol water for 10 min. To finish, the substrates were immediately dried under compressed air and stored until their use.

UV Ozone treatment was performed using a UV-ozone reactor UVO 342 (Jelight company Inc., CA, USA) to remove any remaining organic contamination.

Pyrosil treatment was carried out by combustion chemical vapor deposition (CCVD) using Pyrosil (Pyrosil[®], SURA). Briefly, an organosilicon precursor is injected into a gas flame that is kept in short contact with the substrate leading to a SiO₂-like coating with thickness typically below 50–100 nm. As a result, important changes in the wettability and adhesion are obtained.⁴⁹

Inkjet printing and drop observation

Inkjet printing was carried out using a custom-made inkjet printer system (In-2 Printing Solutions, Navarra, Spain) with Xaar-126/80 piezoelectric printheads (Xaar, Cambridge, United Kingdom). These printheads have 126 nozzles (50 μm diameter) arranged in a line with a pitch of 137 μm. The printhead is fixed in a frame and the substrate moves under the nozzles at a distance between the printhead and the substrate of approximately 1 mm. The line of nozzles is perpendicular to the direction of the substrate motion and as a result the vertical resolution (in the direction of the line of nozzles) is 185 dots per inch (dpi). The horizontal printing resolution (in the direction of the printhead motion) depends on the firing frequency and the speed of the substrate relative to the printhead. The printhead is commanded using Xaar XUSB drive electronics controlled with a PC using the corresponding software (from Xaar) that allows controlling printhead parameters, sample detection and patterns to be printed (bitmap file). During printing operation the target substrate moves under the printhead at a constant speed (typically 20 mm s⁻¹) by using an eTrack linear stage from Newmark systems Inc. (Mission Viejo, CA, USA) commanded by IMS-Terminal software (Marlborough, CT, USA). The printhead is embedded in a metallic block with a heater and a thermocouple connected to a temperature regulator that maintains the block near the desired set point. For the analysis of the characteristics of the ejected drops,

a home-built dropwatcher system was used. This allows the characterization and optimization of the printing system configuration specially parameters that fix the voltage. This visualization system consists of a CCD camera, a strobe led device and a pulse generator to synchronize the piezoelectric signal, the strobe light and the camera acquisition events.

UV-curing fixation

A UV lamp Exfo OmniCure S2000 UV (Gentec, Nivelles, Belgium) has been employed with a UV bandpass filter (wavelength range of 320–390 nm). A power of 10 mW cm⁻² was applied for curing for 5 min. Unless it is specified, curing was carried out in an ambient atmosphere with a relative humidity between 30 and 40% and at room temperature (25 °C). Some of the samples were cured inside a chamber provided with an optical access. A mild vacuum (100 mBar) can be attained inside the chamber by using a vacuum pump. Once the desired pressure level is achieved, UV exposure is immediately carried out to minimize evaporation of the deposited ink components.

Characterization

Fourier Transform Infrared (FTIR) Spectroscopy was performed using a Perkin Elmer Spectrum 100 with ATR accessory. FTIR spectra were recorded between 4000 and 450 cm⁻¹.

UV-Vis absorption measurements of the solutions and the films were carried out using a VARIAN Cary-500 spectrophotometer.

Optical Images of the deposited drops were taken using an optical microscope OLYMPUS Eclipse i80.

Thickness characterization of the deposited layers and profiles of the channel waveguides were characterized using a Bruker Dektak XT Stylus Profiler.

Surface morphology of the cured films was studied using a Field-Emission Scanning Electron Microscope (FE-SEM) Merlin Carl Zeiss (Germany). Atomic Force Microscope (AFM) images were obtained using an Ntegra Aura Scanning Probe Microscope from NT-MDT (Moscow, Russia) working in semi-contact mode.

Mechanical properties of the films were characterized using a Nanoindenter G200 from Agilent Technologies equipped with a Vickers indenter tip. Measurements were carried out at RT and under ambient atmospheric conditions using a continuous stiffness measurement method that applies a small load oscillation (displacement amplitude 2 nm) superimposed to the applied load at a frequency of 45 Hz. As a result hardness and elastic modulus are obtained as a function of penetration depth during the loading–unloading cycle. A maximum penetration depth in the order of 10% the thickness of the film under study was measured so the values obtained are intrinsic of the material. Hardness and elastic modulus are obtained on the basis of the Oliver and Pharr method⁵⁰ assuming a Poisson ratio of 0.38 as done by other authors for similar materials.^{51,52} To eliminate any tip-rounding effect, the data from the first 100 nm are disregarded.⁵³ Below this depth data were consistent and mean values of hardness and elastic modulus were obtained by averaging data between 100 nm and 200 nm, with the maximum penetration depth being 400 nm, (approximately 10% of the film

thickness). The values were calculated on the basis of 4 indentations in 2 identical samples.

Adhesion tests

Adhesion of the cured films to the substrate was characterized using a cross-cut and tape test according to the ASTM D3359 standard method.⁵⁴ Briefly, in a first stage, six parallel scratches are made on the deposit by using a round cutter with 6 parallel blades (Neurtek) separated by 1 mm. The scratches are deep enough to reach the substrate surface. A cross-cut pattern of 6 × 6 cuts was created by applying, in a second stage, the cutter in a direction perpendicular to the first cut. After brushing the scratched area, a normalized adhesion tape (Tesa 4024) is applied over the crosscut pattern and quickly removed at an angle of 180°. The degree of adhesion is evaluated visually by examining the sample using an optical microscope. The adhesion strength is categorized by assessing the amount of deposit removed from 5B (strongest adhesion/no film removal) to 0B (weakest adhesion/complete film removal). Adhesion experiments were reproduced in 3 samples for this adhesion assessment.

Optical characterization of the waveguides. The modes propagating in the planar waveguides were characterized using a prism coupler Metricon 2010 equipped with a HeNe laser at 632.8 nm for the transverse electric (TE) and transverse magnetic (TM) polarization. Essentially a laser beam reaches a prism with a high refractive index and it is reflected to a photodetector. The thin film is placed against the base of the prism and pressed using a pneumatic knee minimizing in this way the air gap between the prism and the sample. The ensemble is rotated with respect to the laser beam. When the angle matches that of the waveguided modes, coupling of light into the waveguide might occur which is manifested by the decrease in the light intensity reaching the photodetector. These measurements allow obtaining the refractive index and film thickness of the films.⁵⁵ The propagation losses of the photopolymerized hybrid waveguides obtained by inkjet printing were also characterized using this same equipment. Briefly an optical fiber scans several cm of the surface where the light is propagating, detecting the scattered light that it is assumed to be proportional to the intensity of light propagating at each position. The intensity remaining in the waveguide after propagating a distance x is given by

$$I(x) = I_0 10^{\left(-\frac{\alpha x}{10}\right)} \quad (1)$$

where I_0 is the initial intensity, $I(x)$ is the transmitted intensity through the waveguide at position x (cm), and α is the attenuation coefficient measured in decibels per centimeter (dB cm^{-1}).

Results and discussion

Ink preparation, jetting properties and ink deposition

Two different inks have been prepared and studied in this work (Table 1). First, we have explored a model ink based on a simple formulation having GPTMS as the main component, a hybrid precursor bearing an epoxide and a triethoxysilyl group. The ink is

Table 1 Composition of the model and high refractive index (HRI) inks in wt%. Additionally 2 wt% triarylsulfonium hexafluorophosphate salts and 0.05 wt% BYK-333 were added as a photoacid generator and a surface tension modifier respectively to both inks

	GPTMS	EPIKOTE 157	dPDMS
Model ink	100	—	—
HRI ink	50	25	25

photosensitized by adding a percentage of 2 wt% triarylsulfonium hexafluorophosphate salts to the GPTMS. These salts show excellent thermal stability and strong absorption in the UV region.^{56,57} In the absence of light the mixture is stable (photolent system). Additionally 0.05 wt% BYK-333 was added to improve the wetting of the ink in the substrate.⁵⁸

A second ink has been prepared based on the same photochemistry but incorporating new monomers to increase the refractive index of the final deposit to be used as a planar waveguide. Besides 50 wt% GPTMS, 25 wt% Epikote 157 and 25 wt% dPDMS were incorporated into this high refractive index (HRI) ink. Additionally 2 wt% triarylsulfonium hexafluorophosphate salts and 0.05 wt% BYK-333 were added as in the model ink. Epikote 157 with eight benzene rings and eight epoxide groups is expected to join the organic part of the polymeric network, while dPDMS, with two benzene rings and two silane groups, the inorganic one. In both cases the aromatic rings will contribute to increase the refractive index of the final material.

Successful inkjet printing requires a full control of the process that essentially consists of the ejection of droplets of ink with controlled properties and their precise positioning and fixation on the final substrate. Starting with the drop ejection process, this involves the generation of a pressure pulse within the printhead that induces the formation of a jet leaving the nozzle. The printhead used in this study employs piezoelectric technology. A pulse of voltage is applied to the piezoelectric element placed close to a nozzle generating a pressure wave in the ink. If enough kinetic energy is transferred to the ink, the fluid can overcome surface tension and generate a jet leaving the nozzle. The correct formation of ink droplets from this jet needs that this thins and breaks up leading to a single drop, which requires specific fluid properties. Surface energy, viscosity and density are the main ones. A series of non-dimensional numbers can be defined relating different magnitudes of the moving jet when leaving the printhead nozzle and help in identifying favorable regimes for correct drop formation. In this way, Reynolds number (Re) relates inertial forces and viscosity while the Weber number (We) compares the kinetic and surface energy of the leaving fluid. Ohnesorge introduced a non-dimensional number that helps in identifying the different regimes of the break up of a jet leaving an orifice. The Ohnesorge number (Oh) relates Re and We and eliminates the speed of the fluid and therefore only depends on the properties of the ink and the dimensions of the orifice.

$$\text{Re} = \frac{v\rho a}{\eta} \quad (2)$$

$$We = \frac{v^2 \rho a}{\gamma} \quad (3)$$

$$Oh = \frac{\sqrt{We}}{Re} = \frac{\eta}{\sqrt{\gamma \rho a}} \quad (4)$$

where v is the speed of the ink leaving the nozzle, η is the ink viscosity, γ its surface tension, ρ its density and a the diameter of the orifice.

To gain insight into the jetting process, calculations of these non-dimensional numbers were carried out for the inks. Viscosity, surface tension and density of the prepared inks were characterized and the results are shown in Table 2. The values of surface tension measurements are obtained at RT (26 °C) slightly below the temperature of the printhead (32 °C). We assume that the values of surface tension do not significantly change in such a small range of temperature (26–32 °C) taking the values at RT for the calculations of the We and Oh numbers. In both inks, the measured value of surface tension is around 27 mN m⁻¹ that is mainly dictated by the presence of polyether-modified polydimethylsiloxane BYK-333. The density is close to 1.1 g cm⁻³ in both cases. Viscosity, which can have a strong dependence on temperature, was measured at 32 °C, the temperature of the printhead. The viscosity of the model ink is quite close to that of its main component GPTMS almost unchanged by the addition of the photoinitiator and other additives. The incorporation of dPDMS and Epikote 157 into the HRI ink resulted in a more viscous solution. This increase in viscosity is mainly due to the addition of Epikote 157 which is an epoxy oligomer solid at RT known to lead to viscous solutions in organic solvents (e.g.: Epikote 157 based SU-8 viscous photoresists in cyclopentanone).

Taking the diameter of the nozzle as 50 μm, the Oh numbers for each of the systems are also given in Table 2. With these figures and assumptions, the Ohnesorge numbers take values of 0.09 and 0.75 for the model and HRI inks, respectively. It is known from the literature that inks with Oh numbers between 0.1 and 1 typically lead to stable droplet formation.⁵⁹ Other authors give even narrower limits for this ejectability criterion (Oh numbers between 0.07 and 0.25 according to Moon and coworkers⁶⁰). In both cases, our inks have acceptable values being within or very close to the established limits. Experimentally, we found, for both inks, that the application of a voltage to the piezoelectric actuators of the printhead slightly above a certain threshold led to stable drop formation without satellites. Fig. 1 shows a sequence of photographs in which the drop formation process can be followed. Application of a voltage to

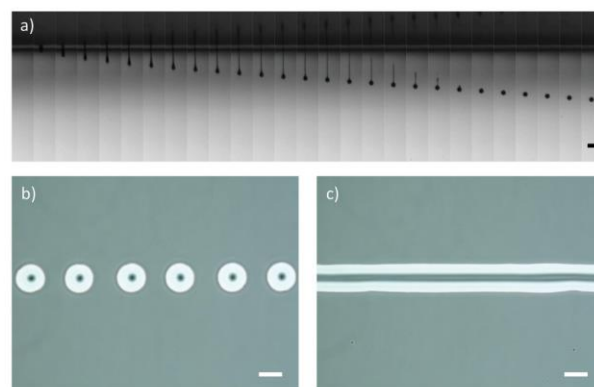


Fig. 1 (a) Temporal sequence of photographs (from left to right) showing the drop formation process for the HRI ink. The time interval between two adjacent frames is 8.5 μs (scale bar: 100 μm). (b and c) Phase contrast microscope images of the inkjet printed drops of the HRI ink deposited along a line in ozone treated substrates at different dpi (scale bar: 100 μm): (b) 120 dpi and (c) 240 dpi.

the piezoelectric element of the printhead induces a jet that leaves the nozzle, thins and breaks up after some time. The long tail formed after jet breaking is completely retracted towards the main drop without breaking in satellites. For these optimum conditions the round droplets with no satellites have the speed shown in Table 2, which corresponds to the We and Re numbers given also in the same table. For these optimum conditions, We numbers for both inks are larger than the threshold of 4 ($We > 4$) established by Duineveld and coworkers.^{25,61} Application of higher voltages to the printhead led to a longer jet that ends up breaking up in a main droplet travelling at higher speed and one or several satellites following the first one (see Fig. S1, ESI[†]). It is important to note that the low viscosity model ink leads, in our printing system, to an Oh number close to the ejectability limit described in the literature. In this regime of low viscosity liquids there is a strong tendency to form satellites during the jet break up which has not been observed in our case. The suppression of satellites in our case can be favored by the presence of the small percentage of the polymeric additive BYK-333. It is well known that the addition of small traces of polymeric additives introduces viscoelasticity in the ink. Besides the forces that, in Newtonian liquids, typically govern droplet formation from the initial jet (inertial and viscous forces and surface tension), elasticity also strongly influences the droplet formation process in fluids incorporating diluted polymers. Elastic forces in these systems arise from the extended polymeric chains along the

Table 2 Density, viscosity, surface tension, droplet speed and Re , We and Oh number values for model and HRI inks

	ρ^a (g cm ⁻³)	η^a (mPa s)	γ^b (mN m ⁻¹)	v^c (m s ⁻¹)	Re^d	We^d	Oh^d
Model ink	1.06	3.44	27.44	1.70	26.2	5.58	0.09
HRI ink	1.1	28.54	26.25	2.04	3.93	8.72	0.75

^a Measured at 32 °C. ^b Measured at 26 °C. ^c Measured under optimum single droplet forming conditions. ^d For Re , We and Oh calculations, surface tension values at 32 °C are approximated by those measured at 26 °C.

elongated jet. Even at small percentages, the presence of these extended chains favors the retraction of the long tail formed after jet breaking towards the main drop precluding satellite formation.^{62,63}

The stability of the ink properties and their jettability were followed for several months. As an example, after 4 months of storage of the model ink in a closed amber flask, the optimum jetting conditions were the same as those of the freshly prepared ink. This test demonstrates the good stability of these photocurable hybrid organic–inorganic inks for this application.

Once the jetting conditions for stable droplet formation have been identified, the interaction of the drop, after landing, with the substrates has also been explored. In order to make functional devices, inkjet printing has to lead on one hand to well-defined patterns and on the other hand to good adhesion of the final deposit to the underlying substrate. In our case, taking into account the hybrid nature of the inks studied, glass was cleaned and treated using two different protocols seeking for functional groups and textures that can promote adhesion of the reactive groups of the inks. In this way, clean glass was treated with UV-Ozone to eliminate surface contaminants leaving silanol groups exposed on the surface.⁶⁴ These hydroxyl groups can later react with the hydroxyl groups generated during the hydrolysis and condensation of the inks. Alternately CCVD using Pyrosil[®] was used to generate a nanoporous silanol rich surface that, as in the case of ozone treated glass, promotes adhesion to the glass through covalent bonding. The roughness added by the CCVD treatment additionally generates an extra bonding surface that could further promote adhesion.⁴⁹

Ink droplets were inkjet printed along a line in ozone treated substrates. If the spacing between droplets is large enough the result is a set of equally spaced dots on the substrate, as seen in Fig. 1b for the HRI ink. If spacing is decreased, coalescence of droplets leads to continuous bead lines as shown in Fig. 1c. For certain dpi around 240 dpi, stable lines are generated and bulging appears above certain dpi for all the cases (> 300 dpi).

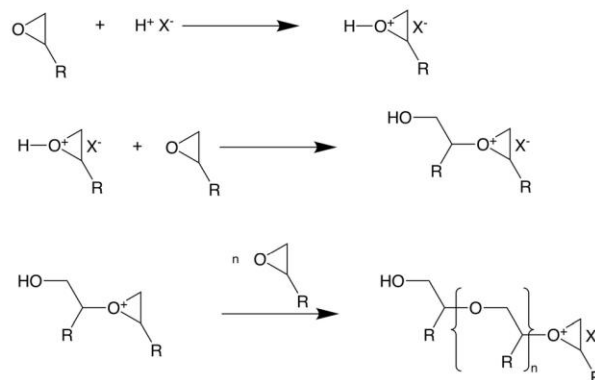
Printing of continuous area features using inks showing partial wetting, as in the present cases, has been achieved in other systems by sequential printing of a spatially offset drop partially overlapping matrixes.⁶⁵ Given the architecture of our printhead, with a distance between nozzles of 137 microns, and the size of the printed dots, covering continuous areas using this approach would require printhead tilting with respect the substrate moving direction. Covering areas with ink can also be achieved by increasing the dpi in the substrate moving direction therefore producing line bulging and coalescence of contiguous lines; however this frequently leads to non-printed regions and faulty printing. Defect-free continuous areas have been achieved with our inks by using a glass substrate treated with ozone or CCVD using pyrosil. While the preparation of defect-free areas using this approach on ozone treated substrates required the use of high dpi in the substrate moving direction (up to 1440 dpi and above), the strong ink spreading in the pyrosil treated substrates led to continuous areas with uniform thickness at low dpi (e.g.: 360 dpi), although the definition of fine features is lost to some extent at the edges of the printed areas in this last case due to ink spreading.

Ink fixation

Continuous films of the model ink were deposited on Pyrosil treated glass substrates using inkjet printing (360 dpi along the substrate moving direction). Irradiation of these films using UV light (320–390 nm, 10 mW cm⁻², 300 s) led to continuous solid films (3.5 μm thick). The films obtained are transparent and present a defect free morphology when observed by SEM (see Fig. S2, ESI[†]) and under an optical microscope. AFM imaging of the film topography (Fig. S3, ESI[†]) reveals a very smooth morphology with a root mean square (rms) surface roughness of 0.44 nm over a 4 × 4 μm² area for a cured deposit of the model ink.

The UV-Vis absorption spectrum of a thin layer of the model ink placed in quartz cells of fixed thickness (Fig. S4, ESI[†]), shows an absorption band centered at 300 nm before irradiation with UV light. Exposure of the liquid layer leads to depletion of this absorption that is ascribed to decomposition of the photoinitiator. This decomposition induces acid generation that triggers polymerization as mentioned above. Scheme 1 presents the epoxy ring-opening cationic photopolymerization. The photoacid H⁺X⁻ generated upon excitation of the photoinitiator attacks the oxygen of the epoxy ring to initiate the formation of the polyether chain. Scheme 2 shows the photoacid-catalyzed sol–gel process for GPTMS that takes place first by hydrolysis of methoxysilane groups and later by condensation to form a siloxane chain. Differently from the classical sol–gel reaction, this photoinduced sol–gel process does not need any additional solvent (water or any other solvent) and simple diffusion of atmospheric moisture is sufficient for the hydrolysis reactions.

FTIR spectroscopy was employed to check the photoinduced polymerization reaction of the inks. Fig. 2 shows the FTIR spectra of the model ink before and after exposure to UV light. The C–H stretching band at 3050 cm⁻¹ of the epoxide disappears indicating that UV irradiation promotes the epoxy ring opening reaction⁶⁶ (see Scheme 1). Regarding the inorganic polymerization, irradiation of the ink produces a noticeable growth of a wide band appearing at 3400 cm⁻¹ corresponding to the vibration of the OH group in the Si–OH bond, all this confirming the hydrolysis reaction.⁶⁷ On the other hand, the



Scheme 1 Cationic ring opening polymerization of epoxy rings.

It is well known that polymerization kinetics in these UV cured hybrid systems is highly dependent on the presence of atmospheric water.⁶⁸ While the cationic reaction is not significantly influenced by the presence of atmospheric water,⁶⁹ this produces a strong effect on the formation of an inorganic network since water is needed for the hydrolysis reaction. Not only the amount of water available but also its ability to diffuse into the sample plays a very important role in the sol-gel polymerization. While thinner films in the order of microns usually lead to higher hydrolysis rates favoring the formation of an inorganic network, thicker ones have a slower supply of water to the deep layers reducing the photoacid catalyzed hydrolysis of the silane. Also the more difficult elimination of byproducts (alcohols) of the condensation in thicker films can induce a slowdown of the hydrolysis.^{58,68} On the other hand phase separation phenomena, leading to light scattering, have been observed in this type of photoacid catalyzed polymerization of hybrid systems. The presence of water and the formation of byproducts such as alcohols due to condensation can induce phase separation and formation of microsegregated phases.⁵⁸ Even more the balance between the formation rates of the two types of networks, organic and inorganic, is crucial to avoid phase segregation.⁶⁸

The drastic reduction of turbidity found in the thicker films of the photocured HRI ink under ambient atmospheric conditions could indicate that the reduction of hydrolysis and condensation rates reduces the phase separation process. Since the ambient atmosphere is the water reservoir for the hydrolysis reaction, elimination of water from it could slow down the sol-gel process and minimize or inhibit phase separation.

To support this hypothesis, curing was carried out in a chamber provided with an optical access in which pressure was diminished to 100 mBar to reduce the water content. Curing under these conditions of isolated deposited droplets of HRI ink led to microlenses free of the microsegregated morphology as observed by SEM (Fig. 3c and d) and optical phase contrast microscopy (Fig. S6c and d, ESI†). When thin films were inkjetted on glass substrates, highly transparent continuous films (even at the edges) in the whole range of

thickness under study were obtained (Fig. S7b, ESI†). AFM was also used to characterize the film topography. The cured films (4 μm thick) also have a smooth morphology with a root mean square (rms) surface roughness of 1.92 nm and 1.03 nm over a $4 \times 4 \mu\text{m}^2$ area for samples exposed to ambient atmospheric (Fig. S8a, ESI†) and under mild vacuum (Fig. S8b, ESI†), conditions respectively. This morphology was observed to be stable over periods of several, at least four, months.

FTIR spectroscopic studies were also carried out on the HRI ink to investigate the curing process in this system under the two considered curing conditions (Fig. 4). Focusing on the photoinduced formation of the inorganic network, which can be affected by the presence of atmospheric water, we have followed the bands at 3400 and 1100 cm^{-1} before and after 10 min UV irradiation. Under ambient atmospheric irradiation conditions (Fig. 4a), a wide band appears at around 3400 cm^{-1} ascribed to the formation of silanols, which confirms the hydrolysis reaction. The peak at 1080 cm^{-1} due to the Si-O-CH₃ group is replaced by a wide band appearing with a peak at around 1100 cm^{-1} associated with the siloxane bonds. This confirms that hydrolysis and condensation have already taken place 10 min after UV irradiation has finished (see Scheme 2). Spectra taken 24 h later did not show significant qualitative differences (only minor changes around 1100 cm^{-1}). The FTIR spectra just described (Fig. 4a) show similar qualitative features to those found for the GPTMS photopolymerization (Fig. 2) involving the same type of reactive group and same curing conditions.

For the samples cured under mild vacuum conditions (Fig. 4b), the changes in the bands associated with the inorganic network followed a different dynamics. Just after the UV exposure under mild vacuum conditions, the sample is let to evolve in an ambient atmosphere. The FTIR spectrum at this point (10 min after UV exposure) reveals that the silanol band in the 3400 cm^{-1} region is already present a few minutes after the sample is exposed to an ambient atmosphere and later evolves shifting toward shorter wavenumbers (see the spectrum at 24 h). The bands around 1100 cm^{-1} also evolve in a different fashion. It can be seen that 10 min after UV exposure the peak at 1080 cm^{-1} decreases but the broad band at 1100 cm^{-1} continues later its

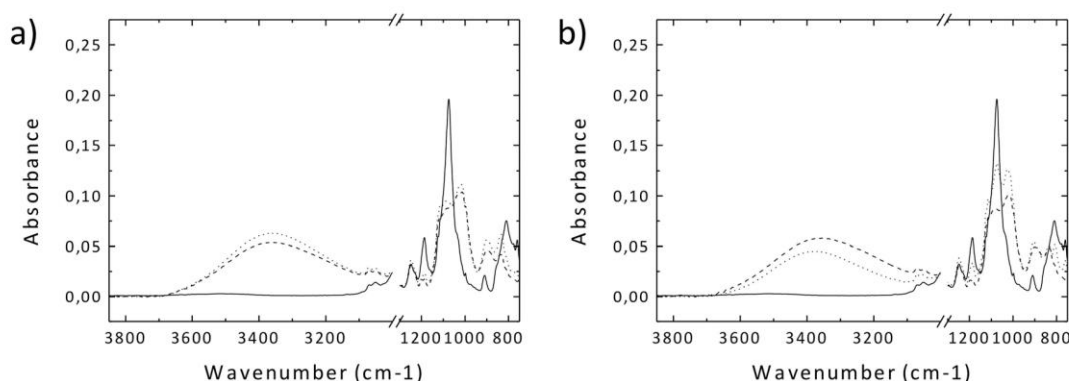


Fig. 4 FTIR spectra of the HRI ink before (continuous line), 10 min after (dotted line) and 24 h after exposure to UV light (dashed line) (a) under ambient atmosphere conditions and (b) under mild vacuum conditions (100 mBar).

evolution over time. Note the relative absorbance change of the two different peaks around 1100 cm^{-1} between the spectra at 10 min and 24 h, which indicates that condensation significantly takes place after the first 10 min for the sample cured under mild vacuum conditions, in contrast to the lack of evolution observed for the sample exposed to ambient atmospheric conditions. After 24 h the spectra do not qualitatively evolve as followed during one month. Despite the differences in the dynamics observed between the samples cured under the two different conditions, the spectra of both films presented qualitatively the same spectra features after 24 h. The differences in the reaction kinetics under these two different curing conditions are responsible for the large differences in morphology for the isolated cured droplets. The experiments above highlight the importance of the presence and the supply of water to the reaction to control the formation of the organic and inorganic networks and therefore the film morphology.⁶⁷ Since no evolution of the FTIR spectra was observed for periods of time longer than 24 h, all the films were allowed to evolve in the dark for at least 24 h before any subsequent characterization to ensure completion of the hydrolysis and condensation processes.

Mechanical properties and adhesion to the substrate

To assess the mechanical properties of the deposited films, elastic modulus and hardness were measured using a nano-indenter. Nanoindentation is a suitable technique to determine the mechanical properties of these types of hybrid organic-inorganic films.⁷⁰ Larger load was necessary for the HRI ink based deposits to reach the 400 nm indentation depth, independently of the curing method, when compared to the model ink ones, which indicates a higher elastic modulus of the HRI deposits. The Young modulus (E) and hardness (H) obtained for the Model and HRI ink deposits are given in Table 3.

The value of Young modulus of 2.6 GPa for the inkjet printed deposits cured using the photoacid catalyzed curing agrees with other values found in the literature for GPTMS networks despite being cured following a different method.^{70,71} Higher values of the Young modulus were obtained for the HRI ink which can be ascribed to the presence of multifunctional Epikote 157 and dPDMS in the formulation leading also to a strongly crosslinked network. No significant differences were found in the mechanical properties between films measured at different times after curing within three months (samples stored in an ambient atmosphere) indicating good mechanical stability of the deposited films.

Concerning adhesion to glass, the SEM images of fractured samples (Fig. 3), demonstrated excellent adhesion between the cured inks and the glass substrate. To assess the adhesion of

the deposited materials towards the substrate, cross-cut and tape tests based on the standard ASTM 3359 were carried out. Optical microscope images of cross-cut areas after the test (film thickness: 3.5–4.5 μm) were taken. For the model ink deposited on glass previously treated with pyrosil, and cured immediately after deposition (Fig. S9a, ESI[†]), almost all the film remained attached after the adhesion test carried out one day after the curing step. Detaching of small flakes along the edges of the cut is observed in the samples with an estimated affected area below 5% and therefore being rated as 4B–5B binding strength, demonstrating a good adhesion of the inkjet printed deposits to the glass substrate. For the HRI ink (Fig. S9b and c, ESI[†]) almost no delamination was observed, being the adhesion strength rating assigned 4B–5B for these films regardless of the photocuring protocol adopted (atmospheric or mild vacuum conditions). The tests were repeated in all the samples, stored under ambient conditions, 3 months later finding similar results.

Inkjet printed planar waveguides

Deposits of the model and HRI inks were directly prepared by inkjet printing on top of glass substrates and subsequently exposed to UV light. As described above, the films presented a stable transparent, defect-free morphology with smooth surface topography, which is a prerequisite for waveguide applications (see Fig. S3 and S8, ESI[†]). Coupling of waveguided modes was demonstrated in our inkjet films of hybrid materials by using the prism coupling technique using 632.8 nm light. This technique enables the characterization of the refractive index and thickness of these so prepared thin films. As an example, Fig. 5a and b show that a thin film of the HRI ink cured at reduced pressure supports several Transversal Electric (TE) and Transversal Magnetic (TM) modes. Only the indicated intensity drops, corresponding to the modes with an effective refractive index higher than that of the substrate ($n_g = 1.514$), are fully supported by the inkjetted film, indicating that the rest of the intensity drops to substrate modes. The effective refractive index of the film modes was used for the calculation of the film refractive index and its thickness.⁵⁵ A refractive index of 1.560 and a thickness of 4.2 μm are calculated from these measurements for the HRI film exposed to reduced pressure. This is in good agreement with the deposit thickness measured using stylus profilometry (4 μm thick). The high values of the refractive index, suitable for waveguide preparation, arise from the aromatic components of the HRI. Thicker films were also prepared using these materials by inkjet leading to planar waveguide supporting a large number of modes (see Fig. S10, ESI[†]). The same characterization was carried out for thin film deposits of the HRI ink cured under ambient atmospheric conditions (Fig. S11, ESI[†]) and of the model ink (Fig. S12, ESI[†]).

To assess the performance of the deposits as planar waveguides we have characterized the optical propagation losses of the TE₀ mode at 632.8 nm. To do this, the scattered light from this mode at each point of the waveguide (Fig. 5c) is measured using a fiber photodetector that moves along the surface following the propagation direction. This enables the estimation of propagation losses by fitting the signal to exponential

Table 3 Mean values for the Young modulus (E) and hardness (H)

	E (GPa)/ H (GPa)
Model ink	2.6/0.19
HRI ink (cured under ambient atmospheric conditions)	4.7/0.31
HRI ink (cured under mild vacuum conditions)	4.7/0.30

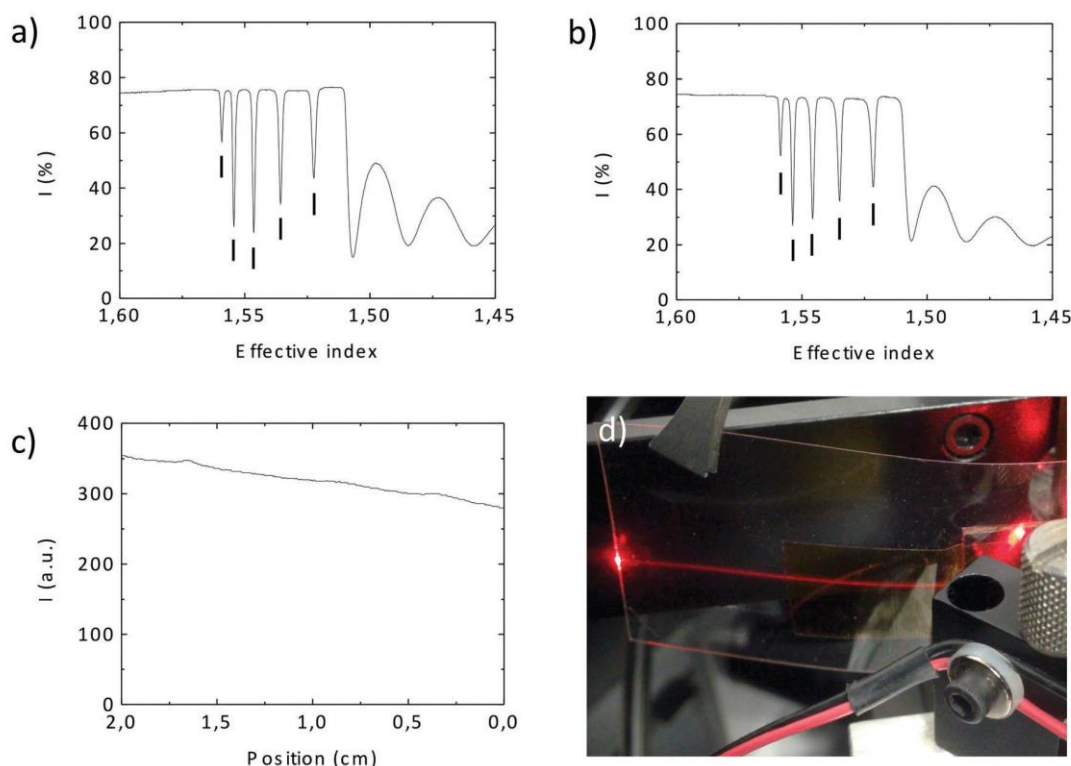


Fig. 5 (a) TE and (b) TM propagation modes (at 632.8 nm) for a HRI ink deposit (4 μm thick) cured under mild vacuum conditions. Modes with an effective refractive index higher than that of the substrate ($n_g = 1.514$), and fully supported by the inkjetted film are indicated with a line. (c) Intensity distribution along an inkjet printed waveguide of the HRI ink cured under mild vacuum conditions. (d) Scattered light streak from an inkjet printed waveguide from the HRI ink on a flexible PET substrate with a model ink printed cladding layer. The substrate and waveguide are bent with the help of a pair of tweezers (top-left).

decay. Optical transmission losses of $0.5\text{--}0.6\text{ dB cm}^{-1}$ at 632.8 nm have been measured for samples exposed under mild vacuum conditions. On the other hand those cured under ambient atmospheric conditions led typically to $1\text{--}1.1\text{ dB cm}^{-1}$. In both cases loss coefficients were stable over periods of 2 months.

Since there is no detectable absorption at the wavelength of measurement (Fig. S4, ESI[†]), the losses have their origin mainly in scattering coming from refractive index spatial variations either from the surface or the volume of the waveguide. Optical losses related to surface variations are proportional to the rms surface roughness.⁷² The morphology studies carried out using AFM already showed that the different curing conditions led to differences in the smoothness of the cured deposits with rms surface roughness values of 1.03 nm and 1.92 nm for the HRI film cured under mild vacuum and under ambient atmospheric conditions, respectively. Even though these roughness values are similar to, even smaller than, those obtained in other materials by using techniques other than inkjet printing, for this same application, the overall losses are larger in our case.^{16,17,20} In this way, Yoon *et al.* prepared channel waveguides by patterned UV photopolymerization of ORMOCER materials with an rms surface roughness of 2–5 nm and propagation losses as small as 0.07 dB cm^{-1} (measured at 850 nm).²⁰ As a result, light losses due to scattering in the bulk

has to be a relevant contribution in our case. The losses due to bulk scattering have their origin at spatial variations of the refractive index arising from density or compositional spatial modulations. In our system we have found that the ratio between the cationic polymerization rate and that of the hydrolysis and condensation strongly affects the microscopic morphology and therefore the scattering properties of the cured material. Consequently, kinetics is very important for optimizing the performance of thin films of these types of materials as optical waveguides. Because of this, polymerization conditions, that is, UV light intensity and the humidity during the process, are key parameters seeking to minimize these losses and to improve the performance of the inkjet printed waveguides.

To exploit the ability of inkjet printing technology to deposit different materials, planar waveguides were manufactured by applying a cladding consisting on a film of the model ink (3.5 μm thick). Once cured, on top of this layer a second deposit of the HRI ink (4 μm thick) was inkjet printed and photocured acting as the core of the planar waveguide. These structures demonstrated to support waveguiding modes with low losses when applied on glass plates. This low attenuation values for the light propagating through the top waveguide were also obtained when a flexible Polyethylene terephthalate (PET) film used in flexible electronics was employed or even conventional

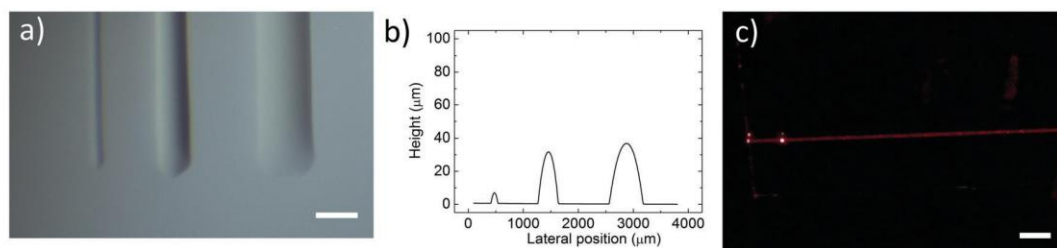


Fig. 6 (a) HRI channel waveguides of different widths (1, 3 and 5 pixels) inkjet printed on a glass substrate (scale bar: 500 μm). (b) Cross section profiles of the waveguides. (c) Scattered light streak from a three-pixel width inkjet printed channel waveguide. Light is coupled by using a prism placed on the right (not shown in the figure) (scale bar: 500 μm).

ceramic glass and metallic substrates were industrially used in conventional applications such as home-appliances like cooktops, fridge or dishwasher front doors. In particular, the deposited waveguides on flexible PET substrates are mechanically stable against bending showing neither detachment or cracking (Fig. 5d) nor increment in propagation losses after ceasing the bending. The lower refractive index cladding applied on top of the rough surface planarizes it and acts as a flat substrate for waveguide core manufacturing. These experiments emphasize the versatility and power of these materials in combination with inkjet printing technology to generate optical circuits in a wide variety of substrates.

Finally, beyond planar waveguides, channel waveguides with different widths have been also printed with these materials on glass substrates to highlight the potential of these fabrication platform to prepare photonic devices. Fig. 6 shows photographs and profiles of inkjet printed HRI waveguides, cured under mild vacuum conditions. Channel waveguides with different widths were prepared in ozone treated substrates. One single-pixel width channel waveguides were obtained by printing ink droplets along a line with a spacing between droplets of 240 dpi. As mentioned above, stable lines (Fig. 6a, left-side waveguide; Fig. 6b, left-side profile) can be obtained. Wider channel waveguides of three-pixel width were prepared by first using two alternate nozzles (with one inactive nozzle in between) to generate, in a first pass, two lines as the one described just above (at 240 dpi). In a second pass, the nozzle in between the two used in the first pass, is used to fill the empty space in between the two lines previously printed depositing a large amount of ink (at 4320 dpi), leading to a channel waveguide with a high profile (Fig. 6a, central waveguide; Fig. 6b, central profile). Wider waveguides, for example five-pixel width (Fig. 6a, right-side waveguide; Fig. 6b, right-side profile), can be prepared using a homologous strategy based on the use of alternate nozzles and two printing passes. After the curing step, light was coupled in these waveguides and losses as low as 0.5 dB cm^{-1} at 632.8 nm have been measured (Fig. 6c).

Putting the obtained values in perspective with respect to other studies in the literature, channel waveguides generated by inkjet of SU-8 solutions by Vacirca and Kurzweg resulted in losses 16.1 dB in 7.5 cm .⁷³ Channel waveguides created by inkjet printing a solvent etchant on a thin film of polystyrene led to optical losses of 2 dB cm^{-1} .⁷⁴ The values obtained in the inkjet printed planar waveguides presented in our work, in the

order of $0.5\text{--}0.6 \text{ dB cm}^{-1}$, are in the same range of values of others obtained by other processing techniques^{75,76} despite improvements in composition and processing are still needed to reach the values, as low as 0.07 dB cm^{-1} , obtained by using photolithography in ORMOCORE materials.²⁰

Conclusions

Jettable inks based on photoacid catalyzed formulations containing monomers with epoxy and silane functionalities have been successfully formulated. Compared to inks based on conventional sol-gel processes, the hydrolysis and condensation in these materials is advantageously delayed in the absence of UV light favoring the long-term stability of the ink properties, mainly viscosity, essential for their applicability in industrial applications. Due to the lack of solvents in the ink formulation, the deposited material can be polymerized immediately after ink deposition upon UV light irradiation and without the need for intermediate baking steps significantly simplifying the process and leading to functional deposits in one single step, allowing also the use of thermally sensitive substrates. UV light triggers the photocuring reaction of the epoxy groups and in the presence of water a crosslinked organic-inorganic polymeric network is obtained. A proper selection of the curing conditions enables obtaining, through a simple process, without the need for postbaking steps, deposits with excellent adhesion to glass and good transparency. Planar and channel waveguides that support modes with propagation losses as low as 0.5 dB cm^{-1} have been demonstrated using this approach. The results here obtained for low attenuation of the propagating light for inkjet printed photocured hybrid waveguides and the possibility to use substrates of different natures demonstrate the suitability of these photoacid catalyzed hybrid formulations and inkjet printing for the preparation photonic devices.

Conflicts of interest

There are no conflicts to declare.

Acknowledgements

Carlos Sánchez-Somolinos thanks the Spanish MINECO project SAF2014-54763-C2-2-R, Gobierno de Aragón, and FEDER (EU).

Authors would like to acknowledge the use of Servicio General de Apoyo a la Investigación-SAI, Universidad de Zaragoza.

References

- 1 R. Hunsperger, *Integrated Optics, theory and technology*, Springer-Verlag, New York, 6th edn, 2009.
- 2 C. Sánchez, B. Lebeau, F. Chaput and J. P. Boilot, *Adv. Mater.*, 2003, **15**, 1969–1994.
- 3 M. Foerthner, M. Rumler, F. Stumpf, R. Fader, M. Rommel, L. Frey, M. Girschikofsky, S. Belle, R. Hellmann and J. J. Klein, *Appl. Phys. A: Mater. Sci. Process.*, 2016, 122–240.
- 4 J. A. Grant-Jacob, S. J. Beecher, T. L. Parsonage, P. Hua, J. I. Mackenzie, D. P. Shepherd and R. W. Eason, *Opt. Mater. Express*, 2016, **6**, 91–96.
- 5 S. Nizamoglu, M. C. Gather, M. Humar, M. Choi, S. Kim, K. S. Kim, S. K. Hahn, G. Scarcelli, M. Randolph, R. W. Redmond and S. H. Yun, *Nat. Commun.*, 2016, **7**, 10374.
- 6 S. Parola, B. Julián-López, L. D. Carlos and C. Sanchez, *Adv. Funct. Mater.*, 2016, **26**, 6506–6544.
- 7 Y. Sun, Q. Liao, Y. Huang, A. Xia, Q. Fu, X. Zhu and Y. Zheng, *Bioresour. Technol.*, 2016, **220**, 215–224.
- 8 S. Guy, B. Baguenard, A. Bensalah-Ledoux, D. Hadiouche and L. Guy, *ACS Photonics*, 2017, **4**, 2916–2922.
- 9 H. K. Kim, S.-J. Kang, S.-K. Choi, Y.-H. Min and C.-S. Yoon, *Chem. Mater.*, 1999, **11**, 779–788.
- 10 P. Coudray, P. Etienne, Y. Moreau, J. Porque and S. I. Najafi, *Opt. Commun.*, 1997, **143**, 199–202.
- 11 R. Houbertz, L. Fröhlich, M. Popall, U. Streppel, P. Dannberg, A. Bräuer, J. Serbin and B. N. Chichkov, *Adv. Eng. Mater.*, 2003, **5**, 551–555.
- 12 P. Coudray, P. Etienne and Y. Moreau, *Mater. Sci. Semicond. Process.*, 2000, **3**, 331–337.
- 13 E. J. Nassar, R. R. Gonçalves, M. Ferrari, Y. Messaddeq and S. Ribeiro, *J. Alloys Compd.*, 2002, **344**, 221–225.
- 14 W. Que and X. Hu, *J. Sol-Gel Sci. Technol.*, 2003, **28**, 319–325.
- 15 R. Houbertz, G. Domann, C. Cronauer, A. Schmitt, H. Martin, J. U. Park, L. Fröhlich, R. Buestrich, M. Popall, U. Streppel, P. Dannberg, C. Wächter and A. Bräuer, *Thin Solid Films*, 2003, **442**, 194–200.
- 16 W. Que, X. Hu and J. Zhou, *Thin Solid Films*, 2005, **484**, 278–282.
- 17 P. Karasiński, C. Tyszkiewicz, A. Domanowska, A. Michalewicz and J. Mazur, *Mater. Lett.*, 2015, **143**, 5–7.
- 18 A. Serra, X. Ramis and X. Fernández-Francos, *Coatings*, 2016, **6**, 8–19.
- 19 K. H. Haas, S. Amberg-Schwab and K. Rose, *Thin Solid Films*, 1999, **351**, 198–203.
- 20 K. B. Yoon, *Macromol. Res.*, 2004, **12**, 290–292.
- 21 R. Woods, S. Feldbacher, D. Zidar, G. Langer, V. Satzinger, V. Schmidt, N. Pucher, R. Liska and W. Kern, *Opt. Mater. Express*, 2014, **4**, 486–498.
- 22 G. Brusatin, D. G. Giustina, M. Guglielmi, M. Casalboni, P. Proposito, S. Schutzmann and G. Roma, *Mater. Sci. Eng., C*, 2007, **27**, 1022–1025.
- 23 J. Alamán, R. Alicante, J. Peña and C. Sánchez-Somolinos, *Materials*, 2016, **9**, 910–947.
- 24 M. Singh, H. M. Haverinen, P. Dhagat and G. E. Jabbour, *Adv. Mater.*, 2010, **22**, 673–685.
- 25 B. Derby, *Annu. Rev. Mater. Res.*, 2010, **40**, 395–414.
- 26 M. Robin, W. Kuai, M. Amela-Cortes, S. Cordier, Y. Molard, T. Mohammed-Brahim, E. Jacques and M. Harnois, *ACS Appl. Mater. Interfaces*, 2015, **7**, 21975–21984.
- 27 R. Danzebrink and M. A. Aegerter, *Thin Solid Films*, 1999, **351**, 115–118.
- 28 R. Danzebrink and M. A. Aegerter, *Thin Solid Films*, 2001, **392**, 223–225.
- 29 J. Y. Kim, N. B. Brauer, V. Fakhfour, D. L. Boiko, E. Charbon, G. Grützner and J. Brugger, *Opt. Mater. Express*, 2011, **1**, 259–269.
- 30 J. Y. Kim, K. Pfeiffer, A. Voigt, G. Gruetzner and J. Brugger, *J. Mater. Chem.*, 2012, **22**, 3053–3058.
- 31 J. Y. Kim, C. Martin-Olmos, N. S. Baek and J. Brugger, *J. Mater. Chem. C*, 2013, **1**, 2152–2157.
- 32 L. Jacot-Descombes, V. J. Cadarso, A. Schleunitz, S. Grützner, J. J. Klein, J. Brugger, H. Schiff and G. Grützner, *Opt. Express*, 2015, **23**, 25365–25376.
- 33 A. Voigt, U. Ostrzinski, K. Pfeiffer, J. Y. Kim, V. Fakhfour, J. Brugger and G. Gruetzner, *Microelectron. Eng.*, 2011, **88**, 2174–2179.
- 34 S. T. Parker, P. Domachuk, J. Amsden, J. Bressner, J. A. Lewis, D. L. Kaplan and F. G. Omenetto, *Adv. Mater.*, 2009, **21**, 2411–2415.
- 35 A. Samusjew, M. Kratzer, A. Moser, C. Teichert, K. K. Krawczyk and T. Griesser, *ACS Appl. Mater. Interfaces*, 2017, **9**, 4941–4947.
- 36 D. J. Lorang, D. Tanaka, C. M. Spadaccini, K. A. Rose, N. J. Cherepy and J. A. Lewis, *Adv. Mater.*, 2011, **23**, 5055–5058.
- 37 T. Wolfer, P. Bollgruen, D. Mager and L. Overmeyer, *Procedia Technol.*, 2014, **15**, 521–529.
- 38 T. Wolfer, P. Bollgruen, D. Mager, L. Overmeyer and J. G. Korvink, *Mechatronics*, 2016, **34**, 119–127.
- 39 M. Hofmann, Y. Xiao, S. Sherman, P. Bollgrün, T. Schmidt, U. Gleissner and H. Zappe, *Inkjet printed single-mode waveguides on hot-embossed foils*, Proc. of SPIE Optical Systems Design, Jena, Germany, 2015.
- 40 P. Bollgruen, U. Gleissner, C. Megnin, D. Mager, J. Korvink and T. Hanemann, *Ink-jet printing of host-guest systems based on acrylates with fluorescent dopants*, Proc. SPIE 9888 Micro-Optics, Brussels, Belgium, 2016.
- 41 P. Bollgruen, U. Gleissner, T. Wolfer, C. Megnin, D. Mager, L. Overmeyer, J. G. Korvink and T. Hanemann, *Opt. Eng.*, 2016, **55**, 107107.
- 42 P. Bollgruen, T. Wolfer, U. Gleissner, D. Mager, C. Megnin, L. Overmeyer, T. Hanemann and J. G. Korvink, *Flexible Printed Electron.*, 2017, **2**, 045003.
- 43 E. Amerio, M. Sangermano, G. Malucelli, A. Priola and B. Voit, *Polymer*, 2005, **46**, 11241–11246.
- 44 E. Amerio, M. Sangermano, G. Malucelli, A. Priola and G. Rizza, *Macromol. Mater. Eng.*, 2006, **291**, 1287–1292.
- 45 M. Sangermano, M. Messori, M. M. Galleco, G. Rizza and B. Voit, *Polymer*, 2009, **50**, 5647–5652.

- 46 A. Chemtob, M. Peter, C. Belon, C. Dietlin, C. Croutxé-Barghorn, L. Vidal and S. Rigolet, *J. Mater. Chem.*, 2010, **20**, 9104–9112.
- 47 C. Croutxé-Barghorn, C. Belon and A. Chemtob, *J. Photopolym. Sci. Technol.*, 2010, **23**, 129–134.
- 48 C. Belon, A. Chemtob, C. Croutxé-Barghorn, S. Rigolet, M. Schmitt, S. Bistac, V. Le Houérou and C. Gauthier, *Polym. Int.*, 2010, **59**, 1175–1186.
- 49 B. Schuhmacher, W. Müschenborn, M. Stratmann, B. Schultrich, C.-P. Klages, M. Kretschmer, U. Seyfert, F. Förster and H.-J. Tiller, *Adv. Eng. Mater.*, 2001, **3**, 681–689.
- 50 W. C. Oliver and G. M. Pharr, *J. Mater. Res.*, 1992, **7**, 1564–1583.
- 51 C. Belon, A. Chemtob, C. Croutxé-Barghorn, S. Rigolet, V. Le Houérou and C. Gauthier, *J. Polym. Sci., Part A: Polym. Chem.*, 2010, **48**, 4150–4158.
- 52 C. Belon, A. Chemtob, C. Croutxé-Barghorn, S. Rigolet, V. Le Houérou and C. Gauthier, *Macromol. Mater. Eng.*, 2011, **296**, 506–516.
- 53 A. C. Fischer-Cripps, *Surf. Coat. Technol.*, 2006, **200**, 4153–4165.
- 54 Standard ASTM D3359-02, Standard Test Methods for Measuring Adhesion by Tape Test, West Conshocken, PA, USA, 2002.
- 55 C. X. Tong, *Advanced Materials for Integrated Optical Waveguides*, Springer International Publishing, Switzerland, 1st edn, 2014, vol. 46, pp. 53–102.
- 56 J. V. Crivello, *J. Polym. Sci., Part A: Polym. Chem.*, 1999, **37**, 4241–4254.
- 57 S. Shi, C. Croutxé-Barghorn and X. Allonas, *Prog. Polym. Sci.*, 2017, **65**, 1–41.
- 58 A. Chemtob, D.-L. Versace, C. Belon, C. Croutxé-Barghorn and S. Rigolet, *Macromolecules*, 2008, **41**, 7390–7398.
- 59 B. Derby, N. Reis, K. Seerden, P. S. Grant and J. Evans, *MRS Proc.*, 2000, **625**, 195–201.
- 60 D. Jang, D. Kim and J. Moon, *Langmuir*, 2009, **25**, 2629–2635.
- 61 P. C. Duineveld, M. M. de Kok, M. Buechel, A. Sempel, K. A. Mutsaers, P. van de Weijer, I. G. Camps, T. van de Biggelaar, J.-E. J. Rubingh and E. I. Haskal, *Proc. SPIE*, 2002, **4464**, 59–67.
- 62 S. D. Hoath, I. M. Hutchings, G. D. Martin, T. R. Tuladhar, M. R. Mackley and D. Vadiello, *J. Imaging Sci. Technol.*, 2009, **53**, 041208.
- 63 S. D. Hoath, D. C. Vadiello, O. G. Harlen, C. McIlroy, N. F. Morrison, W.-K. Hsiao, T. R. Tuladhar, S. Jung, G. D. Martin and I. M. Hutchings, *J. Non-Newtonian Fluid Mech.*, 2014, **205**, 1–10.
- 64 C. K. Fink, K. Nakamura, S. Ichimura and S. J. Jenkins, *J. Phys.: Condens. Matter*, 2009, **21**, 183001.
- 65 E. Tekin, B.-J. de Gans and U. S. Schubert, *J. Mater. Chem.*, 2004, **14**, 2627–2632.
- 66 A. Chemtob, L. Ni, C. Dietlin, C. Croutxé-Barghorn, P. Kitzmann, M. Brogly and L. Vidal, *Surf. Coat. Technol.*, 2012, **209**, 64–72.
- 67 H. De Paz, A. Chemtob, C. Croutxé-Barghorn, D. Le Nouen and S. Rigolet, *J. Phys. Chem. B*, 2012, **116**, 5260–5268.
- 68 L. Ni, N. Moreau, A. Chemtob and C. Croutxé-Barghorn, *J. Sol-Gel Sci. Technol.*, 2012, **64**, 500–509.
- 69 M. Sangermano, N. Razza and J. V. Crivello, *Macromol. Mater. Eng.*, 2014, **299**, 775–793.
- 70 F. Mammari, E. L. Bourhis, L. Rozes and C. Sanchez, *J. Mater. Chem.*, 2005, **15**, 3787–3811.
- 71 M. A. Robertson, R. A. Rudkin, D. Parsonage and A. Atkinson, *J. Sol-Gel Sci. Technol.*, 2003, **26**, 291–295.
- 72 F. P. Payne and J. A. Lacey, *Opt. Quantum Electron.*, 1994, **26**, 977–986.
- 73 N. A. Vacirca and T. P. Kurzweg, in *Advanced Fabrication Technologies for Micro/Nano Optics and Photonics III*, ed. W. V. Schoenfeld, J. J. Wang, M. Loncar and T. J. Suleski, Society of Photo-Optical Instrumentation Engineers (SPIE), San Francisco, 2010, vol. 7591, pp. 75910A–75910A8.
- 74 C. Zhang, C. L. Zou, Y. Zhao, C. H. Dong, C. Wei, H. Wang, Y. Liu, G. C. Guo, J. Yao and Y. S. Zhao, *Sci. Adv.*, 2015, **1**, e1500257.
- 75 V. Prajzler, P. Hyps, R. Mastera and P. Nekvindova, *Radio Eng.*, 2016, **25**, 230–235.
- 76 D. Hadiouche, C. Le Luyer, L. Guy, A. Bensalah-Ledoux, S. Saoudi, H. Khireddine and S. Guy, *Opt. Mater.*, 2014, **36**, 885–891.

SUPPLEMENTARY INFORMATION

Photoacid catalyzed organic-inorganic hybrid inks for the manufacturing of Inkjet-Printed Photonic Devices

*Jorge Alamán,^{a, b} María López-Valdeolivas,^a Raquel Alicante,^a Francisco J. Medel,^c Jorge Silva-Treviño,^a Jose Ignacio Peña,^d and Carlos Sánchez-Somolinos,^{a, e, *}*

^aInstituto de Ciencia de Materiales de Aragón (ICMA), CSIC-Universidad de Zaragoza,
Departamento de Física de la Materia Condensada, Zaragoza, Spain

^bBSH Electrodomésticos España, S.A., Polígono Industrial de PLA-ZA, Ronda del Canal
Imperial de Aragón, 18-20, 50197 Zaragoza, Spain

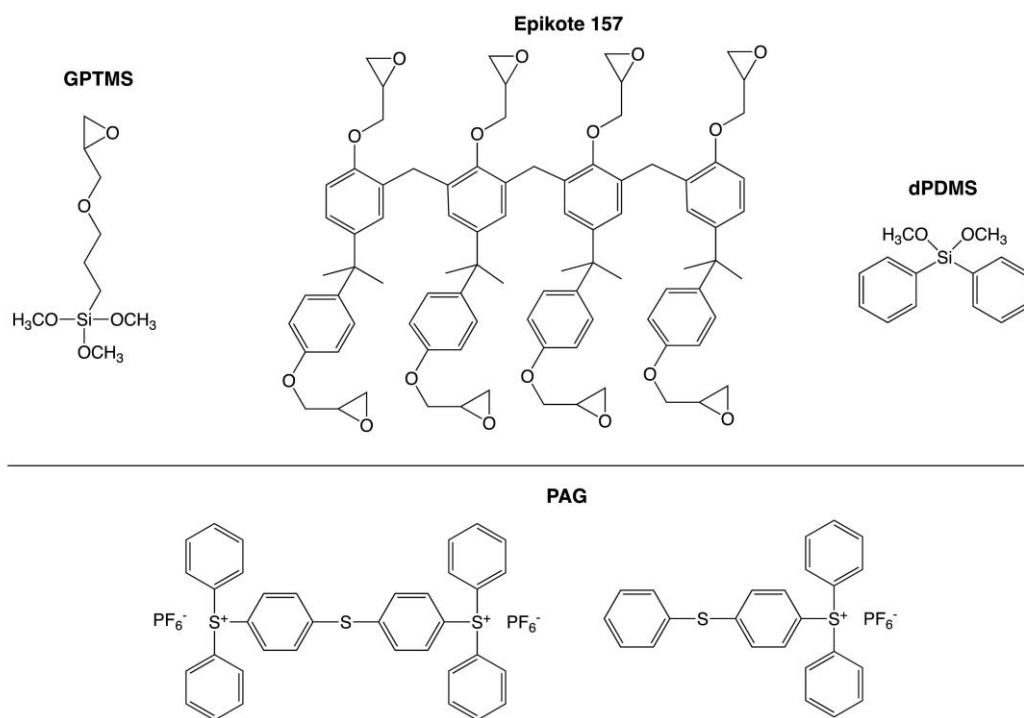
^cInstituto de Ciencia de Materiales de Aragón (ICMA), CSIC-Universidad de Zaragoza,
Departamento de Ingeniería Mecánica, Zaragoza, Spain

^dInstituto de Ciencia de Materiales de Aragón (ICMA), CSIC-Universidad de Zaragoza,
Departamento de Ciencia y Tecnología de Materiales y Fluidos, Zaragoza, Spain

^eCIBER in Bioengineering, Biomaterials and Nanomedicine (CIBER-BBN), Spain

*Correspondence: carlos.s@csic.es

Supplementary figures



Scheme S1 Chemical structure of the main components of the inks. GPTMS (3-glycidoxypropyltrimethoxysilane), Epikote 157, dPDMS (Dimethoxydiphenylsilane) and PAG (triarylsulfonium hexafluorophosphate salts, 50% in propylene carbonate).

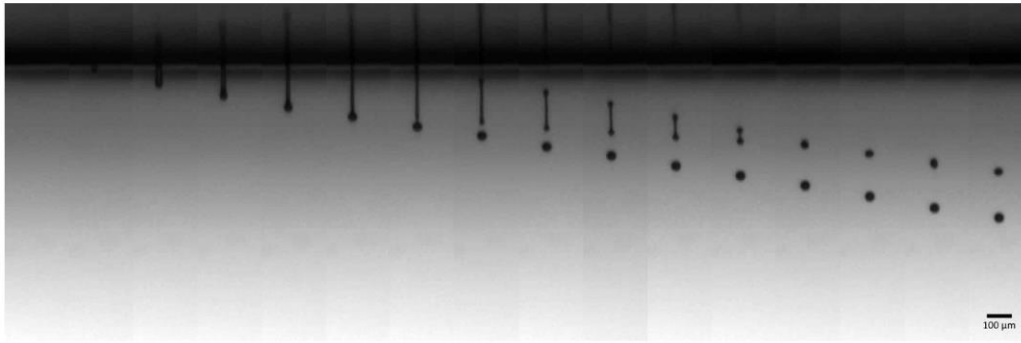


Fig. S1 Sequence of photographs (from left to right) showing the drop formation process for the Model ink under overvoltage conditions. Application of higher voltage to the printhead led to a longer jet that ends up breaking up in a main droplet travelling at higher speed and one or several satellites following the first one. The time interval between two adjacent frames is 11 μ s (scale bar: 100 μ m).

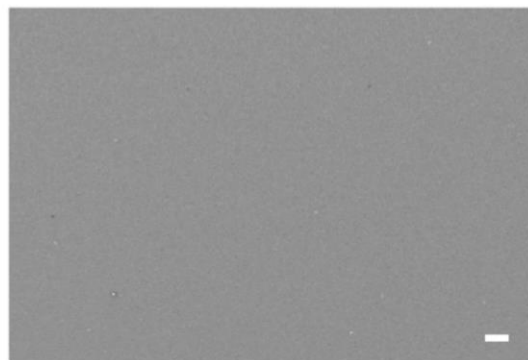


Fig. S2 SEM morphology of 3.5 μ m thick cured film of Model ink (scale bar: 2 μ m).

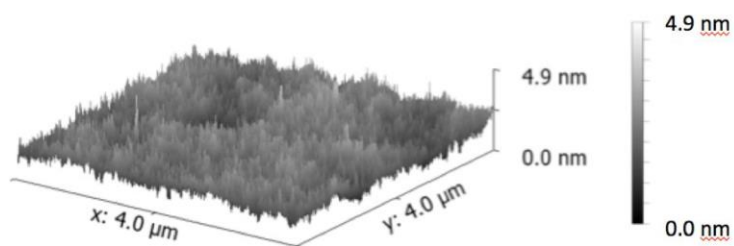


Fig. S3 AFM topography of a cured Model ink deposit (3.5 μ m thick film).

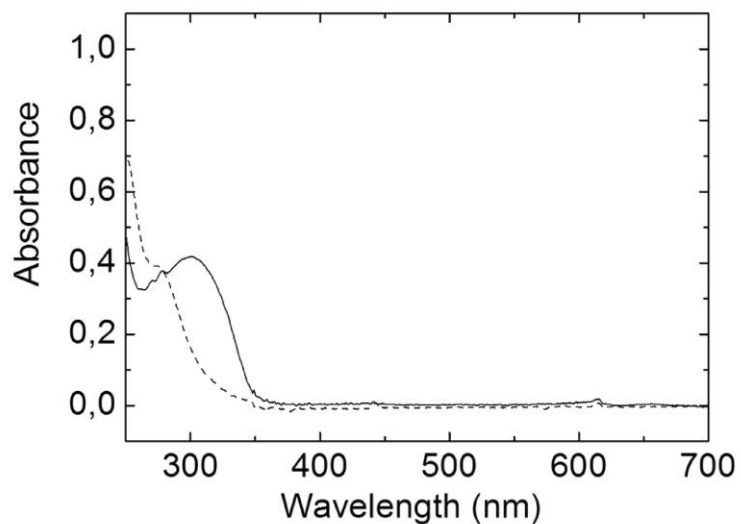


Fig. S4 UV-Vis absorption spectrum of thin films of the Model ink placed between quartz glass plates (10 μm gap) before (continuous line) and after UV irradiation (dashed line).

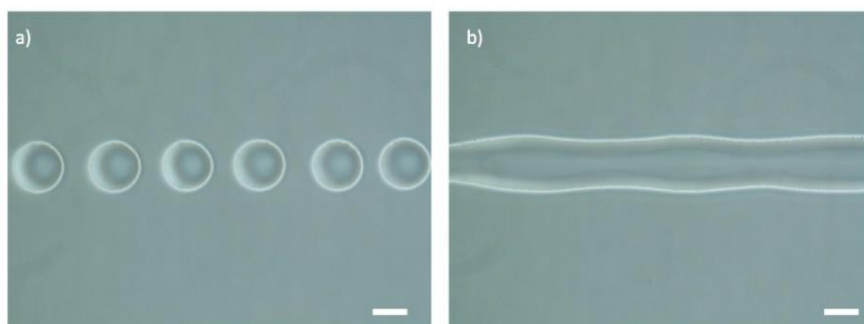


Fig. S5 Phase contrast microscope images of the inkjet printed drops of Model ink deposited along a line in ozone treated substrates at different dpi (scale bar: 100 μm): (a) 120 dpi and (b) 300 dpi. Bulging appears in this last case.

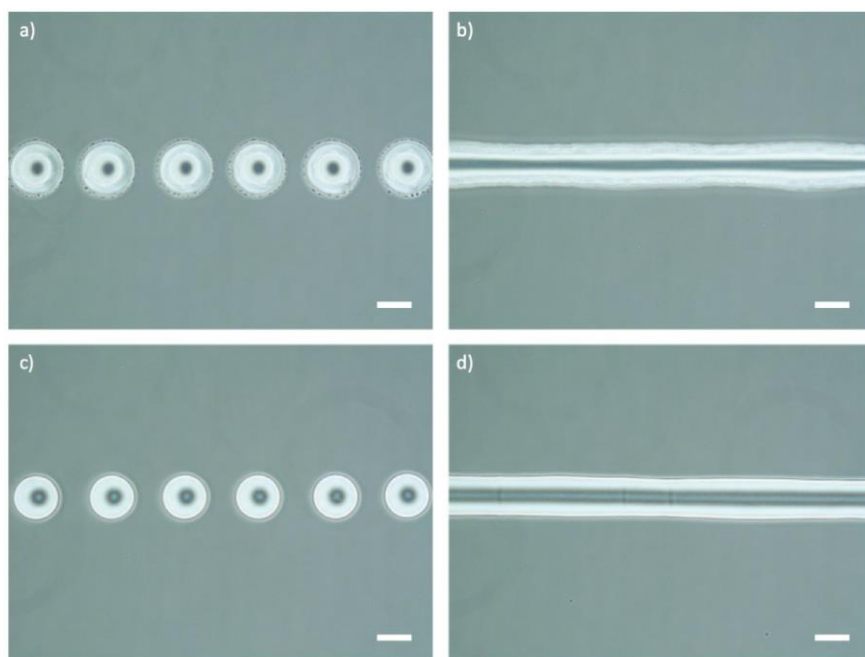


Fig. S6 Phase contrast images of inkjet printed drops of HRI ink deposited along a line in ozone treated substrates cured (a and b) in ambient atmospheric conditions and (c and d) under mild vacuum (100 mBar) (scale bar: 100 μm).

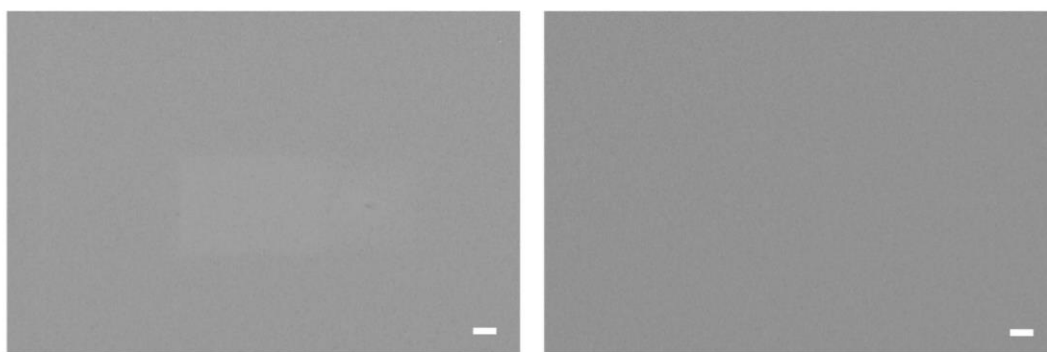


Fig S7 SEM morphology of 4 μm thick films of HRI ink cured (a) in ambient atmosphere conditions and (b) under mild vacuum (100 mBar) (scale bar: 2 μm).

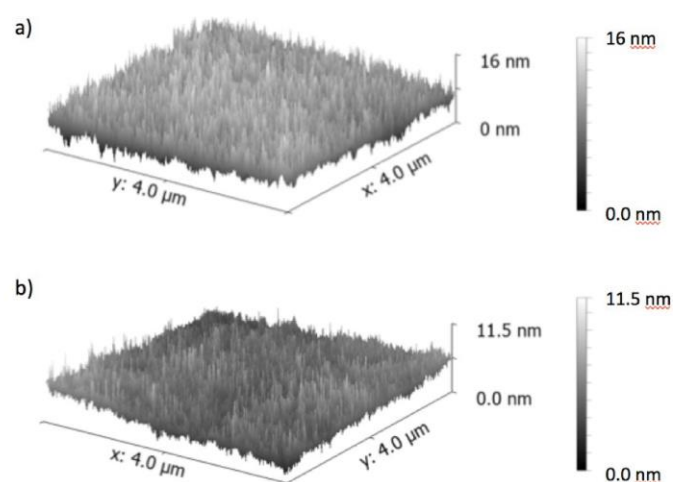


Fig. S8 AFM topography of HRI ink deposits (16 μm thick film) exposed (a) in ambient atmospheric conditions and (b) under mild vacuum.

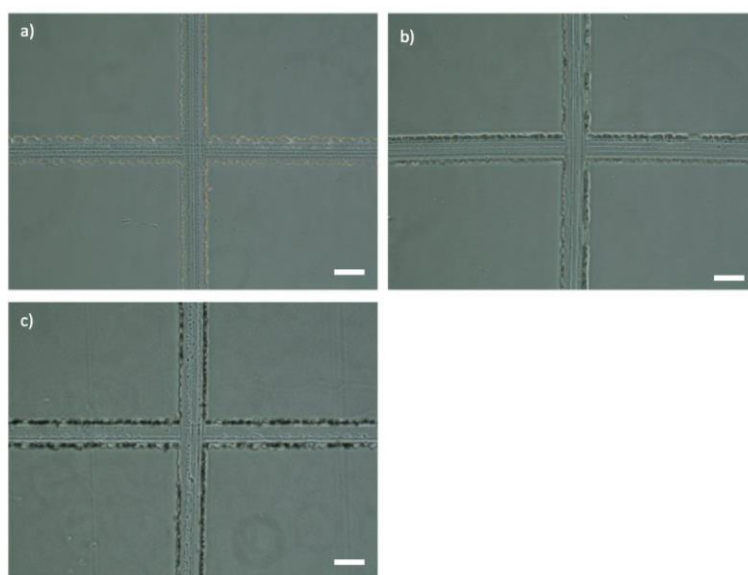


Fig. S9 Optical microscope images of cross-cut areas after the ASTM 3359 adhesion test for thin cured films deposited by inkjet. (a) Model ink film (thickness: 3.5 μm) and (b and c) HRI ink film (thickness: 4 μm) cured (b) in atmosphere and (c) under mild vacuum conditions.

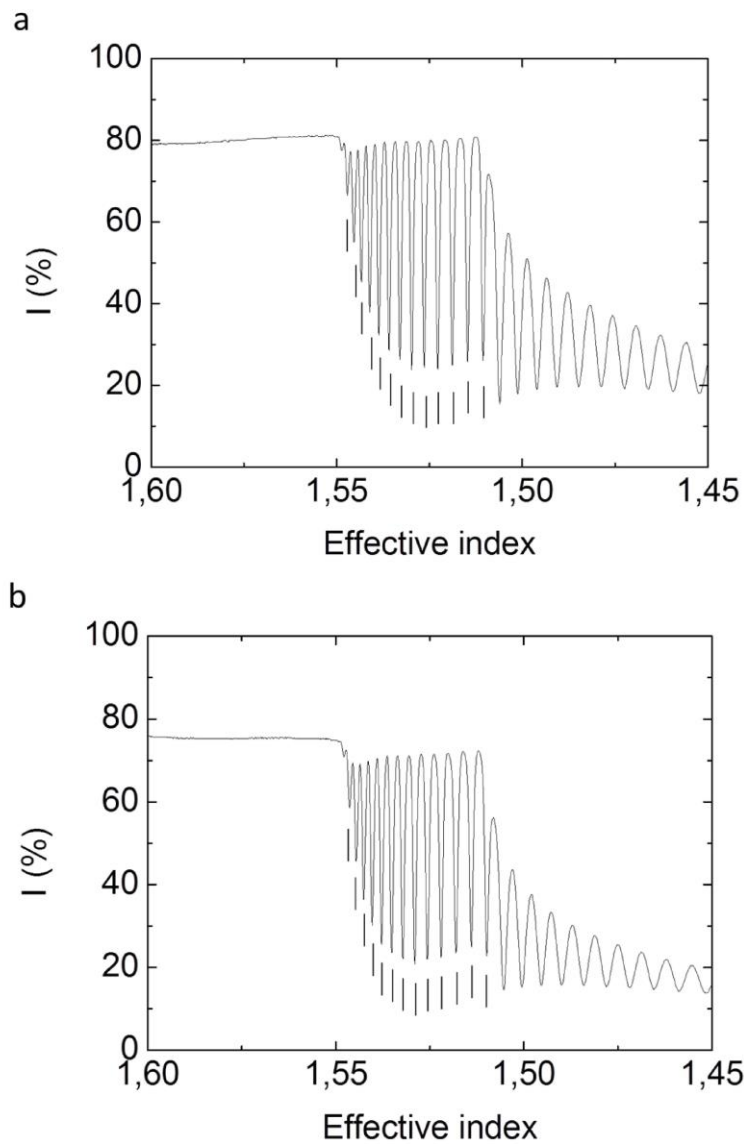


Fig. S10 (a) TE and (b) TM propagation modes (at 632.8 nm) for a HRI ink deposit (16 microns thick film) cured under mild vacuum conditions. Modes with effective refractive index higher than that of the substrate ($n_g = 1.514$), and fully supported by the inkjet printed film are indicated with a line.

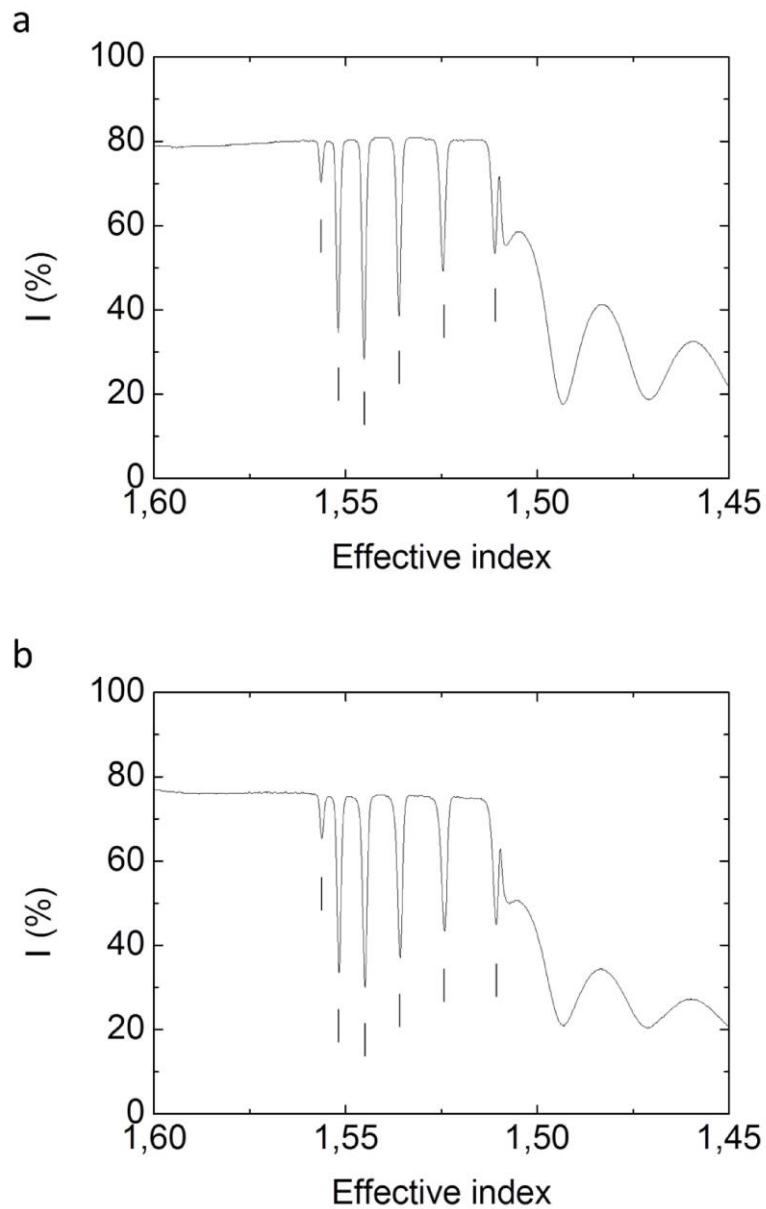


Fig. S11 (a) TE and (b) TM propagation modes (at 632.8 nm) for a HRI ink deposit cured in ambient atmosphere (4.4 μm thick film). Modes with effective refractive index higher than that of the substrate ($n_g = 1.514$), and fully supported by the inkjet printed film are indicated with a line.

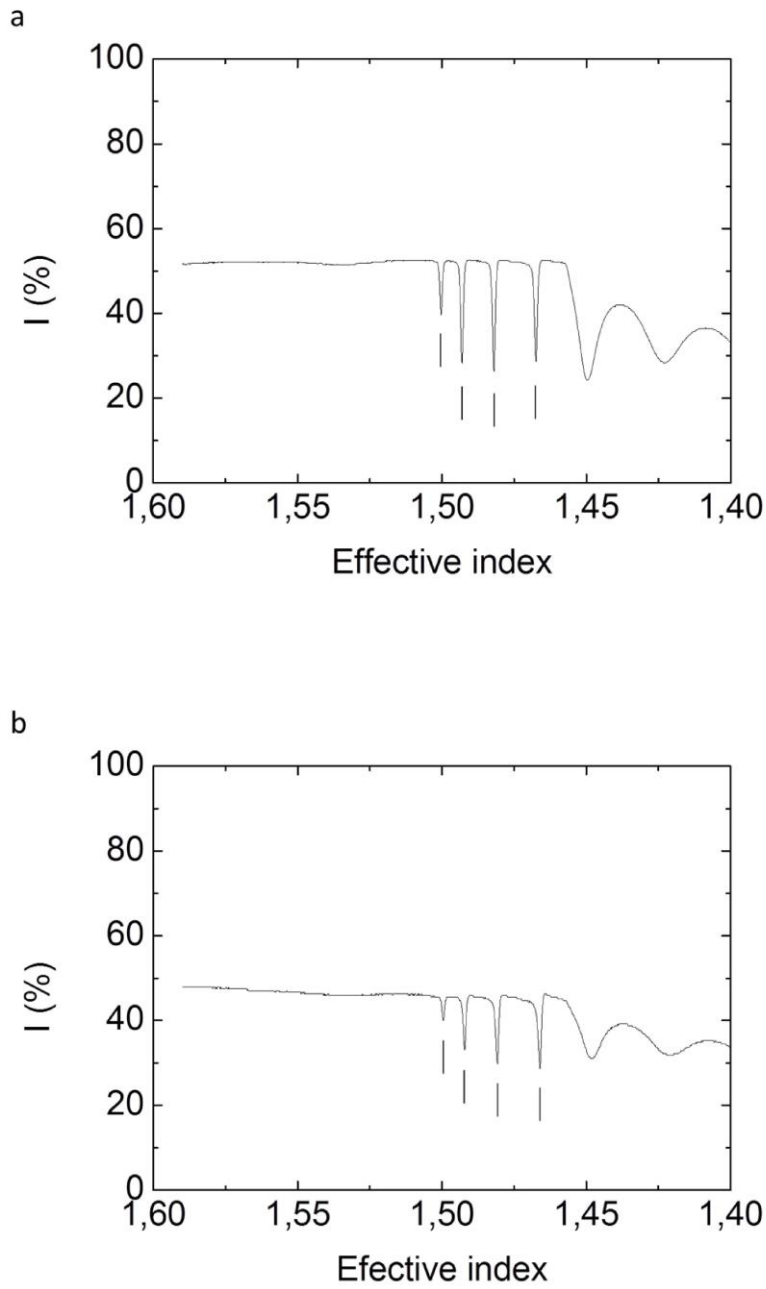
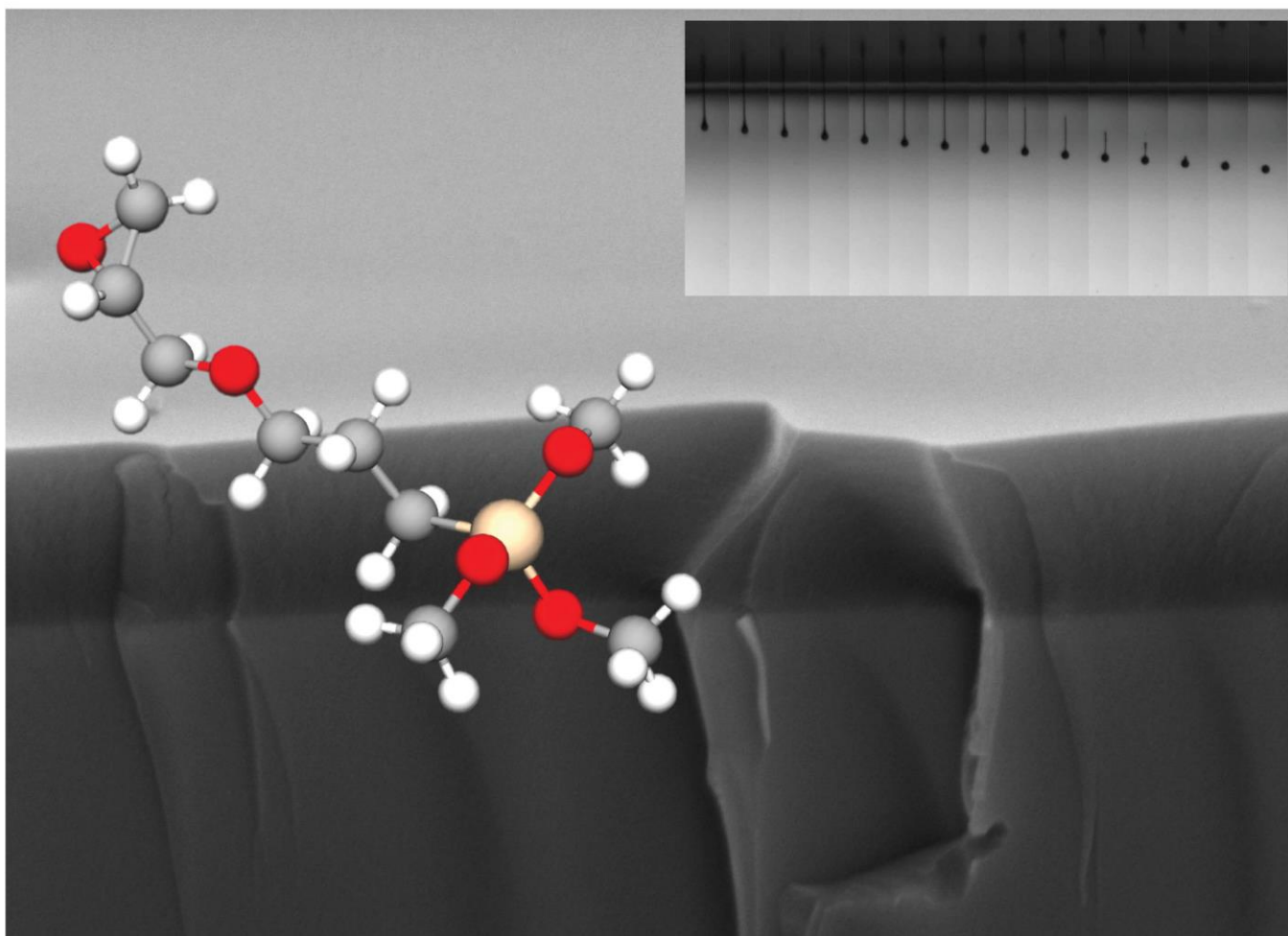


Fig. S12 (a) TE and (b) TM propagation modes (at 632.8 nm) for a Model ink deposit (3.4 μm thick film). Modes with effective refractive index higher than that of the substrate ($n_q = 1.457$), and fully supported by the inkjet printed film are indicated with a line.

Back Cover

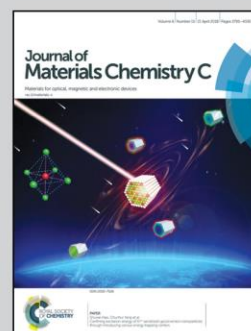


Showcasing research from the Advanced Manufacturing Laboratory at the Institute of Materials Science of Aragón.

Photoacid catalyzed organic–inorganic hybrid inks for the manufacturing of inkjet-printed photonic devices

Inkjet printing of photoacid catalyzed organic–inorganic hybrid formulations has been used for the digital manufacturing of low optical-loss photonic waveguides.

As featured in:



See Carlos Sánchez-Somolinos *et al.*,
J. Mater. Chem. C, 2018, 6, 3882.



rsc.li/materials-c

Registered charity number: 207890


3. Publication 3.

Journal: Polymers

Title: Digital Luminescence Patterning via Inkjet Printing of a Photoacid Catalysed Organic-Inorganic Hybrid Formulation

Article

Digital Luminescence Patterning via Inkjet Printing of a Photoacid Catalysed Organic-Inorganic Hybrid Formulation

Jorge Alaman^{1,2}, María López-Valdeolivas¹, Raquel Alicante¹, Jose Ignacio Peña³ and Carlos Sánchez-Somolinos^{1,4,*} 

¹ Departamento de Física de la Materia Condensada, Instituto de Ciencia de Materiales de Aragón (ICMA), CSIC-Universidad de Zaragoza, 50009 Zaragoza, Spain; jorge.alaman@bshg.com (J.A.); m_lopez@unizar.es (M.L.-V.); raquela@unizar.es (R.A.)

² BSH Electrodomésticos España, S.A., Polígono Industrial de PLA-ZA, Ronda del Canal Imperial de Aragón, 18-20, 50197 Zaragoza, Spain

³ Departamento de Ciencia y Tecnología de Materiales y Fluidos, Instituto de Ciencia de Materiales de Aragón (ICMA), CSIC-Universidad de Zaragoza, 50018 Zaragoza, Spain; jipena@unizar.es

⁴ CIBER in Bioengineering, Biomaterials and Nanomedicine (CIBER-BBN), C Mariano Esquillor s.n., 50018 Zaragoza, Spain

* Correspondence: carlos.s@csic.es; Tel.: +34-876-55-3770

Received: 15 February 2019; Accepted: 28 February 2019; Published: 6 March 2019



Abstract: Accurate positioning of luminescent materials at the microscale is essential for the further development of diverse application fields including optoelectronics, energy, biotechnology and anti-counterfeiting. In this respect, inkjet printing has recently attracted great interest due to its ability to precisely deposit with high throughput and no contact, functional materials on different types of substrates. Here, we present a novel photoacid catalysed organic-inorganic hybrid luminescent ink. The formulation, containing monomers bearing epoxy and silane functionalities, a photoacid generator and a small percentage of Rhodamine-B, shows good jetting properties and adequate wetting of the deposited droplets on the receiving substrates. Ultraviolet exposure of the deposited material triggers the cationic ring-opening polymerization reaction of the epoxy groups. Concomitantly, if atmospheric water is available, hydrolysis and condensation takes place, overall leading to a luminescent crosslinked hybrid organic-inorganic polymeric material obtained through a simple one-step curing process, without post baking steps. Advantageously, protection of the ink from actinic light delays the hydrolysis and condensation conferring long-term stability to the ink. Digital patterning leads to patterned emissive surfaces and elements with good adhesion to different substrates, mechanical and optical properties for the fabrication of optical and photonic elements and devices.

Keywords: organic-inorganic hybrid materials; highly crosslinked polymers; photoacid generators; UV-photopolymerization; inkjet printing; luminescent materials

1. Introduction

The development of luminescent systems is key for the further progress and expansion of a variety of application fields spanning from optoelectronics, solar energy harvesting and biotechnology to documents and goods anti-counterfeiting [1–7]. Light emissive centres typically used in these systems include organic fluorophores, organometallic luminescent molecules, rare earth ions or semiconductor quantum dots, many times incorporated in a solid matrix [8–14]. The selection of the type of luminescent entity and the host medium for each specific application responds to criteria of

emission efficiency, emission wavelength and stability against temperature and illumination conditions, among other requirements.

Inkjet printing has gained a lot of interest over the last years as a tool to create functional elements and devices [15–20] due to its ability to precisely deposit, with no contact, controlled-volume ink droplets on substrates of different nature, all this with high throughput despite being a serial process. In particular inkjet has been explored to generate luminescent patterns. Inks explored for this purpose need to incorporate luminescent entities, such as emissive chromophores or nanoparticles [21–28]. As inkjet is an additive printing method, all the deposited material, except for the solvents, is employed in the final device thus making an optimum use of these precious luminescent additives. Besides this, multiple materials can be sequentially added, enabling the integration of different functional elements and layers in the same device. This is of great potential for example in the formation of pixels in OLED displays, the preparation of sensor bioarrays or the printing of multifunctional security feature elements for documents and goods protection [29–32]. The development and optimization of inks require multiple variables to be considered [30,31]. As an example, appropriate ink viscosity and surface tension are critical to ensure jettability. Besides, adequate interaction between the ink and the target substrate is also needed to have well-defined prints. Many advanced applications require the precise microdeposition of the functional material onto a nonporous substrate [32–36]. Drying of the solvent usually leads to a concentration of the solid at the drop edge through the so called coffee ring effect, a phenomenon that can be, to a large extent, inhibited by a judicious selection of solvents [37,38]. Another approach to circumvent this problem is the use of phase change inks that quickly solidify after impact. Similarly, UV reactive inks, once deposited, can be fixed through polymerization when exposed to actinic light [36,37,39]. This last approach has been employed in the preparation of luminescent inks comprising acrylate or epoxy monomers together with emitting chromophores. After deposition, these are fixed through a light induced reaction leading to an organic polymeric material showing luminescent properties [21,24,40].

Besides these organic based matrix systems, hybrid materials encompass advantages from both, organic and inorganic materials [41]. Hybrid systems show good processability at low temperatures, by means of different patterning techniques. Additionally the final systems typically present good optical quality, tunability of their properties via the selection of proper monomers and their proportions, as well as excellent mechanical properties and adhesion to different types of substrates [42–45]. Additionally the inclusion of luminescent centres in hybrid hosts usually lead to more efficient emission as well as thermal and environmental stability of the light emitting entities [45]. Despite all these advantages, the inclusion of the luminescent functionality in hybrid formulations for inkjet has been scarcely studied and the preparation of luminescent curable hybrid systems that can be directly fixed after deposition remains nearly unexplored. As one of the few examples, the group of Valiyaveetil has recently demonstrated inkjet printing of thermally curable inks based on the polydimethylsiloxane elastomer kit Sylgard 184[®] (Dow Corning Corporation, Midland, MI, USA) with luminescent silica nanoparticles dispersed on it [46]. In another example a sol-gel derived YAG:Er³⁺ precursor is used to generate, through inkjet printing, fine line patterns that, after firing of the samples, lead to miniaturized scintillators [47].

Recently we have demonstrated that photoacid catalysed formulations containing monomers with epoxy and silane functionalities are suitable systems for the preparation of inks with long-term stability leading, after printing and curing, to deposits with excellent optical and mechanical properties [48]. When compared to other sol-gel methods, this approach is a solvent-free process starting with the low molecular weight monomers that advantageously enable the preparation of formulations with appropriate viscosity for inkjet. The use of suitable photoinitiators in the formulation, allows to concomitantly cure the organic and inorganic network by irradiating with UV light [49–51]. The process is carried out at room temperature (RT) without the need of post baking steps. Additionally, in this approach, in comparison to conventional hybrid inks containing prehydrolysed–condensed reactive inorganic precursors [52,53], the hydrolysis and condensation beneficially takes place after the printing

step, when the sample is irradiated with UV light. This favours the long-term stability of the ink properties (e.g., viscosity) needed to preserve its jettability and therefore its applicability in industrial applications. To further explore the potential of this polymerization reaction in the preparation of photocurable functional formulations for inkjet, we have incorporated the luminescent functionality in these reactive systems. Here we report a new light emitting, jettable, solvent-free ink, based on a photoacid catalysed organic-inorganic hybrid formulation, containing monomers with epoxy and silane functionalities and a luminescent dye. Rhodamine B, which has been successfully integrated in other hybrid matrices, has been chosen here as light emissive moiety [54–60]. After deposition, UV irradiation of the inks leads to the cationic ring-opening polymerization of epoxy functionalities and the hydrolysis and condensation of silanes. The resulting cured material presents excellent adhesion to glass and good mechanical properties without any further postprocessing step. Luminescent properties of the deposited materials after curing have been characterized too. To further leverage the potential of these photocurable systems, the use of this luminescent ink in the preparation of light emissive digital patterns on substrates of different nature has also been explored.

2. Materials and Methods

2.1. Materials

The chemical structure of the molecules employed for the ink preparation is presented in Scheme S1 in the Supplementary Information. 3-Glycidoxypropyltrimethoxysilane (GPTMS), a hybrid organic-inorganic molecule provided with an epoxy and a trialkoxysilane, was acquired from Alfa Aesar (Haverhill, MA, USA). GPTMS is a low viscosity liquid at RT. The polymeric epoxy resin Epikote 157, that is a monomer having an average of eight aromatic benzene rings and eight epoxide groups, was purchased from Momentive (Waterford, NY, USA). Epikote 157 appears as flakes at RT. Dimethoxydiphenylsilane (dPDMS) is a liquid disilane monomer bearing two aromatic rings, from Aldrich. As a photoacid generator (PAG), triarylsulfonium hexafluorophosphate salts (50% in propylene carbonate), acquired from Aldrich (Madrid, Spain), were used. This compound, when excited with UV actinic light, triggers the polymerization of the organic epoxide groups and, concurrently, act as a catalyst for the hydrolysis and condensation of the alkoxides. To regulate the surface tension of the ink, BYK-333 (BYK Chemie), a polyether-modified polydimethylsiloxane that also improves the surface wetting, was employed. To provide the ink with luminescent properties, 2-[6-(diethylamino)-3-(diethylimino)-3H-xanthen-9-yl] benzoic acid, usually known as Rhodamine B, was added to the formulation. Rhodamine B was purchased from Lambda Physic (Santa Clara, CA, USA), under the reference Lambdachrome LC6100. All the materials were used as received.

2.2. Experimental Procedures

2.2.1. Ink Preparation

Photocurable luminescent formulations were prepared by directly mixing the above mentioned materials in the corresponding percentages. To facilitate homogenization, Epikote 157 was thoroughly grinded previously to its addition to the mixture. The mixtures were stirred at RT using a magnetic stirrer at 600 rpm until a homogeneous formulation was obtained.

2.2.2. Substrates and Cleaning Procedure

Conventional microscope glass slides were employed as substrates. A pre-cleaning of these substrates was carried out using a solution of soapy water by gently hand rubbing the surface, using nitrile gloves. After thoroughly rinsing the substrates with water, they were introduced in an ultrasonic bath with soapy water for 10 min. After this, the substrates were refluxed with milli-Q water and ultrasonicated again in milli-Q water for 10 min. After cleaning with water, the substrates were refluxed with isopropyl alcohol (IPA) and a third ultrasonic bath was carried out, in this case with

IPA for 10 min. Finally, the glass substrates were immediately dried with compressed air and stored until their use. Cyclic olefin polymer (COP) from Zeonor (188 μm thick polymer foil and microscope slides), uncoated poly(ethylene terephthalate) (PET) film as well as indium tin oxide (ITO) coated PET (220 μm thick polymer foil) from Aldrich were used as thermoplastic substrates for demonstrators. All these plastic substrates are provided with a protective foil that is removed just before printing.

2.2.3. Substrate Treatments

UV Ozone treatment was performed on a UV-ozone reactor UVO 342 (Jelight company Inc., Irvine, CA, USA) to remove any remaining organic contamination of glass [61]. In some of the samples, a Pyrosil treatment (Pyrosil[®], SURA, Jena, Germany), consisting in a combustion chemical vapor deposition (CCVD), was also carried out for the activation of the surfaces. An organosilicon precursor is injected into a gas flame that is put in short contact with the substrate, leading to a SiO₂-like coating with thickness typically below 50–100 nm. As a result, important changes in wettability and adhesion are obtained [62].

2.2.4. Inkjet Printing

For the inkjet printing a custom-made inkjet printer system was used (In-2 Printing Solutions, Navarra, Spain) with Xaar-126/80 piezoelectric printheads (Xaar, Cambridge, UK). These printheads have 126 nozzles (50 μm diameter) arranged in a line with a pitch of 137 μm . The line of nozzles is perpendicular to the direction of the substrate motion, that moves under the fixed printhead. As a result, the vertical resolution (in the direction of the line of nozzles) is 185 dots per inch (dpi). The horizontal resolution (in the direction of the substrate movement) depends on different factors such as firing frequency and relative speed of the substrate with the printhead. The printhead is commanded by the Xaar XUSB drive electronics that is controlled with a PC and its corresponding software (from Xaar, Cambridge, UK). This software enables a precise control of the parameters that command the printhead, detection of the samples and definition of the patterns to be printed (bitmap file). The movement of the substrate while printing takes usually place at constant speed of 20 mm/s by using an eTrack linear stage from Newmark systems Inc. (Mission Viejo, CA, USA) commanded by IMS-Terminal software (Marlborough, MA, USA). The printhead is mounted in a metallic block, provided with a heater and thermocouple connected to a temperature relay that regulates the temperature of the printhead at the desired set point.

2.2.5. UV-Curing Fixation

An UV lamp Exfo OmniCure S2000 UV (Gentec, Nivelles, Belgium) has been used with an UV bandpass filter (wavelength range of 320–390 nm). To cure the films, a power of 10 mW/cm² was applied during 5 min. Curing was carried out at RT (26 °C) either in an ambient atmosphere, with a relative humidity between 30% and 40% or under mild vacuum conditions. In this last case, the samples were cured inside a chamber provided with an optical access. A mild vacuum (100 mBar) can be attained inside the chamber by using a vacuum pump. Once the desired pressure level is achieved, UV exposure is immediately carried out to minimize evaporation of the deposited ink components.

2.3. Characterization

2.3.1. Ink Properties Characterization

Viscosity of the ink was measured by using a Haake Rheostress 1 rotational Rheometer from Thermo Scientific, (Waltham, MA, USA). Surface tension was characterized using the pendant droplet method in an Attension Goniometer Theta Lite. The given surface tension values are the result of an average of three independent measurements. Density measurements were carried out using a 10 mL pycnometer.

2.3.2. Flying Droplet Characterization

Together with the printing system, a home-built dropwatcher was employed for the analysis of the characteristics of the ejected drops. This allows the characterization and optimization of the printing system configuration, especially parameters that fix the voltage sent to the printhead piezoelectric elements and so optimize the final drop characteristics. This visualization system consists on a CCD camera, a strobe led device and a pulse generator to synchronize the signal of the printhead, the strobe light and the camera acquisition events.

2.3.3. Deposited Ink and Film Characterization

Fourier Transform Infrared (FTIR) Spectroscopy was performed using a Perkin Elmer Spectrum 100 with ATR accessory. For FTIR spectra, thin films of the formulation were applied using a Meyer Rod bar nominally providing a wet film thickness of 24 μm . FTIR spectra were measured between 4000–450 cm^{-1} . UV-Vis absorption measurements of the solutions and the films were carried out using a VARIAN Cary-500 spectrophotometer. Luminescent properties of the deposited films (emission and excitation spectra) were characterized using a Perkin Elmer LS50B spectrometer. Optical microscope images of the deposited drops were taken using an optical microscope OLYMPUS Eclipse i80. A Field-Emission Scanning electron microscope (FE-SEM) Merlin Carl Zeiss (Oberkochen, Germany) was used to study the morphology of the films. Hardness and elastic module of the films were measured by nanoindentation, using a Nanoindenter G200 from Agilent Technologies (Santa Clara, CA, USA) equipped with a Vickers indenter tip. Values were calculated on the basis of 4 indentations in 2 identical samples. Adhesion of the cured films to the glass substrate was characterized using a cross-cut and tape test according to the ASTM D3359 standard method [63]. First, using a standard cutter with 6 blades and 1 mm of separation between each one (Neurtek), a cross hatch is done, creating a 6×6 pattern. After that, a normalized adhesion tape (Tesa 4024) is applied over the crosscut pattern and quickly removed at an angle of 180° . The adhesion strength is categorized by visually assessing the amount of deposit removed from 5B (strongest adhesion/no film removal) to 0B (weakest adhesion/complete film removal). Adhesion experiments were reproduced in 3 samples for this adhesion assessment. Thickness characterization of the deposited layers was carried out using a Bruker Dektak XT Stylus Profiler.

3. Results and Discussion

3.1. Ink Formulation

The luminescent ink presented in this paper, named HRI-RhodB-02, takes as basis the work previously developed in our group on photoacid catalysed organic-inorganic hybrid inks for the preparation of photonic waveguides [48]. The hybrid organic-inorganic compound GPTMS is taken as main component (50 wt %), mixed with two monomers in the following proportions: 25 wt % of Epikote 157 and 25 wt % of dPDMS. Epikote 157 is expected to polymerize with the organic part of GPTMS through its epoxy rings, while dPDMS will react with the inorganic network. Apart from this, 0.05 wt % of BYK-333 was added to control the surface tension of the ink and to improve its wetting to the substrate [49]. Additionally, 2 wt % of triarylsulfonium hexafluorophosphate salt is incorporated as photoacid generator to initiate the sol-gel and epoxy groups polymerization processes of the deposited ink when irradiated with UV light. Our luminescent hybrid formulation includes Rhodamine B, a luminescent chromophore that has been previously incorporated in hybrid organic-inorganic systems [54–60]. A 0.2 wt % of Rhodamine B was added to incorporate the luminescence functionality to the ink.

3.2. Inkjet Printing

As mentioned, inkjet printing requires a highly precise control of the rheology of the ink as well as the jetting process itself. The overall process as well as the theoretical laws, based on non-dimensional

numbers, that drive ink jetting and drop formation, have been thoroughly described in the literature [30,31]. These non-dimensional numbers, Reynolds (Re), Weber (We) and Ohnesorge (Oh), given by the following equations, overall describe the behaviour of the ink droplets according to their inertial forces, viscosity, kinetics and surface energy.

$$\text{Re} = \frac{v\rho a}{\eta} \quad (1)$$

$$\text{We} = \frac{v^2\rho a}{\gamma} \quad (2)$$

$$\text{Oh} = \frac{\sqrt{\text{We}}}{\text{Re}} = \frac{\eta}{\sqrt{\gamma\rho a}} \quad (3)$$

where v is the speed of the ink when it is leaving the nozzle, η is the viscosity, γ the surface tension, ρ the density and a the diameter of the printhead orifice. This theoretical framework enables to rationally understand and predict to some extent the proper jettability and deposition of the ink. Trying to gain insight in this respect for the formulated luminescent ink, its relevant properties have been characterized and these non-dimensional numbers have been calculated. Assuming that the surface tension does not significantly change in the small range from RT (26 °C) to the printhead operation temperature (32 °C), the value measured at RT, 25.9 mN/m, was taken for the calculations of the We and Oh numbers. On the other hand, density and viscosity, with a strong dependence on temperature, were measured at 32 °C, obtaining values of 1.1 g/cm³ and 28.5 mPas respectively.

Surface tension, viscosity and density are intrinsic values of the ink however drop velocity, that has a direct influence in We and Re numbers, depends on the printing configuration. The signal sent by the electronics of the printer, which is derived to the piezoelectric actuators of the printhead, is a critical variable that will determine the behaviour of the ink when jetting. Observation of the ink drops being ejected from the printhead nozzles by using a Dropwatcher system, enables the optimization of the voltage signal to obtain a good printability. Too low voltage can derive in the absence of printing as not enough energy is delivered to the fluid to generate a jet. On the other hand, too high voltages can cause the formation of satellites that result in inaccurate printing (Figure S1 in the Supporting information).

Figure 1a shows luminescent ink droplets ejected, in an optimized configuration, at different delay time with respect the piezoelectric actuation: An ink jet leaves the nozzle after piezo actuation. The ink filament after the leading jet front becomes narrower on time until it breaks. The tail following the main part of the flying ink drop is then retracted towards this, finally leading to a spherical drop of ink. The presence in the formulation of chain like polymeric molecules (BYK-333) favours the retraction of the tail that forms after jet rupture, toward the ink flying drop, minimizing the formation of satellite droplets [64,65]. Speed of the droplets can also be characterized by taking a picture of the same droplet at two different times using a double strobe configuration in our dropwatcher system. Average speed is estimated by taking the ratio of the flying distance and the time difference between light pulses. Figure S2 in the Supporting information shows a double strobe image of a set of luminescent ink drops with a temporal delay of 50 μs between light pulses. Through the analysis of the image, the drop velocity was estimated to be 2.5 m/s assuming no deceleration takes place in this short distance.

Taking the values above for viscosity, surface tension and density of the ink, speed of the droplet and the diameter of nozzle as 50 μm, (as provided by the printhead manufacturer), the Reynolds, Weber and Ohnesorge numbers were calculated, giving 4.83, 13.4 and 0.75 respectively. These values are within the range that is typically defined for inkjet printable materials [30,31,66–69] and remarkably this is achieved using a solvent-free ink. The low molecular weight monomers, precursor components for the final deposit, enable the preparation of tailored formulations with appropriate properties for inkjet printing. Apart from the jettability, the luminescent ink presents good stability when stored in a closed amber flask protected from the UV light. Storage over periods longer than 4 months did not significantly change the optimum printing parameters.

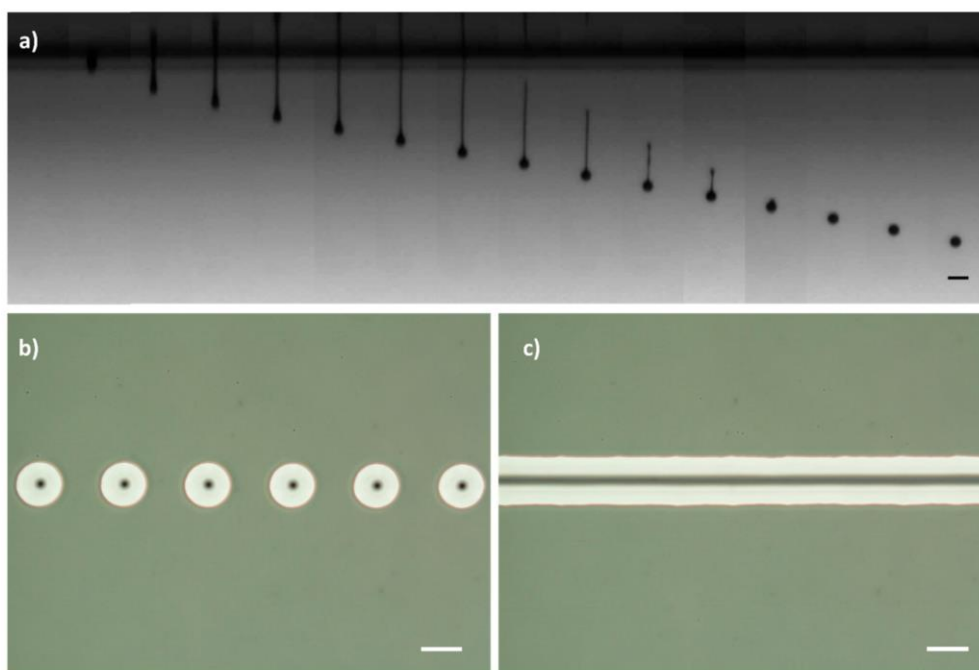


Figure 1. (a) Temporal sequence of photographs (from left to right) showing the drop formation process for the luminescent ink. The time interval between two adjacent frames is $20 \mu\text{s}$ (scale bar: $100 \mu\text{m}$). (b,c) Phase contrast microscope images of the inkjet-printed drops of luminescent ink deposited along a line in an ozone treated glass substrate at different dpi (scale bar: $100 \mu\text{m}$): (b) 120 dpi and (c) 360 dpi.

In order to take advantage of the printing technology and deposit well-defined luminescent patterns, it is also necessary to control the interaction between the flying ink droplet and the receiving substrate. Due to the hybrid nature of our ink and the glass substrate initially used, specific cleaning protocols have been used to improve the wettability on glass, allowing the appropriate deposition of the ink drops and to promote the reaction of the functional groups of the ink monomers to the glass surface. Substrate treatment using UV-Ozone eliminates organic contaminants at the surface and leave the silanol groups exposed at the glass surface. These will afterwards react with the forming hydroxyl groups of the silanes, generated after UV exposure of the ink [61].

Over the ozone-treated surface, drops have been printed at different spacing between drops, that is, at different dots per inch (dpi). In Figure 1b, with 120 dpi, each droplet is isolated after deposition, presenting a circular shape and monodisperse size giving an indication of the reproducibility of the jetting and deposition process). If the space between drops is reduced (increasing to 360 dpi), as shown in Figure 1c, drops coalesce, leading to continuous, well-defined lines of ink on the substrate.

Besides lines, preparation of homogeneous and continuous deposits requires a similar strategy, printing contiguous droplets that coalesce in both axis into well-defined areas. In contrast to UV-Ozone activation that easily leads to dewetted regions and faulty printing, CCVD using Pyrosil[®] treatment was used in the search of these continuous printed regions. Through this CCVD process, a silanol porous nanolayer is created in the surface (see SEM image in Figure S3 in the Supporting information), prior to the deposition of the ink, which favours wetting. Printing on these treated surfaces with suitable dots density (e.g., 360 dpi in the substrate moving direction), led to homogenous films with uniform thickness ($\sim 4 \mu\text{m}$).

3.3. Photocuring process

The effect of UV light exposure of the formulation including the luminescent dye has been studied. A thin film of luminescent HRI-RhodB-02 ink was formed between two quartz plates with a fixed gap in between (determined by the presence of spacers of fixed diameter spheres). The exact gap of the quartz cell before filling the cell with the photocurable ink was determined by interferometry, being 11 μm . Once filled by capillary action, UV-Vis absorption of the liquid thin layer was measured. The spectrum (Figure S4a in the Supporting information) shows two well-differentiated absorption peaks: First, at around 300 nm, which is assigned to the maximum absorption band of the photoacid generator (see Figure S4b of the photocurable ink without dye in the Supporting information) and a second one, at around 560 nm, corresponding to the maximum of the absorption band of the Rhodamine B dye. This dye, previously incorporated in hybrid materials, was selected due to its compatibility and solubility with the rest of components of the ink, as well as its little absorption in the UV region [70] where the photoinitiator strongly absorbs actinic radiation needed to initiate the photopolymerization reaction. Exposure of the liquid layer of our luminescent formulation to UV light irradiation (320–390 nm, 10 mW/cm², 300 s) leads to a decrease of the absorption band in this UV region of the spectra, a change that is ascribed to the photoinitiator decomposition (Figure S4a in the Supporting information). A slight increase in the absorption is observed for the Rhodamine B band at 560 nm after UV exposure. Polymerization taking place in the host material can be responsible of this change in the absorption spectrum as previously reported in hybrid rhodamine B containing systems [60].

Macroscopically, the UV irradiation of a liquid film of photocurable formulation immediately leads to a solid layer indicating that polymerization has efficiently taken place. As mentioned, decomposition of the photoinitiator leads to acid generation that can trigger the epoxy ring-opening cationic photopolymerization as well as the photoacid-catalysed sol-gel process as described elsewhere (see Schemes S2 and S3 in the Supporting information) [48]. To study more in detail this polymerization process, FTIR spectroscopic characterization was carried out. Figure 2 shows the FTIR spectra of the HRI-RhodB-02 luminescent formulation before UV exposure and 10 min after exposure under atmospheric curing conditions. On one hand, the appearance of a broad band at 3400 cm⁻¹, which is assigned to the vibration of the OH group in the Si-OH bond, indicates that the hydrolysis reaction has efficiently taken place [71]. Besides, the narrow band at 1080 cm⁻¹, observed in the uncured material and corresponding to the stretching vibration assigned to the Si-O-CH₃ group, is substituted in the cured material by a complex multipeak band, wider than the original, with maxima in the 1000–1080 cm⁻¹ region, which is attributed to the stretching vibrations of the siloxane Si-O-Si bonds. All these observations confirm that the condensation reaction that leads to the inorganic network has already taken place. On the other hand, the C-H stretching band of the epoxide at 3050 cm⁻¹ diminished just after (10 min. after) UV irradiation (inset Figure 2) indicating that the epoxy ring-opening reaction has taken place forming the organic polymer [72]. Despite the reaction progression, this band did not completely disappear after UV exposure. This could be ascribed to the increase of the viscosity of the system due to polymerization. As the reaction progresses the diffusion of the photoacid generator and the monomers is more and more limited thus favouring the presence of unreacted epoxy groups [73]. This was further supported by the fact that an homologous model luminescent formulation comprising GPTMS as only reactive monomer, thus eliminating the DPDMS and EPIKOTE157 crosslinkers, showed complete depletion of the C-H stretching band of the epoxide at 3050 cm⁻¹, 10 min. after UV irradiation (see Figure S5 and detailed composition of this model formulation in the Supporting information). The lower crosslinking density in this model system allows better monomer diffusion to complete the epoxy polymerization reaction.

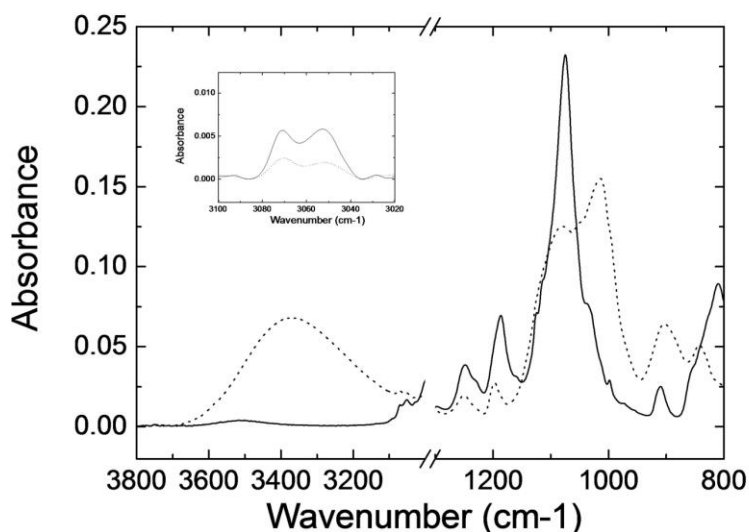


Figure 2. FTIR spectra of the HRI-RhodB-02 luminescent ink before (continuous line) and 10 min after UV exposure (dotted line) under atmospheric conditions. Inset shows the band of the epoxide at 3050 cm^{-1} corrected by using a linear baseline.

FTIR spectra of films of the cured photopolymerizable ink were recorded 10 min and 24 h after the irradiation to assess the evolution of the system in darkness (Figure S6 in the Supporting information). Small differences in the $1000\text{--}1080\text{ cm}^{-1}$ region were appreciated between the spectra at 10 min and 24 h, indicating that hydrolysis and condensation have significantly taken place right after the first 10 min for samples cured under these ambient atmospheric conditions. The spectra do not qualitatively evolve after 24 h, as followed over one month. Overall it can be concluded that the presence of this percentage of this luminescent dye (0.2 wt %) in the ink does not preclude the photoreaction to proceed. As in previously studied systems, without the luminescent dye, the two polymerization processes, cationic ring-opening polymerization of the epoxide groups and the hydrolysis and condensation of the silanes, take place simultaneously after the light excitation of the photoacid generator.

Figure 3a,b shows SEM microscopy images of droplets deposited under optimum jetting conditions and cured in ambient atmosphere (at $26\text{ }^{\circ}\text{C}$ and relative humidity between 30%–40%). The SEM morphology of deposited ink droplets presents inhomogeneous structures in the surface after curing, indicating phase segregation [48]. This effect appears during the curing process in these hybrids multicomponent inks and can be due to the different kinetics of the organic and inorganic parts during their polymerization. The presence of atmospheric water, needed for the hydrolysis step, causes acceleration in the formation of the inorganic network, while the influence of water presence in the cationic ring-opening polymerization reaction of the organic network is less pronounced [74]. This can be used to adjust the relative polymerization rates of the two networks. To avoid this phenomenon, the luminescent ink has been exposed to UV light irradiation at mild vacuum conditions (100 mBar), reducing the amount of available atmospheric water. Figure 3c,d shows SEM microscopy images of isolated deposited droplets cured under these mild vacuum conditions. The cured droplets present a homogeneous, scattering-free, surface morphology. In this last case, due to the reduction of the humidity in the atmosphere, both organic and inorganic network could progress uniformly without phase segregation, leading to a smooth surface of the cured droplet. FTIR experiments were also carried out on a sample cured under mild vacuum conditions to reduce the water content. The spectrum taken 24 h after UV irradiation (Figure S7 in the Supporting information) in this sample did not qualitatively differ from the one taken in a homologous sample cured in ambient atmospheric conditions despite the important differences in morphology. In all cases, regardless of the curing atmosphere, no evolution of

the FTIR spectrum was observed for periods of time longer than 24 h and therefore all the films in this work were allowed to evolve in darkness for at least 24 h before any subsequent characterization to ensure completion of the polymerization process.

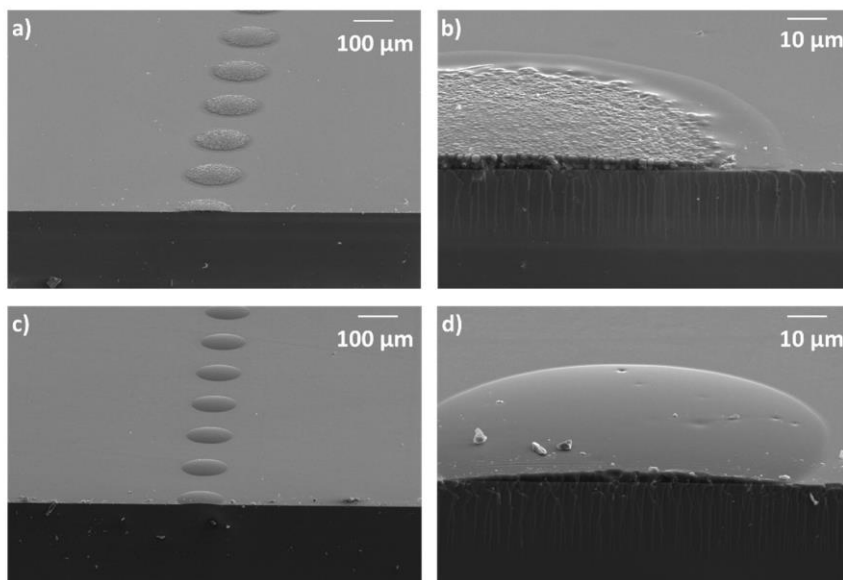


Figure 3. SEM morphology observed at different magnifications of (a) isolated inkjet-printed droplets and (b) fractured cross section of one droplet, cured in ambient atmospheric conditions. SEM morphology observed at different magnifications of (c) isolated inkjet-printed droplets and (d) fractured cross section of one droplet, cured under mild vacuum conditions (100 mBar).

For subsequent studies, we focused in the curing conditions under mild vacuum, leading to non-segregated morphology and therefore homogenous and scattering-free printed elements more suitable for optical applications. The hardness and Young modulus, determined by nanoindentation in 4 μm thick films, were 0.26 and 4.3 GPa, respectively. These values are similar to those measured for homologous deposits without the luminescent dye [48]. Excellent adhesion to the substrate was also found for the cured luminescent ink as can already be anticipated from the SEM images of the fractured cured isolated drops (Figure 3). To assess the adhesion of the cured ink to the glass substrate, a cross-cut and tape test according to the standard ASTM 3359 was carried out. The samples were evaluated in detail with optical microscope after cross cutting the films and removing the tape. As can be seen in Figure S8 in the Supporting information, the cross cut areas do not show significant damages and only slightly detached flakes can be appreciated where the blade has passed, however delamination is below 5% of the affected area resulting in a classification of 4B-5B binding strength according to the defined standard.

3.4. Luminescent Properties of the Printed Films

Deposits of luminescent ink with homogeneous thickness were prepared using the previously described process (inkjet-printed film cured under mild vacuum conditions) and their optical properties were analysed afterwards. Photoluminescence emission and excitation spectra were measured and are shown in Figure 4. It can be seen that the maximum of the excitation spectrum is reached at 562 nm that coincides with the maximum of the absorption spectrum (Figure S4 in the Supporting information). The maximum of emission is red-shifted to 585 nm. These optical properties are given by the excitation of Rhodamine-B dye as the rest of the matrix components present no light absorption in this wavelength range [48].

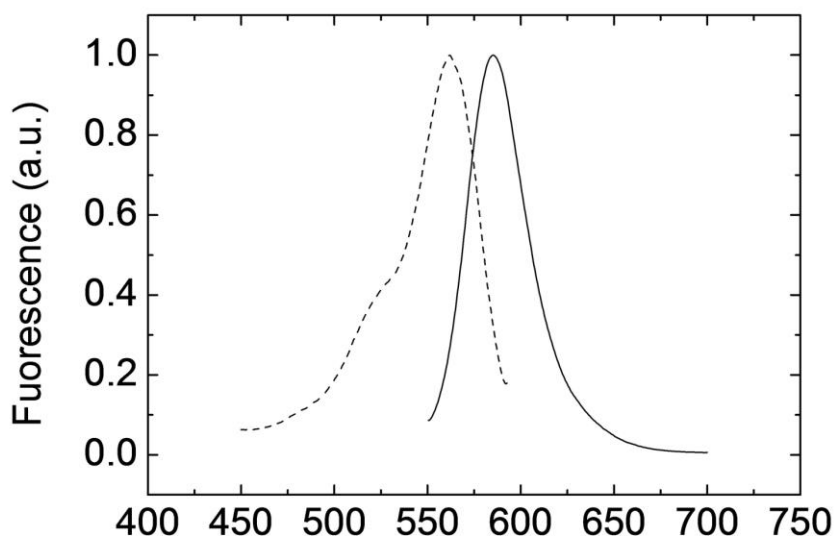


Figure 4. Photoluminescence emission (continuous line) and excitation (dashed line) spectra of deposited films of HRI-RhodB-02 cured at mild vacuum. Photoluminescence emission spectrum is taken with excitation at 530 nm and excitation spectrum is measured at 610 nm.

3.5. Digital Patterning on Different Substrates

Fine control of the spatial positioning provided by inkjet printing enables the preparation of well-defined luminescent patterns, such as the marks or the QR codes shown in Figure 5. Besides the printing of luminescent patterns on glass (Figure 5a), the ink has also been applied on top of thermoplastic substrates such as COP, a material typically used in the preparation of microfluidic devices [75] to put in value the versatility of these photoacid catalysed systems. As an example, Figure 5b shows a print of luminescent ink on top of a rigid COP microscope slide. Printing has also been performed on top of flexible substrates. Figure 5c shows an image printed with the luminescent ink on top of a flexible PET foil coated with ITO. Figure 5d presents a luminescent QR code printed on a flexible COP foil. The orange emitted light from this QR code, when excited with green light, can be immediately recognized by standard QR code recognition software of a conventional mobile phone (Camera app from iPhone 8 by Apple, iOS 12.1.4). Reading of the code is done through a long-pass red filter (Cut-On Wavelength: 600 nm) to ensure that the emitted light is use for code recognition. Neither detachment, nor cracking of the luminescent marks was observed against sample bending, as shown in Figure 5c,d, demonstrating good mechanical stability of the deposited marks also on these flexible substrates. All these demonstrators prove the versatility of these luminescent organic-inorganic single-step curing inks to generate well-defined luminescent functional marks on a variety of industrially relevant substrates.

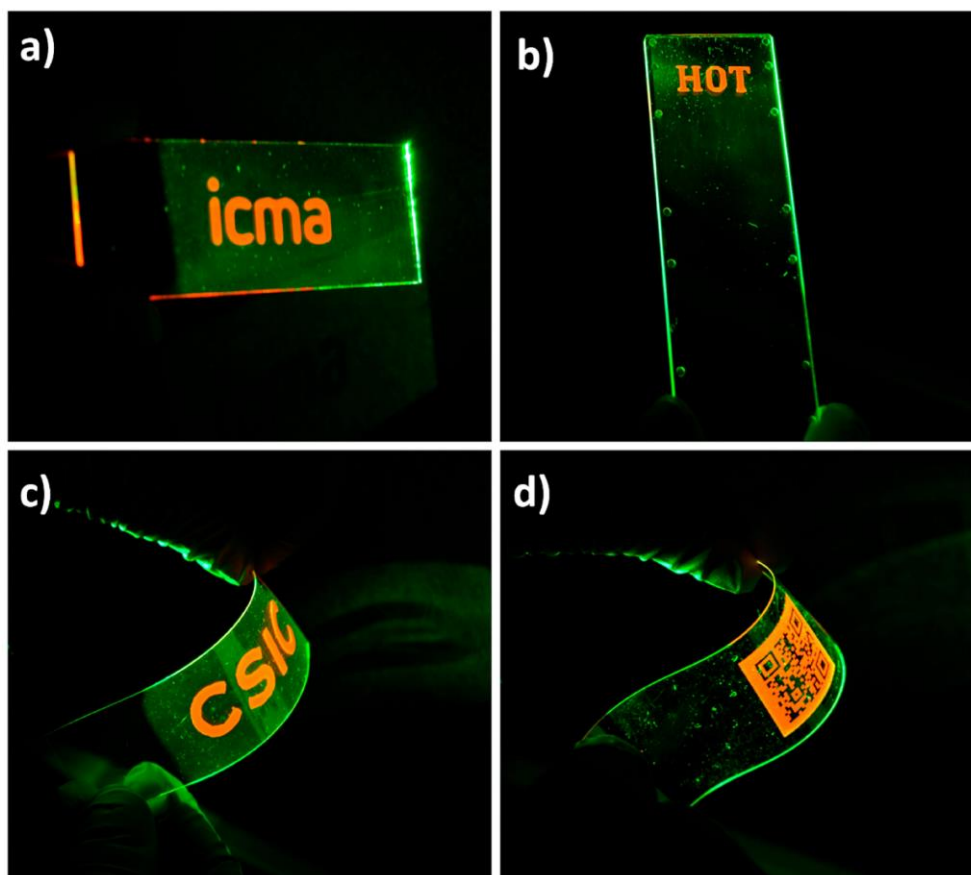


Figure 5. Luminescent prints on different substrates (7.5 cm × 2.5 cm) shown under green light excitation. Luminescent marks on (a) glass, (b) rigid COP and (c) flexible ITO coated PET. (d) Luminescent QR code printed on flexible COP.

4. Conclusions

A luminescent ink based on photoacid catalysed organic-inorganic hybrid formulations has been prepared. The incorporation of a small percentage of Rhodamine-B in photopolymerizable formulations containing monomers with epoxy and silane functionalities as well as photoacid generators, led to a jettable, photocurable ink. UV light exposure triggered the cationic ring-opening polymerization reaction of the epoxy groups and, in the presence of atmospheric water, the hydrolysis and condensation of the inorganic network, overall leading to a crosslinked organic-inorganic polymeric material. Control of the curing conditions led to deposits presenting excellent adhesion to glass, reduced light scattering and luminescence, all this through a simple one-step curing process without the need of any post baking steps that could degrade the luminescent dye. Overall, the present photoacid catalysed strategy allows, through an adequate selection of monomers and functional additives, the preparation of functional inks with tailored optical properties. The photolateness of the presented system, that delays the hydrolysis and condensation reactions in the absence of actinic light, favours the long-term stability of the ink properties overcoming problems arising in inks based on conventional sol-gel processes. Digital patterning of these inks leads to luminescent patterns that can be deposited on different industrially relevant substrates such as glass, PET or COP demonstrating the suitability of these photoacid catalysed organic-inorganic hybrid inks for the preparation of optical elements and devices.

Supplementary Materials: The following are available online at <http://www.mdpi.com/2073-4360/11/3/430/s1>.

Author Contributions: J.A., J.I.P. and C.S.-S. conceived and designed the experiments; J.A., M.L.-V. and R.A. performed the experiments; J.A. and C.S.-S. analyzed the data; J.A., M.L.-V. and R.A. contributed reagents/materials/analysis tools; J.A. and C.S.-S. wrote the paper. All the authors revised the paper.

Funding: This research was funded by the Spanish MINECO project BIO2017-84246-C2-1-R, Gobierno de Aragón and FEDER (EU).

Acknowledgments: Authors would like to acknowledge the use of Servicio General de Apoyo a la Investigación-SAI, Universidad de Zaragoza. The authors thank Beonchip S.L. for kindly supplying COP substrates.

Conflicts of Interest: The authors declare no conflict of interest

References

1. Kobayashi, S.; Mikoshiba, S.; Lim, S. Flat Panel Display Manufacturing. In *LCD Backlights*; John Wiley & Sons, Ltd.: West Sussex, UK, 2009.
2. Konstantatos, G.; Sargent, E.H. *Colloidal Quantum Dot Optoelectronics and Photovoltaics*; Cambridge University Press: Cambridge, UK, 2013.
3. Debije, M.G.; Verbunt, P.P.C. Thirty Years of Luminescent Solar Concentrator Research: Solar Energy for the Built Environment. *Adv. Energy Mater.* **2012**, *2*, 12–35. [[CrossRef](#)]
4. Liang, R.-Q.; Li, W.; Li, Y.; Tan, C.-Y.; Li, J.-X.; Jin, Y.-X.; Ruan, K.-C. An oligonucleotide microarray for microRNA expression analysis based on labeling RNA with quantum dot and nanogold probe. *Nucleic Acids Res.* **2005**, *33*, e17. [[CrossRef](#)] [[PubMed](#)]
5. Brites, C.D.S.; Lima, P.P.; Silva, N.J.O.; Millan, A.; Amaral, V.S.; Palacio, F.; Carlos, L.D. A luminescent molecular thermometer for long-term absolute temperature measurements at the nanoscale. *Adv. Mater.* **2010**, *22*, 4499–4504. [[CrossRef](#)] [[PubMed](#)]
6. Baride, A.; Meruga, J.M.; Douma, C.; Langerman, D.; Crawford, G.; Kellar, J.J.; Cross, W.M.; May, P.S. A NIR-to-NIR upconversion luminescence system for security printing applications. *RSC Adv.* **2015**, *5*, 101338–101346. [[CrossRef](#)]
7. You, M.; Lin, M.; Wang, S.; Wang, X.; Zhang, G.; Hong, Y.; Dong, Y.; Jin, G.; Xu, F. Three-dimensional quick response code based on inkjet printing of upconversion fluorescent nanoparticles for drug anti-counterfeiting. *Nanoscale* **2016**, *8*, 10096–10104. [[CrossRef](#)] [[PubMed](#)]
8. Binnemans, K. Lanthanide-based luminescent hybrid materials. *Chem. Rev.* **2009**, *109*, 4283–4374. [[CrossRef](#)] [[PubMed](#)]
9. Bao, B.; Li, M.; Li, Y.; Jiang, J.; Gu, Z.; Zhang, X.; Jiang, L.; Song, Y. Patterning fluorescent quantum dot nanocomposites by reactive inkjet printing. *Small* **2015**, *11*, 1649–1654. [[CrossRef](#)] [[PubMed](#)]
10. Shirasaki, Y.; Supran, G.J.; Bawendi, M.G.; Bulovic, V. Emergence of colloidal quantum-dot light-emitting technologies. *Nat. Photon.* **2013**, *7*, 13–23. [[CrossRef](#)]
11. Guillou, O.; Daiguebonne, C.; Calvez, G.; Bernot, K. A long journey in lanthanide chemistry: From fundamental crystallography studies to commercial anticounterfeiting taggants. *Acc. Chem. Res.* **2016**, *49*, 844–856. [[CrossRef](#)] [[PubMed](#)]
12. Frath, D.; Massue, J.; Ulrich, G.; Ziessel, R. Luminescent materials: Locking p-conjugated and heterocyclic ligands with boron(III). *Angew. Chem. Int. Ed.* **2014**, *53*, 2290–2310. [[CrossRef](#)] [[PubMed](#)]
13. Wang, F.; Xie, Z.; Zhang, B.; Liu, Y.; Yang, W.; Liu, C.Y. Down- and up-conversion luminescent carbon dot fluid: Inkjet printing and gel glass fabrication. *Nanoscale* **2014**, *6*, 3818–3823. [[CrossRef](#)] [[PubMed](#)]
14. Deng, C.; Yang, Z.; Zheng, Z.; Liu, N.; Ling, J. Photoluminescent nanoparticles in water with tunable emission for coating and ink-jet printing. *J. Mater. Chem. C* **2015**, *3*, 3666–3675. [[CrossRef](#)]
15. Lee, W.-H.; Park, Y.D. Inkjet Etching of Polymers and Its Applications in Organic Electronic Devices. *Polymers* **2017**, *9*, 441. [[CrossRef](#)]
16. Homola, T.; Shekargoftar, M.; Dzik, P.; Krumpolec, R.; Durasova, Z.; Vesely, M.; Cernak, M. Low-temperature (70 °C) ambient air plasma-fabrication of inkjet-printed mesoporous TiO₂ flexible photoanodes. *Flex. Print. Electron.* **2017**, *2*, 035010. [[CrossRef](#)]

17. Ma, S.; Ribeiro, F.; Powell, K.; Lutian, J.; Møller, C.; Large, T.; Holbery, J. Fabrication of Novel Transparent Touch Sensing Device via Drop-on-Demand Inkjet Printing Technique. *ACS Appl. Mater. Interfaces* **2015**, *7*, 21628–21633. [[CrossRef](#)] [[PubMed](#)]
18. Sun, J.Z.; Guo, Y.Z.; Cui, B.; Chu, F.Q.; Li, H.Z.; Li, Y.; He, M.; Ding, D.; Liu, R.P.; Li, L.H.; et al. Inkjet printing bendable circuits based on an oil-water interface reaction. *Appl. Surf. Sci.* **2018**, *445*, 391–397. [[CrossRef](#)]
19. Sun, J.Z.; Yun, C.; Cui, B.; Li, P.; Liu, G.; Wang, X.; Chu, F. A Facile Approach for Fabricating Microstructured Surface Based on Etched Template by Inkjet Printing Technology. *Polymers* **2018**, *10*, 1209. [[CrossRef](#)]
20. Sun, J.Z.; Cui, B.; Chu, F.Q.; Yun, C.H.; He, M.; Li, L.H.; Song, Y.L. Printable nanomaterials for the fabrication of high-performance supercapacitors. *Nanomaterials* **2018**, *8*, 528. [[CrossRef](#)] [[PubMed](#)]
21. Bollgruen, P.; Gleissner, U.; Wolfer, T.; Megnin, C.; Mager, D.; Overmeyer, L.; Korvink, J.G.; Hanemann, T. Ink-jet printed fluorescent materials as light sources for planar optical waveguides on polymer foils. *Opt. Eng.* **2016**, *55*, 107107. [[CrossRef](#)]
22. Zhang, H.-B.; Liu, M.; Lei, X.; Wen, T.; Zhang, J. Digital controlled luminescent emission via patterned deposition of lanthanide coordination compounds. *ACS Appl. Mater. Interfaces* **2014**, *6*, 12594–12599. [[CrossRef](#)] [[PubMed](#)]
23. daLuz, L.L.; Milani, R.; Felix, J.F.; Ribeiro, I.R.B.; Talhavi, M.; Neto, B.A.D.; Chojnacki, J.; Rodrigues, M.O.; Júnior, S.A. Inkjet printing of lanthanide–organic frameworks for anti-counterfeiting applications. *ACS Appl. Mater. Interfaces* **2015**, *7*, 27115–27123. [[CrossRef](#)] [[PubMed](#)]
24. Robin, M.; Kuai, W.; Amela-Cortes, M.; Cordier, S.; Molard, Y.; Mohammed-Brahim, T.; Jacques, E.; Harnois, M. Epoxy based ink as versatile material for inkjet-printed devices. *ACS Appl. Mater. Interfaces* **2015**, *7*, 21975–21984. [[CrossRef](#)] [[PubMed](#)]
25. Haverinen, H.M.; Myllyla, R.A.; Jabbour, G.E. Inkjet printing of light emitting quantum dots. *Appl. Phys. Lett.* **2009**, *94*, 073108. [[CrossRef](#)]
26. Andres, J.; Hersch, R.D.; Moser, J.-E.; Chauvin, A.-S. A new anti-counterfeiting feature relying on invisible luminescent full color images printed with lanthanide-based inks. *Adv. Funct. Mater.* **2014**, *24*, 5029–5036. [[CrossRef](#)]
27. You, M.; Zhong, J.; Hong, Y.; Duan, Z.; Lin, M.; Xu, F. Inkjet printing of upconversion nanoparticles for anti-counterfeit applications. *Nanoscale* **2015**, *7*, 4423. [[CrossRef](#)] [[PubMed](#)]
28. Wang, Y.-M.; Tian, X.-T.; Zhang, H.; Yang, Z.-R.; Yin, X.-B. Anticounterfeiting quick response code with emission color of invisible metal—Organic frameworks as encoding information. *ACS Appl. Mater. Interfaces* **2018**, *10*, 22445–22452. [[CrossRef](#)] [[PubMed](#)]
29. Singh, M.; Haverinen, H.M.; Dhagat, P.; Jabbour, G.E. Inkjet printing-process and its applications. *Adv. Mater.* **2010**, *22*, 673–685. [[CrossRef](#)] [[PubMed](#)]
30. Derby, B. Inkjet printing of functional and structural materials: Fluid property requirements, feature, stability, and resolution. *Annu. Rev. Mater. Res.* **2010**, *40*, 395–414. [[CrossRef](#)]
31. Alaman, J.; Alicante, R.; Pena, J.; Sanchez-Somolinos, C. Inkjet printing of functional materials for optical and photonic applications. *Materials* **2016**, *9*, 910. [[CrossRef](#)] [[PubMed](#)]
32. Coenen, M.J.J.; Slaats, T.M.W.L.; Eggenhuisen, T.M.; Groen, P. Inkjet printing the three organic functional layers of two-colored organic light emitting diodes. *Thin Solid Films* **2015**, *583*, 194–200. [[CrossRef](#)]
33. Samusjew, A.; Kratzer, M.; Moser, A.; Teichert, C.; Krawczyk, K.K.; Griesser, T. Inkjet Printing of Soft, Stretchable Optical Waveguides through the Photopolymerization of High-Profile Linear Patterns. *ACS Appl. Mater. Interfaces* **2017**, *9*, 4941–4947. [[CrossRef](#)] [[PubMed](#)]
34. Kim, J.Y.; Martin-Olmos, C.; Baek, N.S.; Brugger, J. Simple and easily controllable parabolic-shaped microlenses printed on polymeric mesas. *J. Mater. Chem. C* **2013**, *1*, 2152–2157. [[CrossRef](#)]
35. Descombes, L.J.; Cadarso, V.J.; Schleunitz, A.; Grutzner, S.; Klein, J.J.; Brugger, J.; Schiff, H.; Grutzner, G. Organic-inorganic-hybrid-polymer microlens arrays with tailored optical characteristics and multi-focal properties. *Opt. Express* **2015**, *23*, 25365–25376. [[CrossRef](#)] [[PubMed](#)]
36. Eggenhuisen, T.M.; Galagan, Y.; Biezemans, A.F.K.V.; Slaats, T.M.W.L.; Voorthuijzen, W.P.; Kommeren, S.; Shanmugam, S.; Teunissen, J.P.; Hadipour, A.; Verhees, W.J.H.; et al. High efficiency, fully inkjet printed organic solar cells with freedom of design. *J. Mater. Chem. A* **2015**, *3*, 7255–7262. [[CrossRef](#)]
37. Tekin, E.; Smith, P.J.; Hoeppe, S.; van den Berg, A.M.J.; Susha, A.S.; Rogach, A.L.; Feldmann, J.; Schubert, U.S. Inkjet printing of luminescent CdTe nanocrystal–polymer composites. *Adv. Funct. Mater.* **2007**, *17*, 23–28. [[CrossRef](#)]

38. Tekin, E.; de Gans, B.-J.; Schubert, U.S. Ink-jet printing of polymers from single dots to thin film libraries. *J. Mater. Chem.* **2004**, *14*, 2627–2632. [[CrossRef](#)]
39. Jacot-Descombes, L.; Gullo, M.R.; Cadarso, V.J.; Brugger, J. Fabrication of epoxy spherical microstructures by controlled drop-on-demand inkjet printing. *J. Micromech. Microeng.* **2012**, *22*, 074012. [[CrossRef](#)]
40. Bollgruen, P.; Gleissner, U.; Megnin, C.; Mager, D.; Korvink, J.; Hanemann, T. Ink-jet printing of host-guest systems based on acrylates with fluorescent dopants. *SPIE Proc.* **2016**. [[CrossRef](#)]
41. Serra, A.; Ramis, X.; Fernández-Francos, X. Epoxy sol-gel hybrid thermosets. *Coatings* **2016**, *6*, 8. [[CrossRef](#)]
42. Sanchez, C.; Lebeau, B.; Chaput, F.; Boilot, J.-P. Optical properties of functional hybrid organic-inorganic nanocomposites. *Adv. Mater.* **2003**, *15*, 1969–1994. [[CrossRef](#)]
43. Houbertz, R.; Frohlich, L.; Popall, M.; Streppel, U.; Dannberg, P.; Bräuer, A.; Serbin, J.; Chichkov, B.N. Inorganic-Organic Hybrid Polymers for Information Technology: From Planar Technology to 3D Nanostructures. *Adv. Eng. Mater.* **2003**, *5*, 551–555. [[CrossRef](#)]
44. Sanchez, C.; Belleville, P.; Popall, M.; Nicole, L. Applications of advanced hybrid organic-inorganic nanomaterials: From laboratory to market. *Chem. Soc. Rev.* **2011**, *40*, 696–753. [[CrossRef](#)] [[PubMed](#)]
45. Parola, S.; Julian-Lopez, B.; Carlos, L.D.; Sanchez, C. Optical properties of hybrid organic-inorganic materials and their applications. *Adv. Funct. Mater.* **2016**, *26*, 6506–6544. [[CrossRef](#)]
46. Sriramulu, D.; Turaga, S.P.; Yi, A.X.; Bettiol, A.A.; Valiyaveetil, S. Synthesis, characterization and application of luminescent silica nanomaterials. *J. Mater. Chem. C* **2016**, *4*, 11190–11197. [[CrossRef](#)]
47. Hong, Y.; Chen, Z.; Trofimov, A.A.; Lei, J.; Chen, J.; Yuan, L.; Zhu, W.; Xiao, H.; Xu, D.; Jacobssohn, L.G.; et al. Direct inkjet printing of miniaturized luminescent YAG:Er³⁺ from sol-gel precursor. *Opt. Mater.* **2017**, *68*, 11–18. [[CrossRef](#)]
48. Alamán, J.; López-Valdeolivas, M.; Alicante, R.; Medel, F.J.; Silva-Treviño, J.; Peña, J.I.; Sánchez-Somolinos, C. Photoacid catalyzed organic-inorganic hybrid inks for the manufacturing of inkjet-printed photonic devices. *J. Mater. Chem. C* **2018**, *6*, 3882–3894. [[CrossRef](#)]
49. Chemtob, A.; Versace, D.-L.; Belon, C.; Croutxe-Barghorn, C.; Rigolet, S. Concomitant organic-inorganic UV-curing catalyzed by photoacids. *Macromolecules* **2008**, *41*, 7390–7398. [[CrossRef](#)]
50. Chemtob, A.; Peter, M.; Belon, C.; Dietlin, C.; Croutxé-Barghorn, C.; Vidal, L.; Rigolet, S. Macroporous organosilica films via a template-free photoinduced sol-gel process. *J. Mater. Chem.* **2010**, *20*, 9104–9112. [[CrossRef](#)]
51. Croutxé-Barghorn, C.; Belon, C.; Chemtob, A. Polymerization of hybrid sol-gel materials catalyzed by photoacids generation. *J. Photopolym. Sci. Technol.* **2010**, *23*, 129–134. [[CrossRef](#)]
52. Danzebrink, R.; Aegerter, M.A. Deposition of micropatterned coating using an ink-jet technique. *Thin Solid Films* **1999**, *351*, 115–118. [[CrossRef](#)]
53. Danzebrink, R.; Aegerter, M.A. Deposition of optical microlens arrays by ink-jet processes. *Thin Solid Films* **2001**, *392*, 223–225. [[CrossRef](#)]
54. Fujii, T.; Isbii, A.; Anpo, M. Absorption and fluorescence spectra of rhodamine B molecules encapsulated in silica gel networks and their thermal stability. *J. Photochem. Photobiol. A* **1990**, *54*, 231–237. [[CrossRef](#)]
55. Severin-Vantilt, M.M.E.; Oomen, E.W.J.L. The incorporation of Rhodamine B in silica sol-gel layers. *J. Non-Cryst. Solids* **1993**, *159*, 38–48. [[CrossRef](#)]
56. Zareba-Grodz, I.; Pazik, R.; Hermanowicz, K.; Streck, W.; Maruszewski, K. Preparation and optical properties of hybrid coatings based on epoxy-modified silane and rhodamine B. *J. Lumin.* **2006**, *119–120*, 148–152. [[CrossRef](#)]
57. del Monte, F.; Levy, D. Formation of fluorescent Rhodamine B J-dimers in sol-gel glasses induced by the adsorption geometry on the silica surface. *J. Phys. Chem. B* **1998**, *102*, 8036–8041. [[CrossRef](#)]
58. Schulz-Ekloff, G.; Wöhrle, D.; van Duffel, B.; Schoonheydt, R.A. Chromophores in porous silicas and minerals: Preparation and optical properties. *Microporous Mesoporous Mater.* **2002**, *51*, 91–138. [[CrossRef](#)]
59. Nedelcev, T.; Racko, D.; Krupa, I. Preparation and characterization of a new derivative of rhodamine B with an alkoxysilane moiety. *Dyes Pigm.* **2008**, *76*, 550–556. [[CrossRef](#)]
60. Negishi, N.; Fujino, M.; Yamashita, H.; Fox, M.A.; Anpo, M. Photophysical properties and photochemical stability of Rhodamine B encapsulated in SiO₂ and Si-Ti binary oxide matrices by the sol-gel method. *Langmuir* **1994**, *10*, 1772–1776. [[CrossRef](#)]
61. Fink, C.K.; Nakamura, K.; Ichimura, S.; Jenkins, S.J. Silicon oxidation by ozone. *J. Phys. Condens. Matter* **2009**, *21*, 183001–183020. [[CrossRef](#)] [[PubMed](#)]

62. Schuhmacher, B.; Muschenborn, W.; Stratmann, M.; Schultrich, B.; Klages, C.-P.; Kretschmer, M.; Seyfert, U.; Forster, F.; Tiller, H.-J. Novel coating systems and surface technologies for continuous processing of steel sheet. *Adv. Eng. Mater.* **2001**, *3*, 681–689. [[CrossRef](#)]
63. Standard ASTM D3359-02. *Standard Test Methods for Measuring Adhesion by Tape Test*; ASTM International: West Conshocken, PA, USA, 2002.
64. Hoath, S.D.; Hutchings, I.M.; Martin, G.D.; Tuladhar, T.R.; Mackley, M.R.; Vadillo, D. Links between ink rheology, drop-on-demand jet formation, and printability. *J. Imaging Sci. Technol.* **2009**, *53*, 412081–412088. [[CrossRef](#)]
65. Hoath, S.D.; Vadillo, D.C.; Harlen, O.G.; McIlroy, C.; Morrison, N.F.; Hsiao, W.-K.; Tuladhar, T.R.; Jung, S.; Martin, G.D.; Hutchings, I.M. Inkjet printing of weakly elastic polymer solutions. *J. Non-Newton. Fluid Mech.* **2014**, *205*, 1–10. [[CrossRef](#)]
66. Derby, B.; Reis, N.; Seerden, K.A.M.; Grant, P.S.; Evans, J.R.G. Freeform fabrication of ceramics by hot-melt ink-jet printing. *MRS Proc.* **2000**. [[CrossRef](#)]
67. Duineveld, P.C.; de Kok, M.M.; Buechel, M.; Sempel, A.; Mutsaers, K.A.; van de Weijer, P.; Camps, I.G.J.; van de Biggelaar, T.; Rubingh, J.-E.J.M.; Haskal, E.I. Ink-jet printing of polymer light-emitting devices. *Proc. SPIE* **2002**. [[CrossRef](#)]
68. Stow, C.D.; Hadfield, M.G. An experimental investigation of fluid flow resulting from the impact of a water drop with an unyielding dry surface. *Proc. R. Soc. Lond. A Math. Phys. Eng. Sci.* **1981**, *373*, 419–441. [[CrossRef](#)]
69. Bhola, R.; Chandra, S. Parameters controlling solidification of molten wax droplets falling on a solid surface. *J. Mater. Sci.* **1999**, *34*, 4883–4894. [[CrossRef](#)]
70. Bartasun, P.; Cieslinski, H.; Bujacz, A.; Wierzbicka-Wos, A.; Kur, J. A study on the interaction of Rhodamine B with Methylthioadenosine Phosphorylase protein sourced from an antarctic soil metagenomic library. *PLoS ONE* **2013**, *8*, e55697. [[CrossRef](#)] [[PubMed](#)]
71. De Paz, H.; Chemtob, A.; Croutxé-Barghorn, C.; Le Nouen, D.; Rigolet, S. Insights into Photoinduced Sol-Gel Polymerization: An in Situ Infrared Spectroscopy Study. *J. Phys. Chem. B* **2012**, *116*, 5260–5268. [[CrossRef](#)] [[PubMed](#)]
72. Chemtob, A.; Ni, L.; Dietlin, C.; Croutxé-Barghorn, C.; Kitzmann, P.; Brogly, M.; Vidal, L. Spontaneous photoinduced formation of hybrid polymer films with functionalized macroporous patterns. *Surf. Coat. Technol.* **2012**, *209*, 64–72. [[CrossRef](#)]
73. Keller, S.; Blagoi, G.; Lillemose, M.; Haefliger, D.; Boisen, A. Processing of thin SU-8 films. *J. Micromech. Microeng.* **2008**, *18*, 125020. [[CrossRef](#)]
74. Sangermano, M.; Razza, N.; Crivello, J.V. Cationic UV-Curing: Technology and Applications. *Macromol. Mater. Eng.* **2014**, *299*, 775–793. [[CrossRef](#)]
75. Nunes, P.S.; Ohlsson, P.D.; Ordeig, O.; Kutter, J.P. Cyclic olefin polymers: Emerging materials for lab-on-a-chip applications. *Microfluid. Nanofluid.* **2010**, *9*, 145–161. [[CrossRef](#)]



© 2019 by the authors. Licensee MDPI, Basel, Switzerland. This article is an open access article distributed under the terms and conditions of the Creative Commons Attribution (CC BY) license (<http://creativecommons.org/licenses/by/4.0/>).

Supplementary information

Digital luminescence patterning via inkjet printing of a photoacid catalyzed organic-inorganic hybrid formulation

Jorge Alamán^{a, b}, María López-Valdeolivas^a, Raquel Alicante^a, Jose Ignacio Peña^c, and Carlos Sánchez-Somolinos^{a, d}*

^a Instituto de Ciencia de Materiales de Aragón (ICMA), CSIC-Universidad de Zaragoza, Departamento de Física de la Materia Condensada, Zaragoza, Spain

^b BSH Electrodomésticos España, S.A., Polígono Industrial de PLA-ZA, Ronda del Canal Imperial de Aragón, 18-20, 50197 Zaragoza, Spain

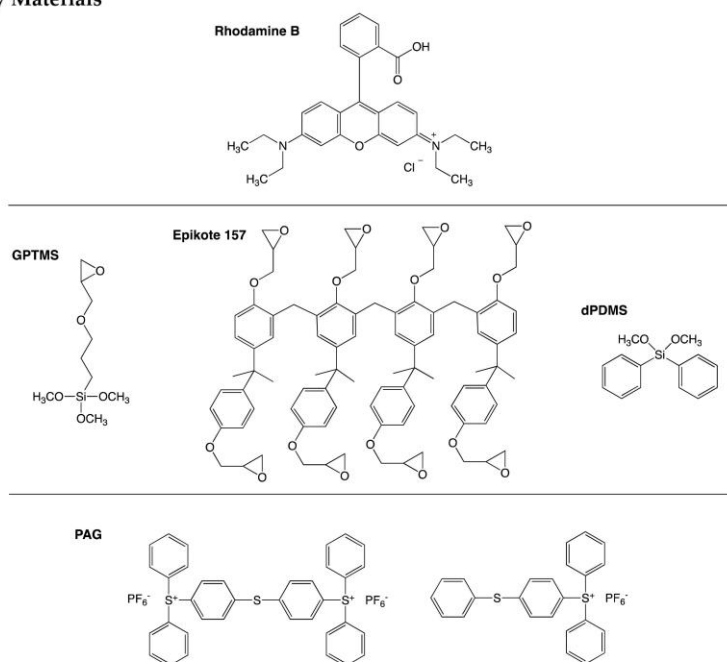
^c Instituto de Ciencia de Materiales de Aragón (ICMA), CSIC-Universidad de Zaragoza, Departamento de Ciencia y Tecnología de Materiales y Fluidos, Zaragoza, Spain

^d CIBER in Bioengineering, Biomaterials and Nanomedicine (CIBER-BBN), Spain

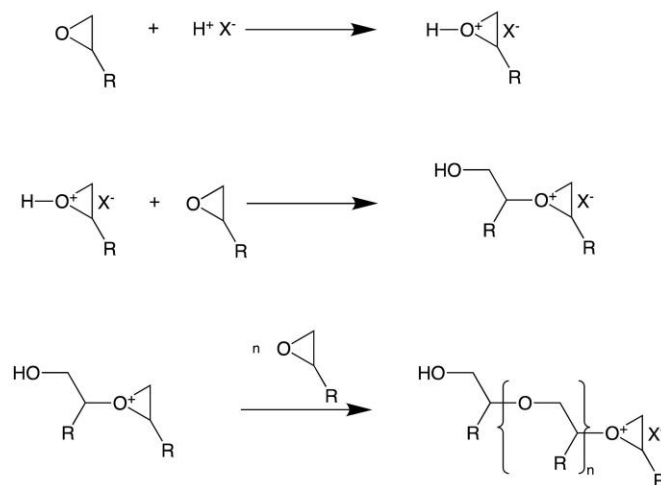
* Correspondence author: carlos.s@csic.es

Telephone: +34 876 55 3770

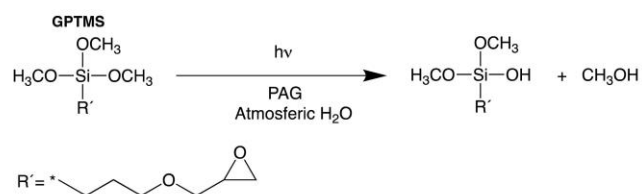
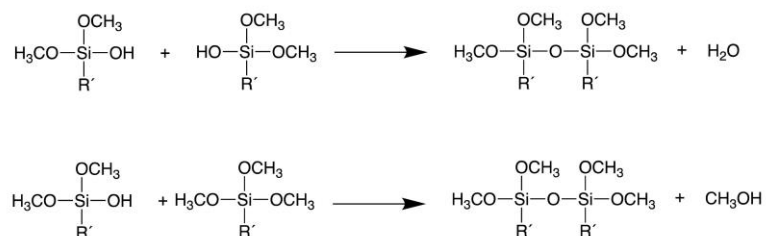
Supplementary Materials



Scheme S1. Chemical structure of the main components of the inks. Rhodamine B, GPTMS (3-glycidoxypropyltrimethoxysilane), Epikote 157, dPDMS (Dimethoxydiphenylsilane) and PAG (triarylsulfonium hexafluorophosphate salts, 50% in propylene carbonate).

Cationic ring-opening polymerization

Scheme S2. Cationic ring-opening polymerization of epoxy monomers.

Hydrolysis**Condensation**

Scheme S3. Hydrolysis and condensation steps of the photoinduced sol-gel process for GPTMS monomer.

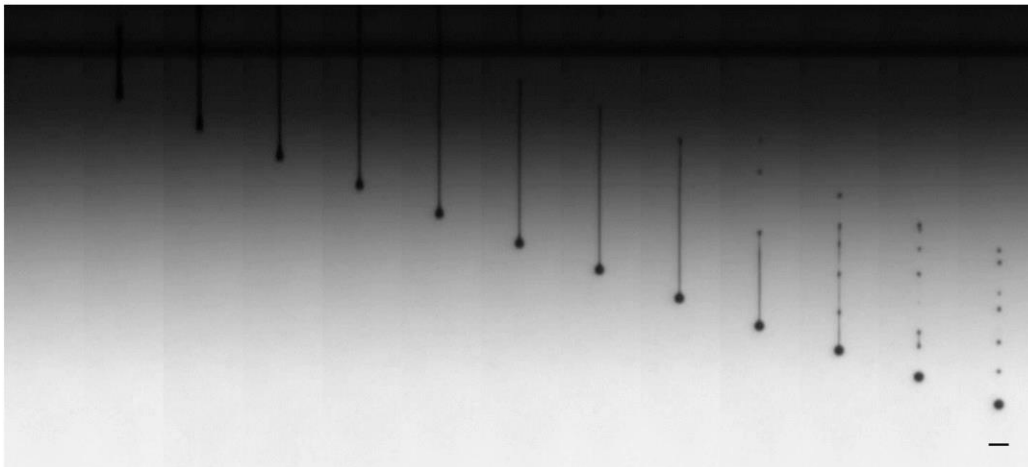


Figure S1. Temporal sequence of photographs (from left to right) showing the drop formation process for the luminescent ink with excess of energy in the jet. The time interval between two adjacent frames is $24 \mu\text{s}$ (scale bar: $100 \mu\text{m}$).

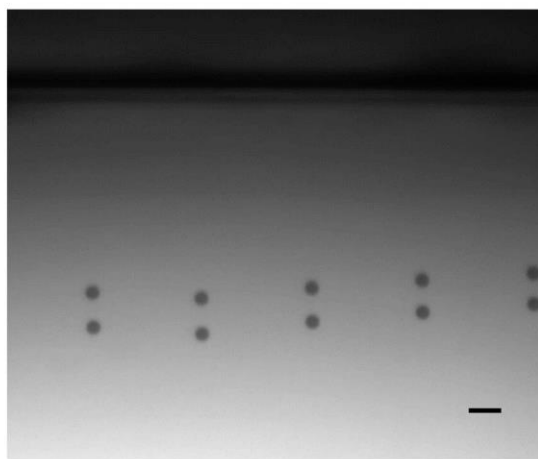


Figure S2. Double strobe image of a set of ejected droplets. The five droplets at the upper row are the same as the ones in the lower row. The five droplets are imaged twice with a delay of $50 \mu\text{s}$. The distance between the images corresponding to the same droplets are used for the calculation of speed (scale bar: $100 \mu\text{m}$).

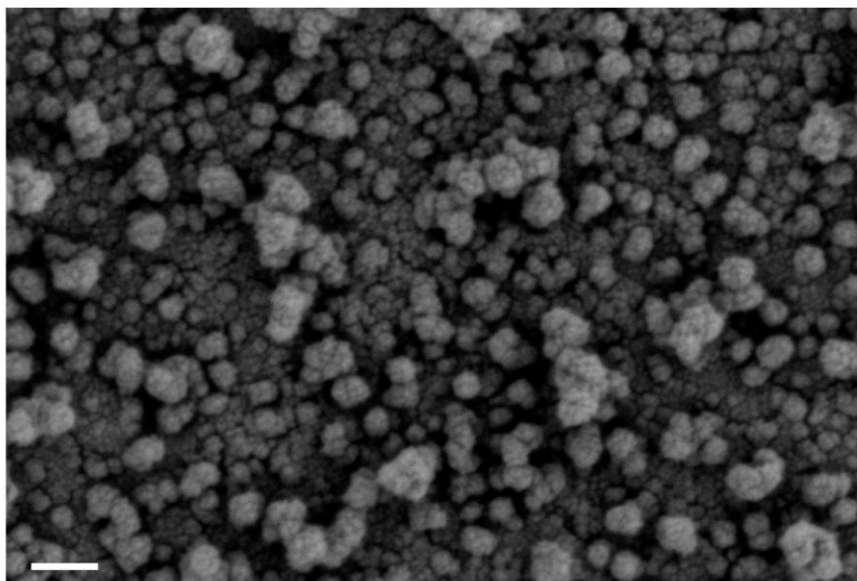


Figure S3. SEM image of a Pyrosil treated glass surface (scale 100 nm).

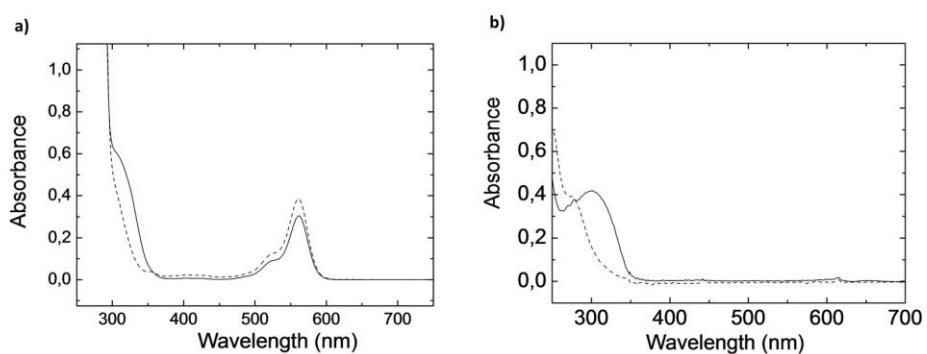


Figure S4. UV-Vis absorption spectra of (a) a thin film of luminescent ink and (b) the same formulation without dye, between quartz glass plates (11 μm gap) before (continuous line) and after UV irradiation (dashed line).

Model-RhodB-02 ink

A model luminescent system, named Model-RhodB-02, based of the organic-inorganic hybrid GPTMS as only reactive monomer, has been prepared as a reference system to follow the photocuring reaction. A small percentage of 2 wt % of triarylsulfonium hexafluorophosphate salts is incorporated to the formulation as a PAG. Additionally 0.05 wt % of BYK-333 and 0,2 wt % of Rhodamine B were added.

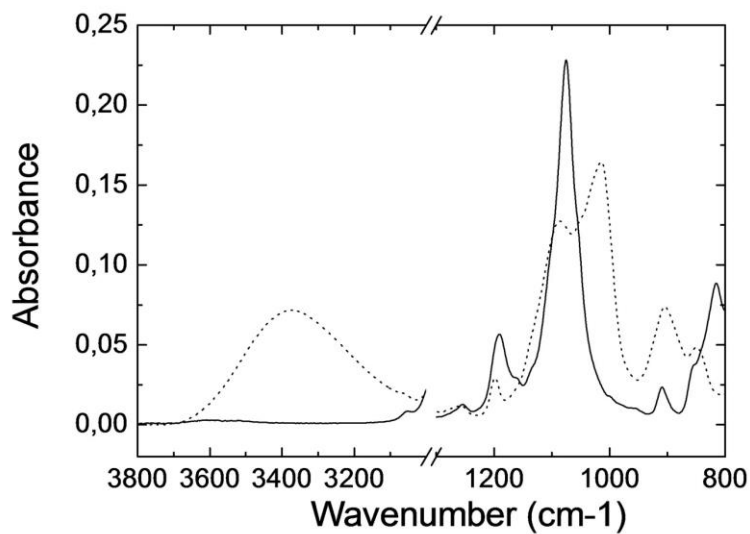


Figure S5. FTIR spectra of Model-RhodB-02 ink before (continuous line) and 10 minutes after UV exposure (dotted line) under atmospheric conditions.

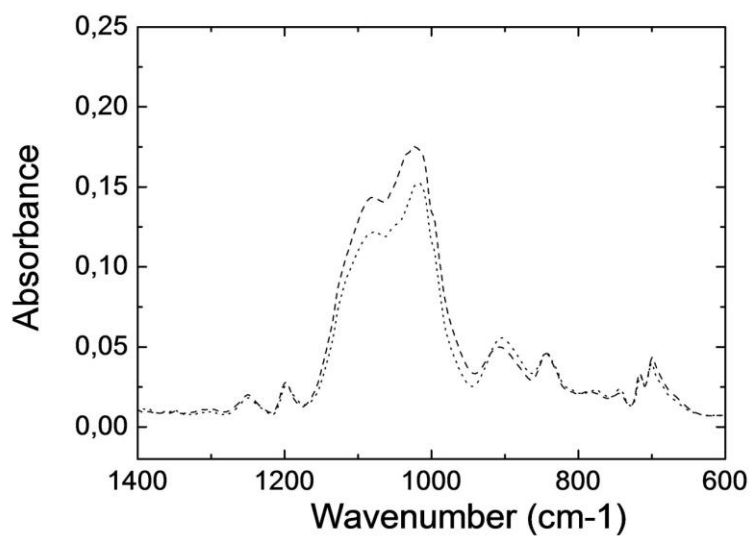


Figure S6. FTIR spectra of a thin film of HRI-RhodB-02 luminescent formulation 10 minutes (dots line) and 24 hours after curing (dashed line) cured under atmospheric conditions.

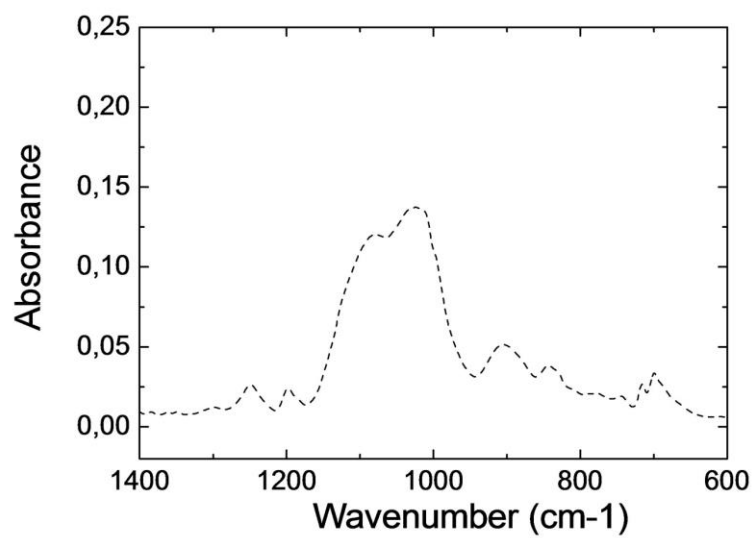


Figure S7. FTIR spectrum of a thin film of HRI-RhodB-02 luminescent formulation 24 hours after curing (dashed line) under mild vacuum conditions (100 mBar).

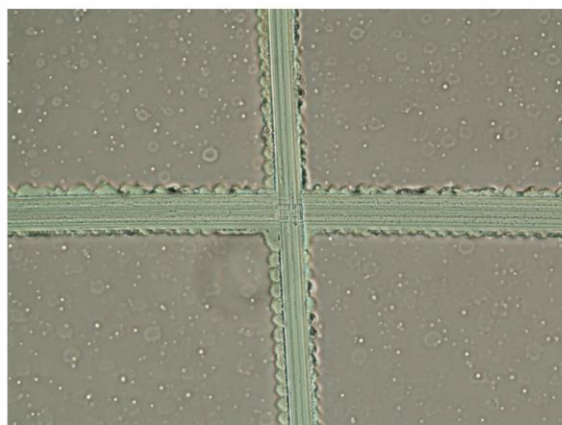


Figure S8. Optical microscope images of deposited films cured under mild vacuum conditions after the ASTM 3359 adhesion test. Film thickness: 4 μm .

4. Publication 4.

Journal: Sensors

Title: Optical Planar Waveguide Sensor with Integrated Digitally-Printed Light Coupling-in and Readout Elements

Article

Optical Planar Waveguide Sensor with Integrated Digitally-Printed Light Coupling-in and Readout Elements

Jorge Alamán ^{1,2}, María López-Valdeolivas ¹, Raquel Alicante ¹ and Carlos Sánchez-Somolinos ^{1,3,*} 

¹ Instituto de Ciencia de Materiales de Aragón (ICMA), CSIC-Universidad de Zaragoza, Departamento de Física de la Materia Condensada, 50009 Zaragoza, Spain

² BSH Electrodomésticos España, S.A., Polígono Industrial de PLA-ZA, Ronda del Canal Imperial de Aragón, 50197 Zaragoza, Spain

³ Centro de Investigación Biomédica en Red de Bioingeniería, Biomateriales y Nanomedicina (CIBER-BBN), C Mariano Esquillor s.n., 50018 Zaragoza, Spain

* Correspondence: carlos.s@csic.es; Tel.: +34-8765-53770

Received: 17 May 2019; Accepted: 25 June 2019; Published: 27 June 2019



Abstract: Optical planar waveguide sensors, able to detect and process information from the environment in a fast, cost-effective, and remote fashion, are of great interest currently in different application areas including security, metrology, automotive, aerospace, consumer electronics, energy, environment, or health. Integration of networks of these systems together with other optical elements, such as light sources, readout, or detection systems, in a planar waveguide geometry is greatly demanded towards more compact, portable, and versatile sensing platforms. Herein, we report an optical temperature sensor with a planar waveguide architecture integrating inkjet-printed luminescent light coupling-in and readout elements with matched emission and excitation. The first luminescent element, when illuminated with light in its absorption band, emits light that is partially coupled into the propagation modes of the planar waveguide. Remote excitation of this element can be performed without the need for special alignment of the light source. A thermoresponsive liquid crystal-based film regulates the amount of light coupled out from the planar waveguide at the sensing location. The second luminescent element partly absorbs the waveguided light that reaches its location and emits at longer wavelengths, serving as a temperature readout element through luminescence intensity measurements. Overall, the ability of inkjet technology to digitally print luminescent elements demonstrates great potential for the integration and miniaturization of light coupling-in and readout elements in optical planar waveguide sensing platforms.

Keywords: integrated optical planar waveguide sensors; flexible sensors; organic-inorganic hybrid materials; liquid crystalline thermoresponsive materials; inkjet printing; luminescent materials

1. Introduction

Sensors are often described as platforms able to detect information, for example temperature, pressure, humidity, or the presence of chemical compounds, from the environment and transform this information into different signals. Most common sensors usually respond to an external stimulus with an electrical signal that is later transmitted and processed by other electronic systems to which they are interfaced. The language spoken between sensors and devices in these cases is therefore based on the flux of electrons; however, the flux of photons can similarly be used to transfer information in sensing platforms. Optical sensors present attractive features when compared with electrical ones, since, for example, they are not subjected to electromagnetic interference, so they can be used

in a harsh environment with high voltages or intense magnetic fields. Besides, the possibility to transfer information through optical waveguides enables the generation of sensor networks that can be connected and monitored remotely without the need to transform the detected information into an electrical signal at each sensing site. The use of light with different properties (e.g., wavelength) also provides the possibility to multiplex several signals in a single waveguide easily. Even more, the employed waveguides can be lightweight, flexible, and inexpensive. All these characteristics make optical sensing platforms of great interest in different application areas including metrology, quality and process control, security, or (bio)medicine [1–5].

An optical sensor typically entails different components such as photonic sources to generate the probing light, optical elements to condition and direct this light towards the sensing region, as well as readout devices to obtain the analysis results. In this field, optical fiber sensors have reached a high degree of development. Coupling of light from lasers or light-emitting diodes (LEDs) is routinely performed currently by means of optical fiber couplers, and progress in sensing materials has enabled the implementation of sensors with improved sensitivity, portability, and reduced size [6,7].

Besides sensors relying on optical fibers, optical sensing systems integrated in planar waveguide geometries have also been extensively explored as they can integrate networks of sensing elements over large areas [8–10]. In these planar systems, it is highly desirable to miniaturize and integrate optical elements of the sensing platform such as detection and readout systems or light sources in the planar waveguide [11–14]. Moreover, for application areas such as biomedicine, microfluidics, or electronic skin, other specific requirements such as the compatibility with materials of different natures (e.g., glass, polymer, or metal), conformability, bendability, or stretchability need to be properly addressed to contribute to the overall sensing device performance [15–18]. Besides, the use of easily scalable, flexible, and reliable high-throughput fabrication techniques to synergistically combine photonic and sensing elements in thin films is required for the further development of these technologies. In this direction, a large effort is currently being made towards the development of materials and compatible manufacturing technologies enabling the large-scale, high-speed, and low-cost production and preparation of microoptical elements, as well as planar photonic systems on polymer foils. Waveguides have been generated in flexible substrates through, for example, lamination or inkjet-printing methods [19–25]. Interestingly, luminescent acrylate formulations have been applied through inkjet printing on polymeric waveguides generated on poly(methyl methacrylate) (PMMA) substrates by Bollgruen and coworkers to create remotely-addressable light sources that can couple light into flexible waveguides [26]. Moreover, regarding the sensing method, it is well known that the use of luminescence intensity measurements to perform magnitude readout advantageously leads to sensitivity improvement when there is no overlap between the exciting and emitted light spectra [27]. Even more, in a waveguide geometry, the light not absorbed in the readout element can be guided away from the detection region, further facilitating discrimination of the luminescence from the excitation light, leading to improved quality of the detectable signal.

In this paper, we present an optical temperature sensor having a planar waveguide architecture and including two luminescent layers with matched emission properties. These two emissive elements allow integrating light coupling-in and readout functions in the planar waveguide structure (Figure 1). Illumination of the first luminescent element with light in its absorption band induces emission of light that is partially coupled into the guided modes of the planar waveguide. Excitation of this element can be remotely performed without the need for special alignment of the light source. As temperature sensing materials, we include liquid crystalline polymers (LCP). The changes of molecular order in these systems, in response to temperature variations, make them suitable materials for this purpose [28–31]. Changes in light scattering of the liquid crystalline (LC) polymeric film with temperature enable the regulation of the light coupled out from the waveguide at this location. Besides temperature sensing, used in this paper as a simple example, LC materials could be tailored to be responsive to other stimuli such as moisture, pH, or chemical compounds as well [32–37]. After passing the region of the sensing element, light remaining in the waveguide reaches the second luminescent element. The emission

wavelength range of the first element is chosen to overlap with the excitation band of the second one, so the light generated in the first element, which is partially coupled into the waveguide, serves as excitation for the second element that emits light at longer wavelengths. Temperature readout can be carried out by measuring the luminescence intensity of this element. For the implementation of the two luminescent functional layers, we make use of our recently-developed inkjet printing platform based on photoacid-catalyzed organic-inorganic hybrid formulations including light-emissive molecules [24,38]. Inkjet printing, enabling the digital deposition of materials, has been demonstrated to be a powerful tool for the preparation and integration of functional elements and devices in a flat geometry [25,39–46]. In our case, inkjet printing technology allows the integration in planar waveguide structures of light coupling-in and readout elements. With the presented architecture, photonic elements such as light sources or detectors can be physically separated from the sensing device, still allowing remote and easy light coupling-in and readout; and therefore, the use of the sensor in adverse environments with, for example, extreme humidity or high electrical or magnetic fields. The implementation of the sensors in rigid and flexible waveguides is also demonstrated.

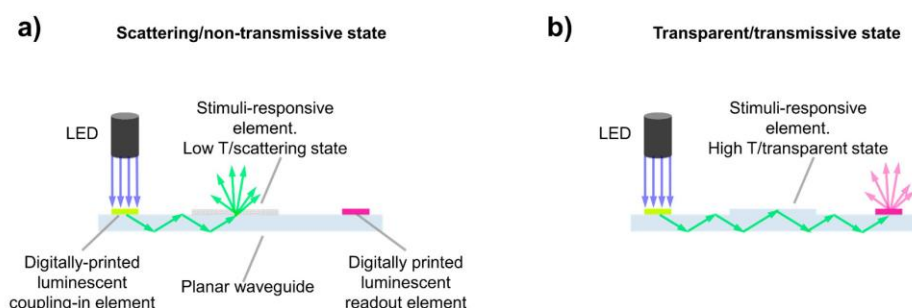


Figure 1. Optical planar waveguide sensor with integrated digitally-printed luminescent light coupling-in and readout elements. Remote excitation of the first luminescent element, by using an LED for example, enables coupling of light into the waveguide. Light is guided towards the thermoresponsive LCP element that regulates the light intensity transmitted towards the end of the waveguide where the second luminescent element is placed. (a) Scattering/non-transmissive state, at low temperature: light is scattered out of the waveguide at the stimuli-responsive element. (b) Transparent/transmissive state, at high temperature: light is not scattered at the stimuli-responsive element, and therefore, light further propagates in the waveguide and reaches the second luminescent layer. Remote luminescence intensity measurements allow quantifying the temperature in the sensor range.

2. Materials and Methods

2.1. Planar Waveguides

Cleaning procedure: Microscope glass slides (Thermo Scientific™ SuperFrost®, extra-white soda-lime glass, dimensions: 76 mm × 26 mm, 1 mm thick, $n = 1.517$ at 546 nm) were employed as planar waveguides in some of the experiments. Pre-cleaning of these glass slides using soapy water was carried out by gently rubbing the glass surface, using nitrile gloves. The slides were rinsed with water and introduced in an ultrasonic bath with soapy water for 10 min. After this, the glass slides were refluxed with Milli-Q water and ultrasonicated again in Milli-Q water for 10 min. The slides were then flushed with isopropyl alcohol. A third ultrasonic bath was carried out, in this case with isopropyl alcohol for 10 min. Finally, the substrates were dried with compressed air.

Cyclic olefin polymer (COP) foil from Zeonor (188 μm -thick polymer foil, $n = 1.53$ at 589 nm, Dusseldorf, Germany) and microscope COP slides, supplied from BeonCHIP (Zaragoza, Spain), were used as polymeric waveguides. COP rigid slides were pre-cleaned and were used as received. The flexible foil substrate was provided with a protective foil that was removed just before processing.

2.2. Substrate Treatments

UV ozone treatment was performed on a UV ozone reactor UVO 342 (Jelight company Inc., Irvine, CA, USA) to remove any contamination in the glass substrates, leaving silanol groups exposed on the surface [38]. As a result, important changes in the wettability and in the adhesion were obtained [24].

2.3. Surface Functionalization with Fluorosilane

The glass substrates, cleaned as described above, and UV ozone treated for 1 hour, were placed in a desiccator containing a glass slide with 50 μ L of 1H,1H,2H,2H-perfluorooctyltrichlorosilane (PFOTCIS) from Aldrich. A vacuum was applied in the desiccator until a pressure of 100 mbar was achieved. After 30 min, the substrates were taken out, thoroughly rinsed with isopropyl alcohol, dried with compressed air, and heated for 10 min at 110 °C in air [47].

2.4. Temperature-Responsive Liquid Crystalline Material

6-(4-Cyano-biphenyl-4'-yloxy)hexyl acrylate (A6OCB, also known as RM 105), a pro-mesogenic molecule functionalized with one reactive acrylate group, was acquired from Synthron GmbH under the reference STO3474. A6OCB presents a crystalline phase at room temperature (RT) and melts at 70–71 °C. 1,4-Bis-[4-(6-acryloyloxyhex-yloxy)benzoyloxy]-2-methylbenzene (RM82) from Merck is a mesogen functionalized with two acrylate end groups. 1-Hydroxycyclohexyl phenyl ketone, also known as Irgacure 184 (IRG184), was used as a UV photoinitiator. A mixture comprising 99 wt% of A6OCB and 1 wt% of RM82 was prepared as a precursor of the thermoresponsive LCP. Besides, 3 wt% of IRG184 photoinitiator was added. To help mixture homogenization, dichloromethane (CH_2Cl_2) in an equivalent wt% to the weight of the solid material was added. The solids immediately dissolved just after a mild shaking of the containing flask. Afterwards, the flask remained open overnight in a fume hood, and the weight was controlled the day after, confirming that all the dichloromethane had been eliminated from the mixture.

2.5. Ink Materials

The following materials were used for the formulation of the inks: 3-glycidoxypropyltrimethoxysilane (GPTMS), a hybrid organic-inorganic monomer bearing an epoxy and a trialkoxysilane group purchased from Alfa Aesar; the epoxy resin Epikote 157, with an average of eight aromatic benzene rings and eight epoxide reactive groups, acquired from Momentive; dimethoxydiphenylsilane (dPDMS), a disilane monomer with two aromatic rings, supplied by Aldrich; a photoacid generator (PAG), triarylsulfonium hexafluorophosphate salt (50% in propylene carbonate), from Aldrich that, upon excitation with UV actinic light, triggers the polymerization reaction of the organic epoxides and, concurrently, catalyzes the hydrolysis and condensation of the alkoxide groups; besides, BYK-333, a polyether-modified polydimethylsiloxane from BYK Chemie, was used to regulate the surface tension of the inks and to promote surface wetting.

To provide the inks with luminescent properties, two different dyes were employed: (i) fluorescein 27 (F27), a luminescent dye having an emission centered at 520 nm (green light) [48,49]; and (ii) Rhodamine B, which strongly absorbs in the green and emits light in the orange-red region of the spectrum, centered at 585 nm [50]. F27 and Rhodamine B were purchased from Lambda Physik under the references Lambdachrome LC 5530 and LC6100, respectively. All the materials were used as received.

2.6. Ink Preparation

The two photopolymerizable luminescent formulations employed in this work were based on the addition of a small amount of emissive dye to a jettable ink, previously developed in our laboratory, incorporating different monomers. Namely, 50 wt% of GPTMS, 25 wt% of Epikote 157, and 25 wt% of dPDMS were the components of the basic formulation. To the weight of these reactive monomers,

a percentage of 2 wt% of triarylsulfonium hexafluorophosphate salts was added to the mixture. Additionally, 0.05 wt% of BYK-333 was added to improve the wetting of the inks in the substrate [51] and to introduce viscoelasticity in the inks [24]. The first luminescent ink, named HRI-F27-02, contained fluorescein 27 (F27), and it was based on the abovementioned basic formulation [24]. Then, 0.2 wt% of F27 was added to the total weight to provide the printed layers with luminescence in the region of 520 nm upon excitation with light in the UV or blue regions. The second luminescent formulation, containing Rhodamine B and named HRI-RhodB-02, had the same composition except for the luminescent dye. To provide HRI-RhodB-02 with orange-red luminescence when excited in the green, 0.2 wt% of Rhodamine B was added to the basic formulation.

2.7. Inkjet Printing

Inkjet printing was carried out using a custom-made inkjet printer system (In-2 Printing Solutions, Navarra, Spain) with Xaar-126/80 piezoelectric printheads (Xaar, Cambridge, U.K.). The printhead had 126 nozzles (50 μm in diameter) arranged in a line with a distance of 137 μm between them. The line of nozzles was perpendicular to the direction of the substrate motion, which moved along a line under the fixed printhead. As a result, the vertical resolution (in the direction of the line of nozzles, perpendicular to the substrate motion) was 185 dots per inch (dpi). The horizontal resolution (in the direction of the substrate movement) depended on the firing frequency and the relative speed of the substrate with respect to the printhead. The printhead was commanded by a Xaar XUSB drive electronics, controlled with a PC. The software (from Xaar) enables the control of the parameters of the printhead, synchronization of the different elements, and transfer of patterns to be printed (bitmap file) to the printhead. The movement of the substrate while printing was at a constant speed of 20 mm/s by using an eTrack linear stage from Newmark systems Inc. (Mission Viejo, CA, USA) commanded by IMS-Terminal software (Marlborough, MO, USA). The printhead was mounted in a metallic block, provided with a heater and thermocouple connected to a temperature control unit that fixed the printhead temperature at the set point (32 $^{\circ}\text{C}$) [24,38].

2.8. Thermoresponsive LCP Film Preparation

The photopolymerizable mixture together with spherical silica spacers (50 μm) was applied on top of the waveguide plate. The waveguide was heated at 75 $^{\circ}\text{C}$, and the photopolymerizable mixture was molten at this temperature. A fluorinated glass plate (previously heated to 75 $^{\circ}\text{C}$) was applied and pressed on top of the photopolymerizable mixture provided with spacers that defined the thickness of the final film. Careful application of this glass cover resulted in a liquid layer free of bubbles ready for photopolymerization. A UV lamp Exfo OmniCure S2000 UV (Gentec, Nivelles, Belgium) was used with a UV bandpass filter (wavelength range of 320–390 nm) for this purpose. Photocuring of the photopolymerizable mixture was carried out by heating the sample at 75 $^{\circ}\text{C}$ and then exposing to UV light with a power of 140 mW/cm² for 30 s. A subsequent post-curing step was carried out by exposing the film with a power of 10 mW/cm² for 5 min. The fluorinated glass was carefully removed, leaving the photopolymerized film in contact with the air.

2.9. Ink Photocuring

For the UV photopolymerizable inks, after inkjet deposition, the samples were exposed to UV light, using the same light source as in the thermoresponsive curing, with a power of 10 mW/cm² for 5 min. The curing process was carried out under mild vacuum conditions placing the printed samples inside a chamber with an optical access. A vacuum of 100 mBar was attained inside the chamber by using a vacuum pump [38]. To reduce the evaporation of the components of the ink while the vacuum reach the desired pressure, UV exposure was immediately activated once this pressure level was reached.

2.10. Characterization

Luminescence of the deposited films was characterized using a Perkin Elmer LS 50B spectrometer. Polarization optical microscope (POM) images of the liquid crystalline textures were taken using an optical microscope OLYMPUS Eclipse i80 provided with crossed polarizers. For temperature-dependent observations, the microscope was equipped with a Linkam LTSE420 heating stage.

Thermogravimetric analysis (TGA) was performed using a Netzsch TG 209 Libra F1 Instrument to obtain the temperature of the onset of the decomposition weight loss curve and the maximum of the derivative of the TGA curve.

3. Results

Prior to integrating, through digital inkjet printing, the light coupling-in and readout luminescent elements depicted in Figure 1, we integrated, as a first step, the temperature sensing element in a planar waveguide geometry. As mentioned in the Introduction, a stimuli-responsive LCP element that changes its scattering properties in response to temperature was incorporated into the central part of the planar waveguide structure. A microscope glass slide was initially used as the planar waveguide structure in this work. This type of simple thick planar waveguide has been used for example in the implementation of different biosensing devices [9]; however, the different described elements, thermoresponsive and luminescent films, could be easily integrated in more sophisticated planar waveguiding structures. The thin layer of LCP presented a highly scattering morphology at low temperature and a transition to an isotropic state at higher temperature, at the clearing point (T_c). To apply this layer on top of the waveguide, first, a photopolymerizable mixture comprising 99 wt% of A6OCB monoacrylate and 1 wt% of RM82 diacrylate was prepared. The monofunctional promesogenic monomer A6OCB was chosen as the main component of the mixture since the resultant side chain liquid crystal polymer (SCLCP), obtained after radical polymerization, presented liquid crystalline behavior [52]. The small amount of mesogenic diacrylate added to the mixture was incorporated to stabilize the resultant film and to hinder dewetting upon heating at high temperature. To enable photopolymerization, a small amount (3 wt%) of UV photoinitiator was added. The prepolymer mixture presented a transition from the crystalline solid to an isotropic liquid at 70 °C, as determined by POM, essentially at the same temperature as the majority monomer component A6OCB. A thin film with a fixed square-shape geometry of the photopolymerizable mixture was applied on top of the waveguide, in its central part, as schematically shown in Figure 1. Film thickness was fixed by using 50- μm spacers dispersed in the mixture and a second fluorinated glass plate, as described in the Section 2. Exposure at 75 °C to UV light led to a noticeable change in the transmission properties of the material. The sample, which was transparent at 75 °C before UV exposure, became turbid in seconds just after actinic light was switched on, keeping the sample at a constant temperature of 75 °C. Excitation of the photoinitiator with UV light produced radicals that initiated the chain growth polymerization of the acrylate monomers. Once the photocuring process (see the Section 2) was completed, the sample was cooled down to RT keeping the same turbid appearance (see Figure 2a), and the fluorinated glass was carefully removed, leaving a highly scattering solid polymeric film attached to the waveguide.

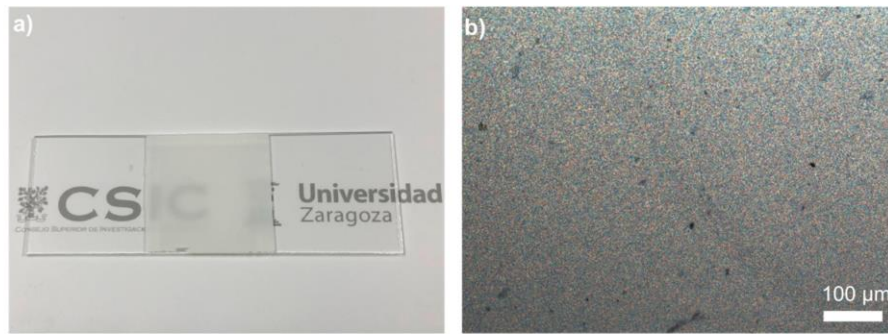


Figure 2. (a) Photograph of a 50 μm -thick sample of LCP (26 mm \times 26 mm) applied in the central part of a glass microscope slide (76 mm \times 26 mm). The LCP film shows high turbidity at RT when compared to the bare glass (at the two sides of the LCP). (b) POM image of an LCP thin film sample at RT.

As mentioned before, cyanobiphenyl acrylate monomers tend to lead to polymers showing liquid crystalline behavior [52]. POM observation of a thin LCP film as a function of temperature revealed a birefringent grainy texture in the cured samples at the curing temperature (75 $^{\circ}\text{C}$), as shown in Figure 2b. The birefringent texture, observed at the POM, totally disappeared when heating at 134 $^{\circ}\text{C}$, at which isotropization takes place. Cooling down below the clearing point recovered essentially the same birefringent fine grainy texture as the as-polymerized film. This recovery was ascribed to the slightly cross-linked nature of the system. The presence of crosslinking sites provided memory to the system, typical of LC elastomers, when it was heated above its isotropization temperature and then cooled back to the mesophase range. The heating and cooling process was repeated several times (>20 times), showing the same optical qualitative behavior with no performance degradation. Indeed, the material showed good thermal stability at temperatures well above this transition temperature to the isotropic state, as assessed by TGA, giving an onset of the decomposition weight loss curve at temperatures above 300 $^{\circ}\text{C}$ (see Figure S1 in the Supplementary Information).

In order to characterize the temperature dependence of the light transmission of the constructed thermosensitive waveguide, the sensing area, provided with the LCP layer, was placed on top of a temperature-controlled metallic block. In this simplified configuration (Figure 3a,b), light was coupled into the waveguide by placing an LED (520-nm peak wavelength) at the edge of the waveguide. This is an efficient way to couple energy into waveguides that can be even further optimized by the use of lenses or reflectors at the LED-waveguide edge interface [9]. A Si photodetector was placed at the other extreme of the planar waveguide, enabling quantification of the light reaching this side. The inset of Figure 3b shows a plot of the light intensity measured at the edge of the waveguide as a function of the temperature of the sensing region. It can be seen that the level of light reaching the detector remained low at temperatures below 126 $^{\circ}\text{C}$ and gradually increased as temperatures went above this temperature. At temperatures below 126 $^{\circ}\text{C}$, within the liquid crystal mesophase, the light travelling from the LED through the waveguide reached the highly scattering LCP film, coupling out light, as can be identified by its green glowing appearance (see Figure 3a). Glow strongly attenuates from left to right in the image, showing the efficiency of the LCP extracting light from the waveguide. As temperature increased from 126–134 $^{\circ}\text{C}$, the intensity of transmitted light gradually increased as the scattering of the LCP layer progressively decreased. At temperatures above 134 $^{\circ}\text{C}$, the LCP layer became transparent (see Figure 3b) and light remained waveguided, reaching the waveguide extreme. The large ratio between the light intensity measured at the high and the low temperature states demonstrated that only a small portion of the light coupled into the waveguide modes reached the extreme of the planar waveguide in the low-temperature, high-scattering state of the LCP layer, demonstrating its good performance as a thermo-optical valve.

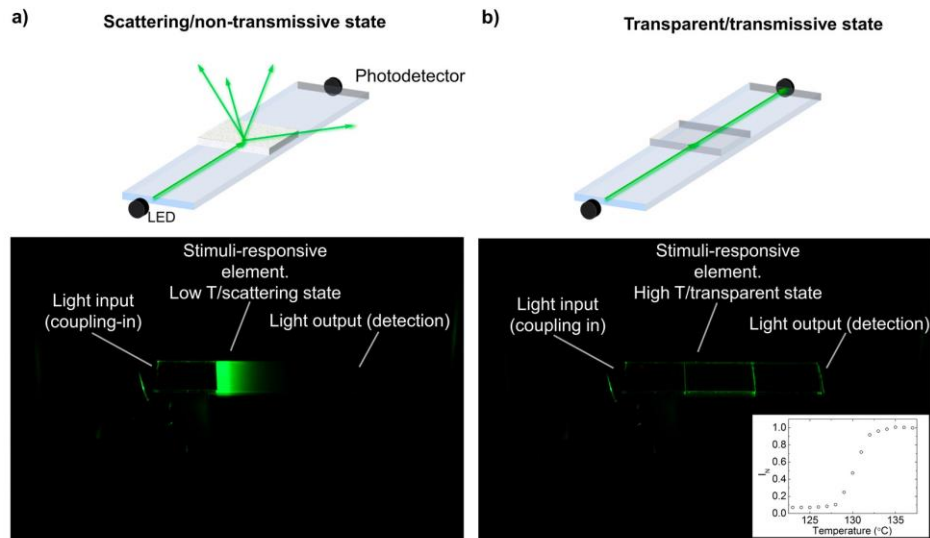


Figure 3. (a) and (b) Schematic representation (top) and photograph (bottom) of the optical planar waveguide sensor using a green LED (peak wavelength of 520 nm) to couple light into the waveguide at one of the waveguide extremes and a photodetector to measure transmitted light at the other extreme (a) in the scattering/non-transmissive state, at low temperature, and (b) in the transparent/transmissive state, at high temperature. The inset in (b) shows a plot of the green light intensity measured at the detection edge of the waveguide as a function of the temperature of the sensing area.

Trying to simplify the injection of light into the waveguided modes, the incorporation of an alternative light coupling-in system was attempted in the waveguide sensor structure. Traditional methods to couple light into a planar waveguide include the incorporation of diffractive gratings or the use of coupling prisms in combination with lasers [53]. Light can also be coupled by the incorporation of luminescent entities (organic dyes, phosphors, quantum dots, etc.) in the waveguide structure [54,55]. Light with a wavelength matching the absorption band of the luminescent layer can be absorbed when passing through it. The absorbed light can be re-emitted at longer wavelengths in all directions. Part of this emitted light is trapped in the waveguided structure by total internal reflection (TIR), at the waveguide-air interface. Emission light rays travelling through the waveguide and reaching this interface at an angle above the critical angle θ_c for TIR ($\theta_c = n_s/n_{air}$; being n_s and n_{air} the refractive indexes of substrate and air, respectively) cannot propagate in the air. As a result, energy remained confined in the waveguide, that is, this emitted light was coupled into its propagation modes. This principle has also been recently used by Bollgruen et al. to couple light in channel waveguides in plastic foils [26]. Despite being less efficient, in terms of energy coupled, in comparison to grating and prism coupling systems, luminescent couplers constitute a simple way to implement and a simple-to-use principle without the need for complex optical alignment systems or specific light sources (e.g., lasers). The use of sunlight as the excitation light source is even possible.

We made use of this principle by incorporating, through digital inkjet printing, a luminescent layer that acted as a light coupling-in element for the waveguide when remotely excited with light of the appropriate wavelength (see Figure 4). Besides, the digital character of inkjet deposition enabled precise placement of the light coupling-in element. To implement this, a luminescent layer of a hybrid organic-inorganic material containing the F27 chromophore (HRI-F27-02) was applied in one side of the planar waveguide sensor structure. This dye (molecular structure shown in Figure 4a) emitted green light when excited at shorter wavelengths as shown in the emission spectrum of Figure S2 in the Supplementary Information. The emitted light was partly coupled into the waveguide structure propagating towards the thermo-optical sensor. Printing of these continuous areas was achieved

with our printer by using 2880 dpi in the substrate moving direction, while keeping 185 dpi in the perpendicular direction. These printing conditions resulted in drop coalescence leading to continuous features in the substrate, as previously described elsewhere [38]. Besides the luminescent light coupling-in element, we incorporated a second inkjet-printed luminescent layer (HRI-RhodB-02) on the other side of the planar waveguide sensor structure. This second element contained Rhodamine B (molecular structure shown in Figure 4b), a dye that absorbs in the green region of the spectra and emits orange-red light, as shown in the emission spectrum of Figure S3 in the Supplementary Information. The light emitted by this element was partly coupled out into the air, becoming visible and therefore acting as a luminescent temperature readout enabling remote sensing. As in the case of the light coupling-in element, this second mark can also be digitally structured, as we have previously demonstrated [38].

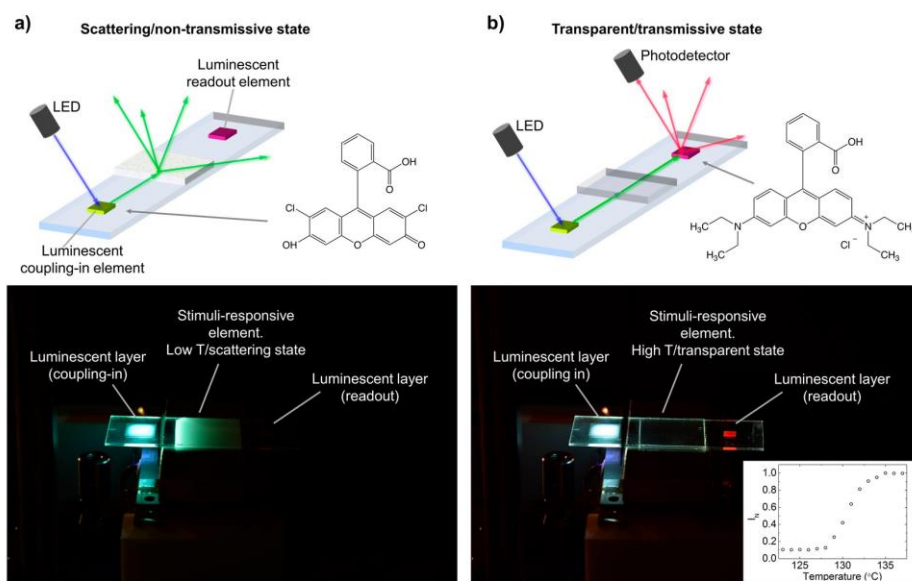


Figure 4. (a,b) Schematic representation (top) and photograph (bottom) of the optical planar waveguide sensor including a luminescent coupling element and a luminescent temperature readout element (a) in the scattering/non-transmissive state, at low temperature, and (b) in the transmissive state, at high temperature. Light from a UV LED (peak wavelength at 365 nm) excites from the top the photocured HRI-F27-02 layer that emits light, partly coupled in the planar waveguide and travelling towards the thermoresponsive liquid crystal polymer sensor material. Waveguided light reaching the HRI-RhodB-02 layer is partly absorbed and re-emitted as orange-red light. A photodetector measures the red light (633 nm) intensity emitted by this luminescent layer as a function of the LCP layer temperature. The molecular structures of F27 and RhodB are shown in (a) and (b), respectively. The inset in (b) shows a plot of the emitted red light (633 nm) measured as a function of temperature at the sensing region.

In this case, light was coupled into the planar waveguide structure by exciting, with UV light coming from an LED (Thorlabs M362L2-C1, peak wavelength at 365 nm, spectrum of reference [56]) placed on top, the HRI-F27-02 layer previously deposited on one side of the waveguide. Part of the coupled light propagated and reached the thermo-optical element that regulated, as a function of temperature, the light passing to the other extreme of the planar waveguide structure where the mark made with HRI-RhodB-02 was placed. The intensity of the luminescence of this HRI-RhodB-02 mark (measured at 633 nm by using a Si photodetector provided with an interferential filter with 10-nm FWHM) as a function of temperature of the thermo-optical layer is presented in the inset of Figure 4b. A low level of red emitted light was measured at temperatures below 126 °C, temperatures at which

the LCP was in the high scattering state. The light intensity increased as temperature went above 126 °C and reached a plateau level at temperatures higher than 134 °C. As in the previously-described configuration, a sufficient ratio between the light intensity at the high and the low temperature of around 10 was measured, demonstrating the suitability of the coupling and the readout abilities using the luminescence to implement the temperature optical planar sensor. A qualitatively similar behavior was observed when excitation of the HRI-F27-02 layer was done with blue light of 455 nm, instead of using UV light (see Figure S4 in the Supplementary Information).

The employed photoacid-catalyzed luminescent inks were demonstrated to be very versatile in terms of their compatibility with different types of substrates [38]. As mentioned, printing on polymeric substrates such as poly(ethylene terephthalate) (PET), acrylonitrile butadiene styrene (ABS), or polycarbonate (PC) has been demonstrated to lead to thin layers of hybrid material showing good adhesion, as well as mechanically flexible. Trying to expand the scope of the present study and show the possibilities of the disclosed sensor, we have explored its implementation in substrates different from glass. As a proof of principle, the sensor was built on a cyclic olefin copolymer (COP) substrate that acts as a planar waveguide. Inkjet printing of the luminescent materials was directly carried out in the as-cleaned substrates without further treatment. Similarly, as done with the glass substrates, a continuous area of luminescent ink containing F27 dye was applied and cured. Excitation of this layer with UV light coupled green light into the COP waveguide. The luminescent indicator printed using the Rhodamine B-containing ink was digitally applied and cured. The thermoresponsive liquid crystal mixture was applied and cured using a similar protocol to that used in the glass-based sensors. A qualitatively similar response was obtained in this prototype compared to that observed in glass. Both a rigid COP waveguide (1.2 mm thick) and a flexible version of the sensor, based on a thin film of COP that can be easily conformed to sense curved surfaces, were generated, as shown in Figure 5.

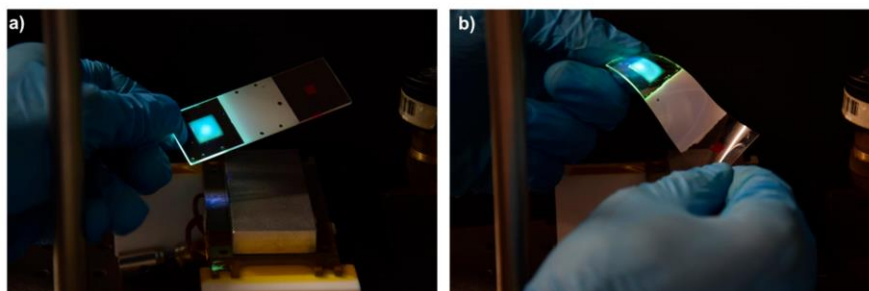


Figure 5. (a) Optical planar waveguide sensor including a luminescent coupling element and a luminescent temperature readout element fabricated on (a) a rigid cyclic olefin polymer (COP) substrate and (b) a flexible COP thin sheet. The sensor, at RT, is in the low T/high scattering state, and the luminescent coupling element is excited with a UV LED placed on top.

4. Conclusions

An optical planar waveguide temperature sensor integrating digitally-printed luminescent light coupling-in and readout elements in the waveguide was presented. The remote excitation of the first luminescent element enabled the coupling of light into the planar waveguide, without the need for special alignment of the light source. When waveguided light propagated through the sensing region, a thermoresponsive LCP regulated the amount of light reaching the readout region. By matching the emission and excitation properties of the luminescent light coupling-in and readout elements, respectively, quantification of the temperature of the sensing region can be carried out through simple remote luminescence intensity measurements of the readout element. The digital character of inkjet technology, allowing the selective deposition of luminescent elements at precise locations and with well-defined geometries, offers great potential for the integration of light coupling-in and miniaturized readout luminescent elements in optical planar waveguide sensors. The hybrid organic-inorganic

nature of the photoacid catalyzed formulations employed in the luminescent inks has led to deposits with excellent adhesion to substrates of different natures such as rigid glass sheets or flexible COP thin films. Despite the range of temperature of the presented sensor, around 130 °C, being narrow, by using other thermoresponsive LC materials, sensors with tailored properties and other ranges of sensing temperature could be generated using the same architecture. As a result, the fabrication platform, which included materials and processing techniques, can lead to flexible, compact, and robust digital integration of different elements to generate fully-reversible, cost-effective, portable, and versatile sensing devices. The prepared sensor, based on luminescence, can be remotely addressed and read using external photonic elements without complex optical alignment, therefore having great potential in diverse application areas including electronics, automotive, aerospace, environment, or health.

Supplementary Materials: Supplementary materials can be found at <http://www.mdpi.com/1424-8220/19/13/2856/s1>. Figure S1: TGA analysis and derivative of the TGA curve for the photocured LCP, Figure S2: Photoluminescence emission spectrum of a deposited film of HRI-F27-02 cured under mild vacuum conditions. Photoluminescence emission spectrum is taken with excitation at 390 nm, Figure S3: Photoluminescence emission spectrum of a deposited film of HRI-RhodB-02 cured under mild vacuum conditions. Photoluminescence emission spectrum is taken with excitation at 530 nm, Figure S4: Optical planar waveguide sensor including a luminescent coupling element and a luminescent temperature readout element (a) in the non-transmissive state, at low temperature, and (b) in the transmissive state, at high temperature. Light from a blue LED (peak wavelength at 455 nm), excites the photocured HRI-F27-02 layer that emits light, partly coupled in the planar waveguide and travelling towards the thermoresponsive liquid crystal polymer sensor material. Waveguided light reaching the HRI-RhodB-02 layer is partly absorbed and re-emitted as orange-red light. A photodetector measures the red light (632 nm) intensity emitted by this emissive layer as a function of the LCP layer temperature.

Author Contributions: Conceptualization, J.A. and C.S.-S.; funding acquisition, C.S.-S.; investigation, J.A., M.L.-V. and R.A.; methodology, J.A., M.L.-V., R.A. and C.S.-S.; supervision, C.S.-S.; writing, original draft, J.A. and C.S.-S.; writing, review and editing, M.L.-V. and R.A.

Funding: This research was funded by the Spanish Ministerio de Ciencia, Innovación y Universidades for Project BIO2017-84246-C2-1-R, Gobierno de Aragón, FEDER (EU).

Conflicts of Interest: The authors declare no conflict of interest.

References

1. Wang, X.-D.; Wolfbeis, O.S. Fiber-Optic Chemical Sensors and Biosensors (2013–2015). *Anal. Chem.* **2016**, *88*, 203–227. [[CrossRef](#)] [[PubMed](#)]
2. Pospíšilová, M.; Kuncová, G.; Trögl, J. Fiber-Optic Chemical Sensors and Fiber-Optic Bio-Sensors. *Sensors* **2015**, *15*, 25208–25259. [[CrossRef](#)] [[PubMed](#)]
3. Caucheteur, C.; Guo, T.; Albert, J. Review of plasmonic fiber optic biochemical sensors: Improving the limit of detection. *Anal. Bioanal. Chem.* **2015**, *407*, 3883–3897. [[CrossRef](#)] [[PubMed](#)]
4. Matias, I.R.; Ikezawa, S.; Corres, J. *Fiber Optic Sensors: Current Status and Future Possibilities*; Springer International Publishing: Basel, Switzerland, 2017.
5. Udd, E.; Spillman, W.B. *Fiber Optic Sensors: An Introduction for Engineers and Scientists*, 2nd ed.; Wiley: New York, NY, USA, 2011.
6. Rivero, P.J.; Goicoechea, J.; Arregui, F.J. Optical Fiber Sensors Based on Polymeric Sensitive Coatings. *Polymers* **2018**, *10*, 280. [[CrossRef](#)] [[PubMed](#)]
7. Wang, X.-D.; Wolfbeis, O.S.; Meier, R.J. Luminescent probes and sensors for temperature. *Chem. Soc. Rev.* **2014**, *42*, 7834. [[CrossRef](#)] [[PubMed](#)]
8. Budach, W.; Abel, A.P.; Bruno, A.E.; Neuschäfer, D. Planar Waveguides as High-Performance Sensing Platforms for Fluorescence-Based Multiplexed Oligonucleotide Hybridization Assays. *Anal. Chem.* **1999**, *71*, 3347–3355. [[CrossRef](#)]
9. Shi, H.-C.; Song, B.-D.; Long, F.; Zhou, X.-H.; H, M.; Lv, Q.; Yang, H.-Y. Automated Online Optical Biosensing System for Continuous Real-Time Determination of Microcystin-LR with High Sensitivity and Specificity: Early Warning for Cyanotoxin Risk in Drinking Water Sources. *Environ. Sci. Technol.* **2013**, *47*, 4433–4441. [[CrossRef](#)]
10. Mukundan, H.; Anderson, A.S.; Grace, W.K.; Grace, J.M.; Hartman, N.; Martinez, J.S.; Swanson, B.I. Waveguide-Based Biosensors for Pathogen Detection. *Sensors* **2009**, *9*, 5783–5809. [[CrossRef](#)]

11. Savvate'ev, V.; Chen-Esterlit, Z.; Aylott, J.W.; Choudhury, B.; Kim, C.H.; Zou, L.; Friedl, J.H.; Shinar, R.; Shinar, J.; Kopelman, R. Integrated organic light-emitting device/fluorescence-based chemical sensors. *Appl. Phys. Lett.* **2002**, *81*, 4652–4654. [[CrossRef](#)]
12. Klantsataya, E.; Jia, P.; Ebendorff-Heidepriem, H.; Monro, T.; François, A. Plasmonic Fiber Optic Refractometric Sensors: From Conventional Architectures to Recent Design Trends. *Sensors* **2017**, *17*, 12. [[CrossRef](#)]
13. Gruber, P.; Marques, P.C.; Szita, N.; Mayr, T. Integration and application of optical chemical sensors in microbio-reactors. *Lab Chip* **2017**, *17*, 2693–2712. [[CrossRef](#)] [[PubMed](#)]
14. Pfeiffer, S.A.; Nagl, S. Microfluidic platforms employing integrated fluorescent or luminescent chemical sensors: A review of methods, scope and applications. *Methods Appl. Fluoresc.* **2015**, *3*, 034003. [[CrossRef](#)] [[PubMed](#)]
15. Guo, J.; Niu, M.; Yang, C. Highly flexible and stretchable optical strain sensing for human motion detection. *Optica* **2017**, *4*, 1285–1288. [[CrossRef](#)]
16. Choi, M.; Choi, J.W.; Kim, S.; Nizamoglu, S.; Hahn, S.K.; Yun, S.H. Light-guiding hydrogels for cell-based sensing and optogenetic synthesis in vivo. *Nature Photon.* **2013**, *7*, 987–994. [[CrossRef](#)] [[PubMed](#)]
17. Yang, H.; Gijjs, M.A.M. Micro-optics for microfluidic analytical applications. *Chem. Soc. Rev.* **2018**, *47*, 1391. [[CrossRef](#)] [[PubMed](#)]
18. To, C.; Hellebrekers, T.L.; Park, Y.-L. Highly Stretchable Optical Sensors for Pressure, Strain, and Curvature Measurement. In Proceedings of the IEEE/RSJ International Conference on Intelligent Robots and Systems (IROS), Hamburg, Germany, 28 September–2 October 2015.
19. Hoffmann, G.-A.; Wolfer, T.; Zeitler, J.; Franke, J.; Suttman, O.; Overmeyer, L. Manufacturing of polymer optical waveguides using self-assembly effect on pre-conditioned 3D-thermoformed flexible substrates. In Proceedings of the Advanced Fabrication Technologies for Micro/Nano Optics and Photonics X, San Francisco, CA, USA, 29 January–1 February 2017; SPIE: Bellingham, WA, USA, 2017; Volume 1011503.
20. Körner, M.; Prucker, O.; Rühle, J. Polymer hybrid materials for planar optronic systems. In Proceedings of the Optical Systems Design 2015: Optical Design and Engineering VI, Jena, Germany, 7–10 September 2015; SPIE: Bellingham, WA, USA, 2015; Volume 96262.
21. Kelb, C.; Rother, R.; Schuler, A.-K.; Hinkelmann, M.; Rahlves, M.; Prucker, O.; Müller, C.; Rühle, J.; Reithmeier, E.; Roth, B. Manufacturing of embedded multimode waveguides by reactive lamination of cyclic olefin polymer and polymethylmethacrylate. *Opt. Eng.* **2016**, *55*, 037103. [[CrossRef](#)]
22. Samusjew, A.; Kratzer, M.; Moser, A.; Teichert, C.; Krawczyk, K.K.; Griesser, T. Inkjet Printing of Soft, Stretchable Optical Waveguides through the Photopolymerization of High-Profile Linear Patterns. *ACS Appl. Mater. Interfaces* **2017**, *9*, 4941–4947. [[CrossRef](#)] [[PubMed](#)]
23. Bollgruen, P.; Wolfer, T.; Gleissner, U.; Mager, D.; Megnin, C.; Overmeyer, L.; Hanemann, T.; Korvink, J.G. Ink-jet printed optical waveguides. *Flex. Print. Electron.* **2017**, *2*, 045003. [[CrossRef](#)]
24. Alamán, J.; López-Valdeolivas, M.; Alicante, R.; Medel, F.J.; Silva-Treviño, J.; Peña, J.I.; Sánchez-Somolinos, C. Photoacid catalyzed organic–inorganic hybrid inks for the manufacturing of inkjet-printed photonic devices. *J. Mater. Chem. C* **2018**, *6*, 3882–3894. [[CrossRef](#)]
25. Alamán, J.; Alicante, R.; Peña, J.; Sánchez-Somolinos, C. Inkjet Printing of Functional Materials for Optical and Photonic Applications. *Materials* **2016**, *9*, 910. [[CrossRef](#)]
26. Bollgruen, P.; Gleissner, U.; Wolfer, T.; Megnin, C.; Mager, D.; Overmeyer, L.; Korvink, J.G.; Hanemann, T. Ink-jet printed fluorescent materials as light sources for planar optical waveguides on polymer foils. *Opt. Eng.* **2016**, *55*, 107107. [[CrossRef](#)]
27. Liu, L.; Zhou, X.; Wilkinson, J.S.; Hua, P.; Song, B.; Shi, H. Integrated optical waveguide-based fluorescent immunosensor for fast and sensitive detection of microcystin-LR in lakes: Optimization and Analysis. *Sci. Rep.* **2017**, *7*, 3655. [[CrossRef](#)] [[PubMed](#)]
28. Algorri, J.; Urruchi, V.; Bennis, N.; Sánchez-Pena, J. A Novel High-Sensitivity, Low-Power, Liquid Crystal Temperature Sensor. *Sensors* **2014**, *14*, 6571–6583. [[CrossRef](#)] [[PubMed](#)]
29. Torres, J.; García-Cámara, B.; Pérez, I.; Urruchi, V.; Sánchez-Pena, J. Wireless Temperature Sensor Based on a Nematic Liquid Crystal Cell as Variable Capacitance. *Sensors* **2018**, *18*, 3436. [[CrossRef](#)] [[PubMed](#)]
30. Li, Y.; Liu, Y.; Luo, D. Optical thermal sensor based on cholesteric film refilled with mixture of toluene and ethanol. *Opt. Express* **2017**, *25*, 26349–26355. [[CrossRef](#)] [[PubMed](#)]
31. Oh, S.-W.; Kim, S.-H.; Yoon, T.-H. Thermal control of transmission property by phase transition in cholesteric liquid crystals. *J. Mater. Chem. C* **2018**, *6*, 6520. [[CrossRef](#)]

32. Herzer, N.; Guneyesu, H.; Davies, D.J.D.; Yildirim, D.; Vaccaro, A.R.; Broer, D.J.; Bastiaansen, C.W.M.; Schenning, A.P.H.J. Printable Optical Sensors Based on H-Bonded Supramolecular Cholesteric Liquid Crystal Networks. *J. Am. Chem. Soc.* **2012**, *134*, 7608–7611. [[CrossRef](#)]
33. Stumpel, J.E.; Wouters, C.; Herzer, N.; Ziegler, J.; Broer, D.J.; Bastiaansen, C.W.M.; Schenning, A.P.H.J. An Optical Sensor for Volatile Amines Based on an Inkjet-Printed, Hydrogen-Bonded, Cholesteric Liquid Crystalline Film. *Adv. Opt. Mater.* **2014**, *2*, 459–464. [[CrossRef](#)]
34. Davies, D.J.D.; Vaccaro, A.R.; Morris, S.M.; Herzer, N.; Schenning, A.P.H.J.; Bastiaansen, C.W.M. A Printable Optical Time-Temperature Integrator Based on Shape Memory in a Chiral Nematic Polymer Network. *Adv. Funct. Mater.* **2013**, *23*, 2723–2727. [[CrossRef](#)]
35. Schenning, A.; Crawford, G.P.; Broer, D.J. *Liquid Crystal Sensors*; Taylor & Francis Group: Boca Raton, FL, USA, 2018.
36. Moirangthem, M.; Arts, R.; Merckx, M.; Schenning, A.P.H.J. An Optical Sensor Based on a Photonic Polymer Film to Detect Calcium in Serum. *Adv. Funct. Mater.* **2016**, *26*, 1154–1160. [[CrossRef](#)]
37. Stumpel, J.E.; Broer, D.J.; Schenning, A.P.H.J. Stimuli-responsive photonic polymer coatings. *Chem. Commun.* **2014**, *50*, 15839–15848. [[CrossRef](#)] [[PubMed](#)]
38. Alamán, J.; López-Valdeolivas, M.; Alicante, R.; Peña, J.; Sánchez-Somolinos, C. Digital Luminescence Patterning via Inkjet Printing of a Photoacid Catalysed Organic-Inorganic Hybrid Formulation. *Polymers* **2019**, *11*, 430. [[CrossRef](#)] [[PubMed](#)]
39. Homola, T.; Shekargoftar, M.; Dzik, P.; Krumpolec, R.; Durasova, Z.; Vesely, M.; Cernak, M. Low-temperature (70 °C) ambient air plasma-fabrication of inkjet-printed mesoporous TiO₂ flexible photoanodes. *Flex. Print. Electron.* **2017**, *2*, 035010. [[CrossRef](#)]
40. Ma, S.; Ribeiro, F.; Powell, K.; Lutian, J.; Møller, C.; Large, T.; Holbery, J. Fabrication of Novel Transparent Touch Sensing Device via Drop-on-Demand Inkjet Printing Technique. *ACS Appl. Mater. Interfaces* **2015**, *7*, 21628–21633. [[CrossRef](#)] [[PubMed](#)]
41. Sun, J.Z.; Guo, Y.Z.; Cui, B.; Chu, F.Q.; Li, H.Z.; Li, Y.; He, M.; Ding, D.; Liu, R.P.; Li, L.H.; et al. Inkjet printing bendable circuits based on an oil-water interface reaction. *Appl. Surf. Sci.* **2018**, *445*, 391–397. [[CrossRef](#)]
42. Sun, J.Z.; Yun, C.; Cui, B.; Li, P.; Liu, G.; Wang, X.; Chu, F. A Facile Approach for Fabricating Microstructured Surface Based on Etched Template by Inkjet Printing Technology. *Polymers* **2018**, *10*, 1209. [[CrossRef](#)] [[PubMed](#)]
43. Sun, J.Z.; Cui, B.; Chu, F.Q.; Yun, C.H.; He, M.; Li, L.H.; Song, Y.L. Printable nanomaterials for the fabrication of high-performance supercapacitors. *Nanomaterials* **2018**, *8*, 528. [[CrossRef](#)]
44. Singh, M.; Haverinen, H.M.; Dhagat, P.; Jabbour, G.E. Inkjet Printing-Process and Its Applications. *Adv. Mater.* **2010**, *22*, 673–685. [[CrossRef](#)]
45. Hutchings, I.M.; Martin, G.D. *Inkjet Technology for Digital Fabrication*; Wiley: Chichester, UK, 2013.
46. Fink, C.K.; Nakamura, K.; Ichimura, S.; Jenkins, S.J. Silicon oxidation by ozone. *J. Phys. Condens. Matter* **2009**, *21*, 183001. [[CrossRef](#)]
47. Trimbach, D.; Feldman, K.; Spencer, N.D.; Broer, D.J.; Bastiaansen, C.W.M. Block Copolymer Thermoplastic Elastomers for Microcontact Printing. *Langmuir* **2003**, *19*, 10957–10961. [[CrossRef](#)]
48. Hilgendorff, M.; Sundström, V. Ultrafast electron injection and recombination dynamics of dye sensitised TiO₂ particles. *Chem. Phys. Lett.* **1998**, *287*, 709–713. [[CrossRef](#)]
49. Nagachandra, K.H.; Mannekutla, J.R.; Amarayya, S.M.; Inamdar, S.R. Solvent effect on the spectral properties of dipolar laser dyes: Evaluation of ground and excited state dipole moments. *Eur. J. Chem.* **2012**, *3*, 163–171. [[CrossRef](#)]
50. Zareba-Grodź, I.; Pazik, R.; Hermanowicz, K.; Streck, W.; Maruszewski, K. Preparation and optical properties of hybrid coatings based on epoxy-modified silane and rhodamine B. *J. Lumin.* **2006**, *119*, 148–152. [[CrossRef](#)]
51. Chemtob, A.; Versace, D.-L.; Belon, C.; Croutxé-Barghorn, C.; Rigolet, S. Concomitant Organic–Inorganic UV-Curing Catalyzed by Photoacids. *Macromolecules* **2008**, *41*, 7390–7398. [[CrossRef](#)]
52. Craig, A.A.; Imrie, C.T. Effect of Backbone Flexibility on the Thermal Properties of Side-Group Liquid-Crystal Polymers. *Macromolecules* **1999**, *32*, 6215–6220. [[CrossRef](#)]
53. Zappe, H. *Fundamentals of Micro-Optics*, 1st ed.; Cambridge University Press: Cambridge, UK, 2010.
54. Goetzberger, A.; Greubel, W. Solar-Energy Conversion with Fluorescent Collectors. *App. Phys.* **1977**, *14*, 123–139. [[CrossRef](#)]

55. Debije, M.G.; Verbunt, P.P.C. Thirty Years of Luminescent Solar Concentrator Research: Solar Energy for the Built Environment. *Adv. Energy Mater.* **2012**, *2*, 12–35. [[CrossRef](#)]
56. Thorlabs. LED Emission Spectrum. Available online: https://www.thorlabs.com/images/popupImages/M365L2_Spectrum.gif (accessed on 19 June 2019).



© 2019 by the authors. Licensee MDPI, Basel, Switzerland. This article is an open access article distributed under the terms and conditions of the Creative Commons Attribution (CC BY) license (<http://creativecommons.org/licenses/by/4.0/>).

Optical Planar Waveguide Sensor with Integrated Digitally-Printed Light Coupling-in and Readout Elements

Jorge Alamán ^{1,2}, María López-Valdeolivas ¹, Raquel Alicante ¹ and Carlos Sánchez-Somolinos ^{1,3,*}

¹ Instituto de Ciencia de Materiales de Aragón (ICMA), CSIC-Universidad de Zaragoza, Departamento de Física de la Materia Condensada, Zaragoza 50009, Spain; m_lopez@unizar.es (M.L.-V.); raquela@unizar.es (R.A.)

² BSH Electrodomésticos España, S.A., Polígono Industrial de PLA-ZA, Ronda del Canal Imperial de Aragón, 50197 Zaragoza, Spain; jorge.alaman@bshg.com

³ Centro de Investigación Biomédica en Red de Bioingeniería, Biomateriales y Nanomedicina (CIBER-BBN), C Mariano Esquillor s.n., Zaragoza 50018, Spain

* Correspondence author: carlos.s@csic.es; Tel.: +34-8765-53770

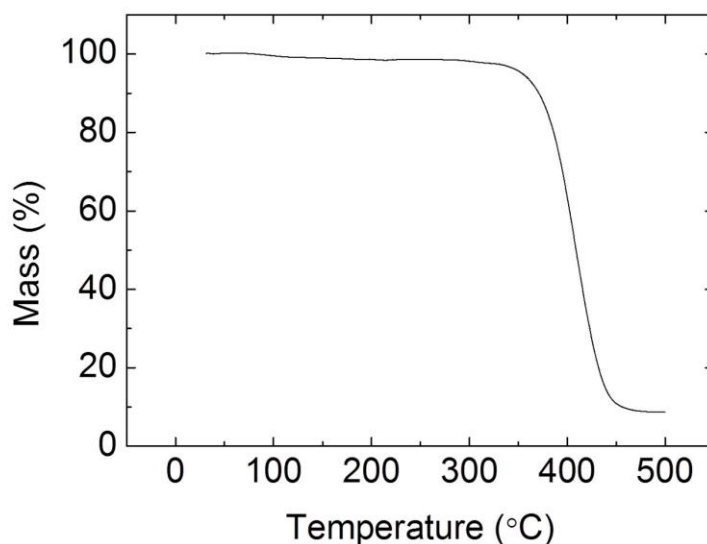


Figure S1. TGA analysis and derivative of the TGA curve for the photocured LCP.

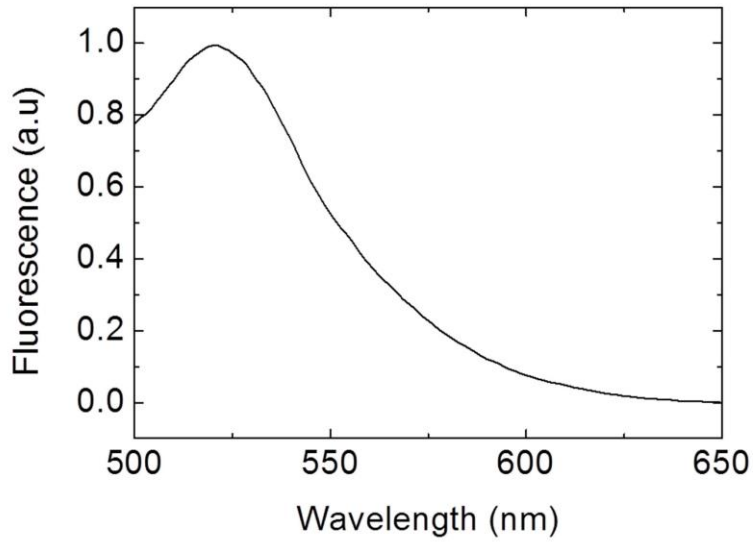


Figure S2. Photoluminescence emission spectrum of a deposited film of HRI-F27-02 cured under mild vacuum conditions. Photoluminescence emission spectrum is taken with excitation at 390 nm.

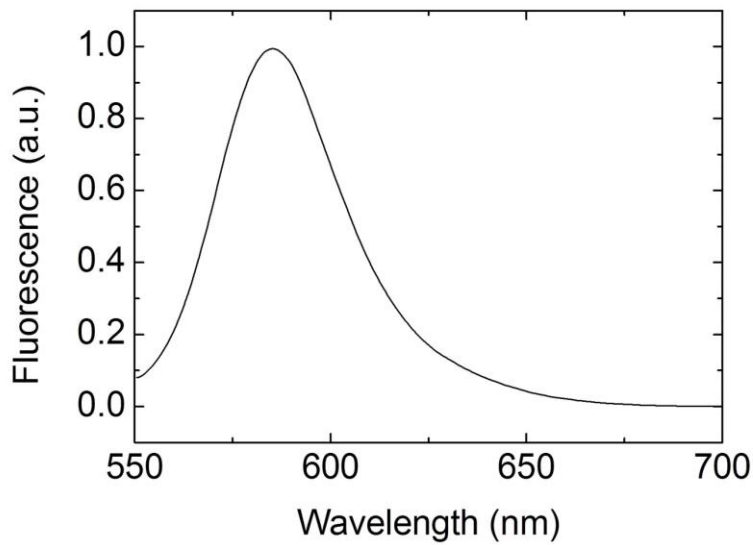


Figure S3. Photoluminescence emission spectrum of a deposited film of HRI-RhodB-02 cured under mild vacuum conditions. Photoluminescence emission spectrum is taken with excitation at 530 nm.

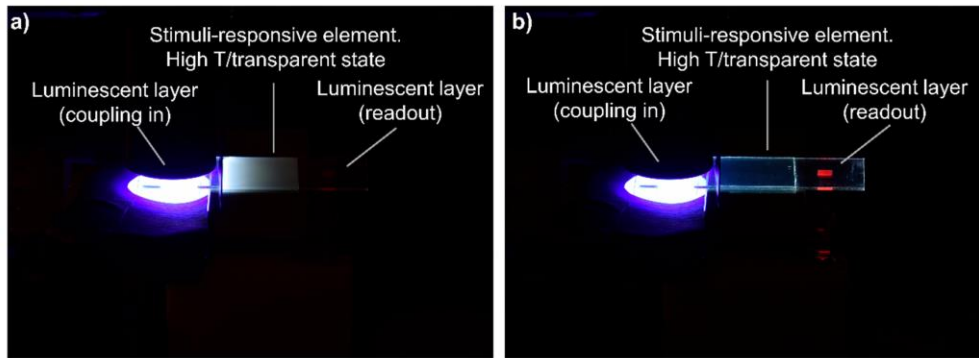


Figure S4. Optical planar waveguide sensor including a luminescent coupling element and a luminescent temperature readout element a) in the non-transmissive state, at low temperature, and b) in the transmissive state, at high temperature. Light from a blue LED (peak wavelength at 455 nm), excites the photocured HRI-F27-02 layer that emits light, partly coupled in the planar waveguide and travelling towards the thermoresponsive liquid crystal polymer sensor material. Waveguided light reaching the HRI-RhodB-02 layer is partly absorbed and re-emitted as orange-red light. A photodetector measures the red light (632 nm) intensity emitted by this emissive layer as a function of the LCP layer temperature.

5. Publication 5.

Journal: Applied Surface Science

Title: Facile Fabrication of Microlenses with Controlled Geometrical Characteristics by Inkjet Printing on Nanostructured surfaces prepared by combustion chemical vapour deposition



Full Length Article

Facile fabrication of microlenses with controlled geometrical characteristics by inkjet printing on nanostructured surfaces prepared by combustion chemical vapour deposition



Jorge Alamán^{a,b}, Ana María López-Villuendas^a, María López-Valdeolivas^a, María Pilar Arroyo^c, Nieves Andrés^c, Carlos Sánchez-Somolinos^{a,d,*}

^a Instituto de Ciencia de Materiales de Aragón (ICMA), CSIC-Universidad de Zaragoza, Departamento de Física de la Materia Condensada, Zaragoza, Spain

^b BSH Electrodomésticos España, S.A., Polígono Industrial de PLA-ZA, Ronda del Canal Imperial de Aragón, 18-20, 50197 Zaragoza, Spain

^c Instituto Universitario de Investigación en Ingeniería de Aragón (I3A), Universidad de Zaragoza, Departamento de Física Aplicada, Zaragoza, Spain

^d CIBER in Bioengineering, Biomaterials and Nanomedicine (CIBER-BBN), Spain

ARTICLE INFO

Keywords:

Photoacid catalyzed polymerization
Inkjet printing
Microlenses
Combustion chemical vapour deposition
Superhydrophobic surfaces

ABSTRACT

Precise positioning of microlenses with well-defined optical characteristics is key in the further development of CCD cameras, biosensors or optical fiber interconnects. Inkjet printing enables accurate microfabrication of microlenses however inks generally employed for this purpose contain solvents that need to be evaporated before the lens solidification process. Besides, the receiving substrate needs to be conditioned, sometimes using complex photolithographic steps to lead to large contact angles of the deposited ink drop that are needed to attain large numerical aperture microlenses. This paper describes the fabrication of microlenses with controlled geometrical characteristics by inkjet printing a solvent-free photocurable formulation. The employed photoacid catalyzed organic-inorganic hybrid ink can be cured just after deposition, without any intermediate evaporation or annealing step, enormously simplifying microlens fabrication process. Besides, a simple combustion chemical vapour deposition process, leading to a porous layer with nano-roughness, followed by a silanization step using a fluorosilane enables the generation of a surface that provides access to a large range of contact angles for the ink drops that are printed on this surface. Single droplet microball lenses with contact angles up to 115°, beyond the hemispherical microlenses, are demonstrated with this industrially viable, cost-effective and high-throughput method.

1. Introduction

Microlenses and microlens arrays are used to redirect light and improve collection efficiency in sensing devices, light-coupling in optical fiber communication systems, light extraction from light emitting diodes (LEDs) or optical performance in displays [1–9]. In many of these applications, the precise positioning of microlenses with short focal lengths and high numerical aperture (NA) is highly demanded. For example, microball lenses beyond the hemispherical geometry, adequately integrated and precisely positioned, are useful elements to efficiently focus light from a laser diode into single-mode fibers for communication systems. The development of photolithographic techniques, that enabled the extraordinary progress of the semiconductor industry, also facilitated the first practical miniaturization of lenses into microlenses [10]. These were prepared starting with circular microposts created by using a photoresist.

The posts were later thermally treated to melt the resist leading, through a thermal reflow process, to a lens with a spherical profile dictated by surface tension. Curing of the photoresist ultimately stabilizes the final microlens shape [11,12]. Other photolithographic approaches such as gray-scale microlens projection as well as other chemical or mechanical methods, for example hot embossing, have also been used in the production of microlens arrays with well-defined profiles redirecting light in a controlled fashion [13–16]. The preparation of microlenses has also been undertaken using inkjet printing technology. Compared to photolithographic or embossing based methods, inkjet printing digitally positions droplets of ink leading to microlenses at well-defined locations on virtually any type of substrate, with no contact and minimal post-processing [17–30].

Typically a polymerizable material solution is used as a base material for the microlens fabrication. The final refractive index of the

* Corresponding author at: Instituto de Ciencia de Materiales de Aragón (ICMA), CSIC-Universidad de Zaragoza, Departamento de Física de la Materia Condensada, Zaragoza, Spain.

E-mail address: carlos.s@csic.es (C. Sánchez-Somolinos).

<https://doi.org/10.1016/j.apsusc.2020.145422>

Received 27 September 2019; Received in revised form 9 January 2020; Accepted 15 January 2020

Available online 18 January 2020

0169-4332/ © 2020 Elsevier B.V. All rights reserved.

microlens, key in its optical performance, can be tailored to a large extent through the ink formulation. A solvent, not present in the final solid lens, is usually employed to adjust the ink properties so jetting is possible without clogging of the printhead nozzle [19,23,24,27]. The prepolymer solution is then jetted and deposited on top of a substrate. After all the solvents are evaporated, the so generated microlens, can be fixed by polymerization [18,19]. Disadvantageously, this solvent evaporation post-printing step complicates the manufacturing process and it can additionally result in undesired changes in the geometry and the optical properties of the final solid microlenses.

Besides the intrinsic properties of the ink, the interaction of this ink with the target substrate is also of key importance for the resultant microlens geometry and therefore for its optical characteristics. For the typical volumes of single droplets deposited by inkjet printing, their final shape on the substrate is not influenced by gravity, generally reaching a spherical cap geometry [31]. For a flat surface, the solid angle of the spherical cap is dictated by the contact angle and their volume determined by the amount of deposited ink [32]. For example, in order to generate microlenses with high NA, modified substrates leading to sessile ink droplets with large contact angles have been generated to create, on top of them, high NA microlenses by inkjet printing, however the preparation process is complex and involves sophisticated and expensive equipment [20–22,33,34]. Interestingly, Luo et al [27] prepared nanostructured layers consisting on fluorinated nanopillars to create high NA microlenses on top of these layers. The method to prepare them comprises the generation of a thin ZnO seed layer (30 nm thick) onto a glass substrate using a radio frequency (RF) magnetron sputter-deposition technique. Afterwards, ZnO nanopillars are synthesized onto the substrate in an aqueous solution of zinc nitrate hexahydrate and methenamine in deionized water. Finally a C_4F_8 coating is done by inductively coupled plasma chemical vapour deposition process, using C_4F_8 and CHF_3 gases. The so prepared surfaces can be used to generate microlenses beyond the hemisphere (contact angle of 115°). Overall, despite all these advances and the intense efforts, the developed techniques involve complicated steps, difficult to implement in an industrial environment and in a cost-effective way.

Here we report a facile, robust, cost-effective and high-throughput method for the preparation of microlenses with well-defined optical characteristics on flat substrates by inkjet printing technology. A solvent-free photoacid catalyzed hybrid organic–inorganic polymerizable formulation has been used as an ink for microlens preparation. The deposited ink is directly cured just after deposition without need of any evaporation post-printing step. As a result, the lens geometry is immediately fixed after deposition, with no post-processing, facilitating the control of the lens optical properties. In order to tune the contact angle of the prepolymer droplets, a simple two-step method to modify the receiving substrate has been developed. Firstly, the combustion chemical vapour deposition (CCVD) of a silane leads to a nanostructured layer on top of the substrate. Secondly, this layer is chemically coated with a fluorosilane by conventional chemical vapour deposition (CVD) [35]. The introduction of the nanoroughness on the surface by CCVD and its subsequent fluorination by CVD leads to larger contact angles of the photopolymerizable ink droplets and microball lenses beyond the hemisphere can be attained. The drops can be immediately fixed by ultraviolet (UV) photopolymerization. The preparation of microlenses with controlled geometrical characteristics using this simple method, compatible with a continuous industrial production process, together with the lens morphological and optical characterization are described in this paper.

2. Material and methods

2.1. Ink material

3-glycidoxypolytrimethoxysilane (GPTMS), a monomer with an epoxy and a trialkoxysilane group, was purchased from Alfa Aesar (Haverhill, MA, USA). The epoxy resin Epikote 157, a monomer with eight epoxide groups, was obtained from Momentive (Waterford, NY, USA). Dimethoxydiphenylsilane (dPDMS), a disilane monomer bearing two aromatic rings was acquired from Aldrich (Madrid, Spain). Triarylsulfonium hexafluorophosphate salts (50% in propylene carbonate) purchased from Aldrich (Madrid, Spain) were used as a photoacid generator (PAG) system. BYK-333, a polyether-modified polydimethylsiloxane, from BYK Chemie (Wesel, Germany) was used to regulate the surface tension of the ink.

2.2. Substrate modification

2.2.1. Substrates and cleaning procedure

Conventional microscope glass slides were used as substrates for our studies. First, substrates were pre-cleaned by gently hand rubbing them using nitrile gloves and a solution of soapy water. After this, the substrates were thoroughly rinsed with milli-Q water and they were put in an ultrasonic bath containing soapy water for 10 min. The substrates were then flushed with milli-Q water and put in an ultrasonic bath containing again milli-Q water for 10 min more. After this, the substrates were flushed with isopropyl alcohol (IPA) and put again 10 more min in an ultrasonic bath, containing this time IPA. After the wet cleaning steps, the glass substrates were dried using compressed air.

2.2.2. Ozone modified glass.

Cleaned substrates were UV-Ozone treated for 1 h. UV-ozone treatment was carried out in a UV-ozone reactor UVO 342 (Jelight company Inc., CA, USA).

2.2.3. CCVD treatment

CCVD treatment of the glass was carried out using the Pyrosil® technique (Sura Instruments GmbH (Jena, Germany)). The equipment (Pyrosil® ST system 180 MD 1B) generates a propane-air flame with the air stream containing vapour of tetramethylsilane (TMS). The substrates placed on a metallic platform at RT are moved with a conveyor belt with a speed of 100 mm/s through the outer, reactive part of the flame, where the TMS transforms into amorphous silicon oxide [36]. The distance between the exit of the burner and the substrate platform is 64 mm. This process can be repeated as many times as desired, increasing subsequently the amount of deposited material. Along this paper, the number of passes has been varied from 0 to 14.

2.2.4. CVD treatment with fluorosilane

The substrates, either treated with ozone or with CCVD, are then placed in a desiccator containing a glass slide in the middle with 10 Pasteur pipette drops of 1H,1H,2H,2H-Perfluorooctyltrichlorosilane (FOTS). A mild vacuum of 100 mbar was then applied for 30 min all at room temperature (RT). The substrates are taken out of the desiccator, thoroughly flushed with isopropanol, dried with compressed air and finally baked for 10 min at 110°C in air.

2.3. Inkjet printing

A custom-made inkjet printer system (In-2 Printing Solutions, Navarra, Spain) was employed to generate the microlenses. The system uses Xaar-126/80 piezoelectric printheads (Xaar, Cambridge, United Kingdom). The printhead is fitted in a temperature stabilized metallic block provided with heating elements and a thermocouple all connected to a temperature controller. The printhead has 126 nozzles ($50\ \mu\text{m}$ diameter) arranged in a line with a pitch of $137\ \mu\text{m}$. The line of

nozzles is orthogonal to the direction of the substrate displacement. Consequently, the vertical resolution (in the direction of the line of nozzles) is 185 dots per inch (dpi). The horizontal resolution (in the direction of the substrate movement) depends on jetting frequency and speed of the substrate relative to the printhead. A Xaar XUSB drive electronics and associated software, controlled with a PC, is used to command the printhead. The substrate stage is linearly moved under the printhead by an eTrack linear stage (Newmark systems Inc.; Mission Viejo, CA, USA) with IMS-Terminal software (Marlborough, CT, USA)

2.4. Photocuring

An Exfo OmniCure S2000 (Gentec, Nivelles, Belgium) UV lamp provided with an UV bandpass filter (320–390 nm) has been used. A power of 10 mW/cm² has been applied on the samples during 5 min for curing. UV light exposure was carried out at RT (25 °C) under mild vacuum conditions. More into detail, for curing, the samples were placed inside a metallic chamber provided with an optical access. A mild vacuum of 100 mBar was achieved inside the chamber by using a vacuum pump. Once the pressure level is achieved, UV light is immediately applied to minimize ink evaporation.

2.5. Water contact angle measurements

Water contact angles were characterized using an Attension Goniometer Theta Lite. Distilled water droplets (8 μl) were dispensed using a flat-tipped needle. The given values are the result of an average of three independent measurements.

2.6. Morphological characterization

Morphological studies of the microlenses were performed using a field-emission scanning electron microscope (FE-SEM) Merlin from Carl Zeiss (Oberkochen, Germany).

2.7. Optical characterization

A home-made digital transmission microscope has been used for the estimation of the geometrical characteristics of the microlenses. The illumination beam is a collimated laser beam ($\lambda = 514.5$ nm). Planachromat extra long working distance microscope objectives are used to image the microlenses into a digital camera (2560x2160, 6.5 μm pixels). A home-built holder allows an easy rotation of the glass substrate (where the microlenses are placed) so that the microlenses can be observed from any direction, including top and side views.

3. Results and discussion

3.1. Microlens ink material

To generate the microlenses by inkjet printing we use as ink a solvent-free photoacid catalyzed organic–inorganic hybrid formulation previously developed in our laboratory, named HRI ink [37]. The ink consists mainly of three different monomers: an organic–inorganic hybrid molecule named GPTMS (50 wt%), bearing an epoxy and a triethoxysilane group, the multifunctional epoxide Epikote 157 (25 wt%) and dPDMS (25 wt%) as disilane. These two last monomers, are expected to polymerize with the epoxy rings and the silane groups of GPTMS respectively, finally forming an organic–inorganic hybrid network. Besides Epikote 157 and dPDMS have 8 and 2 aromatic benzene rings respectively, contributing to increase the refractive index of the resultant material. Additionally, 0.05 wt% of BYK-333 is incorporated to the formulation as a surface tension regulator [38]. Finally, 2 wt% of triarylsulfonium hexafluorophosphate salt is added as a photoinitiator system to the formulation. Irradiation with UV light of this photosensitive system generates acidic species that effectively catalyze the

epoxy ring-opening reaction, on one side, and the hydrolysis and condensation polymerization processes of the silanes on the other side.

Overall, the surface tension and rheology of the system have been tailored to obtain jettable ink using industrial piezoelectric printheads. Besides, selection of the components of the ink, described in the paragraph above, has been done to lead, after curing, into solid materials with excellent optical transmission properties [37]. Advantageously, no solvents are used in the formulation of the ink. So, once ejected and deposited on the substrate, fixation to the substrate can be directly done by UV photopolymerization without the need of intermediate evaporation steps that complicate the lens preparation process and can lead to undesired geometry changes of the deposited features. By curing the deposited ink under mild vacuum conditions (100 mBar) solid printed elements, including waveguides, can be obtained with a refractive index of 1.56 and with optical losses of 0.5–0.6 dB/cm, as we have previously reported [37,39,40].

3.2. Surface treatment

As a previous step to generate microlenses, the glass surface is conditioned to receive the inkjet printed droplets and lead to well-defined contact angles of the deposited ink droplets. The interfacial energies involved and the amount of deposited ink regulate the shape and dimensions of the deposited liquid lens [32]. In order to obtain microlenses with high NA, substrates need to be modified seeking for sessile ink droplets with large contact angle. This leads to deposited liquid lenses with smaller lens base diameter (diameter of the flat interface of the lens with the substrate) and larger lens height.

First, a conventional modification process of the glass substrate consisting in an ozone treatment (see Section 2.2.2) followed by CVD of FOTS (see Section 2.2.4) has been performed as a reference treatment. Ozone is applied to pre-clean glass substrates to eliminate any residual organic layers and leave the silanol groups of the glass exposed at the surface [41]. The glass is then exposed to a vapour of FOTS that is adsorbed to the surface at RT and covalently fixed when annealed at high temperature [42]. As a result, this treated glass substrate, that will be named as ozone-fluorosilane modified glass, presents a hydrophobic surface with a water contact angle of 110° (see Fig. S1 in the Supplementary Information). Ink droplets were inkjet printed on top of this ozone-fluorosilane modified glass substrates. Optimized jetting and photocuring conditions for this ink has been described elsewhere, leading to smooth and optically transparent polymerized prints [37]. Briefly, once the ink has been deposited, this is immediately cured by UV exposure at mild vacuum conditions (100 mBar) to reduce the amount of available atmospheric water and balance the organic and inorganic networks formation, inhibiting in this way phase segregation frequently found in polymerization of these multicomponent systems. Fig. 1 shows FESEM images of an array of photocured inkjet printed microlenses on a glass substrate previously modified with ozone and CVD of FOTS. A microlens typical diameter of 80 μm has been measured for these microlenses. Additional geometrical characterization of these lenses will be provided in Section 3.3.

To get access to larger contact angles of the ink with the target substrate, it is needed to explore alternative surface treatments that keep the good optical transmission properties of glass and, at the same time, are compatible with inkjet printing. It is well known that fluorinated flat surfaces leads in the best case to water contact angles below 120° [43] and that roughness introduced in the surface at different length-scales is a key ingredient to increase this water contact angle value [43–47]. Nature has been a continuous source of inspiration in this context providing a collection of microtextures leading to large hydrophobicity. In many examples, bumps at scale of tens of microns have demonstrated to contribute to increase hydrophobicity. However, many times the coexistence of these micron-size features together with nanostructures in the range of tens or hundreds of nanometers leads to further enhancement of this property [48–50]. Despite the origin of

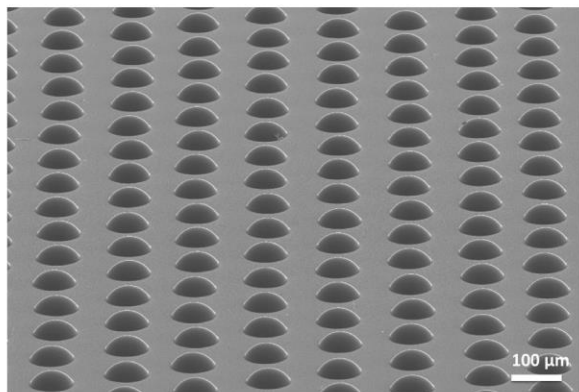
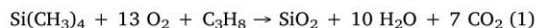


Fig. 1. Oblique view FESEM images of an array of cured inkjet printed microlenses using HRI-ink on an ozone-fluorosilane modified glass.

superhydrophobic behaviour in this hierarchically structured surfaces is not fully understood, the coexistence of low surface energy materials (such as fluorinated solids) and roughness is a well-established approach to engineer surfaces with high degrees of hydrophobicity. As surface roughness can lead to a decrease of transparency, the use of these corrugated surfaces for optical applications is majorly focused in surface treatments leading to nanoscale roughness with features well below the wavelength of light, therefore significantly reducing light scattering. Different methods have been used to generate this surface roughness, including surface chemical etching, hydrothermal growth or deposition of nanoparticles, nanorods or nanofilaments [51–59]. For effective industrial implementation simplicity in the preparation process is of paramount importance.

Here we introduce a simple and industrially viable two-step process to create surfaces leading to large contact angles of the deposited ink. First, the CCVD of an organosilicon precursor, TMS, is used for the introduction of surface roughness at the nanoscale in flat surfaces (see Section 2.2.3). Second, following the CCVD process, a simple CVD of a fluorosilane is carried out [35] (see Section 2.2.4). More in detail, as schematically shown in Fig. 2a, the substrate is put on a metallic plate,

all at RT. The plate and the samples are moved with a conveyor belt with a constant speed (100 mm/s) through the outer part of a gas flame fed with TMS in ambient atmosphere (see details in Section 2.2.3). As a result, an amorphous nanotextured SiO₂ layer with thickness typically in the range of tens of nanometres is deposited [60,61]. The reaction of the monomer with flame to generate SiO₂ is exemplified by Equation 1. As previously reported in the literature, these types of layers present hydroxyl groups in surface. This property has been extensively used to generate adhesion promotion layers and constitutes an excellent opportunity for postfunctionalization [60–62].



Taking clean glass substrates at RT as starting point for the process, thin SiO₂ films were deposited using this CCVD method. Several passes of the substrate through the reactive flame of the CCVD system can be carried out to add additional SiO₂. Afterwards, these samples are CVD treated with FOTS, as described in Section 2.2.4, by placing them inside a desiccator containing a small volume of this compound, all at low pressure (100 mBar) at RT. The presence of atmospheric water produces hydrolysis of the labile chlorosilane groups of the FOTS. Annealing leads to condensation and covalent fixation of the fluorosilane to the deposited SiO₂ nanoparticles as schematically presented in Fig. 2b.

Water contact angles (WCAs) were characterized on CCVD-fluorosilane treated glass substrates with different number of passes through the reactive flame of the CCVD system. As mentioned above, ozone-fluorosilane modified glass (ozone treatment followed by CVD of FOTS process) led to a WCA of 110°. In contrast, the samples treated with 4 or more passes of CCVD and a subsequent CVD of FOTS resulted in substantially larger WCAs with values between 164° and 170°.

Water droplets were deposited on top of the surface of samples with ozone-fluorosilane treatment and CCVD-fluorinated samples with 2, 4, 6, 8, 10, 12 and 14 passes through the flame to further study their wetting behaviour. On one side, ozone-fluorosilane modified glass pin the water droplets showing no slipping of these drops. On the other side, for all CCVD-fluorosilane modified substrates, a sliding angle below 3° was found, defining this angle as the angle of the sample with respect the horizontal plane at which droplet roll-off takes place. This demonstrates superhydrophobic behaviour. As an example, Fig. 2c shows a droplet of water on top of the CCVD-fluorinated surface with 4

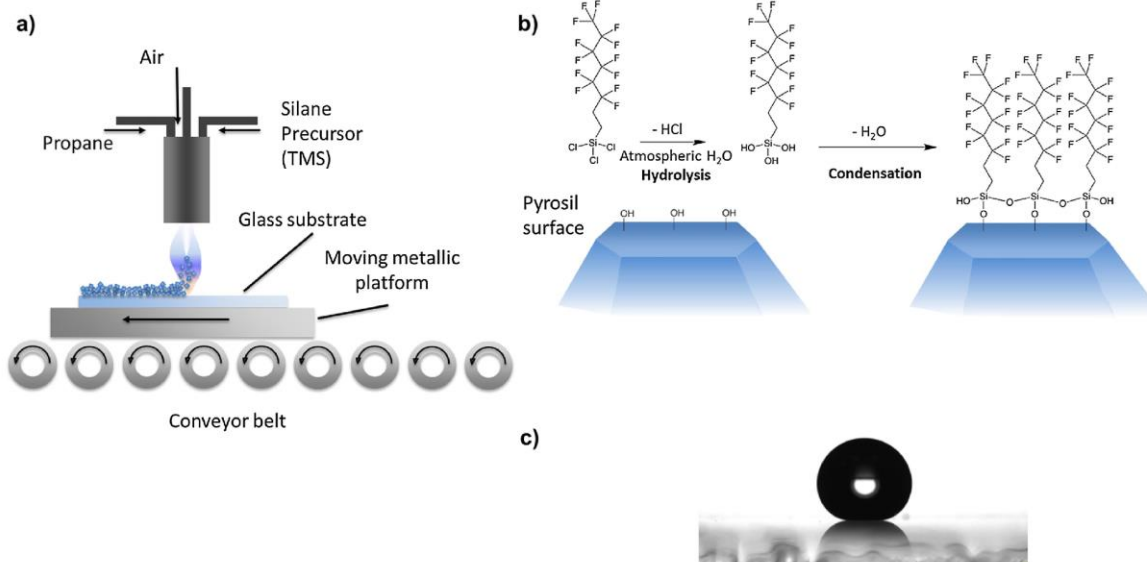


Fig. 2. (a) Schematic representation of the CCVD process and the deposited nanoparticles. (b) Schematic illustration of the surface functionalization of the deposited particles with 1H,1H,2H,2H-Perfluorooctyltrichlorosilane by CVD. (c) Water droplet on top of a CCVD-fluorosilane modified glass (4 passes through the reactive flame of the CCVD system).

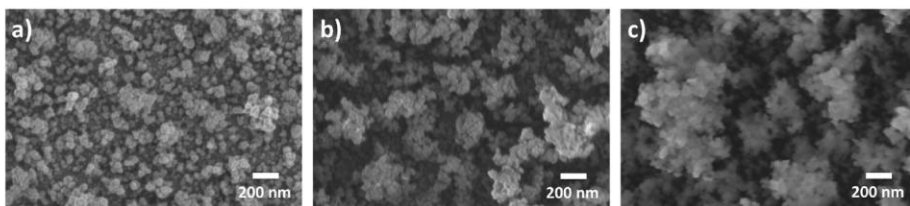


Fig. 3. FESEM images of CCVD treated substrates with (a) 2, (b) 4 and (c) 8 passes through the reactive flame before silanization with FOTS.

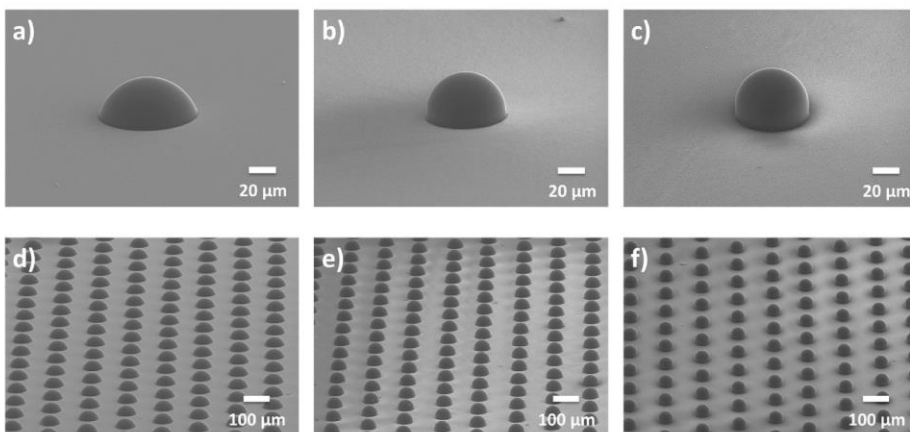


Fig. 4. Oblique view FESEM images of a single-drop inkjet printed microlens using HRI-ink on a CCVD-fluorosilane treated glass substrate with (a) 2, (b) 4 and (c) 8 passes through the reactive flame of the CCVD system. Oblique view FESEM images of arrays of single-drop inkjet printed microlenses on a CCVD-fluorosilane treated glass substrate with (d) 2, (e) 4 and (f) 8 passes through the flame.

CCVD passes leading after fluorosilane treatment to water contact angle of 165° and sliding angle of less than 1° .

Morphological studies have been carried out in these CCVD modified substrates to better understand the origin of the enhanced hydrophobicity. Fig. 3 shows SEM images of CCVD treated substrates, using 2, 4 and 8 passes of the substrate through the flame before the silanization with FOTS. Fig. 3a, corresponding to the SEM image of the sample with 2 passes, clearly shows the existence of a large number of particles with diameter in the range of 20–40 nm randomly distributed on the glass surface. As the number of passes of the substrate through

the reactive flame increases, the SEM image reveals the formation of particle aggregates as seen in Fig. 3b and 3c for samples with 4 and 8 passes through the flame respectively. Subsequent silanization with the fluorinated modifier does not change the surface morphology (see Fig. S2).

These results indicate that the nanoroughness created by the fluorosilane coated hierarchical structures is responsible of the enhanced hydrophobicity. Overall it can be stated that the combination of CCVD of TMS and a subsequent chemical modification through the fluorosilanization with FOTS is a simple and industrially viable

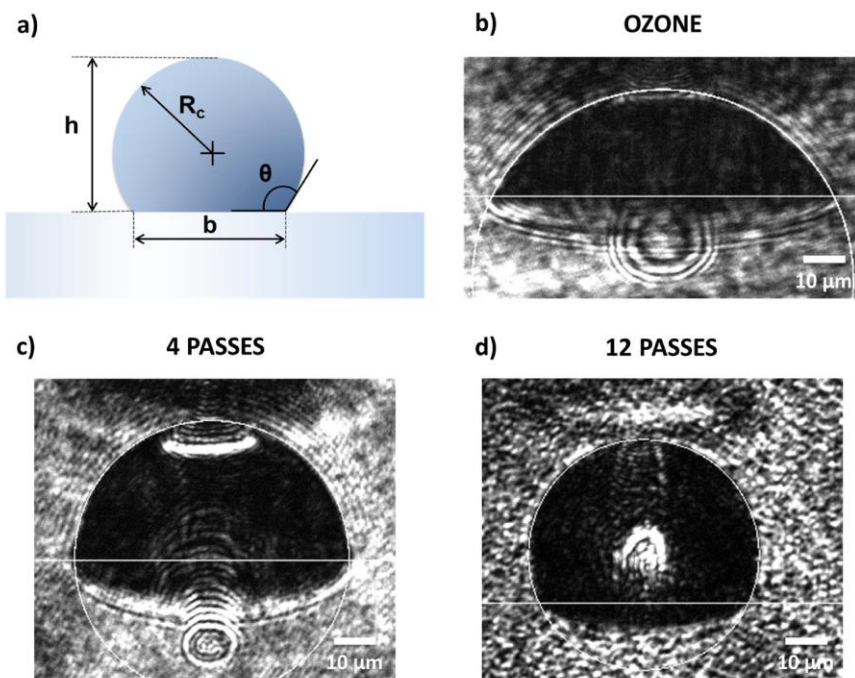


Fig. 5. (a) Definition of geometrical parameters of single-drop inkjet printed microlenses using HRI-ink: radius of curvature (R_c), height (h), base diameter (b) and angle (θ) at the contact point. Side view microscope images of microlenses with (b) ozone-fluorosilane modified glass, (c) 4 and (d) 12 passes through the reactive flame of the CCVD system. A white circle and a line are drawn in each image to outline the lens position and the substrate baseline.

Table 1

Geometrical parameters of inkjet printed microlenses on CCVD-fluorosilane modified glass. As a reference, parameters for lenses deposited on ozone-fluorosilane modified glass are also included as having zero passes through the flame.

# passes	R _c (μm)	b (μm)	h (μm)	θ (°)
0 (Ozone)	46.2	80.3	23.4	60.4
2	39.7	77.5	31.1	77.5
4	32.5	65.0	33.1	91
6	28.8	56.2	35.2	102.8
8	29.4	57.7	35.1	101.2
10	28.5	53.2	38.7	110.9
12	27.3	49.6	38.7	114.7
14	27.3	50.2	38.1	113.2

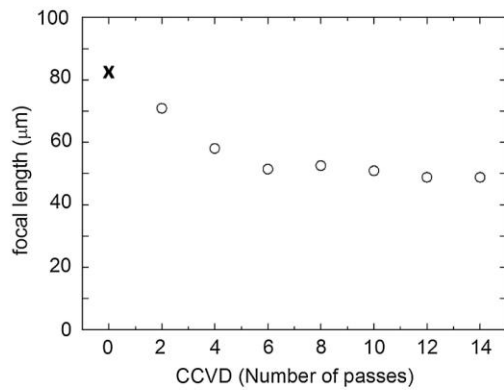


Fig. 6. Theoretically calculated focal length of inkjet printed microlenses on CCVD-fluorosilane modified glass with different number of passes of the substrate through the reactive flame (circles). As a reference, the calculated focal length for lenses deposited on ozone-fluorosilane modified glass is also included as having zero passes through the flame (cross).

processing methodology for the preparation of superhydrophobic surfaces.

3.3. Microlens preparation and characterization

We have prepared inkjet printed microlenses on top of CCVD-fluorosilane treated glass substrates. Fig. 4a, b and c present oblique SEM images of a single-drop microlens, inkjet printed and UV cured under mild vacuum conditions on CCVD-fluorosilane modified glass with 2, 4 and 8 passes through the reactive flame respectively. The microlenses present a spherical profile and a smooth morphology after processing. The increase of the substrate nanoroughness is accompanied with an increase of the contact angle of the ink and therefore a larger curvature (smaller radius of curvature) of the resultant microlenses (*vide infra*). Advantageously for our methodology, these deposited HRI ink droplets, with large contact angles, are pinned in the substrate. As a result, these CCVD-fluorosilane treated substrates with ink droplets arrays deposited on top can be taken and observed under the microscope before curing without special precaution in the handling, this not

generating any damage of the quality of the microlenses arrays. Fig. 4d, e and f show FESEM images of arrays of microlenses deposited on CCVD-fluorosilane modified glass treated with 2, 4 and 8 passes through the flame respectively, and subsequently photocured. Inspection of the shape and dimensions of the microlenses over larger areas of several cm² confirmed the reproducibility both in the surface conditioning and the microlens deposition processes. The digital character of the developed inkjet printing based methodology allows to precisely deposit microlenses with high reproducibility at well-defined positions. As a limitation, and also inherent to inkjet printing, the distance between micro lenses has to be slightly larger than the diameter of the microlenses to avoid coalescence of ink droplets during processing that would result in array quality deterioration. Nevertheless, microlens diameters higher than 90% the distance between adjacent lenses have been nicely demonstrated by other authors using inkjet printing, demonstrating great potential of this technique in the generation of high density microlens arrays [63].

Optical lens parameters (Fig. 5a) of these single-drop microlenses have been investigated using optical microscopy. Fig. 5 presents side view microscope images of microlenses deposited on ozone-fluorosilane modified glass (Fig. 5b), and CCVD-fluorosilane modified glass with 4 (Fig. 5c) and 12 (Fig. 5d) passes through the flame. A software routine recognizes the contour of the microlens adjusting it to a circle shape. The baseline is determined by the two points where the circle fitting deviates from the microlens contour. As previously shown in FESEM images, the side view microscope images corroborate that an increase in the nanoroughness provided by the CCVD treatment followed by the grafting with the fluorosilane leads to larger angles of the inkjet printed microlenses at the contact point with the substrate. It is worth to note that for a number of passes of the substrates through the flame larger than 4, this angle is already larger than 90° (hemisphere).

From these measurements, different microlens parameters, graphically described in Fig. 5a, such as the radius of curvature (R_c), height (h), base diameter (b) and the angle (θ) at the contact point with the substrate have been determined and are presented in Table 1.

From these values the focal length can be theoretically calculated from $f = R_c / (n - 1)$, taking as a refractive index n value of 1.56, previously measured in thin films of this material through a prism-coupling method [37] using a wavelength of 632.8 nm. Fig. 6 shows the focal length values of the different microlenses as a function of surface treatment. A clear trend towards shorter focal lengths is observed as the number of passes through the reactive flame increases, until a saturation value of 50 μm is reached.

3.4. Multidrop microlenses

Microlenses of different size have also been generated by applying different number of microdroplets at the same position in these CCVD-fluorosilane treated substrates. Fig. 7a, b and c present FESEM images of sets of ink-jet printed microlenses on CCVD-fluorosilane treated glass substrate with 2, 4 and 8 passes through the flame respectively. Microlenses have been prepared using a different number of ink droplets (1, 8, 27 and 64 droplets, from left to right) in each position. As in the case of single droplet microlenses, lenses created with larger number of microdroplets show a well-controlled and reproducible geometry.

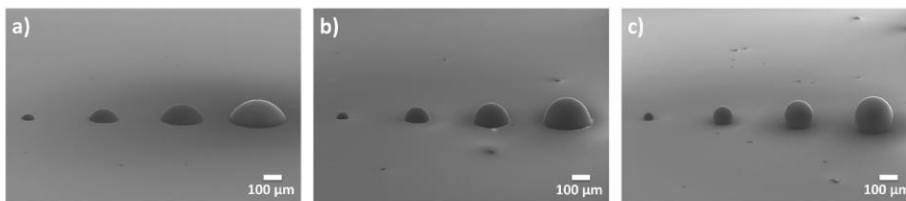


Fig. 7. Oblique FESEM image of ink-jet printed microlenses using HRI-ink on a CCVD-fluorosilane treated glass substrate with (a) 2, (b) 4 and (c) 8 passes through the reactive flame of the CCVD system. Different number of ink droplets has been deposited for the preparation of each microlens (from left to right: 1, 8, 27, 64 ink droplets).

4. Conclusions

In this work we have presented a facile and robust methodology for the preparation of microlenses with controlled geometrical characteristics on flat substrates by using inkjet printing technology. A solvent-free photocurable organic–inorganic hybrid formulation has been used as an ink for microlens fabrication. This ink uses no solvent and therefore can be cured immediately after printing, without any evaporation or annealing post-printing step, notably simplifying the microlens preparation process. A simple two-step surface treatment has been developed to tune the interaction of the ink with the substrate. Firstly, the CCVD of a nanostructured SiO₂ layer is first carried out on a flat substrate. Secondly, conventional CVD is used to coat this nanostructured layer with a fluorosilane. Control of both, the surface treatment and the deposited inkjet printed drop, results in microlenses with controlled geometrical characteristics. Microball lenses beyond the hemispherical microlens have been demonstrated with this simple method reaching single microdroplet lenses with angles at the contact point up to 115°. Even more, it can be envisioned that a subsequent controlled modification of the fluorosilane coating could further tune the contact angle of the ink on these CCVD-fluorinated substrates, leading into photocured microlenses with different focal lengths on the same substrate, thus enabling the preparation of multiscale microlens arrays. Overall the presented industrially viable, cost-effective and high-throughput methodology has demonstrated the precise positioning of microlenses with different contact angles and sizes, including microball lenses, by adjusting the surface treatment and the inkjet printing conditions, having therefore great potential in diverse application areas including communications, displays and sensing applications.

CRedit authorship contribution statement

Jorge Alamán: Conceptualization, Methodology, Investigation, Writing - original draft. **Ana María López-Villuendas:** Investigation. **María López-Valdeolivas:** Investigation. **María Pilar Arroyo:** Methodology, Investigation. **Nieves Andrés:** Methodology, Investigation. **Carlos Sánchez-Somolinos:** Conceptualization, Methodology, Writing - original draft.

Declaration of Competing Interest

The authors declared that there is no conflict of interest.

Acknowledgements

Carlos Sánchez Somolinos acknowledges funding from the Spanish Ministry project BIO2017-84246-C2-1-R, Gobierno de Aragón project LMP150_18 and FEDER (EU). Authors would like to acknowledge the use of Servicio General de Apoyo a la Investigación-SAI, Universidad de Zaragoza.

Appendix A. Supplementary material

Supplementary data to this article can be found online at <https://doi.org/10.1016/j.apsusc.2020.145422>.

References

- [1] K.E. Cai-Jun, Y.I. Xin-Jian, L.A.I. Jian-Jun, C.H.E.N. Si-Hai, Fabrication, testing and integration technologies of polymer microlens for Pt/Si schottky-barrier infrared charge coupled device applications, *Chinese Phys. Lett.* 22 (2005) 135.
- [2] -Y. Jr, C.-P. Hu, S.-Y. Lin, H. Hung, C.-K. Chao Yang, Semi-ellipsoid microlens simulation and fabrication for enhancing optical fiber coupling efficiency, *Sensor Actuat. A-Phys.* 147 (2008) 93–98.
- [3] F. Galeotti, W. Mróz, G. Scavia, C. Botta, Microlens arrays for light extraction enhancement in organic light-emitting diodes: a facile approach, *Org. Electron.* 14 (2013) 212–218.
- [4] Y.M. Song, Y. Xie, V. Malyarchuk, J. Xiao, I. Jung, K.-J. Choi, Z. Liu, H. Park, C. Lu, R.-H. Kim, R. Li, K.B. Crozier, Y. Huang, J.A. Rogers, Digital cameras with designs inspired by the arthropod eye, *Nature* 497 (2013) 95–99.
- [5] C.-H. Tien, C.-H. Hung, T.-H. Yu, Microlens arrays by direct-writing inkjet print for LCD backlighting applications, *J. Disp. Technol.* 5 (2009) 147–151.
- [6] J.M. Pavia, M. Wolf, E. Charbon, Measurement and modeling of microlenses fabricated on single-photon avalanche diode arrays for fill factor recovery, *Opt. Express* 22 (2014) 4202–4213.
- [7] V.K. Shinoj, V.M. Murukeshan, S.B. Tor, N.H. Loh, S.W. Lye, Design, fabrication, and characterization of thermoplastic microlenses for fiber-optic probe imaging, *Appl. Opt.* 53 (2014) 1083–1088.
- [8] J. Arai, H. Kawai, F. Okano, Microlens arrays for integral imaging system, *Appl. Opt.* 45 (2006) 9066–9078.
- [9] J.-H. Lee, Y.-H. Ho, K.-Y. Chen, H.-Y. Lin, J.-H. Fang, S.-C. Hsu, J.-R. Lin, M.-K. Wei, Efficiency improvement and image quality of organic light-emitting display by attaching cylindrical microlens arrays, *Opt. Express* 16 (2008) 21184–21190.
- [10] J. del Barrio, C. Sánchez-Somolinos, Light to shape the future: from photolithography to 4D printing, *Adv. Optical Mater.* 1900598 (2019) 1–33.
- [11] Z.D. Popovic, R.A. Sprague, G.A.N. Connell, Technique for monolithic fabrication of microlens arrays, *Appl. Optics* 27 (1988) 1281–1297.
- [12] R.F. Shyu, H. Yang, W.-R. Tsai, J.-C. Tsai, Micro-ball lens array fabrication in photoresist using PTFE hydrophobic effect, *Microsyst. Technol.* 13 (2007) 1601–1606.
- [13] M.-H. Wu, C. Park, G.M. Whitesides, Fabrication of arrays of microlenses with controlled profiles using gray-scale microlens projection photolithography, *Langmuir* 18 (2002) 9312–9318.
- [14] X.-J. Shen, L.-W. Pan, L. Lin, Microplastic embossing process: experimental and theoretical characterizations, *Sens. Actuators, A* 97–98 (2002) 428–433.
- [15] T. Hou, C. Zheng, S. Bai, Q. Ma, D. Bridges, A. Hu, W.W. Duley, Fabrication, characterization, and applications of microlenses, *Appl. Optics* 54 (2015) 7366–7376.
- [16] Q. Xu, B. Dai, Y. Huang, H. Wang, Z. Yang, K. Wang, S. Zhuang, D. Zhang, Fabrication of polymer microlens array with controllable focal length by modifying surface wettability, *Opt. Express* 26 (2018) 4172–4182.
- [17] Z. Zhang, X. Tang, X. Liu, X. Lei, W. Chen, Fabrication of high quality and low cost microlenses on a glass substrate by direct printing technique, *Appl. Optics* 53 (2014) 7868–7871.
- [18] J.Y. Kim, K. Pfeiffer, A. Voigt, G. Gruetzner, J. Brugger, Directly fabricated multi-scale microlens arrays on a hydrophobic flat surface by a simple ink-jet printing technique, *J. Mater. Chem.* 22 (2012) 3053–3058.
- [19] J.Y. Kim, C. Martin-Olmos, N.S. Baek, J. Brugger, Simple and easily controllable parabolic-shaped microlenses printed on polymeric mesas, *J. Mater. Chem. C* 1 (2013) 2152–2157.
- [20] L. Jacot-Descombes, M.R. Gullo, V.J. Cadarso, J. Brugger, Fabrication of epoxy spherical microstructures by controlled drop-on-demand inkjet printing, *J. Micromech. Microeng.* 22 (2012) 074012.
- [21] V.J. Cadarso, J. Perera-Núñez, L. Jacot-Descombes, K. Pfeiffer, U. Ostrzinski, A. Voigt, A. Llobera, G. Grützer, J. Brugger, Microlenses with defined contour shapes, *Opt. Express* 19 (2011) 18665–18670.
- [22] M. Blattmann, M. Ocker, H. Zappe, A. Seifert, Jet printing of convex and concave polymer micro-lenses, *Opt. Express* 23 (2015) 24525–24536.
- [23] R. Danzebrink, M.A. Aegerter, Deposition of micropatterned coating using an ink-jet technique, *Thin Solid Films* 351 (1999) 115–118.
- [24] R. Danzebrink, M.A. Aegerter, Deposition of optical microlens arrays by ink-jet processes, *Thin Solid Films* 392 (2001) 223–225.
- [25] X. Zhu, L. Zhu, H. Chen, M. Yang, W. Zhang, Fabrication of multi-scale micro-lens arrays on hydrophobic surfaces using a drop-on-demand droplet generator, *Opt. Laser Technol.* 66 (2015) 156–165.
- [26] X. Zhu, L. Zhu, H. Chen, Z. Li, W. Zhang, Fabrication of high numerical aperture micro-lens array based on drop-on-demand generating of water-based molds, *Opt. Laser Technol.* 68 (2015) 23–27.
- [27] Y. Luo, L. Wang, Y. Ding, H. Wei, X. Hao, D. Wang, Y. Dai, J. Shi, Direct fabrication of microlens arrays with high numerical aperture by ink-jetting on nanotextured surface, *Appl. Surf. Sci.* 279 (2013) 36–40.
- [28] X. Zhu, L. Zhu, H. Chen, L. Yang, W. Zhang, Micro-ball lens structure fabrication based on drop on demand printing the liquid mold, *Appl. Surf. Sci.* 361 (2016) 80–89.
- [29] X. Zhu, Q. Xu, Y. Hu, H. Li, F. Wang, Z. Peng, H. Lan, Flexible biconvex microlens array fabrication using combined inkjetprinting and imprint-lithography method, *Opt. Laser Technol.* 115 (2019) 118–124.
- [30] L. Wang, Y. Luo, Z.Z. Liu, X. Feng, B. Lu, Fabrication of microlens array with controllable high NA and tailored optical characteristics using confined ink-jetting, *Appl. Surf. Sci.* 442 (2018) 417–422.
- [31] A.L. Yarin, Drop impact dynamics: splashing, spreading, receding, bouncing, *Annu. Rev. Fluid Mech.* 38 (2006) 159–192.
- [32] D.B. Van Dam, C. Le Clerc, Experimental study of the impact of an ink-jet printed droplet on a solid substrate, *Phys. Fluids* 16 (2004) 3403–3414.
- [33] L. Jacot-Descombes, V.J. Cadarso, A. Schleunitz, S. Grützer, J.J. Klein, J. Brugger, H. Schift, G. Grützer, Organic-inorganic-hybrid-polymer microlens arrays with tailored optical characteristics and multi-focal properties, *Opt. Express* 23 (2015) 25365–25375.
- [34] E. Beckert, F. Kemper, P. Schreiber, M. Reif, P. Dannberg, S. Sauva, Inkjet printing of microlens arrays on large, lithographic structured substrates, *Proc. SPIE Adv. Fabricat. Technol. Micro/Nano Opt. Photon.* XII 10930 (2019) 1–7.
- [35] J. Alamán, R. Alicante, M.C. Artal, C. Gimeno, C. Sanchez-Somolinos, Método para recubrir un elemento base para un componente de aparato doméstico, y componente de aparato doméstico ES Patent No. E52673370 (B1), 3 April 2019.

- [36] R. Janda, J.-F. Roulet, M. Wulf, H.-J. Tiller, A new adhesive technology for all-ceramics, *Dent. Mater.* 19 (2003) 567–573.
- [37] J. Alamán, M. López-Valdeolivas, R. Alicante, F.J. Medel, J. Silva-Treviño, J.I. Peña, C. Sánchez-Somolinos, Photoacid catalyzed organic–inorganic hybrid inks for the manufacturing of inkjet-printed photonic devices, *J. Mater. Chem. C* 6 (2018) 3882–3894.
- [38] A. Chemtob, D.-L. Versace, C. Belon, C. Croutxé-Barghorn, S. Rigolet, Concomitant organic-inorganic UV-curing catalyzed by photoacids, *Macromol.* 41 (2008) 7390–7398.
- [39] J. Alamán, M. López-Valdeolivas, R. Alicante, J.I. Peña, C. Sánchez-Somolinos, Digital luminescence patterning via inkjet printing of a photoacid catalysed organic-inorganic hybrid formulation, *Polymers* 11 (2019) 430.
- [40] J. Alamán, M. López-Valdeolivas, R. Alicante, C. Sánchez-Somolinos, Optical planar waveguide sensor with integrated digitally-printed light coupling-in and readout elements, *Sensors* 19 (2019) 2856.
- [41] C.K. Fink, K. Nakamura, S. Ichimura, S.J. Jenkins, Silicon oxidation by ozone, *J. Phys.: Condens. Matter* 21 (2009) 183001.
- [42] D. Trimbach, K. Feldman, N.D. Spencer, D.J. Broer, C.W.M. Bastiaansen, Block copolymer thermoplastic elastomers for microcontact printing, *Langmuir* 19 (2003) 10957–10961.
- [43] T. Nishino, M. Meguro, K. Nakamae, M. Matsushita, Y. Ueda, The lowest surface free energy based on -CF₃ alignment, *Langmuir* 15 (1999) 4321–4323.
- [44] E.G. Shafrin, W.A. Zisman, Upper Limits for the Contact Angles of Liquids on Solids, Naval Research Laboratory, Surface Chemistry Branch, Chemistry Division, Washington D.C., 1963.
- [45] D. Quere, Wetting and roughness, *Annu. Rev. Mater. Res.* 38 (2008) 71–99.
- [46] A. Lafuma, D. Quéré, Superhydrophobic states, *Nat. Mater.* 2 (2003) 457–460.
- [47] S. Wang, L. Jiang, Definition of superhydrophobic states, *Adv. Mater.* 19 (2007) 3423–3424.
- [48] Z. Guo, W. Liu, B.-L. Su, Superhydrophobic surfaces: from natural to biomimetic to functional, *J. Colloid Interface Sci.* 353 (2011) 335–355.
- [49] T. Darmanin, F. Guittard, Superhydrophobic and superoleophobic properties in nature, *Mater. Today* 18 (2015) 273–285.
- [50] T. Verho, C. Bower, P. Andrew, S. Franssila, O. Ikkala, R.H.A. Ras, Mechanically durable superhydrophobic surfaces, *Adv. Mater.* 23 (2011) 673–678.
- [51] L. Xu, J. He, Fabrication of highly transparent superhydrophobic coatings from hollow silica nanoparticles, *Langmuir* 28 (2012) 7512–7518.
- [52] R.G. Karunakaran, C.-H. Lu, Z. Zhang, S. Yang, Highly transparent superhydrophobic surfaces from the coassembly of nanoparticles (< 100 nm), *Langmuir* 27 (2011) 4594–4602.
- [53] L. Xu, R.G. Karunakaran, J. Guo, S. Yang, Transparent, superhydrophobic surfaces from one-step spin coating of hydrophobic nanoparticles, *ACS Appl. Mater. Interfaces* 4 (2012) 1118–1125.
- [54] T. Wang, T.T. Isimjan, J. Chen, S. Rohani, Transparent nanostructured coatings with UV-shielding and superhydrophobicity properties, *Nanotechnol.* 22 (2011) 265708.
- [55] J. Zimmermann, F.A. Reifler, G. Fortunato, L.C. Gerhardt, S. Seeger, A. Simple, One-step approach to durable and robust superhydrophobic textiles, *Adv. Funct. Mater.* 18 (2008) 3662–3669.
- [56] H. Kim, K. Noh, C. Choi, J. Khamwannah, D. Villwock, S. Jin, Extreme superomniphobicity of multiwalled 8 nm TiO₂ nanotubes, *Langmuir* 27 (2011) 10191–10196.
- [57] R.T.R. Kumar, K.B. Mogensen, P. Bøggild, Simple approach to superamphiphobic overhanging silicon nanostructures, *J. Phys. Chem. C* 114 (2010) 2936–2940.
- [58] Y. Liu, Y. Xiu, D.W. Hess, C.P. Wong, Silicon surface structure-controlled oleophobicity, *Langmuir* 26 (2010) 8908–8913.
- [59] A. Hozumi, T.J. McCarthy, Ultralyophobic oxidized aluminum surfaces exhibiting negligible contact angle hysteresis, *Langmuir* 26 (2010) 2567–2573.
- [60] B. Schinking, R. Petzold, H.-J. Tiller, G. Grundmeier, Chemical structure and morphology of ultrathin combustion CVD layers on zinc coated steel, *Appl. Surf. Sci.* 179 (2001) 79–87.
- [61] H.-J. Tiller, R. Göbel, B. Magnus, A. Garschke, R. Musil, A new concept of metal–resin adhesion using an intermediate layer of SiO_x-C, *Thin Solid Films* 169 (1989) 159–168.
- [62] V. Seitz, K. Arzt, S. Mahnel, C. Rapp, S. Schwaminger, M. Hoffstetter, E. Wintermantel, Improvement of adhesion strength of self-adhesive silicone rubber on thermoplastic substrates – comparison of an atmospheric pressure plasma jet (APPJ) and a Pyrosil® flame, *Int. J. Adhes. Adhes.* 66 (2016) 65–72.
- [63] D. Wallace, D. Hayes, T. Chen, V. Shah, D. Radulescu, P. Cooley, K. Wachtler, A. Nallani, Think Additiv: Ink-Jet Deposition of Materials for MEMS Packaging, 6th Topical Workshop on Packaging of MEMS and Related Micro-Nano-Bio Integrated Systems, November 18–20, Long Beach, California, 2004.

Supplementary Information

Facile fabrication of microlenses with tailored optical properties by inkjet printing on nanostructured surfaces prepared by combustion chemical vapour deposition.

Jorge Alamán,^{a, b} Ana María López-Villuendas,^a María López-Valdeolivas,^a María Pilar Arroyo,^c Nieves Andrés,^c and Carlos Sánchez-Somolinos,^{a, d, *}

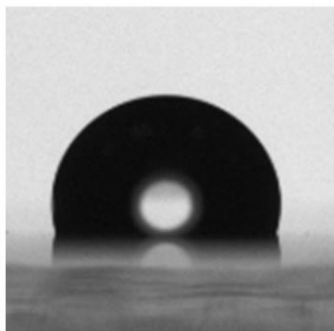
^a Instituto de Ciencia de Materiales de Aragón (ICMA), CSIC-Universidad de Zaragoza, Departamento de Física de la Materia Condensada, Zaragoza, Spain

^b BSH Electrodomésticos España, S.A., Polígono Industrial de PLA-ZA, Ronda del Canal Imperial de Aragón, 18-20, 50197 Zaragoza, Spain

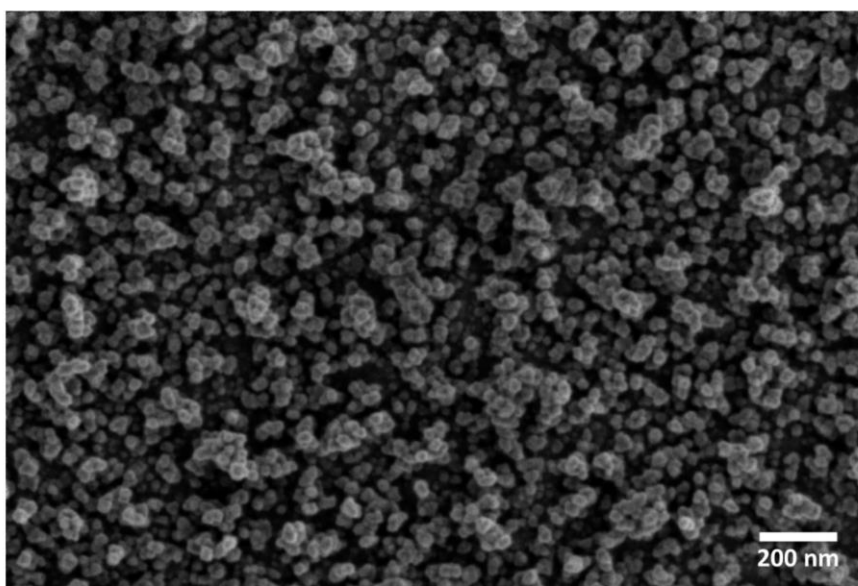
^c Instituto Universitario de Investigación en Ingeniería de Aragón (I3A), Universidad de Zaragoza, Departamento de Física Aplicada, Zaragoza, Spain

^d CIBER in Bioengineering, Biomaterials and Nanomedicine (CIBER-BBN), Spain

* Correspondence: carlos.s@csic.es



FigS1. Sessile drop of water on glass treated with ozone treatment followed by CVD with a fluorosilane



FigS2. FESEM images of a CCVD treated substrate with 2 passes through the flame after silanization with FOTS.

